

**PURDUE UNIVERSITY**  
**GRADUATE SCHOOL**  
**Thesis/Dissertation Acceptance**

This is to certify that the thesis/dissertation prepared

By Alexandra Nicole Mendlein

Entitled

Instrumental and Chemometric Analysis of Automotive Clear Coat Paints by Micro Laser Raman and UV Microspectrophotometry

For the degree of Master of Science

Is approved by the final examining committee:

Jay A. Siegel, PhD.

Chair

John V. Goodpaster, PhD.

Lei Li, PhD.

To the best of my knowledge and as understood by the student in the *Research Integrity and Copyright Disclaimer (Graduate School Form 20)*, this thesis/dissertation adheres to the provisions of Purdue University's "Policy on Integrity in Research" and the use of copyrighted material.

Approved by Major Professor(s): Jay A. Siegel, PhD.

Approved by: John V. Goodpaster, PhD

Head of the Graduate Program

07/01/2011

Date

**PURDUE UNIVERSITY  
GRADUATE SCHOOL**

**Research Integrity and Copyright Disclaimer**

Title of Thesis/Dissertation:

Instrumental and Chemometric Analysis of Automotive Clear Coat Paints by Micro Laser Raman and UV Microspectrophotometry

For the degree of Master of Science

I certify that in the preparation of this thesis, I have observed the provisions of *Purdue University Executive Memorandum No. C-22, September 6, 1991, Policy on Integrity in Research*.\*

Further, I certify that this work is free of plagiarism and all materials appearing in this thesis/dissertation have been properly quoted and attributed.

I certify that all copyrighted material incorporated into this thesis/dissertation is in compliance with the United States' copyright law and that I have received written permission from the copyright owners for my use of their work, which is beyond the scope of the law. I agree to indemnify and save harmless Purdue University from any and all claims that may be asserted or that may arise from any copyright violation.

Alexandra Nicole Mendlein

\_\_\_\_\_  
Printed Name and Signature of Candidate

06/30/2011

\_\_\_\_\_  
Date (month/day/year)

\*Located at [http://www.purdue.edu/policies/pages/teach\\_res\\_outreach/c\\_22.html](http://www.purdue.edu/policies/pages/teach_res_outreach/c_22.html)

INSTRUMENTAL AND CHEMOMETRIC ANALYSIS OF AUTOMOTIVE CLEAR COAT PAINTS  
BY MICRO LASER RAMAN AND UV MICROSPECTROPHOTOMETRY

A Thesis  
Submitted to the Faculty  
of  
Purdue University  
by  
Alexandra Nicole Mendlein

In Partial Fulfillment of the  
Requirements for the Degree  
of  
Master of Science

August 2011  
Purdue University  
Indianapolis, Indiana

For my family: Mom, Dad, Alyssa, and Anna, for all of your love and support in everything I've achieved. I love you. To my friends: Sonja and Jac, for being the best friends I could wish for, and somehow even more excited about grad school than I was; Chrissy, for being my always-supportive Indy Mom; Charlie, for keeping things in perspective; and my Voice of Reason (you know who you are). You have all been amazing during this experience. Thank you so much.

## ACKNOWLEDGMENTS

I would like to thank Dr. Jay Siegel for being my advisor through my graduate career. Your experience and support have been invaluable to me. I would also like to thank Dr. John Goodpaster for being a great teacher and wealth of knowledge over the course of my studies. I am also grateful to Jeanna Feldmann for her work on the MSP samples, and Cheryl Szkudlarek for her help with XLSTAT. A sincere thanks goes to Gina Ammerman, Cary Pritchard, and Karl Dria for all their help with maintaining and troubleshooting the instruments. I also appreciate the support of Simon Clement from Foster and Freeman and Saya Yamaguchi from CRAIC Technologies for their help with the Raman and MSP, respectively. Also, thank you Elisa Liszewski Pozywio, for laying the groundwork on the MSP portion of this study. In addition, my deepest thanks go to everyone who has positively impacted my research.

## TABLE OF CONTENTS

	Page
LIST OF TABLES.....	vi
LIST OF FIGURES.....	vii
LIST OF ABBREVIATIONS .....	ix
ABSTRACT.....	x
CHAPTER 1. INTRODUCTION.....	1
1.1 Automotive Clear Coats and their Analysis.....	1
1.2 Chemometric Techniques for Data Analysis .....	4
1.2.1 Preprocessing Techniques.....	6
1.2.2 Agglomerative Hierarchical Clustering (AHC).....	9
1.2.3 Principal Component Analysis (PCA) .....	11
1.2.4 Discriminant Analysis (DA) .....	13
1.2.5 Analysis of Variance (ANOVA) .....	16
CHAPTER 2. RAMAN SPECTROSCOPY.....	18
2.1 Review of Raman Spectroscopy .....	18
2.2 Materials and Methods .....	19
2.2.1 Instrumental Analysis.....	19
2.2.2 Time Study.....	23
2.2.3 Data Analysis .....	23
2.3 Results and Discussion.....	25
2.3.1 Statistical Results.....	25
2.3.2 External Validation .....	36
2.3.3 Formation of Classes .....	38
2.3.4 Known UV Absorbers.....	41
2.3.5 Limitations of the Study .....	43
2.3.6 Time Study.....	43
2.3.6.1 Aims of the Study.....	45
2.3.6.2 Summary of Results .....	45
2.3.6.3 Limitations of the Study.....	45
2.4 Conclusions.....	46
CHAPTER 3. MICROSPECTROPHOTOMETRY .....	47
3.1 Review of Microspectrophotometry.....	47
3.2 Materials and Methods .....	48
3.2.1 Instrumental Analysis.....	48

	Page
3.2.2 Data Analysis .....	49
3.3 Results and Discussion.....	50
3.3.1 Statistical Results.....	50
3.3.2 External Validation .....	60
3.3.3 Formation of Classes .....	62
3.3.4 Known UV Absorbers.....	65
3.3.5 Limitations of the Study .....	66
3.4 Conclusions.....	67
CHAPTER 4. CONCLUSIONS OF THE STUDY.....	68
CHAPTER 5. FUTURE DIRECTIONS.....	70
LIST OF REFERENCES .....	73
APPENDICES	
Appendix A. Clear Coat Spectra by Raman Spectroscopy.....	77
A.1 Training Samples .....	77
A.2 External Validation Samples.....	118
A.2.1 External Validation Spectra .....	118
A.2.2 Comparison of External Validation and Training Set (averaged spectra) .	124
Appendix B. Clear Coat Spectra by Raman Spectroscopy: Time Study.....	130
B.1 Samples Stored in a Dark Cabinet .....	130
B.2 Samples Stored in a Lit Laboratory.....	134
Appendix C. Clear Coat Spectra by Microspectrophotometry.....	139
C.1 Training Samples .....	139
C.2 External Validation Samples.....	179
C.2.1 External Validation Spectra .....	179
C.2.2 Comparison of External Validation and Training Set (averaged spectra)..	184

## LIST OF TABLES

Table	Page
Table 2.1 Potential Raman bands for known UV absorbers.....	24
Table 2.2 Eigenvalues and variability associated with each principal component (PC)...	28
Table 2.3 Confusion matrix for cross-validation results from DA with three classes.....	34
Table 2.4 Confusion matrix for the external validation results of the supplemental data from DA .....	36
Table 2.5 Possible Raman peak assignments for known UV absorbers .....	42
Table 3.1 Eigenvalues and variability associated with each principal component (PC)...	52
Table 3.2 Confusion matrix for cross-validation results from DA with three classes.....	58
Table 3.3 Confusion matrix for the external validation results of the supplemental data from DA .....	60
Table 4.1 Members of Raman and MSP AHC groups.....	69



## LIST OF FIGURES

Figure	Page
Figure 1.1 Examples of UV absorber types used in clear coats .....	3
Figure 1.2 Comparison of raw and smoothed Raman data .....	7
Figure 1.3 Parts of a dendrogram .....	10
Figure 1.4 Example of a PCA observations plot .....	13
Figure 1.5 Example of a DA observations plot .....	15
Figure 2.1 Formation of Stokes and anti-Stokes lines .....	18
Figure 2.2 Parameter test runs using clear coat PC001 .....	21
Figure 2.3 FORAM background correction procedure .....	22
Figure 2.4 Structures of known UV absorbers .....	22
Figure 2.5 Dendrogram from AHC of averaged clear coat spectra .....	26
Figure 2.6 Centroids of the three classes from the dendrogram .....	26
Figure 2.7 The observations plot from PCA with three classes shown .....	27
Figure 2.8 Scree plot of principal component factor scores F1-F32 .....	29
Figure 2.9 Factor loadings for PC1 plotted versus wavenumber .....	30
Figure 2.10 Factor loadings for PC2 plotted versus wavenumber .....	30
Figure 2.11 Factor loadings for PC3 plotted versus wavenumber .....	31
Figure 2.12 Factor loadings for PC4 plotted versus wavenumber .....	31
Figure 2.13 Factor loadings for PC5 plotted versus wavenumber .....	32
Figure 2.14 Sum of squares of the factor loadings of the first five principal components plotted versus wavenumber .....	32
Figure 2.15 Class central objects with PC1 and PC2 regions highlighted .....	33
Figure 2.16 Observations plot from DA with three classes .....	34
Figure 2.17 F values from ANOVA plotted versus wavenumber .....	35
Figure 2.18 Class central objects with ANOVA regions highlighted .....	35
Figure 2.19 External validation sample EV010 compared to original sample PC066 .....	37
Figure 2.20 External validation sample EV019 compared to original sample PC019 .....	37
Figure 2.21 Samples of the same make and model but different year placed in different classes .....	38
Figure 2.22 Samples of the same make and model but different year placed in the same class .....	39
Figure 2.23 Samples of the same make, model, and year placed in the same class .....	40
Figure 2.24 Samples of the same make, model, and year placed in different classes .....	40
Figure 2.25 Raman spectra of known UV absorbers .....	41

Figure	Page
Figure 2.26 Raman spectra of known UV absorbers compared to class central objects .	42
Figure 2.27 Replicate 1 of PC001 over eight weeks while stored in a dark cabinet.....	44
Figure 2.28 Replicate 1 of PC001 over eight weeks while stored in the lit laboratory ....	44
Figure 3.1 Dendrogram from AHC of averaged clear coat spectra .....	50
Figure 3.2 Centroids of the three classes from the dendrogram .....	51
Figure 3.3 The observations plot from PCA with three classes shown .....	52
Figure 3.4 Scree plot of principal component factor scores F1-F20.....	53
Figure 3.5 Factor loadings for PC1 plotted versus wavelength .....	54
Figure 3.6 Factor loadings for PC2 plotted versus wavelength .....	54
Figure 3.7 Factor loadings for PC3 plotted versus wavelength .....	55
Figure 3.8 Factor loadings for PC4 plotted versus wavelength .....	55
Figure 3.9 Factor loadings for PC5 plotted versus wavelength .....	56
Figure 3.10 Sum of squares of the factor loadings of the first five principal components plotted versus wavelength .....	56
Figure 3.11 Class central objects with PC1 and PC2 regions highlighted .....	57
Figure 3.12 Observations plot from DA with three classes .....	58
Figure 3.13 F values from ANOVA plotted versus wavenumber .....	59
Figure 3.14 Class central objects with ANOVA regions highlighted .....	59
Figure 3.15 External validation sample EV008 compared to original sample PC036.....	61
Figure 3.16 External validation sample EV014 compared to original sample PC150.....	61
Figure 3.17 Samples of the same make and model but different year placed in different classes .....	62
Figure 3.18 Samples of the same make and model but different year placed in the same class.....	63
Figure 3.19 Samples of the same make, model, and year placed in the same class.....	64
Figure 3.20 Samples of the same make, model, and year placed in different classes.....	64
Figure 3.21 MSP spectra of known UV absorbers .....	65
Figure 3.22 MSP spectra of known UV absorbers compared to class central objects .....	66

## LIST OF ABBREVIATIONS

2,4-DHBP	2,4-dihydroxybenzophenone
4-DD-2-HBP	4-dodecyloxy-2-hydroxybenzophenone
AHC	agglomerative hierarchical clustering
ANOVA	analysis of variance
ASTM	American Society for Testing and Materials
cm <sup>-1</sup>	wavenumber/reciprocal centimeter
CV	canonical variate
DA	discriminant analysis
DMF	dimethylformamide
FTIR	Fourier transform infrared spectroscopy
GC	gas chromatography
HALS	hindered amine light stabilizer
IR	infrared
LDA	linear discriminant analysis
MS	mass spectrometry
MSP	microspectrophotometry/microspectrophotometer
mW	milliwatt
NIST	National Institute of Standards and Technology
nm	nanometer
PC	principal component
PC###	paint chip ###
PCA	principal component analysis
Py	pyrolysis
SEM	scanning electron microscopy
SERS	surface-enhanced Raman spectroscopy
SWGMA	Scientific Working Group for Materials Analysis
UV	ultraviolet
VOC	volatile organic compound
x	magnification

## ABSTRACT

Mendlein, Alexandra Nicole. M.S., Purdue University, August, 2011. Instrumental and Chemometric Analysis of Automotive Clear Coat Paints by Micro Laser Raman and UV Microspectrophotometry. Major Professor: Jay Siegel.

Automotive paints have used an ultraviolet (UV) absorbing clear coat system for nearly thirty years. These clear coats have become of forensic interest when comparing paint transfers and paint samples from suspect vehicles. Clear coat samples and their ultraviolet absorbers are not typically examined or characterized using Raman spectroscopy or microspectrophotometry (MSP), however some past research has been done using MSP. Chemometric methods are also not typically used for this characterization. In this study, Raman and MSP spectra were collected from the clear coats of 245 American and Australian automobiles. Chemometric analysis was subsequently performed on the measurements. Sample preparation was simple and involved peeling the clear coat layer and placing the peel on a foil-covered microscope slide for Raman or a quartz slide with no cover slip for MSP. Agglomerative hierarchical clustering suggested three classes of spectra, and principal component analysis confirmed this. Factor loadings for the Raman data illustrated that much of the variance between spectra came from specific regions ( $400 - 465 \text{ cm}^{-1}$ ,  $600 - 660 \text{ cm}^{-1}$ ,  $820 - 885 \text{ cm}^{-1}$ ,  $950 - 1050 \text{ cm}^{-1}$ ,  $1740 - 1780 \text{ cm}^{-1}$ , and  $1865 - 1900 \text{ cm}^{-1}$ ). For MSP, the regions of highest variance were between  $230 - 270 \text{ nm}$  and  $290 - 370 \text{ nm}$ . Discriminant analysis showed that the three classes were well-differentiated with a cross-validation accuracy of 92.92% for Raman and 91.98% for MSP. Analysis of variance attributed differentiability of the classes to the regions between  $400 - 430 \text{ cm}^{-1}$ ,  $615 - 640 \text{ cm}^{-1}$ ,

825 – 880  $\text{cm}^{-1}$ , 1760 – 1780  $\text{cm}^{-1}$ , and 1860 – 1900  $\text{cm}^{-1}$  for Raman spectroscopy. For MSP, these regions were between 240 – 285 nm and 300 – 370 nm. External validation results were poor due to excessively noisy spectra, with a prediction accuracy of 51.72% for Raman and 50.00% for MSP. No correlation was found between the make, model, and year of the vehicles using either method of analysis.

## CHAPTER 1. INTRODUCTION

The aim of this study was to discriminate automotive clear coats using Raman spectroscopy, microspectrophotometry, and subsequent chemometric analysis. This research was intended to determine how many classes of clear coat spectra were present and reliably discernable for both instrumental methods. Also important to investigate was which features of the clear coat spectra were most unique to each class, and which regions of the spectra were most variable and/or differentiable between classes. The work also sought to examine to what extent additional samples could be correctly classified into the existing classes, and whether any correlations between make, model, and year of the automobile were present.

### 1.1 Automotive Clear Coats and Their Analysis

Paints can be valuable forensic evidence. Traces of automotive paints can be found at the scenes of automobile collisions where one vehicle hits another vehicle, an object, or a person. Paint may be transferred from one car to another, a car to an object, or occasionally from a car to the clothing or body of a person. Since paint cannot generally be attributed to a particular source, most forensic analysis of paints centers on physical and chemical testing in order to compare a known sample of paint from a suspect vehicle to transferred paint. Because of the way in which paints from a vehicle may be deposited onto an individual or object, the complete layer structure of automotive paint may not be present in the transfer. Thus differentiating between clear coats has become a focus of several works.<sup>1,2,3,4</sup>

Automotive paints are typically applied to a vehicle by a series of discrete steps. A primer is first electrolyzed onto the body surface of the vehicle. Then finish layers are applied over this primer. These layers consist of one or more colored base coats and finally a clear coat. The clear coat contains no color or pigment, protects the base coat from degradation and weathering, and imparts the final shiny appearance to the vehicle. Clear coats originated in the late 1970s, when the topcoat paint system was split into a pigmented base coat and a clear coat. The clear coat system gained popularity in the 1980s, and is still in use today. In the 1990s, new binders and paints with lower concentrations of volatile organic compounds (VOCs) were developed to comply with new environmental standards. Currently, clear coats use either a liquid application method (i.e., acrylic melamine and acrylic carboxy epoxy) or a powder coating method (i.e., acrylic carboxy epoxy and acrylic urethane).<sup>1</sup> Clear coat manufacturers have been generally reduced to a “big three” consisting of DuPont, BASF, and PPG, although companies such as Nippon, Bayer, and Sherwin-Williams also produce clear coats. These manufacturers supply original automotive paints and clear coats worldwide.<sup>2</sup>

The vast majority of clear coats contain light stabilizers, such as hindered amine light stabilizers (HALS), and ultraviolet (UV) absorbers to protect the paint against weathering, degradation, and UV light. These UV absorbers must absorb within the region of 290 – 350 nm, since this encompasses the wavelengths of light that cause the photodegradation of polymers. Benzotriazoles and triazines are the most commonly used UV absorbers found in automotive clear coats, but benzophenones and oxalanilides may also be used. Examples of some of the UV absorbers used in clear coats are shown in Figure 1.1.<sup>3</sup> Clear coat binders typically consist of acrylics and polyurethanes based on cross-linking hydroxyl-functional polymers.<sup>1,3</sup>

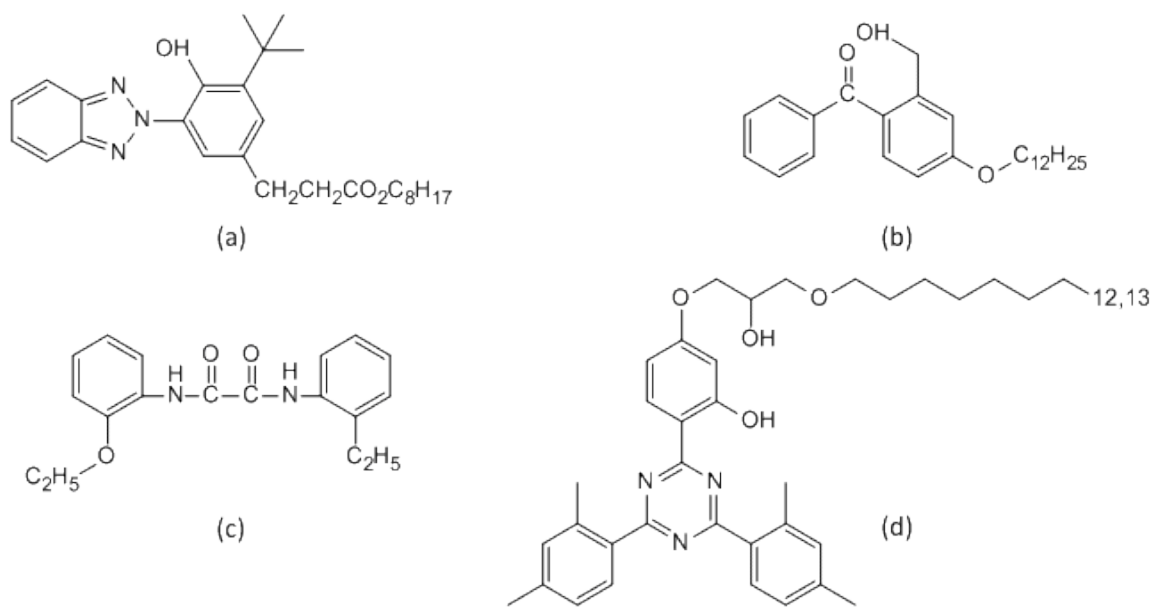


Figure 1.1 Examples of UV absorber types used in clear coats: (a) hydroxyphenylbenzotriazole; (b) benzophenone; (c) oxanilide; and (d) hydroxyphenyl-S-triazine classes.<sup>3</sup>

The procedures used in typical casework follow guidelines developed by the Scientific Working Group for Materials Analysis (SWGMA) and ASTM Standard E1610 (Standard Guide for Forensic Paint Analysis and Comparison).<sup>5</sup> The forensic analysis of automotive paints generally starts with a microscopic examination of the paint samples to note the number and thicknesses of layers, differences in color, and the shape and distribution of any particles present in the sample. Following microscopic examination, a chemical or spectroscopic analysis is then performed. This can include microspectrophotometry (MSP), scanning electron microscopy (SEM), infrared (IR) spectrophotometry, and pyrolysis gas chromatography - mass spectrometry (Py-GC-MS), among others.<sup>6</sup> Infrared spectrophotometry and Py-GC-MS are considered to be especially valuable, even though the latter is a destructive technique. Several authors have examined the differentiability of automotive paints using these techniques.<sup>2,4,7</sup>

SWGMA suggests Raman spectroscopy as a possible analytical technique during forensic paint examinations, especially to gather information about inorganic



compounds present in the paints and binders.<sup>5</sup> IR use is far more common than Raman spectroscopy, but has its drawbacks. For example, many inorganic and organic pigments are weak IR absorbers. These pigments may then be obscured by other compounds found in the paints. Raman spectroscopy can overcome this limitation by examining a lower range of wavenumbers than typical IR instruments. For example, most IR instruments have a range between 600 and 4000  $\text{cm}^{-1}$ , while many Raman spectra can extend below 600  $\text{cm}^{-1}$ . Many extenders and inorganic pigments found in paints have peaks in this region. The data provided by Raman is also complementary to that of IR due to the differing selection rules for each technique.<sup>6</sup> Some bands in automotive paints that overlap in IR spectrophotometry do not overlap using Raman. Kuptsov also found Raman bands to be sharper and easier to assign than IR bands.<sup>8</sup> Past research on paint analysis using Raman has focused more on whether spectra of various paint layers were obtainable, not whether they were differentiable.<sup>6,8</sup> Some darker pigments may not produce usable spectra due to fluorescence or thermal issues.<sup>8</sup> Raman spectra of clear coats will be discussed in Chapter 2.

Because of MSP's ability to differentiate between even small variances in color, MSP has been widely used in automotive paint analysis.<sup>5,9</sup> Visual color analysis can prove difficult in forensic settings, as the samples are typically very small. MSP can provide objective color information about these samples that human observers cannot.<sup>5,10,11</sup> While typically used for color information about paint samples, research has been done on using MSP to examine the UV-absorbers in clear coats.<sup>1,3</sup> Preliminary studies have shown that clear coats can be classified by MSP.<sup>1</sup> This work expands the data set past that of previous studies. The MSP spectra of clear coats will be discussed in Chapter 3.

## 1.2 Chemometric Techniques for Data Analysis

The use of multivariate statistical analysis is a growing practice in forensic chemistry. Forensic scientists often have to identify patterns and interpret differences

in data. Chemometrics make this task more accurate, objective, and manageable. It is especially useful when the scientist is presented with large quantities of spectral data as is the case in this research. Comparing more than 200 spectra by inspection was never a valid scientific technique, but was widely used (and sometimes still is) until the adoption of multivariate statistical techniques became more accessible to forensic chemists. Multivariate statistics have been used on many types of forensic trace evidence, including accelerants, inks, fibers, ammunition, gun powder, glass, and paint.<sup>12</sup>

Statistics used for univariate measurements are easily calculated by hand, using a calculator, or with a spreadsheet. However, these statistics are not robust enough for comparing data from spectroscopy, chromatography, or mass spectrometry, where one sample has many data points at different variables.<sup>12</sup> Rather, multivariate chemical data is often thought of as matrices. Each row corresponds to a number of measurements of a single sample or single experiment. Each column represents the measurements on a single variable, such as that of a spectroscopic peak.<sup>12,13</sup> Using multivariate statistical methods, the statistical significance of the differences in these patterns can be established.<sup>12</sup>

Typically, forensic scientists rely upon visual comparisons of chromatograms and spectra when making determinations of whether known and unknown samples might have come from the same source. As a result, there is no statistical basis for determining the evidentiary value of these comparisons. Given the recent challenges to the reliability of these trace evidence comparisons, many laboratories are seeking to find ways to compare samples in a more quantitative manner. Multivariate statistics could address the relevance and reliability issues raised in *Daubert v. Merrell Dow Pharmaceuticals*. Chemometrics could also help with the implementation of the recommendations from the National Academy of Sciences (NAS) report on strengthening forensic science. Specifically, Recommendations 3 and 5 can be addressed in part by the use of chemometrics. Recommendation 3 deals with issues of accuracy and reliability in the various forensic science disciplines, and Recommendation

5 seeks to address issues of human observer bias and sources of human error (e.g., visual versus chemometric analysis of data).<sup>14</sup>

Multivariate statistics have proven valuable for many years. The underlying principles of some of these statistical methods have been known for nearly a century. The idea of principal component analysis (PCA) as a dimension reduction and data display technique originated with Pearson in 1901. In 1933, Hotelling detailed algorithms for computing principal components (PCs). The multivariate distance bearing Mahalanobis' name was introduced by him in 1936, and linear discriminant analysis (LDA) was first developed by Fisher that same year.<sup>12</sup>

Chemometric methods are typically applied to reducing data, sorting and grouping, investigating the dependence among variables, prediction, or hypothesis testing.<sup>15</sup> Chemometrics can reduce the complexity of a large data set, and can make predictions about unknown samples.<sup>12</sup> Chemometrics can also be used to interpret the results of forensic analyses, especially those involving pattern recognition. When using multivariate statistical techniques, replicate sample measurements should be made to allow for experimental uncertainty and determine the significance of between-sample differences.<sup>12</sup> After preprocessing the data, four chemometric techniques were employed in this study: Agglomerative Hierarchical Clustering (AHC), Principal Component Analysis (PCA), Discriminant Analysis (DA), and Analysis of Variance (ANOVA).

### 1.2.1 Preprocessing Techniques

Preprocessing is defined as the preparation of information before the application of mathematical algorithms.<sup>16</sup> It is often required before performing multivariate statistical analyses. Preprocessing can remove noise and variation that might complicate data interpretation. However, some preprocessing can negatively impact the data, so techniques must be chosen and applied carefully.

The signal-to-noise ratio can be increased and unnecessary noise can be removed by data smoothing.<sup>12,17</sup> Unfortunately, smoothing can cause distortions in peak height and width, can impair resolution of peaks, and can result in the loss of some features.<sup>12</sup> Most smoothing methods involve creating a “window” of a specified number of data points and using the data values within the window to estimate a “noise-free” value for the point in the center of the window. Depending on the method used, the “noise-free” value may be the mean or median of the values in the window, or a predicted value from a polynomial fit to the data. Respectively, these methods are called mean smoothing, median smoothing, and running polynomial smoothing.<sup>12,17</sup> The most common method of smoothing is running polynomial smoothing, including the Savitzky-Golay algorithm. This method is well-documented and often used in instrument software.<sup>12</sup> A comparison of a raw Raman spectrum with its smoothed counterpart is shown in Figure 1.2.

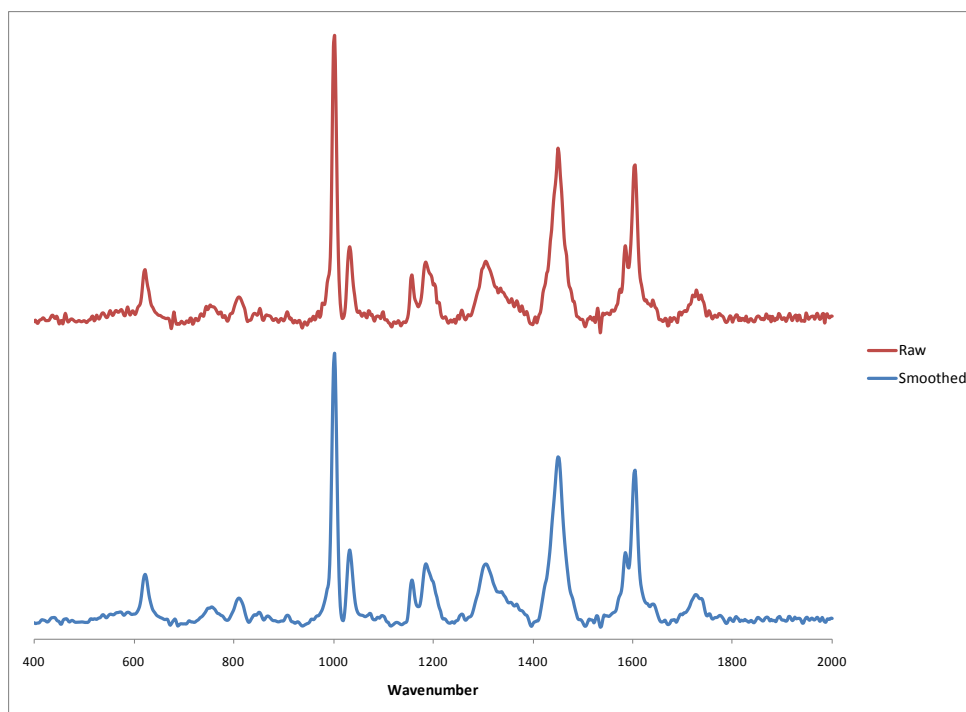


Figure 1.2 Comparison of raw and smoothed Raman data.

Background correction is employed to keep varying background levels from confusing interpretation. For instance, fluorescence interference may dominate the background of a Raman spectrum.<sup>12</sup> Background correction can be accomplished by subtracting a straight line or polynomial from the baseline in a spectrum. It can also be done by replacing sample vectors with their first derivative.<sup>12,17</sup> A Savitzky-Golay algorithm exists for background correction as well, replacing each data point with the derivative of the smoothing polynomial at that point.<sup>17</sup>

Normalization of spectra eliminates variations due to sample size, concentration, amount, and instrument response.<sup>12,17</sup> It is typically conducted after smoothing and background correction have been completed. Normalization divides the values of the variables by a constant value, scaling them to a constant total (e.g., 1 or 100).<sup>13,16</sup> The sample values may be divided by the sum of the absolute values of all intensities, normalizing the sample to unit area. The sample values may also be divided by the square root of the sum of squares of the intensities, normalizing to unit length.<sup>12,17</sup>

Mean centering shifts the origin of the coordinate system to the center of the data.<sup>18</sup> It eliminates constant background without changing differences in variables.<sup>12</sup> It involves subtracting the mean of each variable from the related elements of the sample vectors.<sup>12,18</sup> It essentially calculates the mean spectrum for the data set and subtracting that “centroid” from each spectrum.<sup>12,17,18</sup> Mean centering is often inappropriate for use in signal analysis, because the concern is variability above a baseline rather than around an average.<sup>16</sup> This centering loses information about the origin of the factor space, relative magnitudes of eigenvalues, and relative errors.<sup>18</sup>

Autoscaling is the use of variance scaling and mean centering.<sup>17</sup> It multiplies all of the spectra in the data set by a scaling factor for each wavelength. Autoscaling is done to either increase or decrease the influence on the calibration of each wavelength.<sup>18</sup> It is recommended when variables have different units of measurement or show large differences in variance.<sup>12</sup> However, it can negatively impact the precision or calibration.<sup>18</sup> Also, if absolute intensities are important (e.g., correspond to concentration of a sample component), autoscaling should not be used.<sup>13</sup>

### 1.2.2 Agglomerative Hierarchical Clustering (AHC)

The purpose of cluster analysis is to determine whether individual samples fall into groupings, and what those groupings might be.<sup>16</sup> No prior knowledge of groupings is known, therefore cluster analysis is considered an unsupervised technique. Cluster analysis involves determining the similarities or dissimilarities between objects (i.e., distances). The items that are deemed most similar will be clustered together.<sup>13,16</sup> The distance between objects can be measured using different mathematical approaches. The first is Euclidean distance, or ruler distance. Based on the Pythagorean theorem, it is calculated using Equation 1.1, where  $x$  and  $y$  are two points,  $(x - y)'$  is the transpose of the matrix  $(x - y)$ , and  $d_{xy}$  is the distance between them.<sup>12,15</sup> The smaller the value of  $d_{xy}$ , the more similar the two objects are.<sup>16</sup>

$$d_{xy} = \sqrt{(x - y)'(x - y)} \quad \text{Equation 1.1}$$

Another method is the Manhattan distance. If the Euclidean distance represents the length of the hypotenuse of a right triangle, Manhattan distance represents the distance along the two other sides of the triangle. It is generally greater than, very rarely equal to, Euclidean distance.<sup>16</sup> The Mahalanobis distance is one more method for measuring similarity and dissimilarity. This method accounts for the fact that some variables may be correlated, and uses the inverse of the variance-covariance matrix as a scaling factor. The formula for Mahalanobis distance is shown in Equation 1.2, where  $C$  is the variance-covariance matrix of the variables.<sup>16</sup>

$$d_{xy} = \sqrt{(x - y) \cdot C^{-1} \cdot (x - y)'} \quad \text{Equation 1.2}$$

Hierarchical clustering looks for the most similar or dissimilar pair of objects or clusters, then combines or divides them at each step, until all of the objects have been appropriately clustered.<sup>16</sup> The information is then displayed in a two-dimensional plot called a dendrogram, an example of which is shown in Figure 1.3.<sup>17</sup> There are two main types of hierarchical clustering: agglomerative hierarchical clustering (AHC) and divisive hierarchical clustering. AHC takes every object to be in its own individual cluster at first. The objects are then grouped into larger clusters, such that those in each group are

more closely related than those in different groups. The most similar objects are clustered first, then those clusters are further grouped according to similarity until as few clusters as possible exist.<sup>15,16</sup> Divisive clustering, on the other hand, starts with one group containing all of the objects, and divides them based on their dissimilarity.<sup>15</sup>

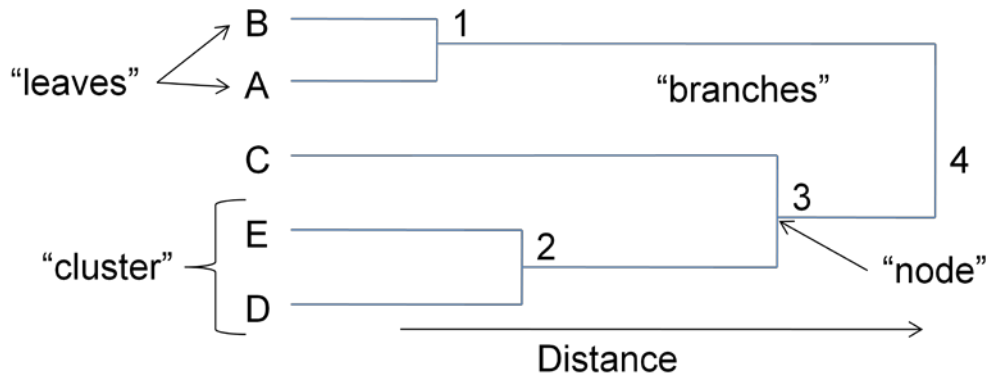


Figure 1.3 Parts of a dendrogram. (Figure courtesy of Dr. John Goodpaster.)

AHC can utilize several linkage methods. These methods include nearest neighbor, furthest neighbor, centroid, and Ward's method, among others. Nearest neighbor linkage, also called single linkage, joins clusters or objects based on the smallest distance between an object in the old cluster and the other objects or clusters. Furthest neighbor, or complete linkage, is the opposite of nearest neighbor and uses the greatest distance to link clusters or objects.<sup>13,16</sup> The centroid method links clusters based on the distance between the calculated centroids of clusters rather than nearest or furthest neighbors. This method is more sensitive to outliers, as they can negatively impact the calculation of the centroid of a group.<sup>17</sup> Ward's method, the method used in this work, seeks to minimize the "loss of information" due to joining two clusters. In this case, "loss of information" is an increase in an error sum of squares. The error sum of squares is calculated by measuring the sum of squared deviations of every data point from the mean of the cluster. Linking clusters involves examining every possible link and determining which linkage results in the smallest increase in the error sum of squares.<sup>15</sup>

In general, AHC is an excellent tool for initial data analysis. It allows users to examine large sets of data for both expected and unexpected clusters. However, AHC does not give any indication of which variables have the greatest influence on the clustering. And while the dendrogram is simple, standardized, and represents the entirety of the data set, it is the only view of the data available using this method. There is no way to interactively view and manipulate the dendrogram so that the user may exploit human pattern-recognition abilities.<sup>17</sup> Clustering analysis has been used on inks<sup>19</sup> and soils,<sup>20</sup> and AHC specifically has been employed with electrical tapes,<sup>21,22</sup> lighter fuels,<sup>23</sup> heroin,<sup>24</sup> and a smaller data set of clear coats.<sup>1</sup>

### 1.2.3 Principal Component Analysis (PCA)

Principal Component Analysis (PCA) is a dimensionality reduction technique that condenses the original variables to a number of significant principal components (PCs).<sup>13,16</sup> It is used to classify variables.<sup>25</sup>

The information gained by PCA can be visually represented in a couple of ways. The first, and most traditional form, is the scores plot, shown in Figure 1.4. This plots the score of one PC against the score of another for each sample. The second method of visualizing PCA is the loadings plot. Factor loadings are plotted against each variable (i.e., wavelength). The factor loadings represent the cosines of the angle between the principal component and each variable. Where the cosines are positive, the variables are positively correlated. Where the cosines are negative, the variables are negatively correlated. Areas where the cosine is nearly zero have no correlation.<sup>16</sup>

The possible number of PCs is the smaller of the number of variables or the number of samples.<sup>12</sup> To find the first PC, the axis that minimizes the orthogonal sum of squares of the data points must be found.<sup>12,13</sup> This principal component will account for the greatest amount of variance in the data set. The second principal component accounts for the next greatest amount of variance in a direction perpendicular to the first PC.<sup>12</sup> Each successive PC captures less of the remaining variability in the data set.



Significant PCs will have larger eigenvalues, or the sum of squares of each principal component or score.<sup>13,16</sup> The sum of the eigenvalues over all principal components is equal to the number of variables present in the data set (i.e., measured wavelengths).<sup>25</sup>

Principal components have eigenvalues associated with them that reflect the variance, percent variance, and cumulative variance for the principal component. A number of principal components must be selected to represent the data set and put through discriminant analysis (DA) if desired. If too many principal components are used, the “noise” from extra principal components may interfere with the formation and verification of classes.<sup>26</sup> To choose the correct number, one of three methods can be employed. The first method involves choosing a cumulative variance that must be met, such as 95%, and using the number of principal components that exceeds that percentage.<sup>16</sup> The second method, introduced by Cattell in 1966, uses a scree plot, which plots eigenvalues against factor number. Where a sudden break in the plot occurs, this location indicates the number of significant principal components. To the right of this location is “factorial scree,” or debris.<sup>25</sup> This is the method that was used in this work. The third method uses the Kaiser criterion, proposed by Kaiser in 1960, to determine the number of principal components. All eigenvalues that are greater than one would be considered significant.<sup>25</sup> The scree plot method was chosen for use in this work because it is more stringent and resulted in a fewer number of factors than the other two methods. This introduces less noise into subsequent discriminant analysis.

PCA is possibly the most widely-used multivariate chemometric technique. It has been used for high explosives mixtures,<sup>27</sup> headlight lens materials,<sup>28</sup> hair dyes,<sup>29</sup> drugs,<sup>24</sup> soils,<sup>20</sup> inks,<sup>19</sup> electrical tapes,<sup>21,22</sup> and accelerants.<sup>23</sup>

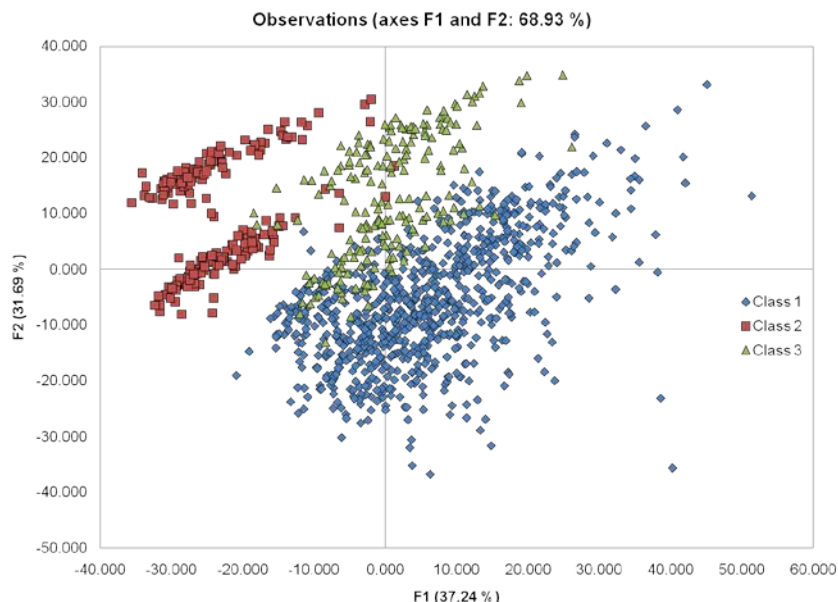


Figure 1.4 Example of a PCA observations plot. (Figure courtesy of Cheryl Szkudlarek.)

#### 1.2.4 Discriminant Analysis (DA)

Linear discriminant analysis (DA) is another dimensionality reduction technique. DA defines the distance of a sample from the center of a class, and creates a new set of axes to place members of the same group as close together as possible, and move the groups as far apart from one another as possible.<sup>12,16</sup> These new axes are discriminant axes, or canonical variates (CVs), that are linear combinations of the original variables.<sup>12</sup> An example observations plot is shown in Figure 1.5. DA is a form of supervised pattern recognition, as it requires knowledge of group memberships for each sample.<sup>12,16</sup>

DA requires that the number of samples (i.e., spectra) exceed the number of variables (i.e., wavelengths).<sup>12</sup> This is due to the equations used in the calculations. The first, shown in Equation 1.3, obtains a measurement comparable to a score. It is often called the linear discriminant function.<sup>16</sup>

$$f_i = (\bar{x}_A - \bar{x}_B) \cdot C_{AB}^{-1} \cdot x_{i_i} \quad \text{Equation 1.3}$$

In this equation,  $x_A$  and  $x_B$  represent the centroids of two groups, and  $x_i$  is a row vector corresponding to sample  $i$ .  $C_{AB}$  is the pooled variance-covariance matrix. The formula

for calculating  $C_{AB}$  is shown in Equation 1.4 for two groups, but can be extended to any number of groups.<sup>16</sup>  $N_A$  represents the number of objects in group A, and  $N_B$  represents the number of objects in group B.  $C_A$  is the variance-covariance matrix for group A, and  $C_B$  is the variance-covariance matrix for group B.<sup>16</sup>

$$C_{AB} = \frac{(N_A-1)C_A + (N_B-1)C_B}{(N_A+N_B-2)} \quad \text{Equation 1.4}$$

If the number of samples does not exceed the number of variables, the pooled variance-covariance matrix cannot be inverted. This is why PCA often precedes DA.<sup>12</sup> Finally, the Mahalanobis distance from the sample to the centroid of any given group is calculated.<sup>16</sup> The procedure for DA is somewhat analogous to that of PCA. However, instead of maximizing the sum of squares of the residuals as PCA does, DA maximizes the ratio of the variance between groups divided by the variance within groups, called the Fisher ratio.<sup>12,13</sup>

Once this procedure has been followed and the new samples have been classified, cross-validation is performed to test the classification accuracy. There are a number of methods available for cross-validation. Resubstitution uses the entire data set as a training set, developing a classification method based on the known class memberships of the samples. The class membership of every sample is then predicted by the model, and the cross-validation determines how often the rule correctly classified the samples. Resubstitution has a major drawback, however. Since it uses the same data set to both build the model and to evaluate it, the accuracy of the classification is typically overestimated. When the classification model is applied to a new data set, the error rate would likely be much higher than predicted.<sup>12</sup>

Another method of cross-validation is the hold-out method. This method separates the data set into two parts: one to be used as a training set for model development, and a second to be used to test the predictions of the model. Separating the data used to train the model from the data used to evaluate it creates an unbiased cross-validation. However, in situations where data is limited, this may not be the best approach, as all of the data is not used to create the classification model. Also,

acquiring enough data to have appropriately-sized training and test sets may be time-consuming or difficult due to resources.<sup>12</sup>

One final method for cross-validation is the leave-one-out method. In this method, a sample is removed from the data set temporarily. The classification model is then built from the remaining samples, and then used to predict the classification of the deleted sample. This process continues through all of the samples, treating each sample as an unknown to be classified using the remaining samples. More than one sample can also be left out at a time. For example, 20% of the samples may be temporarily removed while the model is built using the remaining 80%. The leave-one-out method uses all of the available data for evaluating the classification model. It is time consuming, but usually preferable.<sup>12</sup> DA has been applied to mixtures of high explosives,<sup>27</sup> materials used in the manufacture of headlamp lenses,<sup>28</sup> electrical tapes,<sup>21,22</sup> inks,<sup>19</sup> soils,<sup>20</sup> and hair dyes.<sup>29</sup>

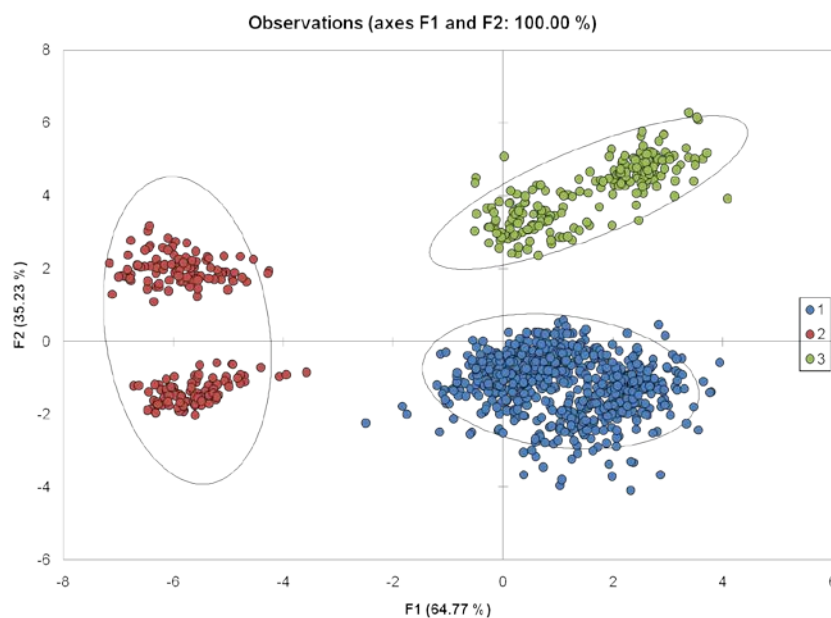


Figure 1.5 Example of a DA observations plot. (Figure courtesy of Cheryl Szkudlarek.)

### 1.2.5 Analysis of Variance (ANOVA)

Analysis of variance (ANOVA) tests the statistical significance of differences in means by examining between-groups and within-groups variability.<sup>12,30</sup> It determines whether the difference between sample means exceeds what can be explained by random error.<sup>26</sup> ANOVA can be used to segregate and estimate the causes of variation, and provides a method for determining whether the independent variable(s) has a significant impact on the dependent variable(s).<sup>26,31</sup>

ANOVA is similar to the statistical  $t$  test, but does not result in the loss of assurance that applying the  $t$  test to these types of data would. For example, if five samples that had been analyzed repeatedly were compared, the  $t$  test would need to be completed at least ten times. If the 0.05% confidence level was chosen, the probability of making the correct choice for the first pair is 95%. This diminishes to 95% of 95% for making the correct decision for both the first and second pairs, and so on.<sup>31</sup> ANOVA also allows the user to test each factor while controlling the others, requiring fewer samples to find significant effects.<sup>30</sup>

ANOVA relies on the fact that variances can be partitioned.<sup>30</sup> Variance is calculated as the sum of squared deviations from the mean, divided by the sample size minus one.<sup>30</sup> The formula for computing variance is found in Equation 1.5.<sup>26</sup>

$$\text{variance} = \sum(x_i - \bar{x})^2 / (n - 1) \quad \text{Equation 1.5}$$

ANOVA begins with a null hypothesis: the within-sample variance and between-sample variance should be the same. For univariate ANOVA, the within-sample variance is calculated using Equation 1.6.<sup>26</sup>

$$\text{within - sample } \sigma_0^2 = \sum_i \sum_j (x_{ij} - \bar{x}_i)^2 / h(n - 1) \quad \text{Equation 1.6}$$

The summation of  $j$  and subsequent division by  $(n - 1)$  calculates the variance of each sample, as in Equation 1.5. The summation over  $i$  divided by  $h$  averages the sample variances. This is called a mean square, as it involves a sum of squares divided by the degrees of freedom. The between-sample variance is calculated using Equation 1.7.<sup>26</sup>

$$\text{between - sample } \sigma_0^2 = n \sum_i (\bar{x}_i - \bar{x})^2 / (h - 1) \quad \text{Equation 1.7}$$

If the initial null hypothesis is incorrect, meaning the two variance estimates differ significantly, the between-sample estimate will exceed the within-sample estimate due to between-sample variation.<sup>26,31</sup> To determine whether the between-sample estimate is significantly greater than the within-sample estimate, a one-tailed F-test would be employed. If the calculated F value is greater than the critical value, the null hypothesis is subsequently rejected, meaning the difference between the sample means is significant.<sup>26,31</sup>

For multivariate ANOVA (MANOVA), instead of the univariate F value, a multivariate F value (Wilks' lambda) is obtained. This value is based on the comparison of the error variance-covariance matrix and the effect variance-covariance matrix. If the overall multivariate test is significant, the univariate F tests for each variable are then examined to determine which variables contributed to the overall result.<sup>30</sup> The use of ANOVA is a newer trend in forensic science. It has been applied to headlight lens materials,<sup>28</sup> illicit drugs,<sup>32,33</sup> document papers,<sup>34</sup> and animal hair.<sup>35</sup>

## CHAPTER 2. RAMAN SPECTROSCOPY

### 2.1 Review of Raman Spectroscopy

Raman spectroscopy is a vibrational spectroscopic technique, as is infrared spectrophotometry. However, while IR deals with absorption of radiation, Raman measures scattering. The scattering phenomena that form the basis for Raman spectroscopy were discovered in 1929 by C.V. Raman and K.S. Krishnan. They found that when a molecule is bombarded with monochromatic light, such as a laser, it exhibits one of three behaviors. The first, Rayleigh scattering, occurs when a molecule begins in its ground state and then returns to it after excitation. This is the most common scattering behavior. The second, called a “Stokes” line, appears when a molecule starts at its ground state but returns to the first excited energy level after excitation. The third, and least frequent, is the “anti-Stokes” line. This occurs when a molecule starts in an excited state, is further excited by the radiation, and returns to its ground state after excitation.<sup>36</sup>

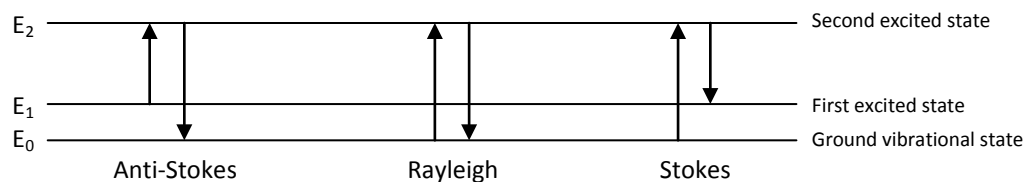


Figure 2.1 Formation of Stokes and anti-Stokes lines.<sup>37</sup>

When using Raman, a laser excitation source is employed. If the polarizability of a functional group in the sample changes, a peak will appear on the Raman spectrum. This is different from IR, which records a peak when a change in dipole moment occurs. Most normal modes are either Raman or IR active, although some can be both.<sup>36</sup>

Raman spectroscopy has the advantage of being non-destructive and requires only a small sample for analysis. When examining items such as ancient works of art or one-of-a-kind pieces of evidence, preservation is key. This makes Raman a good technique for forensic science applications. Sample preparation is generally minimal, and the spectra are also highly reproducible.

Unfortunately, Raman spectroscopy is limited by its inherently low sensitivity and by fluorescence interference. The laser can also be destructive to certain types of samples at full power. Fluorescence interference can sometimes be mitigated by changing the wavelength of the exciting laser.

## 2.2 Materials and Methods

### 2.2.1 Instrumental Analysis

Automobile paint chips were originally collected from junkyards and body shops. Some foreign samples were also collected from repair shops in Australia. A total of 268 samples were collected, and clear coat peels were made of 245 of them. The other samples were not used because the clear coat layer had degraded and/or was no longer present.

To obtain samples of each automobile's clear coat, a microscalpel and an Olympus SZ51 stereomicroscope at 40x magnification were used. Because some of the paint samples contained only one small paint chip, it was decided that three replicates would be created per sample. For most samples, each replicate was taken from a different paint chip. When fewer than three chips were available, the replicates were taken from as far apart on the available chip as possible. The replicates for each sample



were placed on a labeled aluminum foil-covered glass microscope slide using the microscalpel and a Tungsten needle. The Tungsten needle was then used to draw a circle around each replicate and label it. The foil slides were then stored in labeled petri dishes in a cabinet in the laboratory. The latter two thirds of the clear coat peels were made by Jeanna Feldmann, an undergraduate summer intern from Missouri Southern State University.

A Foster and Freeman FORAM Raman Spectral Comparator (Foster and Freeman, Worcestershire UK) with a 30 mW, 785 nm laser was used in the analysis of the clear coat samples. The FORAM can be run at 100%, 25%, and 10% laser power, and has an approximately  $8\text{ cm}^{-1}$  resolution. The instrument was calibrated before each use with polystyrene beads provided by the manufacturer. To perform a sample run, the foil slide containing the sample's replicates was positioned under the 5x objective of the Raman, and a sample was located and placed in focus. The stage was then lowered and the objective was changed to 20x. The sample was then re-focused and the area to be scanned was selected. Some samples had to be unfocused and placed farther away from the lens in order to be scanned successfully. These samples were too thick and oversaturated the Raman when in focus.

Replicates were scanned at 10% power, with 10 scans of 100 seconds each, in almost all cases. Using the laser at full power melted clear coat samples, and as such was deemed unusable. After some experimentation, it was determined that 10% power with a long integration time resulted in the best spectra. Test runs using three different sets of parameters are shown in Figure 2.2. Only five samples were not scanned using these parameters, as they oversaturated the detector regardless of whether they were placed out of focus farther away from the lens. PC004 and PC007 were scanned at 10% power with 20 scans of 12 seconds each. PC014 and PC015 were run using ten 70- and 75-second scans, respectively. PC041 was scanned 10 times with an integration time of 20 seconds. Because the parameters for these five samples were different from those of the rest of the sample set, they were excluded from chemometric analysis. All of the scans were automatically baseline corrected and smoothed using the FORAM software.

For smoothing, the FORAM software uses a Savitzky-Golay filter with a five-point window. The FORAM software's baseline correction method is shown in Figure 2.3.

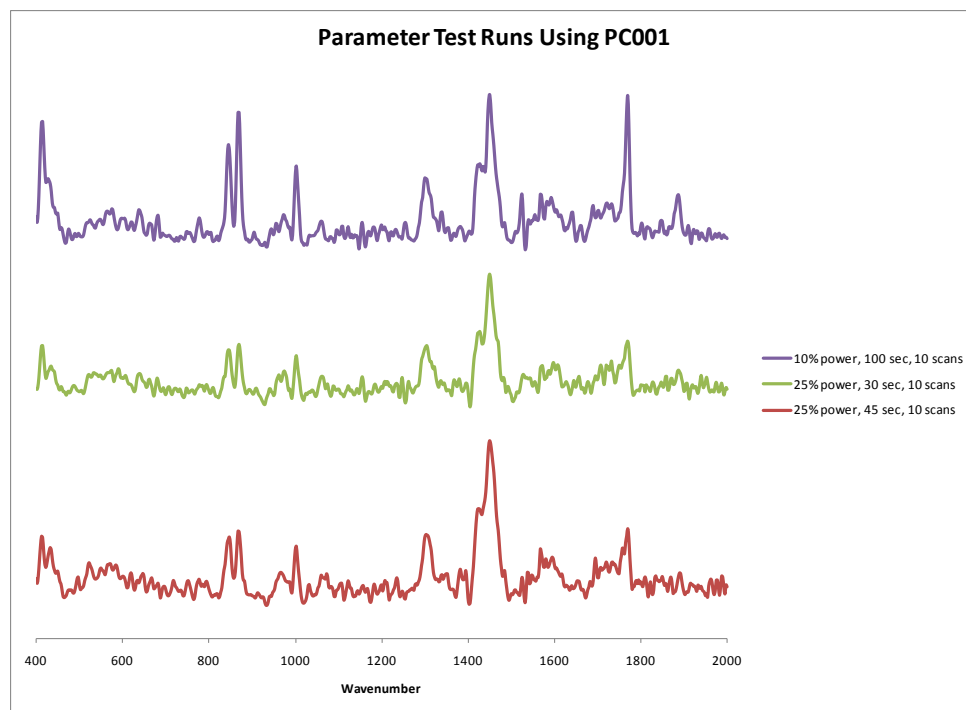


Figure 2.2 Parameter test runs using clear coat PC001.

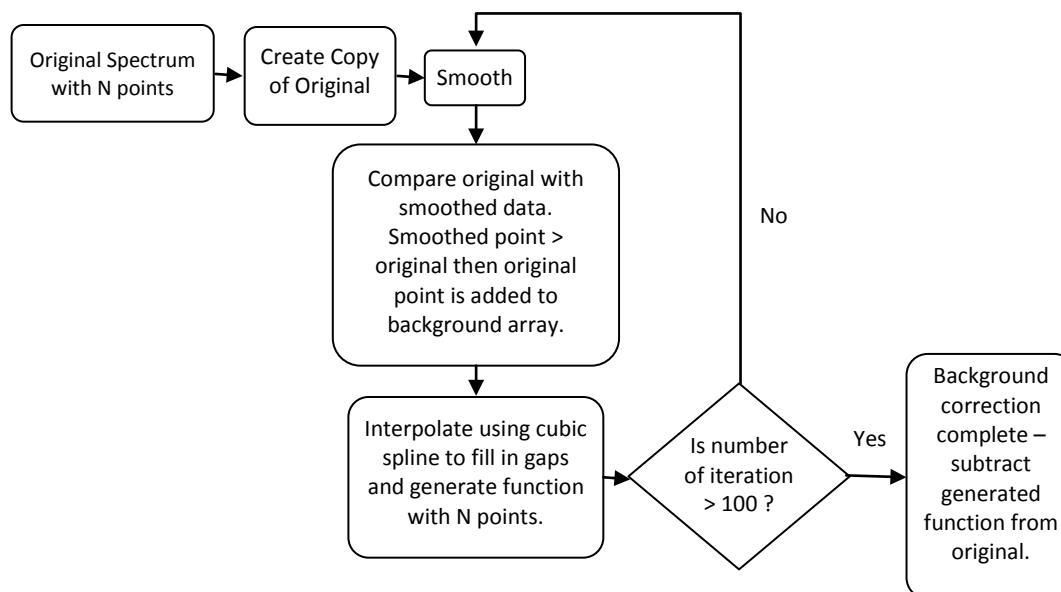


Figure 2.3 FORAM background correction procedure.  
(Figure courtesy of Simon Clement, Foster and Freeman.)

Three known UV absorbers were obtained and run using the same parameters as the clear coat samples. These UV absorbers were 2,4-dihydroxybenzophenone, 4-dodecyloxy-2-hydroxybenzophenone, and Tinuvin 292. The structures of each are shown in Figure 2.4.<sup>38,39</sup> In this work, the first two will be abbreviated as 2,4-DHBP and 4-DD-2-HBP. The three samples were prepared by dissolving a small amount of each absorber in acetone and then spotting the liquid onto a foil-covered microscope slide.

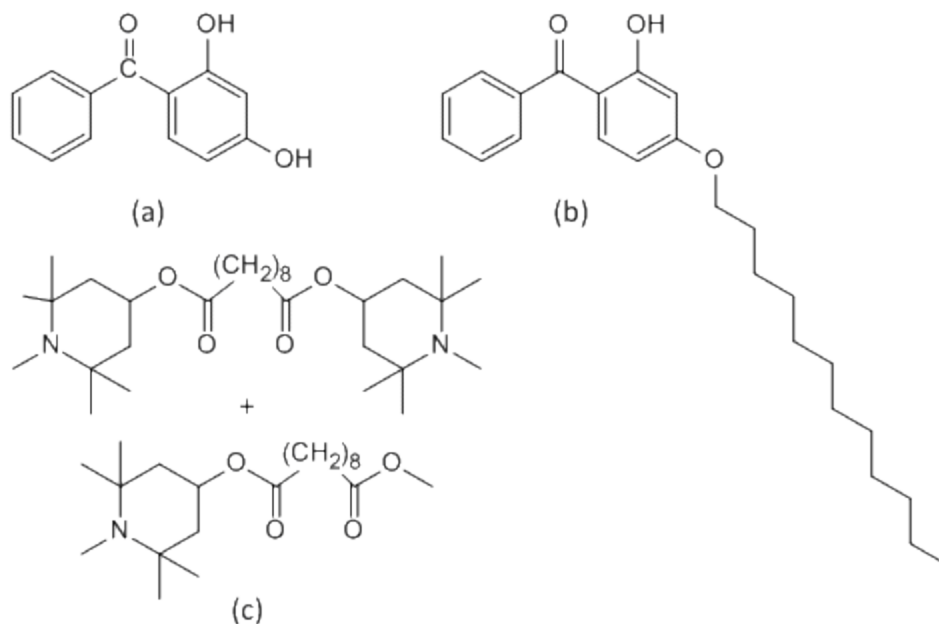


Figure 2.4 Structures of known UV absorbers: (a) 2,4-dihydroxybenzophenone; (b) 4-dodecyloxy-2-hydroxybenzophenone; (c) Tinuvin 292.<sup>38,39</sup>

### 2.2.2 Time Study

A secondary experiment was conducted to determine the effects of time and light exposure on clear coat samples. Three samples were chosen for this study: PC001 (2002 Pontiac Trans Am), PC008 (1998 Toyota Camry), and PC016 (2005 GMC Sonoma). These three samples were scanned initially, and then scanned every week until the end of the eight-week test period. In between scans, these samples were kept in a cabinet in the laboratory. A second set of three replicates was peeled for each sample following the procedures outlined in section 2.2.1. These replicates were stored on their foil-covered slides in a petri dish, then placed out in the laboratory to allow light to reach the samples. These samples were scanned initially, then once a week for eight weeks.

The FORAM Raman Spectral Comparator (Foster and Freeman, Worcestershire UK) with a 30 mW, 785 nm laser was used in the analysis of these clear coat samples. Calibration with polystyrene beads was performed before each use. The replicates were scanned at 10% power, with 10 scans of 100 seconds each. All of the scans were automatically baseline corrected and smoothed using the FORAM software.

### 2.2.3 Data Analysis

Prior to subjecting the data to chemometric analysis, the spectra for all replicates were normalized using Excel 2007 (Microsoft Corporation, Redmond WA). This was accomplished by dividing the intensity values at each wavelength by the square root of the sum of squares of all of that replicate's intensity values. The normalized spectra were then averaged to give one spectrum per sample. These averaged spectra were then used for AHC, PCA, DA, and ANOVA analysis using XLSTAT2010 software (Addinsoft, Paris France).

The clear coat samples were also qualitatively compared to Raman spectra of a few known UV absorbers to determine potential similarities. Based on the bonds present in the three UV absorbers chosen, the bands shown in Table 2.1 might be expected to be visible in the Raman spectra.<sup>40</sup>

Table 2.1 Potential Raman bands for known UV absorbers.<sup>40</sup>

Bond	Found In	Peak Region	Intensity
C-C	2,4-DHBP; 4-DD-2-HBP; Tinuvin 292	1305 - 1295 1175 - 1120 1100 - 1010 900 - 800 540 - 485 ~455 ~300*	strong medium variable medium to strong medium medium weak
C=C	2,4-DHBP; 4-DD-2-HBP	1625 - 1590 1590 - 1575 1525 - 1430 580 - 540 475 - 425	medium to strong medium weak variable weak
C-H	2,4-DHBP; 4-DD-2-HBP; Tinuvin 292	3105 - 3000* 2975 - 2915* 2885 - 2840* 1485 - 1440 1305 - 1295 1220 - 1200 1160 - 1140 1040 - 1020 940 - 885 860 - 840 780 - 760 740 - 690	strong medium medium to strong weak to medium medium weak weak weak weak weak weak weak
C-N	Tinuvin 292	3315 - 3215* 3440 - 3350*	weak to medium weak to medium
C-O	2,4-DHBP; 4-DD-2-HBP; Tinuvin 292	1275 - 1185 1260 - 1180 1160 - 1050 1140 - 820	strong medium to weak weak strong
C=O	2,4-DHBP; 4-DD-2-HBP; Tinuvin 292	1745 - 1715 1700 - 1680 1670 - 1600	medium variable variable
O-H	2,4-DHBP; 4-DD-2-HBP	3200 - 2500* 1440 - 1260	weak medium to weak

\*Peak region outside of instrument wavenumber range

Only qualitative analysis was performed on the time study samples. At the end of the eight weeks, the spectra from a particular replicate over the course of the experiment were normalized and overlaid. The overlaid spectra were then examined for similarities and differences.

## 2.3 Results and Discussion

### 2.3.1 Statistical Results

The AHC dendrogram for automotive clear coats analyzed by Raman spectroscopy is shown in Figure 2.5 below. AHC analysis shows that there are three classes based on the location of the truncation line, as determined by a histogram of node positions. Divisions at nodes to the right of the truncation line are most significant in establishing the number of classes. AHC was performed on averaged spectra for each clear coat sample. The spectra of the class centroids, shown in Figure 2.6, illustrates that, while similar, there are some distinct differences between each group's spectra. For instance, the Class 1 central object contains more intense peaks within the 1300 – 1650 wavenumber region. Class 3's central object has an additional, but small, peak between 900 and 1000 wavenumbers.

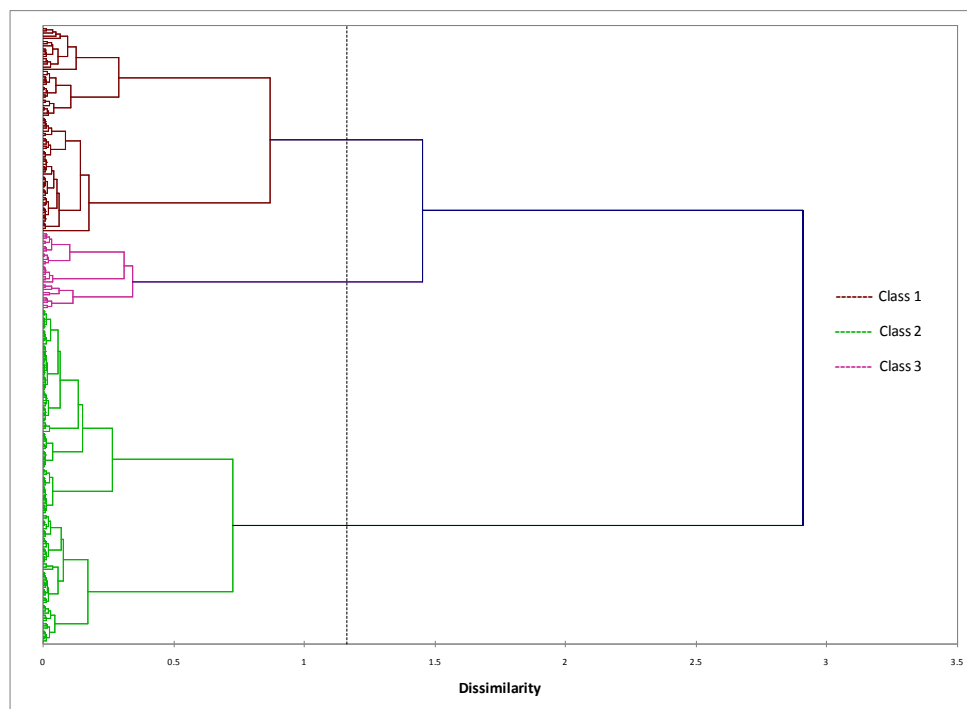


Figure 2.5 Dendrogram from AHC of averaged clear coat spectra.  
Three classes are formed.

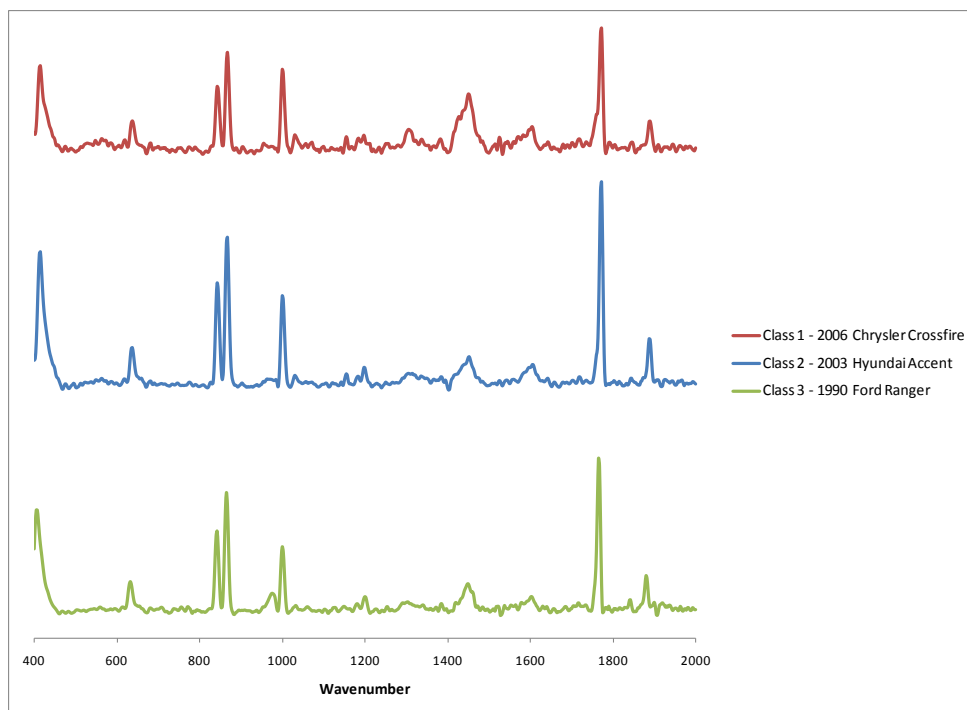


Figure 2.6 Centroids of the three classes from the dendrogram.

Averaged spectra were again used for PCA and subsequent DA. The observations plot created by PCA is shown in Figure 2.7. The plot uses the first two principal components, which account for 59.38% of the total variance in the sample set. The plot is color-coded to show the data when grouped into 3 classes. Overlap is especially evident in the final class on the plot, though the other classes are generally very well-separated. Separation of the final class may occur when more principal components are examined in additional dimensions.

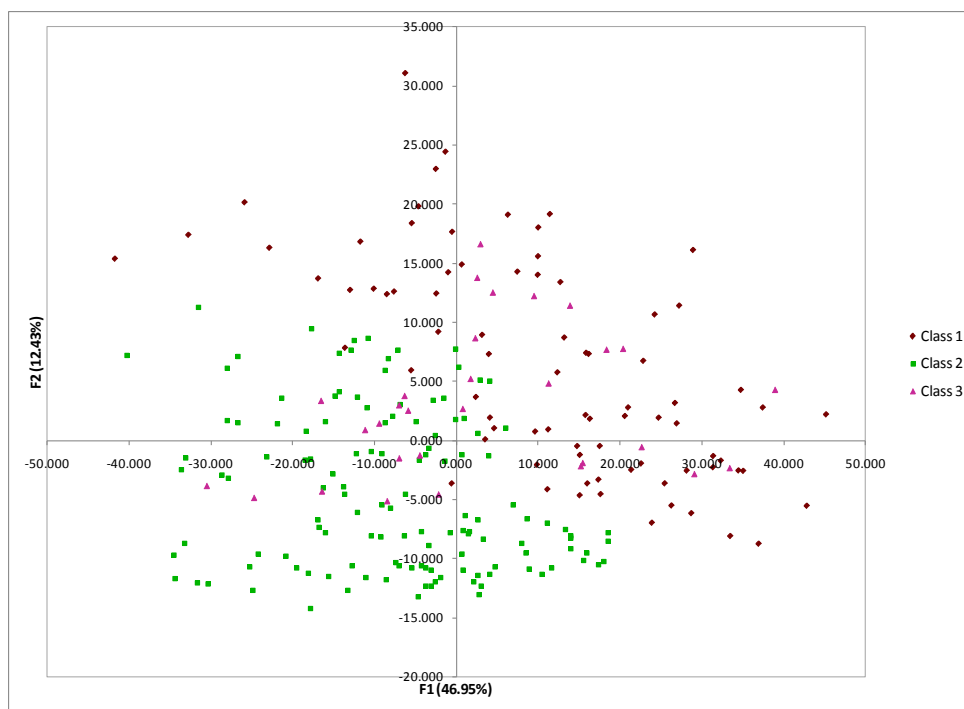


Figure 2.7 The observations plot from PCA with three classes shown.

DA was performed using the data gained from PCA. Table 2.2 shows the eigenvalues pertinent to this study. A number of principal components must be selected to put through DA. To choose the correct number, the scree plot shown in Figure 2.8 was employed. This resulted in the use of five principal components and an approximately 73% cumulative variance. To meet or exceed 95% cumulative variance, 41 principal components would have been required. The Kaiser criterion resulted in 34 principal components.



Table 2.2 Eigenvalues and variability associated with each principal component (PC).

Principal Component (PC)	Eigenvalue	Variability (%)	Cumulative (%)
PC1 (F1)	300.966	46.953	46.953
PC2 (F2)	79.698	12.433	59.386
PC3 (F3)	40.264	6.281	65.667
PC4 (F4)	26.849	4.189	69.856
PC5 (F5)	21.442	3.345	73.201
PC6 (F6)	17.536	2.736	75.937
PC7 (F7)	16.191	2.526	78.463
PC8 (F8)	14.932	2.329	80.792
PC9 (F9)	11.661	1.819	82.611
PC10 (F10)	8.807	1.374	83.985
PC11 (F11)	7.859	1.226	85.211
PC12 (F12)	6.540	1.020	86.232
PC13 (F13)	5.198	0.811	87.043
PC14 (F14)	4.640	0.724	87.766
PC15 (F15)	3.936	0.614	88.380
PC16 (F16)	3.562	0.556	88.936
PC17 (F17)	3.230	0.504	89.440
PC18 (F18)	3.065	0.478	89.918
PC19 (F19)	2.742	0.428	90.346
PC20 (F20)	2.412	0.376	90.722
PC21 (F21)	2.269	0.354	91.076
PC22 (F22)	2.078	0.324	91.400
PC23 (F23)	2.048	0.320	91.720
PC24 (F24)	1.880	0.293	92.013
PC25 (F25)	1.789	0.279	92.292
PC26 (F26)	1.730	0.270	92.562
PC27 (F27)	1.523	0.238	92.800
PC28 (F28)	1.450	0.226	93.026
PC29 (F29)	1.387	0.216	93.242
PC30 (F30)	1.273	0.199	93.441
PC31 (F31)	1.183	0.184	93.626
PC32 (F32)	1.168	0.182	93.808
PC33 (F33)	1.067	0.166	93.974
PC34 (F34)	1.026	0.160	94.134
PC35 (F35)	0.992	0.155	94.289
PC36 (F36)	0.946	0.148	94.436
PC37 (F37)	0.918	0.143	94.580
PC38 (F38)	0.839	0.131	94.711
PC39 (F39)	0.818	0.128	94.838
PC40 (F40)	0.807	0.126	94.964
PC41 (F41)	0.757	0.118	95.082

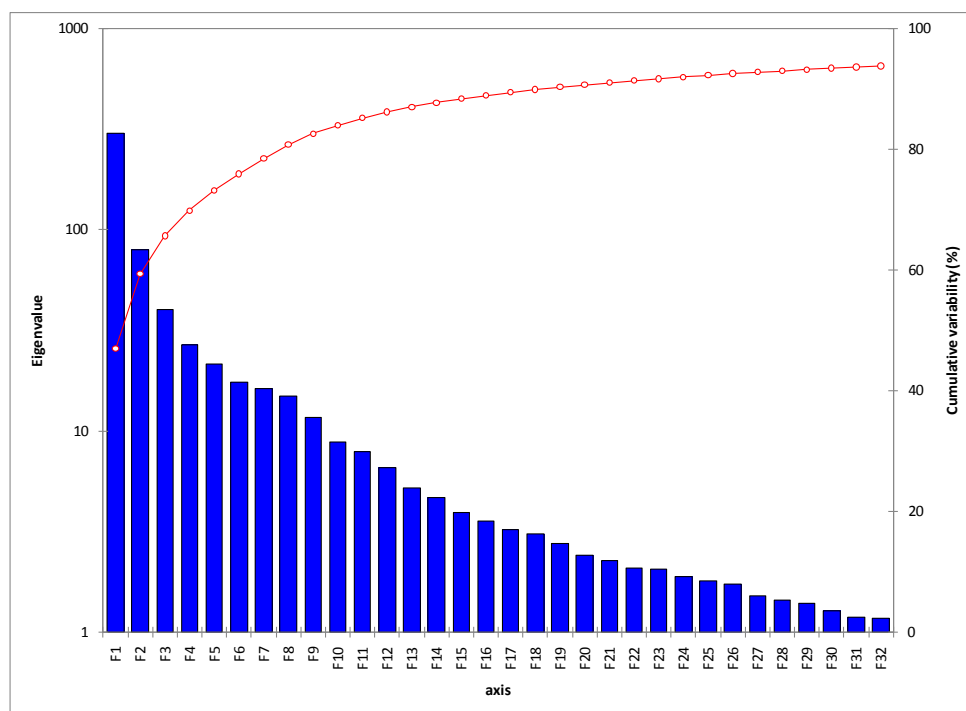


Figure 2.8 Scree plot of principal component factor scores F1-F32.

Figures 2.9 through 2.13 display a different method of representing PCA observations. In these charts, factor loadings for each of the first five principal components are plotted versus wavenumber. The factor loadings represent the cosines of the angle between the principal component and each variable. The areas of the plot where the cosines are positive are areas of positive correlation. Areas where the cosine is negative are areas of negative correlation. Areas where the cosine is nearly zero have no correlation. The first five principal components were chosen for use in subsequent DA. It becomes obvious that the information available from each principal component decreases with an increase in the number of principal components used. However, the first five were deemed to offer sufficient useful information versus noise for DA.

Figure 2.14 shows the sum of squares of the first five principal components plotted versus wavenumber. The sum of squares plot describes communality, or the overall regions of the Raman spectra that reflect the most variability. For instance, the peak on the sum of squares plot around  $985\text{ cm}^{-1}$  corresponds to a peak that is only well-defined in the spectrum of the Class 3 central object. The significant peak at  $1425$

$\text{cm}^{-1}$  corresponds to a broad peak that appears in all three central objects' spectra, but varies in intensity.

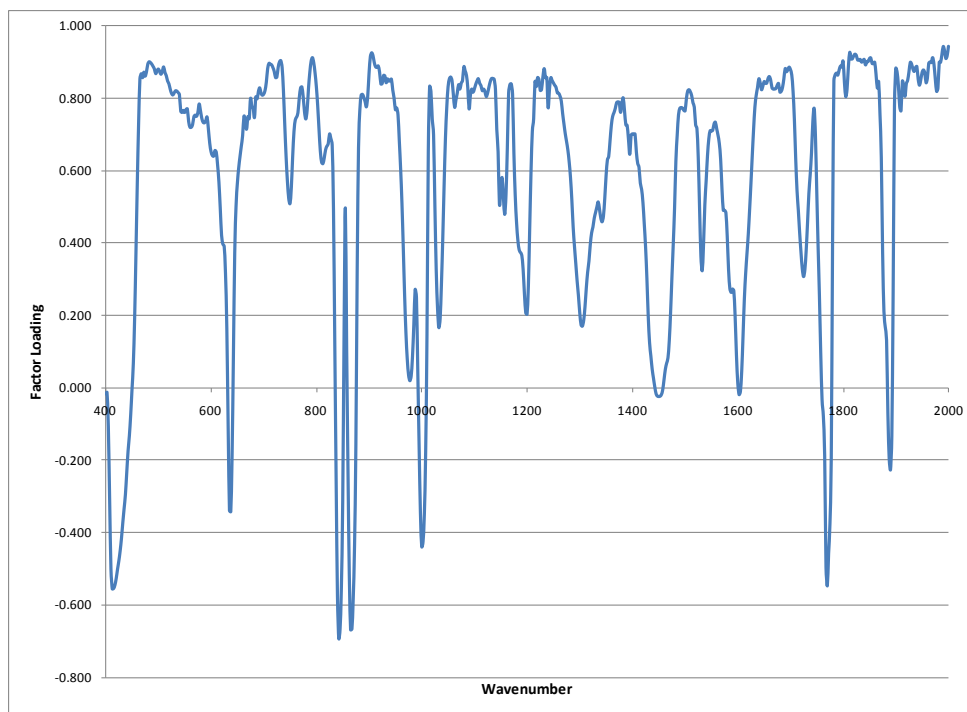


Figure 2.9 Factor loadings for PC1 plotted versus wavenumber.

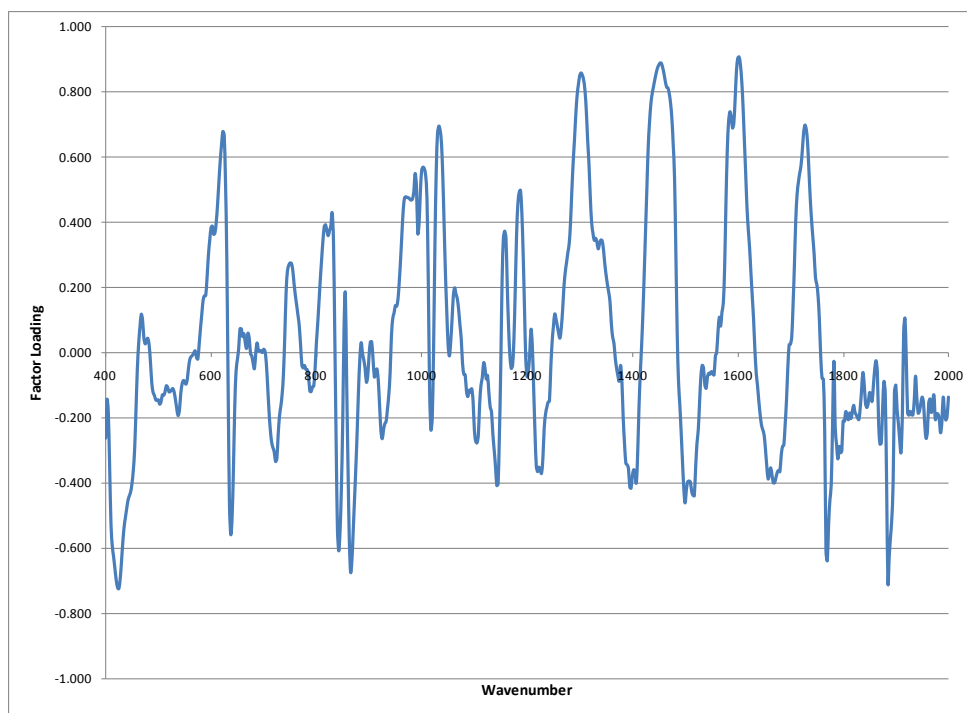


Figure 2.10 Factor loadings for PC2 plotted versus wavenumber.

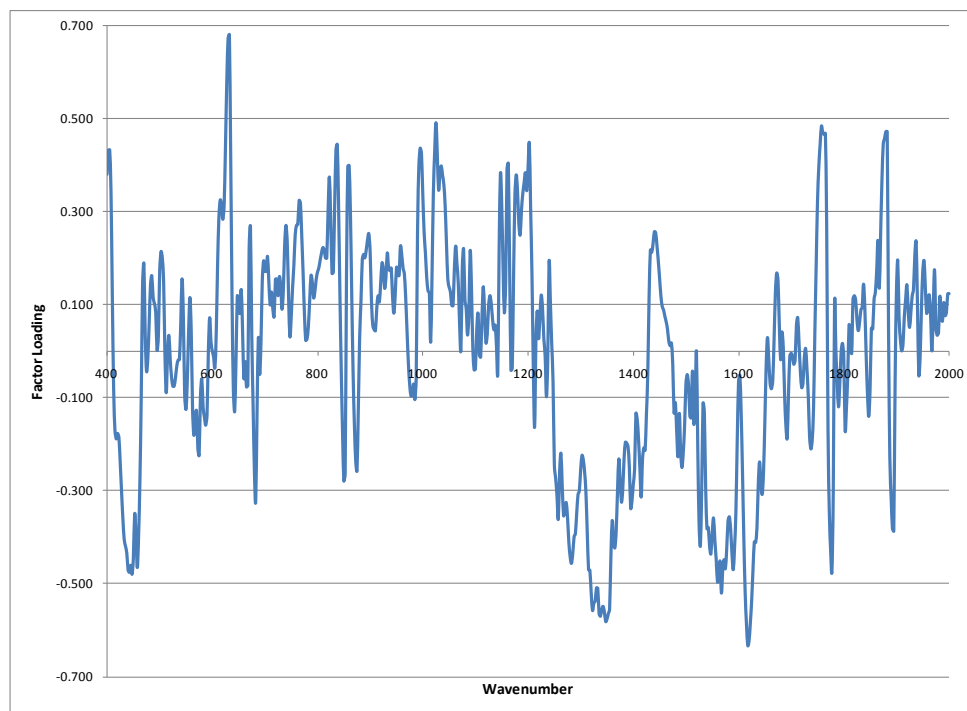


Figure 2.11 Factor loadings for PC3 plotted versus wavenumber.

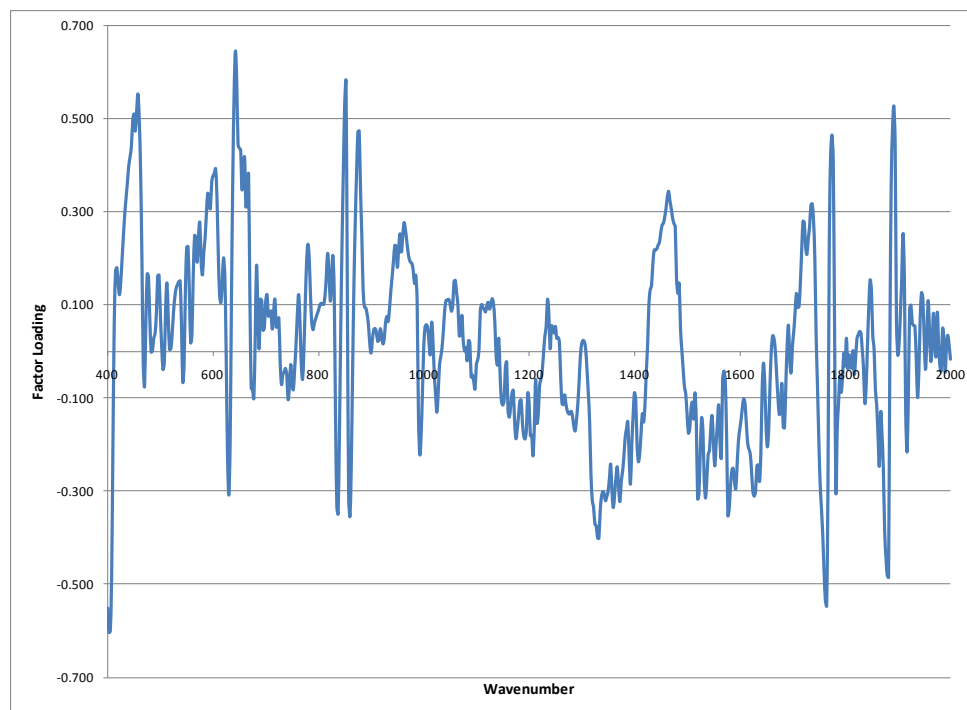


Figure 2.12 Factor loadings for PC4 plotted versus wavenumber.

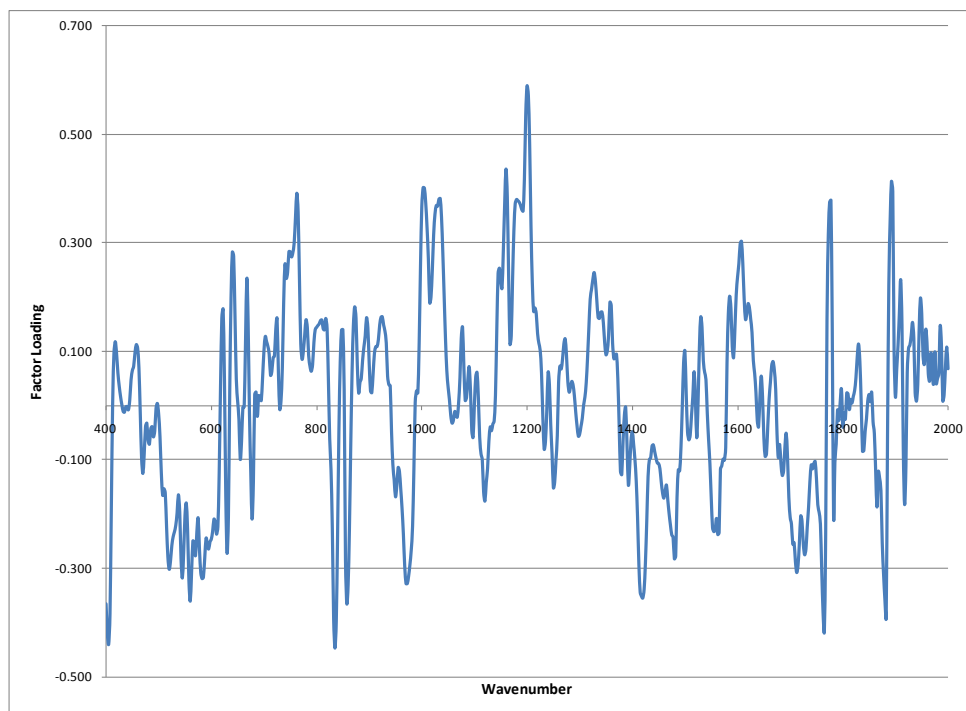


Figure 2.13 Factor loadings for PC5 plotted versus wavenumber.

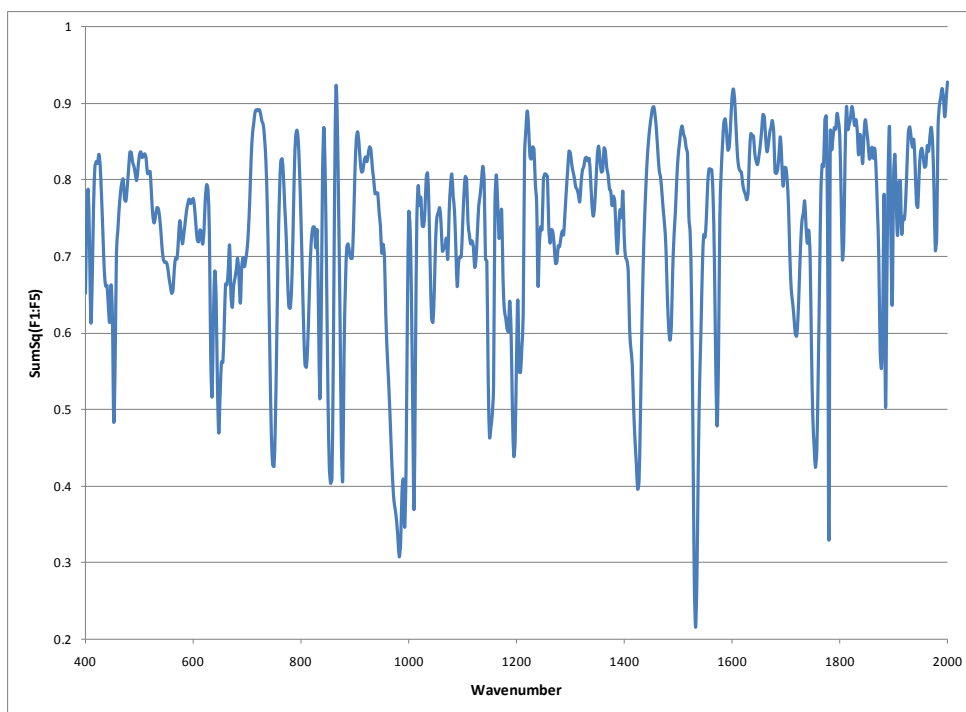


Figure 2.14 Sum of squares of the factor loadings of the first five principal components plotted versus wavenumber.

Looking at the plot of class centroids in Figure 2.15, it is evident that the areas of strong negative correlation from PC1, shown in grey, tend to overlap with the peaks found in the class central objects. The positive correlations from PC2, shown in orange, correspond to features of the class central objects' spectra that appear to vary in intensity between classes.

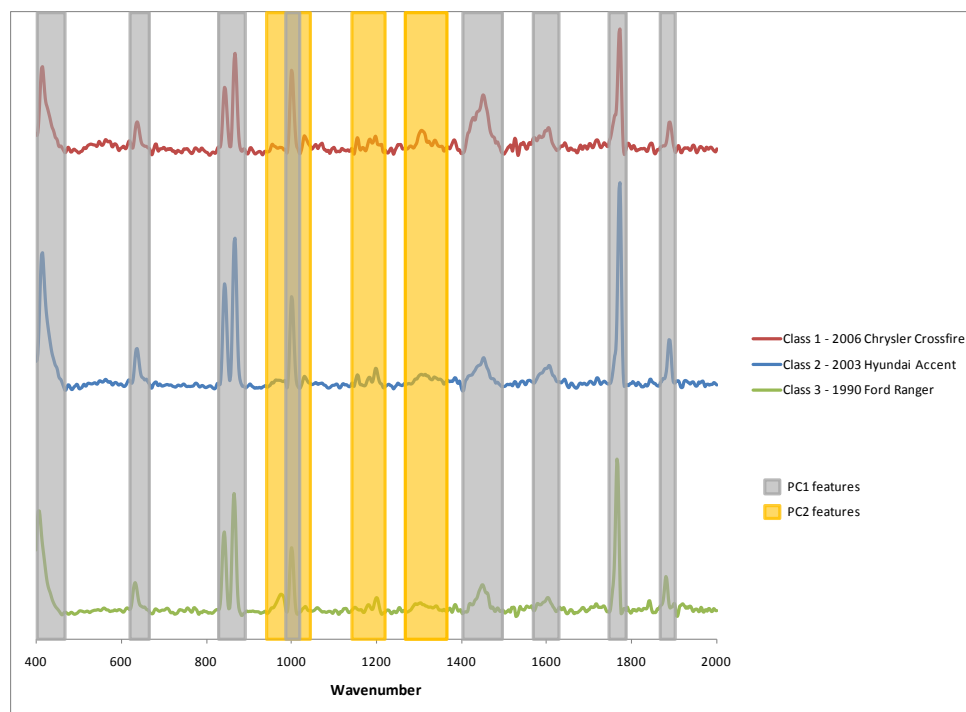


Figure 2.15 Class central objects with PC1 and PC2 regions highlighted.

Figure 2.16 shows the results of DA using the first five principal components. DA was performed with three classes in order to be consistent with AHC results, with 100% of the variance accounted for in two dimensions. Overlap is visible between the classes, which impacts the cross-validation results. This is seen in the confusion matrix results in Table 2.3. The samples located along the diagonal indicate those that were correctly classified, while samples outside of the diagonal were incorrectly grouped. When three classes were used, 92.92% of the samples were correctly classified.

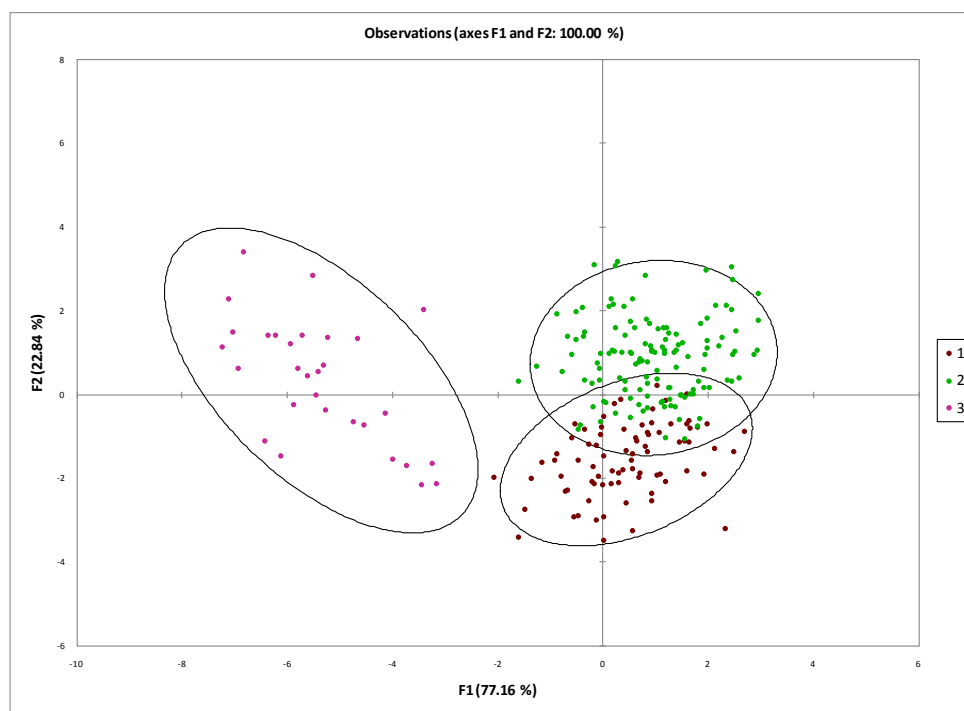


Figure 2.16 Observations plot from DA with three classes.

Table 2.3 Confusion matrix for cross-validation results from DA with three classes.

From/To	1	2	3	Total	% correct
1	70	10	0	80	87.50%
2	7	123	0	130	94.62%
3	0	0	30	30	100.00%
Total	77	133	30	240	92.92%

The final method of chemometric analysis used on the data set was ANOVA.

Where PCA looks for the regions of the spectra that are the most variable, ANOVA finds the areas that are most differentiable. Figure 2.17 shows the ANOVA plot of F values versus wavenumber for the Raman spectra. Compared to the factor loadings plots from PCA, ANOVA analysis finds the region between 900 – 1700  $\text{cm}^{-1}$  to be far less significant. ANOVA also appears to find the areas just around the peaks in the purple regions of Figure 2.18 to be more differentiable than the peaks themselves.

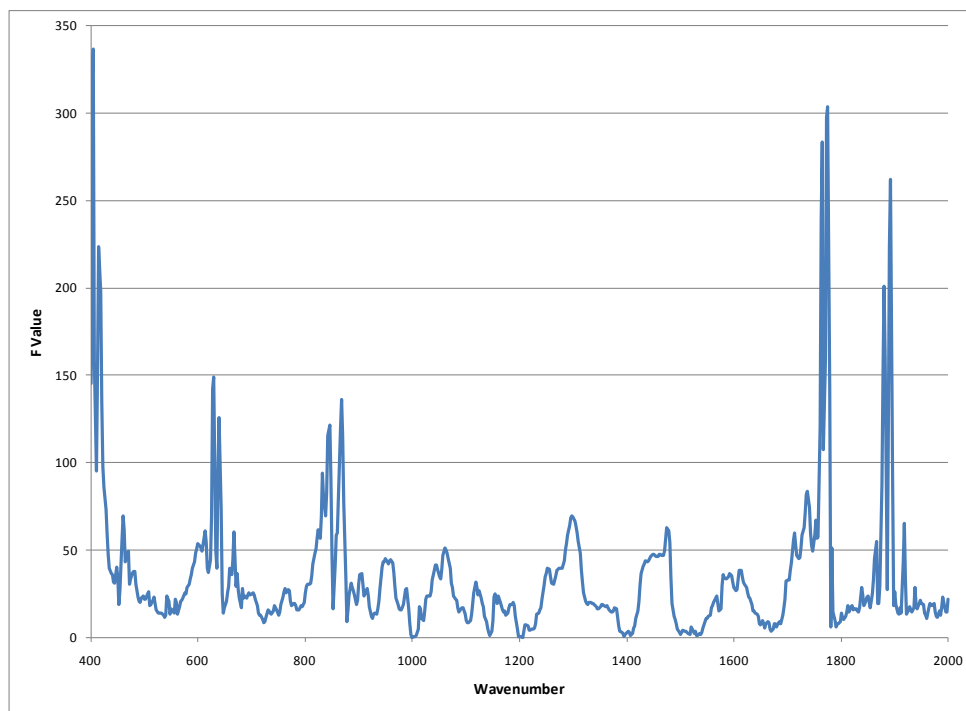


Figure 2.17 F values from ANOVA plotted versus wavenumber.

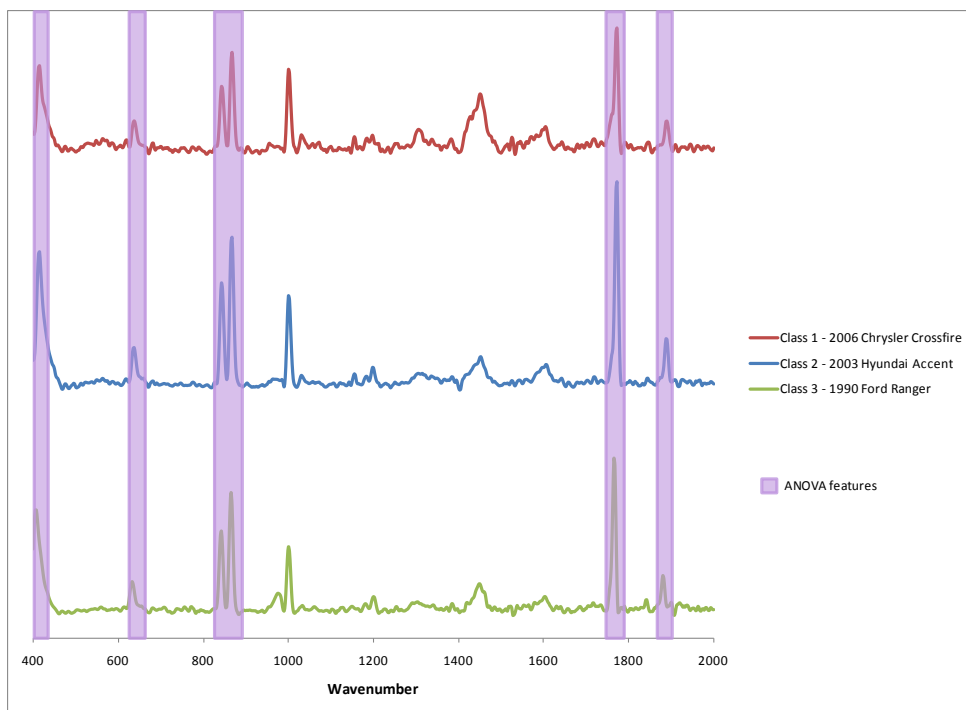


Figure 2.18 Class central objects with ANOVA regions highlighted.



### 2.3.2 External Validation

Thirty of the original samples were run a second time as a blind external validation study. During confusion matrix creation, it was determined that one of the samples chosen was PC041, a sample that had been run initially using different parameters than the rest of the sample set. Since PC041 had been discarded from the data analysis, it was also excluded from the validation set, resulting in 29 validation samples. The results are shown in Table 2.4. DA predicted which classes the supplemental samples should be grouped into, and the correct class was determined by the grouping of the original sample. All of the external validation samples were predicted to be in either the first or second class. The bold number in green represents the number of samples that were correctly classified. The bold numbers in red indicate the numbers of samples that were incorrectly classified. Overall, the external validation correctly assigned 51.72% of the samples. This was considered to be a poor result. In comparing the original and external validation spectra of the various samples, it seems that additional noise in the external validation led to incorrect classifications. Visually, many of the validation spectra were very similar to their original counterparts. Figure 2.19 shows one of the validation samples that was incorrectly classified on the same axes as the original sample. However, some external validation samples were correctly classified when their spectra had very obvious differences compared to the original spectra. Figure 2.20 is an example of such a case.

Table 2.4 Confusion matrix for the external validation results of the supplemental data from DA.

From/To	1	2	3	Total	% correct
1	<b>2</b>	<b>4</b>	0	6	33.33%
2	<b>7</b>	<b>13</b>	0	20	65.00%
3	<b>2</b>	<b>1</b>	0	3	0.00%
Total	11	18	0	<b>29</b>	<b>51.72%</b>

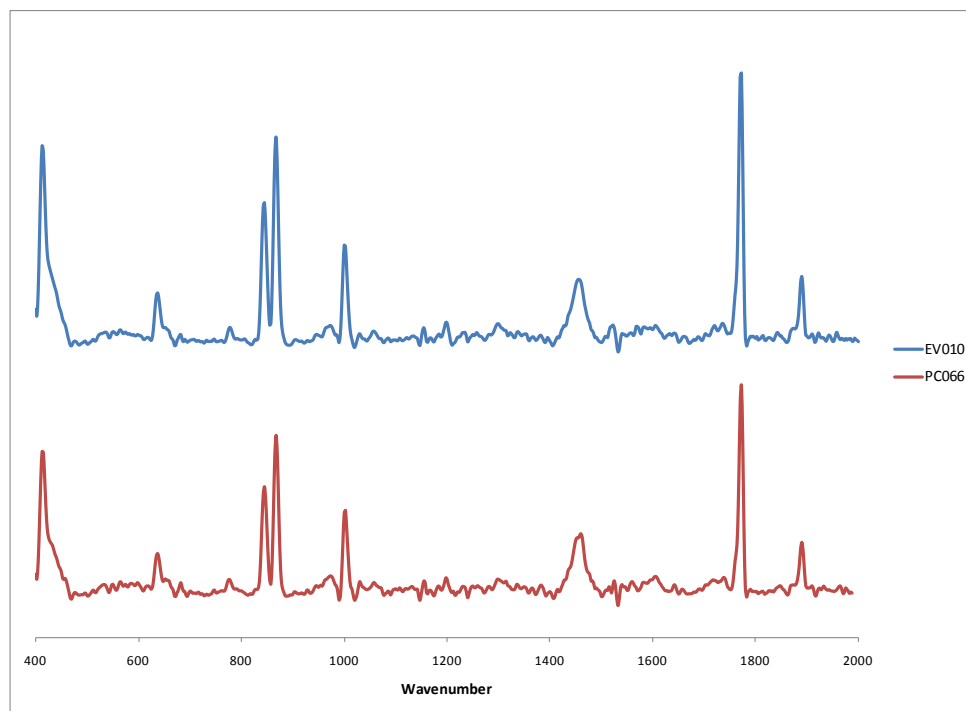


Figure 2.19 External validation sample EV010 compared to original sample PC066. EV010 was incorrectly classified from Class 1 to Class 2.

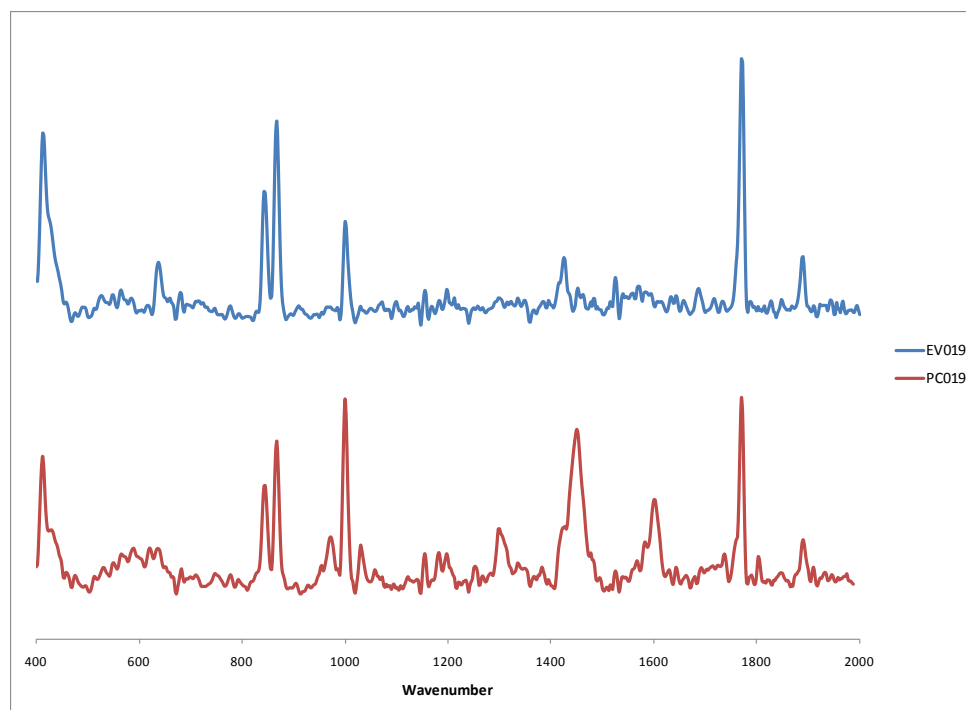


Figure 2.20 External validation sample EV019 compared to original sample PC019. EV019 was correctly classified from Class 1 to Class 1.

### 2.3.3 Formation of Classes

Chemometric analysis showed that there were three classes forming reliably differentiable spectra. The next step of analysis was to determine whether make, model, and year was impacting the formation of these three classes. To accomplish this, spectra of clear coats from the same make and model of vehicle but different years were examined.

Figure 2.21 shows two cars of the same make and model but different years that were sorted into different classes. The samples in this case were both Buick Lesabres. Year 1997 was sorted into Class 2, while year 2001 was sorted into Class 3. Figure 2.22 shows two cars of the same make and model but different years that were sorted into the same class. The samples were Chrysler Town & Countries, year 2001 and 2005, and were both sorted into Class 2. The spectra in Figure 2.22 are more similar to each other than those in Figure 2.21, but there are obvious differences between the two spectra. These two figures show that year does not affect class formation.

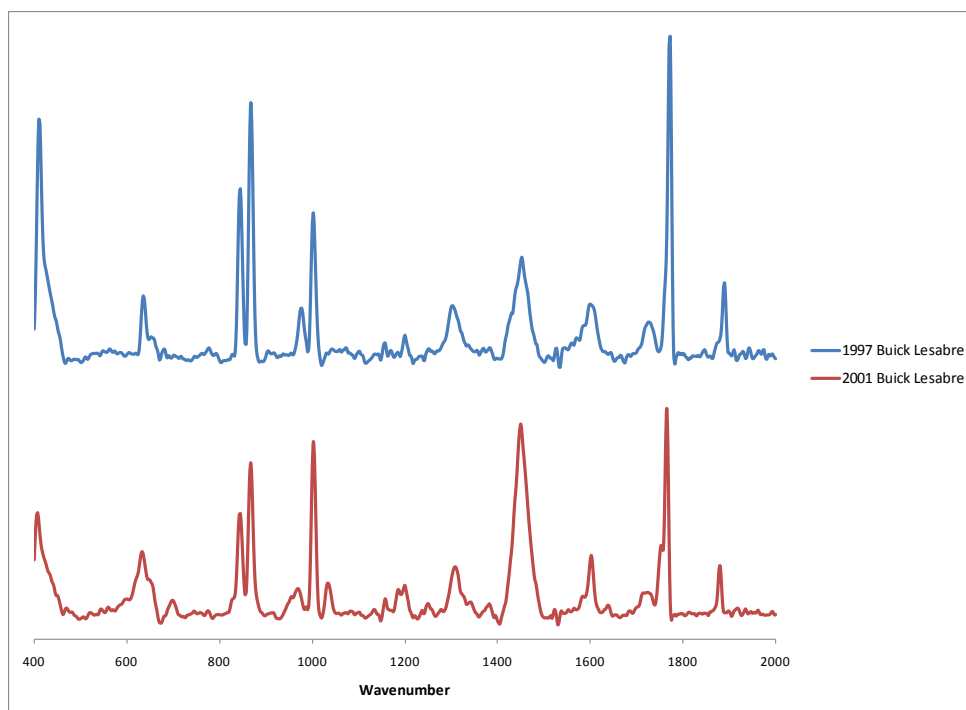


Figure 2.21 Samples of the same make and model but different year placed in different classes.

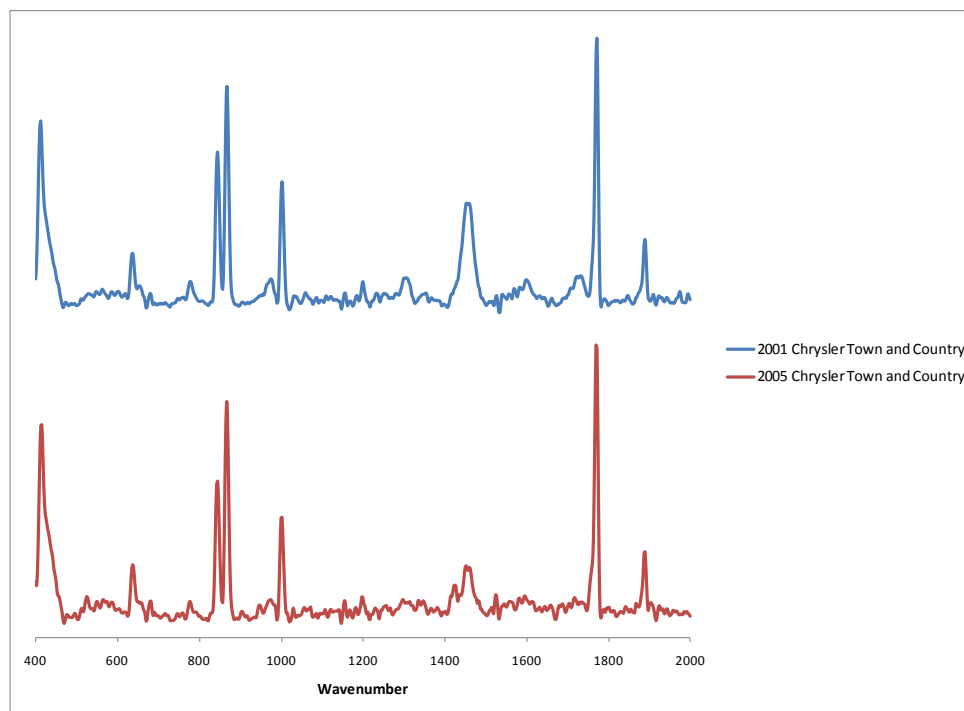


Figure 2.22 Samples of the same make and model but different year placed in the same class.

Figure 2.23 shows three vehicles of the same make, model, and year placed into the same class. The samples in this case were all 1998 Chevrolet Blazers, and were all sorted into Class 2. Figure 2.24 shows two vehicles of the same make, model, and year placed into different classes. The two samples were 2001 Hyundai Sonatas, and one was sorted into Class 1, while the other was sorted into Class 2. This shows that make and model also do not impact the groupings of automotive clear coats.

Examining the types of vehicles that were present in each class further proves that make, model, and year did not affect classification of clear coats. Some models fell into multiple classes, such as the Honda Accord. Some makes had vehicles in all three classes, such as Chevrolet, Ford, Honda, and Toyota. In general, there is no indication that a correlation exists between make, model, or year and classification of the clear coat's Raman spectrum.

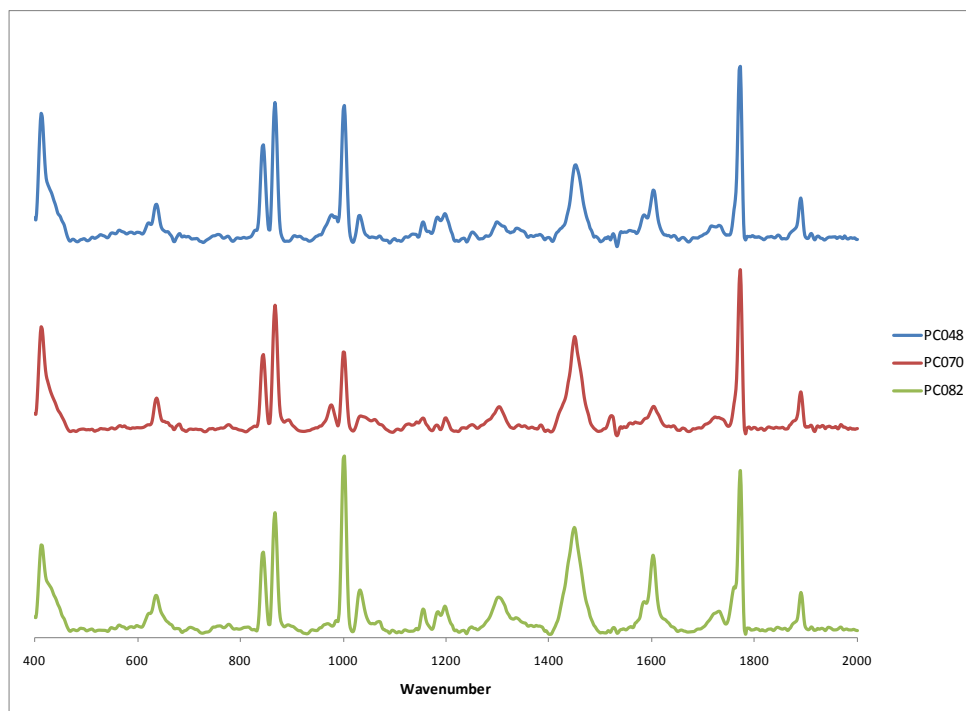


Figure 2.23 Samples of the same make, model, and year placed in the same class.

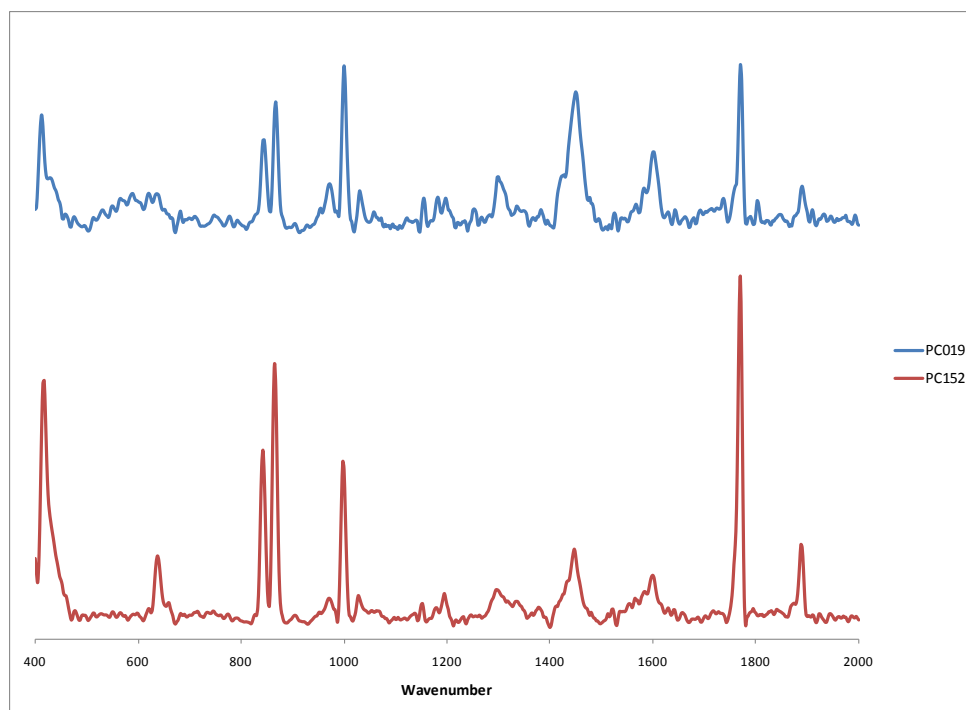


Figure 2.24 Samples of the same make, model, and year placed in different classes.

### 2.3.4 Known UV Absorbers

Raman spectra of three known UV absorbers are shown in Figure 2.25. When compared to the Raman spectra of the class centroids of the three classes of clear coats, it is evident that some of the features of the UV absorbers' spectra are also present in those of the class centroids. The grey regions of Figure 2.26 highlight the common features of the clear coat samples and the known UV absorbers. It is possible that 4-DD-2-HBP or Tinuvin 292 could be present in the clear coat samples. It is less likely that 2,4-DHBP is present in the clear coat samples, although there are some peaks present in its spectrum that also appear in the clear coat samples. The peaks in the 700 – 800, 1300 – 1400, and 1500 – 1650  $\text{cm}^{-1}$  regions of the 2,4-DHBP spectrum don't appear to be in the clear coat samples. Table 2.5 shows the potential peak assignments for the peaks visible in the known UV absorber spectra.

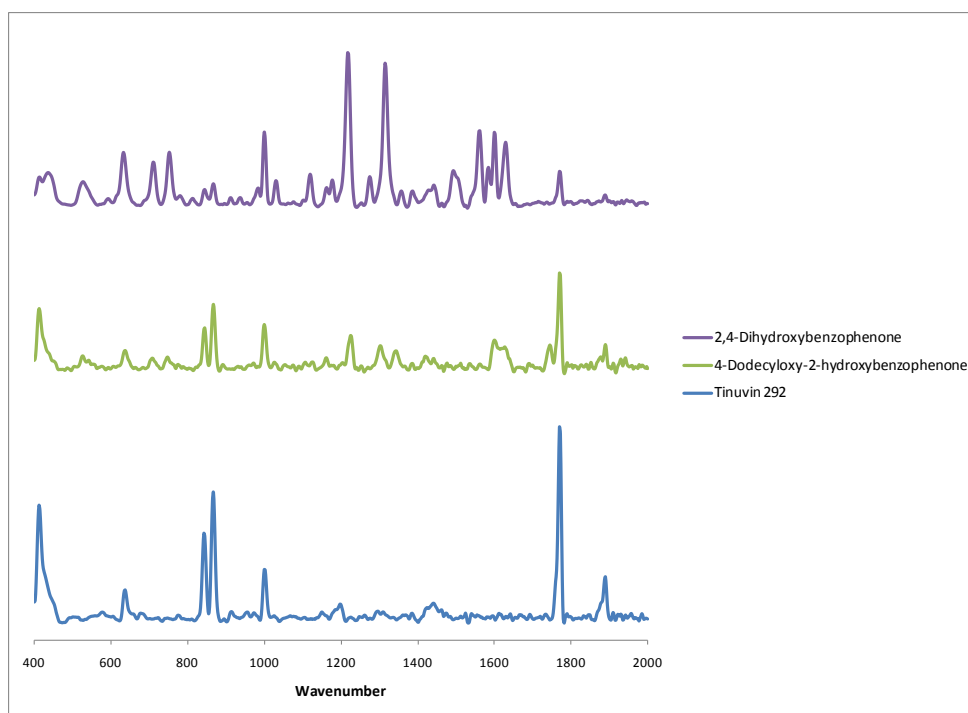


Figure 2.25 Raman spectra of known UV absorbers.

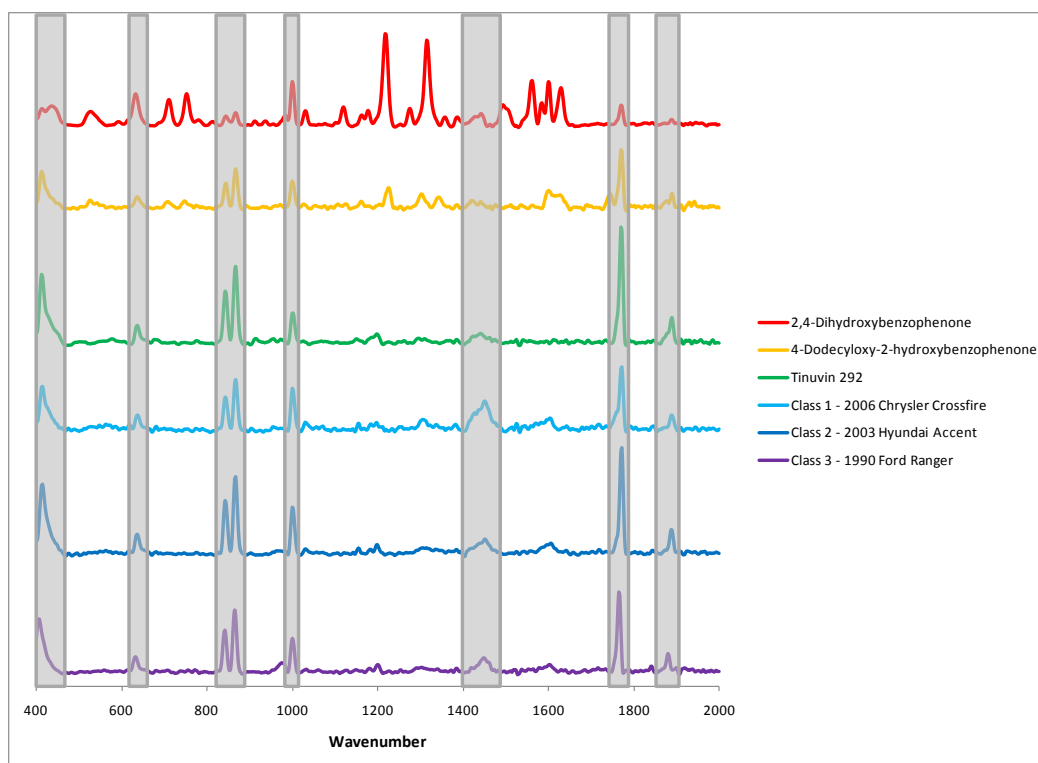


Figure 2.26 Raman spectra of known UV absorbers compared to class central objects.

Table 2.5 Possible Raman peak assignments for known UV absorbers.<sup>40</sup>

Bond	Found In	Peak Region	Intensity
C-C	2,4-DHBP	1305 - 1295	strong
	2,4-DHBP; 4-DD-2-HBP; Tinuvin 292	900 - 800	medium to strong
	2,4-DHBP	540 - 485	medium
C=C	2,4-DHBP; 4-DD-2-HBP	1590 - 1575	medium
	2,4-DHBP	475 - 425	weak
C-H	2,4-DHBP	1485 - 1440	weak
	2,4-DHBP; 4-DD-2-HBP	1305 - 1295	medium
	4-DD-2-HBP	1220 - 1200	weak
	2,4-DHBP; 4-DD-2-HBP; Tinuvin 292	940 - 885	weak
	2,4-DHBP; 4-DD-2-HBP; Tinuvin 292	860 - 840	weak
	2,4-DHBP	780 - 760	weak
C-O	2,4-DHBP	740 - 690	weak
	2,4-DHBP	1275 - 1185	strong
	4-DD-2-HBP	1260 - 1180	weak
	2,4-DHBP; 4-DD-2-HBP; Tinuvin 292	1140 - 820	strong
C=O	2,4-DHBP	1670 - 1600	medium
O-H	2,4-DHBP; 4-DD-2-HBP	1440 - 1260	medium to weak

### 2.3.5 Limitations of the Study

A study of this type has some significant limitations. For one, the initial conditions of a clear coat and its exposure to environmental effects can impact chemical composition of the clear coat. However, the storage conditions of the paint chips collected are unknown. Samples were collected “as-is” from the different vehicles, and environmental factors were not controlled. Paint chips may have been collected from two vehicles of the same make, model, and year, but one vehicle might have been stored in a garage while the other was kept outside in a driveway. The Raman spectra for the two clear coats would potentially be different due to weathering effects. The amount of these differences is unknown. Even though this is a significant limitation, it must be recognized that this is the state of affairs with actual forensic paint cases; the initial and storage conditions are usually unknown.

Another potential limitation to Raman analysis of clear coats is that the chemical makeups and concentrations of the UV absorbers present in the clear coat samples are unknown. Some of the samples may have the same UV absorbers present in different concentrations, which could affect classification. Also, clear coats are commodities. They are not manufactured by the vehicle makers, but purchased. The same clear coat systems could be in use across many different makes and models of vehicles. Again, this is the normal situation with real forensic paint cases.

### 2.3.6 Time Study

The overlaid spectra of replicate 1 of PC001 over the course of eight weeks are shown in Figures 2.27 and 2.28. Figure 2.27 shows PC001, replicate 1, after eight weeks of storage in a dark cabinet in the laboratory. Figure 2.28 shows a replicate of PC001 after eight weeks of storage in a lit area of the laboratory.



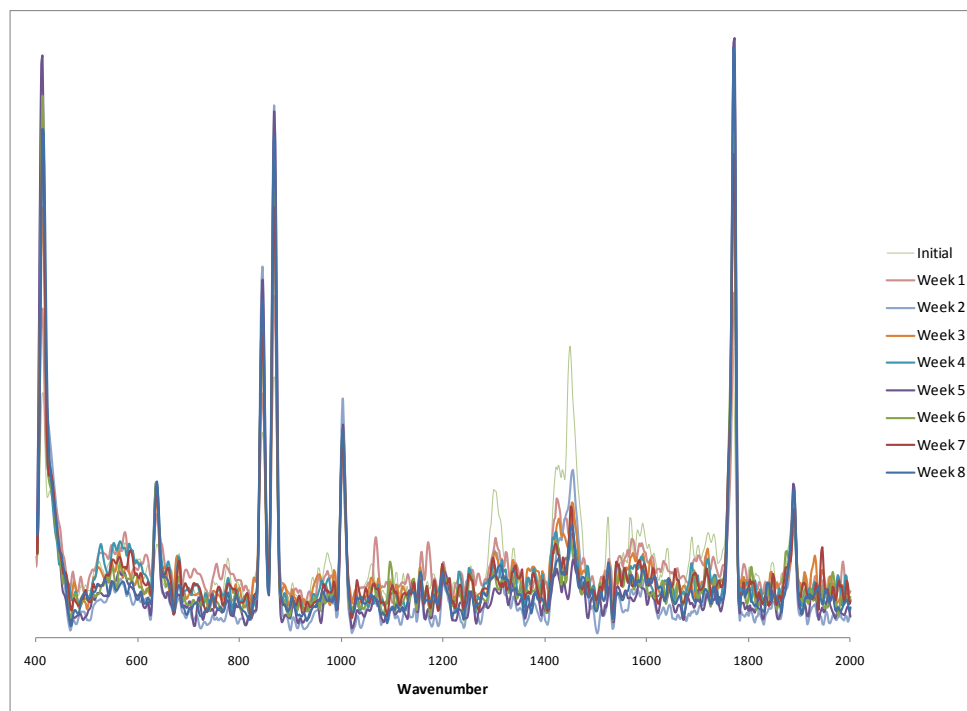


Figure 2.27 Replicate 1 of PC001 over eight weeks while stored in a dark cabinet.

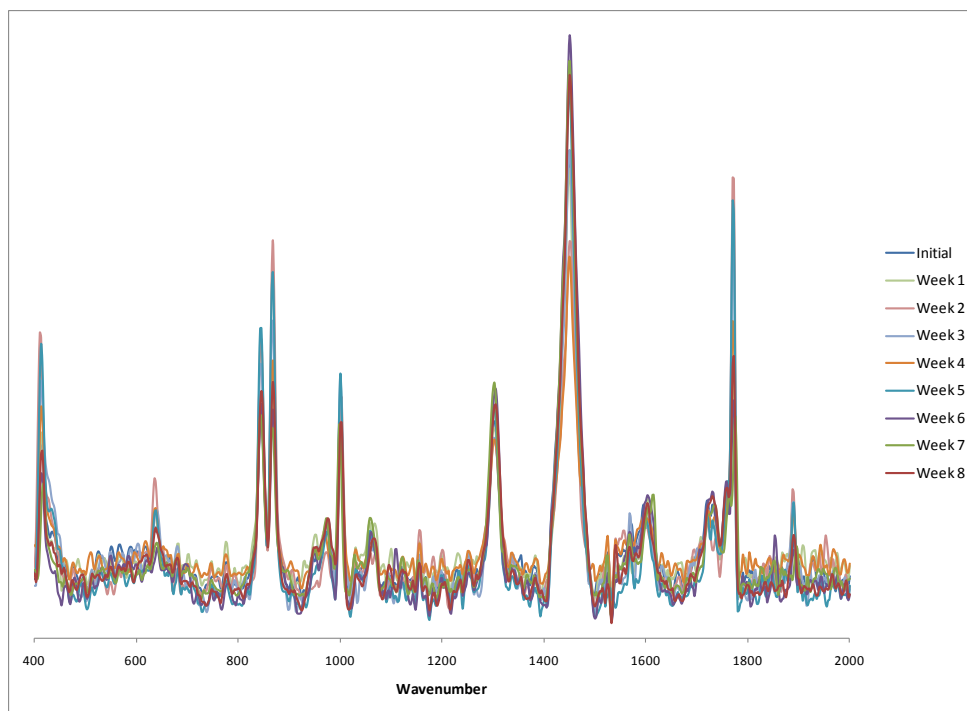


Figure 2.28 Replicate 1 of PC001 over eight weeks while stored in the lit laboratory.

#### 2.3.6.1 Aims of the Study

This secondary study was conducted to determine the effects of time and storage conditions on the Raman spectra of automotive clear coats. It also serves as an investigation into sample preparation of the clear coats.

#### 2.3.6.2 Summary of Results

The overlaid spectra of each replicate over the course of the study showed the spectra were highly reproducible. No peaks were gained or lost during the timeframe of the study. This showed that, for purposes of this work, that samples can be run well after clear coat peels are made without being detrimental to the quality of the data. Also, storing the peels in a lit area of the laboratory versus a dark cabinet does not negatively impact data collection.

#### 2.3.6.3 Limitations of the Study

This time study showed that the Raman spectra of clear coats were very reproducible over time. However, peeling and storing clear coats does not mimic actual wear and weathering conditions on a vehicle. Even storage in a lit laboratory area may not accurately represent the migration and depletion of UV absorbers as a result of repeated exposure to sunlight and the elements.

## 2.4 Conclusions

Raman has proven to be an effective method of analyzing automotive clear coat samples. Sample preparation is minimal and easily accomplished. Spectra are also highly reproducible between replicates and over time.

The chemometric analysis of the sample set using AHC, PCA, DA, and ANOVA resulted in several significant findings. Three classes formed within the sample set. The central objects of these classes show that the areas of the spectra with the highest variability between the classes appear at approximately 975, 1450, and 1600 wavenumbers. These classes were accurately differentiated using cross-validation. However, blind external validation samples were not as successful. The clear coat samples also varied widely by make, model, and year, but no correlations between these variables and the Raman spectra were found.

## CHAPTER 3. MICROSPECTROPHOTOMETRY

### 3.1 Review of Microspectrophotometry

UV-visible microspectrophotometry is an instrumental technique used to acquire information about how samples behave in the ultra-violet (UV) and visible regions of the electromagnetic spectrum. These range between 190-400 nm and 400-800 nm, respectively. The visible region is used to determine the color of the sample being analyzed, and can help compare and discriminate colors in a way human observers cannot. The UV region displays information about only two types of electronic transitions,  $\pi \rightarrow \pi^*$  or  $n \rightarrow \pi^*$ .<sup>37</sup> If  $\pi$  electrons are present in the compound being examined, peaks will appear in the UV region. From this, examiners can determine whether double bonds and conjugation are present in the sample under scrutiny.<sup>9</sup> The more conjugated a compound, the higher the wavelengths it will absorb in, shifting its absorbance into the visible region.

A microspectrophotometer (MSP) can obtain spectra using four different modes. These are transmittance, absorbance, reflectance, and fluorescence. Transmission spectra are obtained by measuring the amount of light that is transmitted by the sample at each wavelength. Absorbance spectra measure the amount of light absorbed at each wavelength. For opaque samples, reflectance spectra measure the amount of light reflected off of the sample at each wavelength. Finally, fluorescence spectra measure the intensity of fluorescence emitted by the sample.<sup>9</sup>

When using MSP, white light passes through the sample. The sample will absorb different wavelengths of the light depending on its molecular structure. Wavelengths of light that are not absorbed encounter a mirrored aperture. This aperture sends an

image of the sample, minus a portion that corresponds to the size of the aperture, to a digital video camera. The portion of light that passes through the aperture enters a monochromator, which separates the wavelengths of light. These wavelengths are then detected by an array detector, which measures the intensity of light at each wavelength. The intensity and wavelength values are then converted to a spectrum.<sup>9</sup>

Because MSPs are single-beam instruments, a reference spectrum must be collected prior to actual sample analysis. This reference spectrum is of the material(s) used to mount the sample (i.e., a quartz slide and glycerin). The sample data is then compared to that of the reference standard, and a spectrum of intensity versus wavelength is produced.

For samples such as clear coats, the visible region of the spectrum is not useful, as there is no color to detect. However, the UV region can give investigators information about the nature of the UV absorbers present in the clear coats. In this study, transmittance spectra were collected and displayed in absorbance values. This combination was chosen because characterizing clear coats based on their UV absorbers, which absorb transmitted UV light, was the focus of the study.

## 3.2 Materials and Methods

### 3.2.1 Instrumental Analysis

Samples were prepared following the procedures outlined previously in section 2.2.1. A CRAIC QDI 2000 microspectrophotometer (CRAIC Technologies, San Dimas CA) was used for the clear coat samples. The analysis was conducted in transmission mode under 15x magnification, with approximately 2 nm resolution. The microspectrophotometer was calibrated before each use with NIST traceable standards. The clear coat peels were removed from the foil slide used for Raman analysis and placed on a quartz slide without a cover slip. Before each set of sample scans, an

autoset optimization, dark scan, and reference scan were run. One sample run was completed for each of the three replicates in a given sample. These sample runs were completed by Ms. Feldmann.

Between the analysis of samples using Raman and subsequent analysis by MSP, 11 replicates were consumed during analysis. These replicates were PC006 replicate 3, PC017 replicate 2, PC020 replicate 1, PC038 replicate 1, PC042 replicate 1, PC048 replicate 3, PC057 replicate 3, PC058 replicate 1, PC059 replicate 2, PC074 replicate 3, and PC078 replicate 2. As one of the goals of this study was to conduct Raman and MSP analyses of the exact same clear coat peels, the missing replicates were not replaced. Rather, subsequent averaging of spectra was done with only two replicates instead of three.

The three known UV absorbers obtained for the Raman study were also analyzed by MSP using the same parameters as the clear coat samples. A small amount of each absorber was dissolved in acetone and then spotted onto a quartz slide.

### 3.2.2 Data Analysis

Because the MSP spectra were not automatically baseline corrected by the software, manual baseline correction had to be completed prior to chemometric analysis. This was done by subtracting the minimum value from each replicate's spectrum. Each spectrum was then normalized by dividing the absorbance values by the square root of the sum of squares of all of the absorbance values for that replicate. Ninety-eight spectra considered to be outliers or of unacceptably poor quality were thrown out of the data set. All of the replicates for each sample were then averaged to yield one spectrum per sample. Baseline correction, normalization, and averaging were all completed using Excel 2007 (Microsoft Corporation, Redmond WA). Using XLSTAT2010 (Addinsoft, Paris France), AHC, PCA, DA, and ANOVA analysis was performed on these averaged spectra.

### 3.3 Results and Discussion

#### 3.3.1 Statistical Results

The AHC dendrogram for automotive clear coats analyzed by MSP is shown in Figure 3.1 below. AHC analysis shows that there are three classes based on the location of the truncation line, as determined by a histogram of node positions. Divisions at nodes to the right of the truncation line are more significant in establishing the number of classes. AHC was performed on averaged spectra for each clear coat sample. The spectra of the class centroids, shown in Figure 3.2, illustrates that there are some distinct differences between each class's spectra. For instance, Classes 1 and 3 exhibit multiple peaks, but with different patterns of intensity. Class 2 has only a single peak.

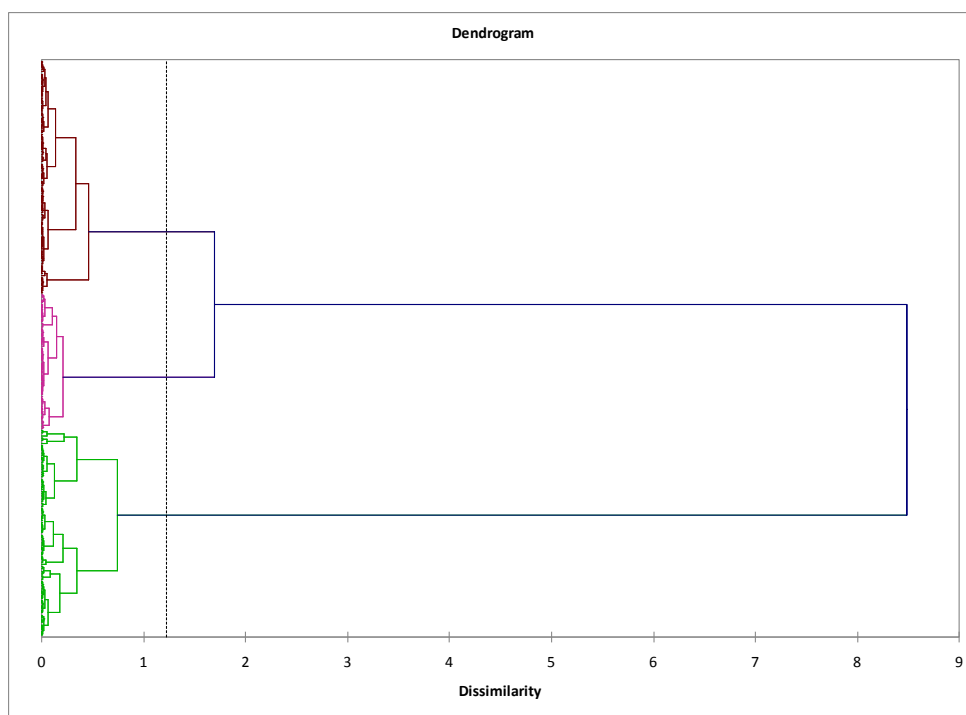


Figure 3.1 Dendrogram from AHC of averaged clear coat spectra.  
Three classes are formed.

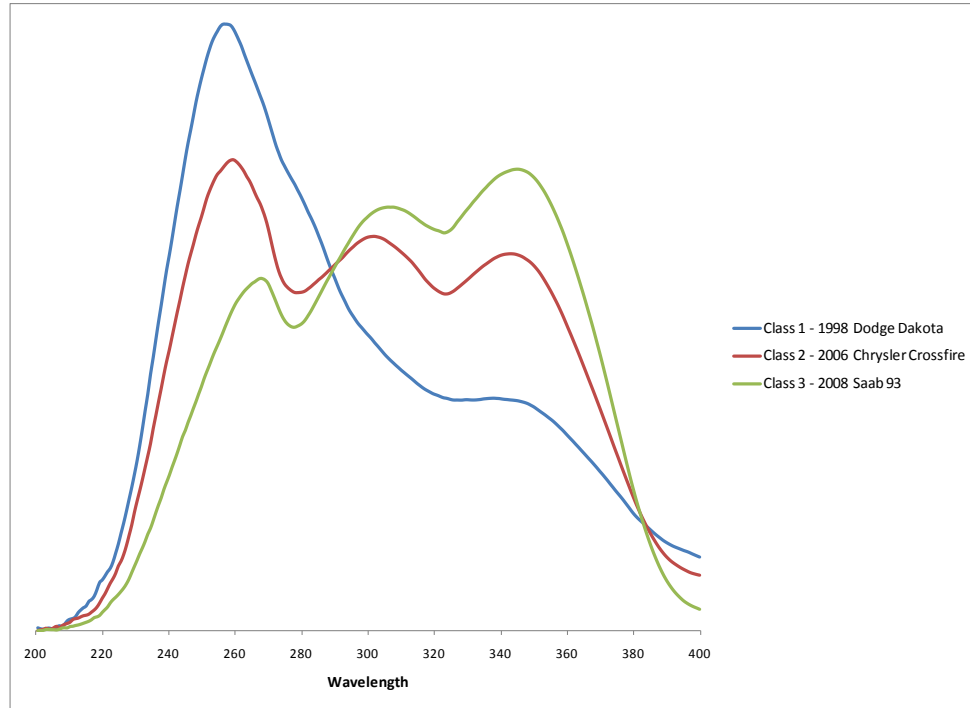


Figure 3.2 Centroids of the three classes from the dendrogram.

Averaged spectra were again used for PCA and subsequent DA. The observations plot created by PCA is shown in Figure 3.3. The plot uses the first two principal components, which account for 73.73% of the total variance in the sample set. The plot is color-coded to show the data when grouped into 3 classes. Overlap between the classes is present, but the classes are generally very well-separated.



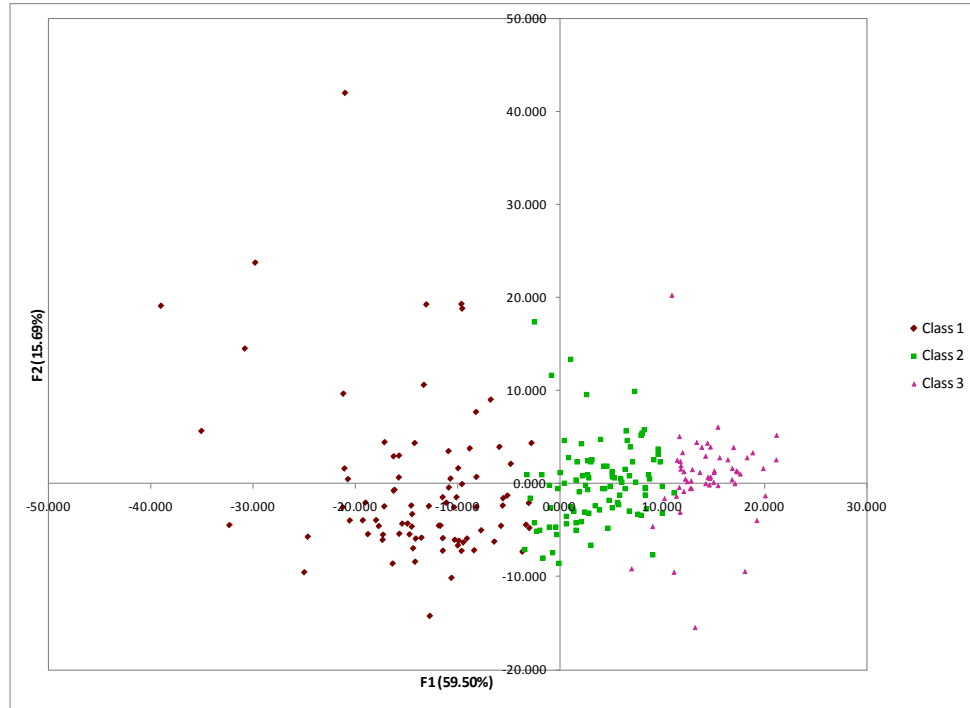


Figure 3.3 The observations plot from PCA with three classes shown.

DA was then performed using the PCA data. Table 3.1 displays the eigenvalues relevant to this research. To choose the correct number of principal components to use for DA, the scree plot shown in Figure 3.4 was used. This resulted in the use of five principal components and over 97% cumulative variance. Using the Kaiser criterion resulted in 7 principal components.

Table 3.1 Eigenvalues and variability associated with each principal component (PC).

Principal Component (PC)	Eigenvalue	Variability (%)	Cumulative (%)
PC1 (F1)	148.761	59.504	59.504
PC2 (F2)	39.235	15.694	75.198
PC3 (F3)	32.544	13.018	88.216
PC4 (F4)	15.563	6.225	94.441
PC5 (F5)	7.080	2.832	97.273
PC6 (F6)	2.748	1.099	98.372
PC7 (F7)	1.990	0.796	99.168

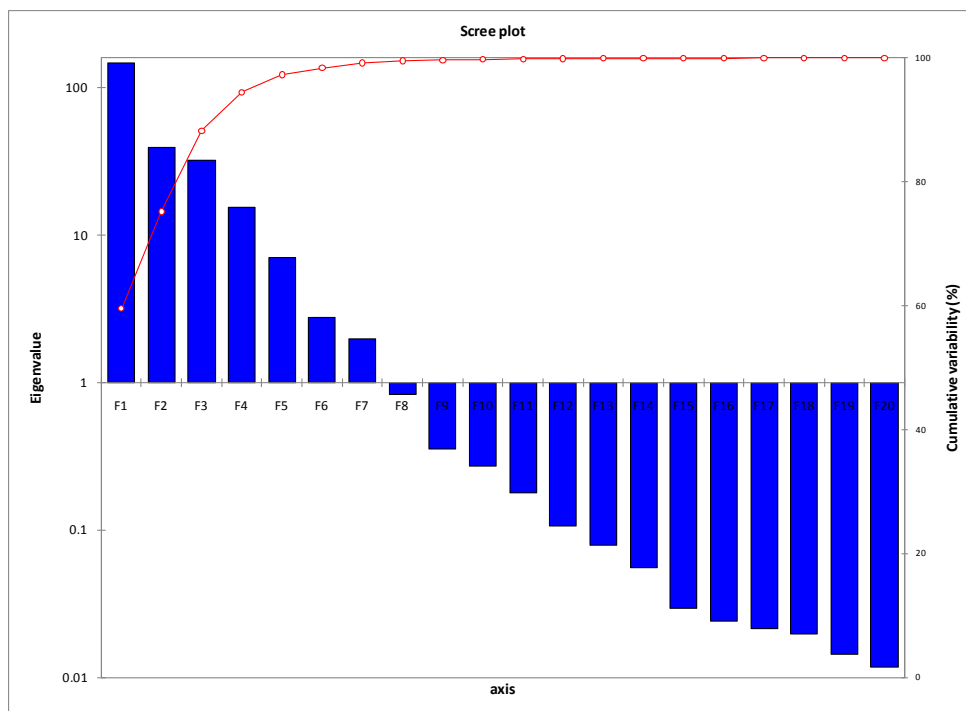


Figure 3.4 Scree plot of principal component factor scores F1-F20.

Figures 3.5 through 3.9 show an alternate method of representing PCA observations. In these charts, factor loadings for each of the first five principal components are plotted versus wavelength. The factor loadings represent the cosines of the angle between the principal component and each variable. The areas of the plot where the cosines are positive are areas of positive correlation. Areas where the cosine is negative are areas of negative correlation. Areas where the cosine is nearly zero have no correlation. The first five principal components were chosen for use in DA. It becomes obvious that the useful information available from each principal component decreases when the number of principal components used increases. However, the first five were determined to offer sufficient useful information versus noise for DA.

Figure 3.10 shows the sum of squares of the first five principal components plotted versus wavenumber. The sum of squares plot describes communality, or the overall regions of the MSP spectra that reflect the most variability. For instance, the peaks on the sum of squares plot around 280 nm and from 300 – 360 nm correspond to

regions on the central objects' spectra where all three classes have very different features.

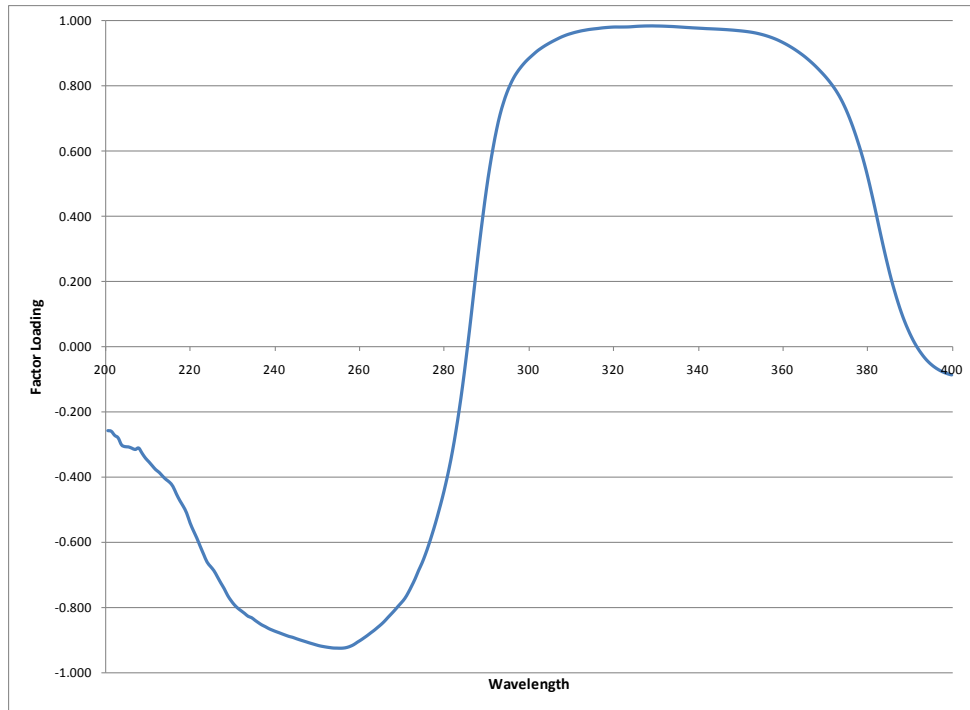


Figure 3.5 Factor loadings for PC1 plotted versus wavelength.

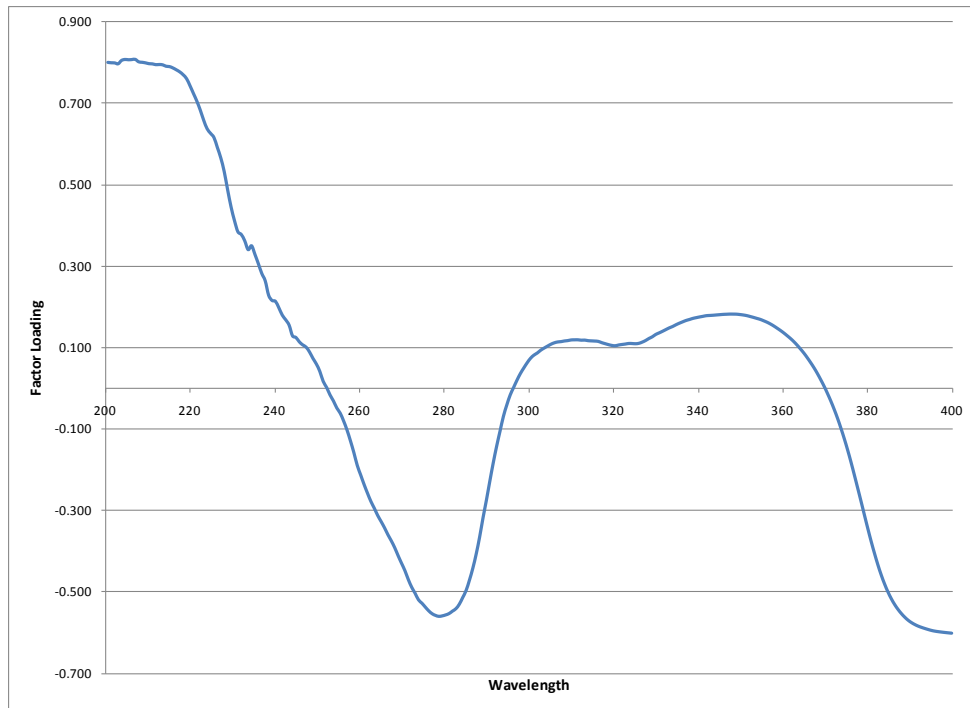


Figure 3.6 Factor loadings for PC2 plotted versus wavelength.

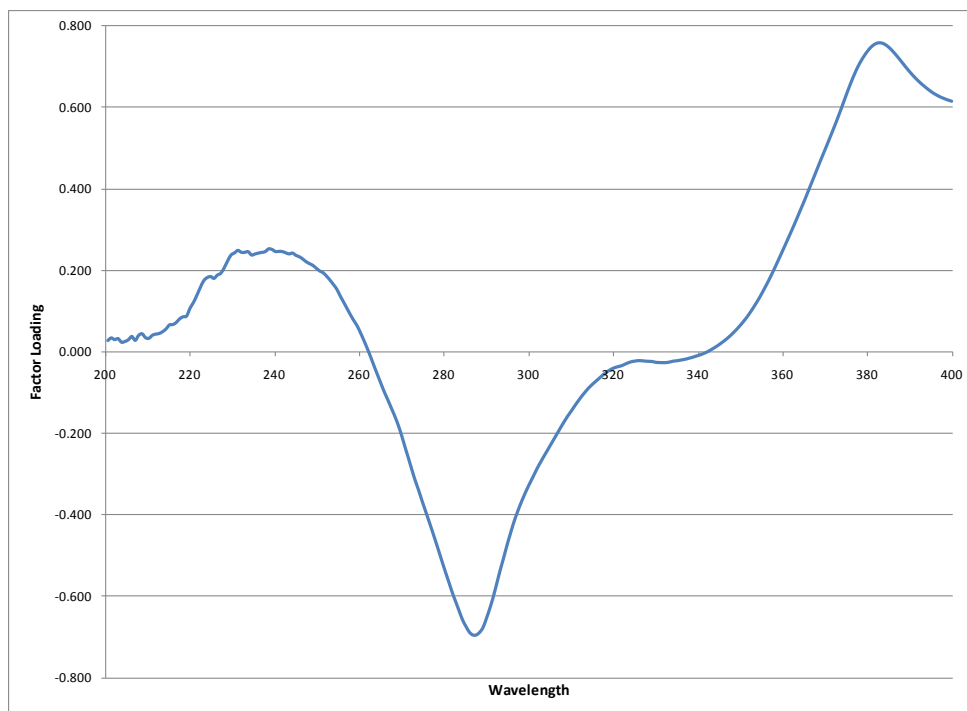


Figure 3.7 Factor loadings for PC3 plotted versus wavelength.

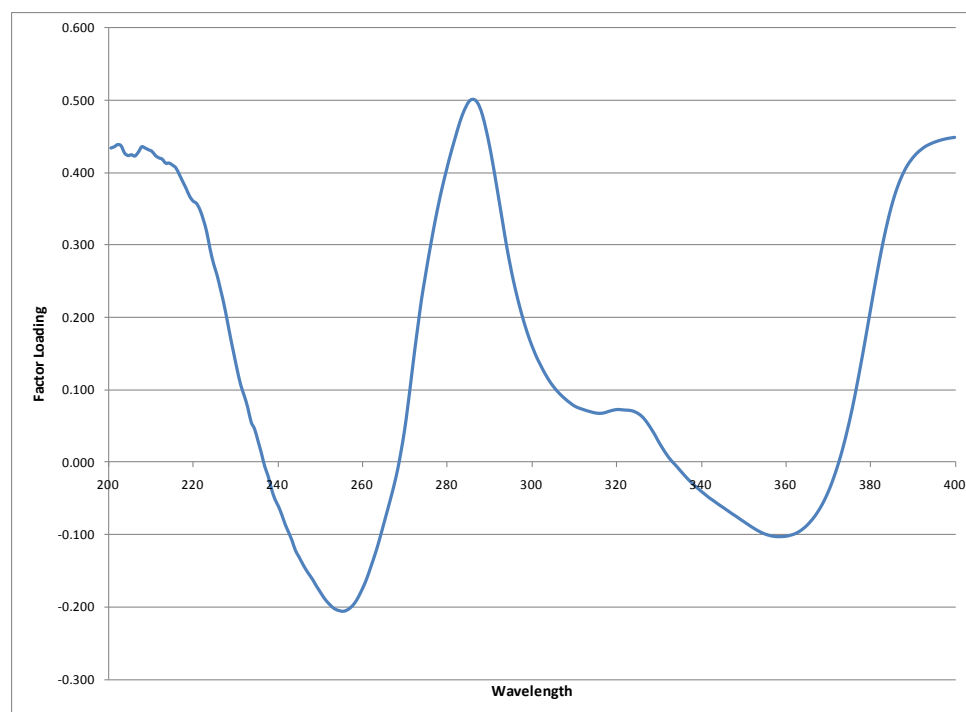


Figure 3.8 Factor loadings for PC4 plotted versus wavelength.

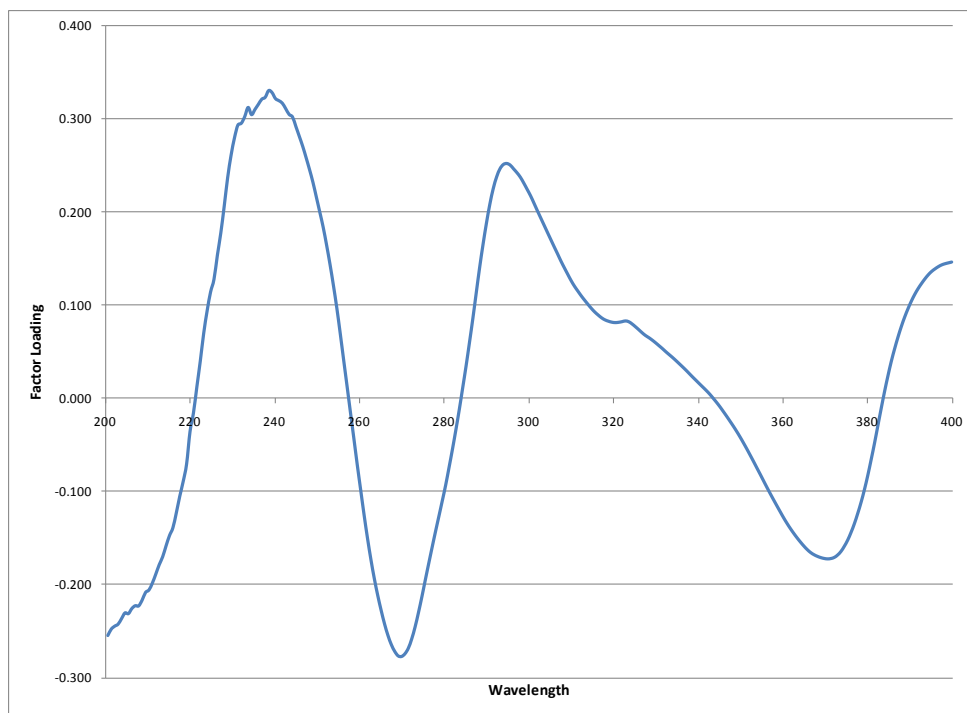


Figure 3.9 Factor loadings for PC5 plotted versus wavelength.

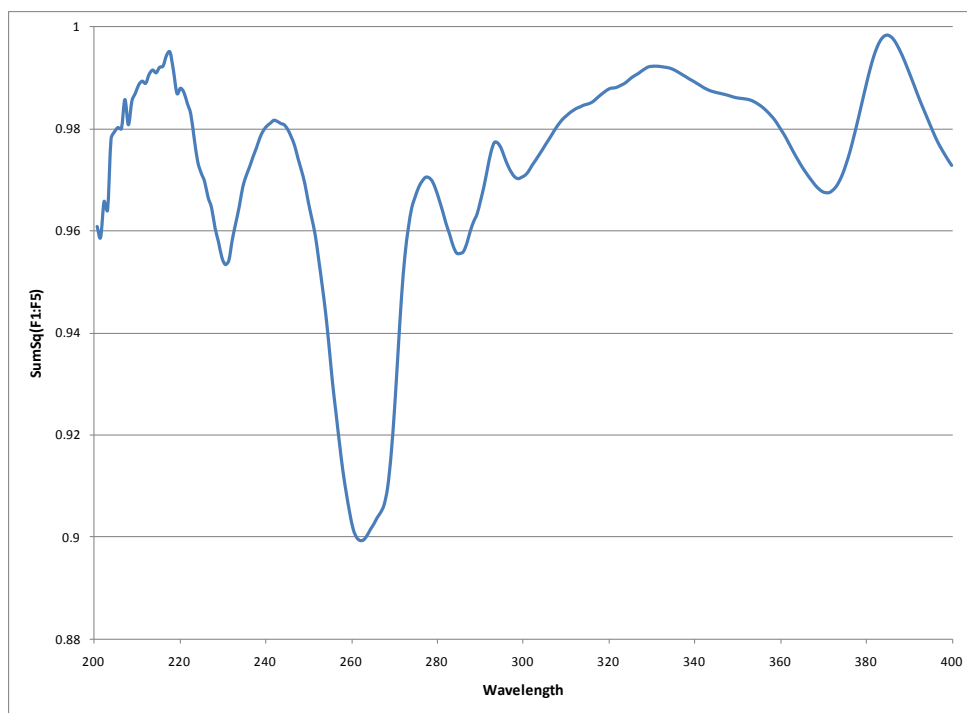


Figure 3.10 Sum of squares of the factor loadings of the first five principal components plotted versus wavelength.

Comparing the factor loadings plot of PC1 to the spectra of the class centroids as shown in Figure 3.11, it appears that the areas of strong negative correlation from PC1 tend to overlap with the peaks found in 230 – 270 nm region of the class centroids. All three of the class centroids contain a peak within this region. The positive correlations from PC1 correspond to features in the 290 – 370 nm region. This region contains the peaks that vary between classes.

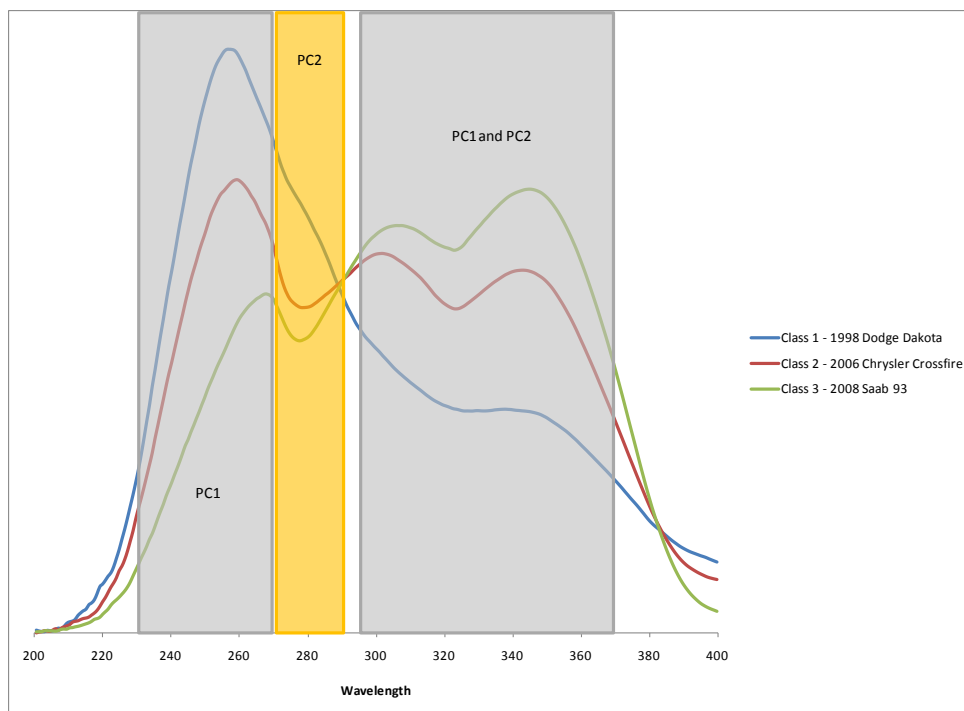


Figure 3.11 Class central objects with PC1 and PC2 regions highlighted.

Figure 3.12 displays the results of DA using the first five principal components. DA was performed with three classes in order to be consistent with AHC results, and 100% of the variance was accounted for in two dimensions. Overlap is very evident between the three classes, which affects the cross-validation results. This is seen in the confusion matrix results in Table 3.2. The samples located along the diagonal indicate those that were correctly classified. Samples outside of the diagonal were incorrectly grouped. When three classes were used, 91.98% of the samples were correctly classified.

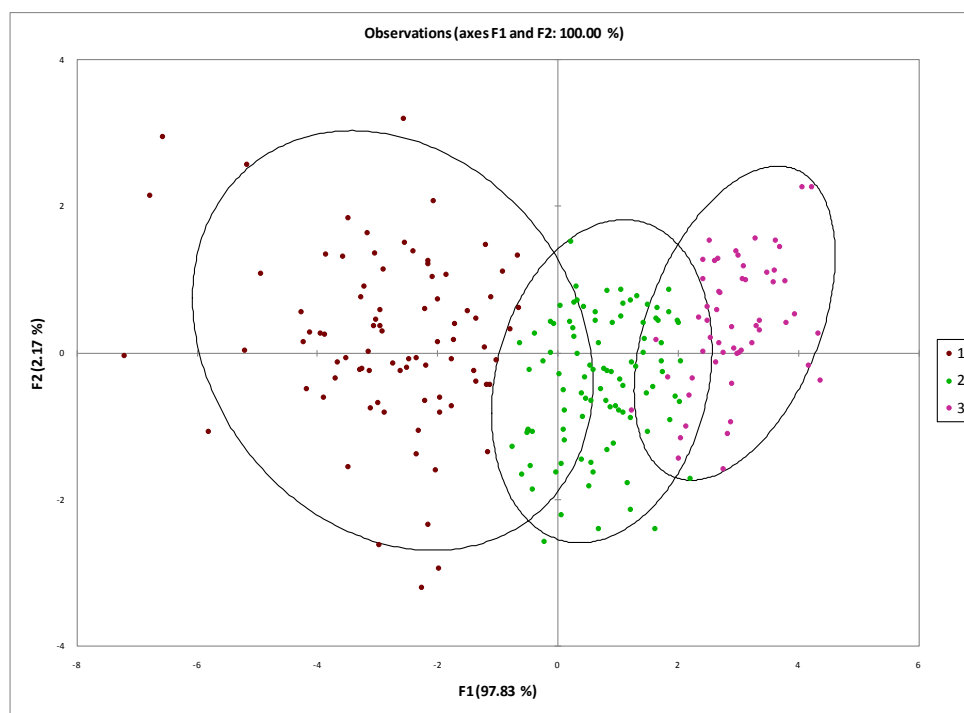


Figure 3.12 Observations plot from DA with three classes.

Table 3.2 Confusion matrix for cross-validation results from DA with three classes.

From \ To	1	2	3	Total	% correct
1	78	7	0	85	91.76%
2	0	92	4	96	95.83%
3	0	8	48	56	85.71%
Total	78	107	52	237	91.98%

The final method of chemometric analysis used on the data set was ANOVA. Where PCA looks for the regions of the spectra that are the most variable, ANOVA finds the areas that are most differentiable. Figure 3.13 shows the ANOVA plot of F values versus wavelength for the MSP spectra. ANOVA analysis finds the peaks around 260 nm to be slightly less significant than those in the 300 – 370 nm region. This corresponds to the regions of negative and positive correlation from the first two principal components as seen in Figure 3.11. Figure 3.14 shows the class central objects with the ANOVA features highlighted.

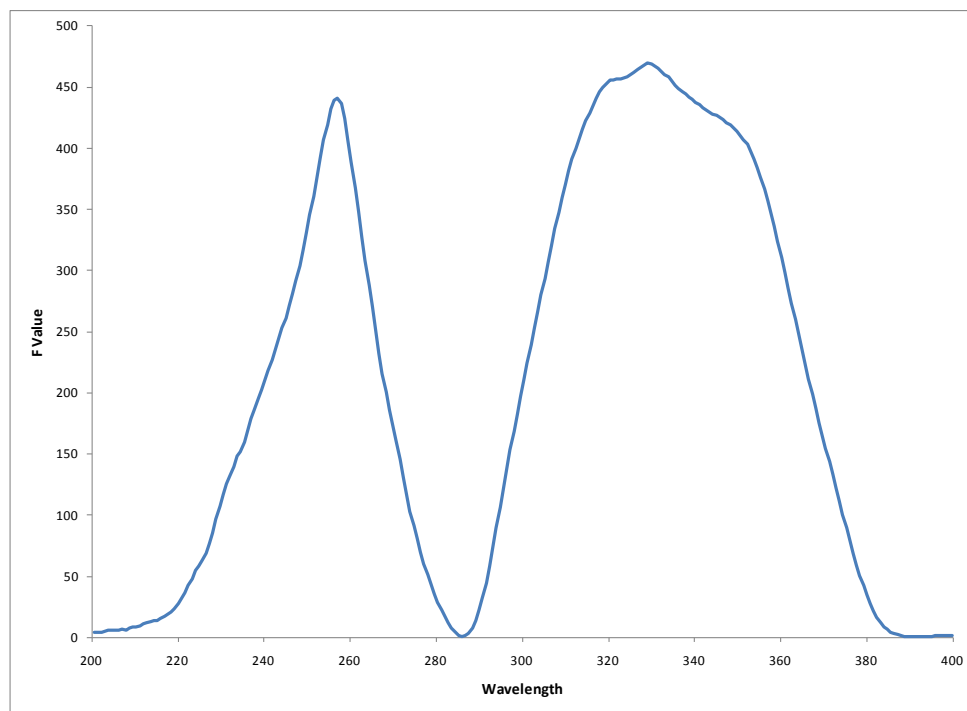


Figure 3.13 F values from ANOVA plotted versus wavenumber.

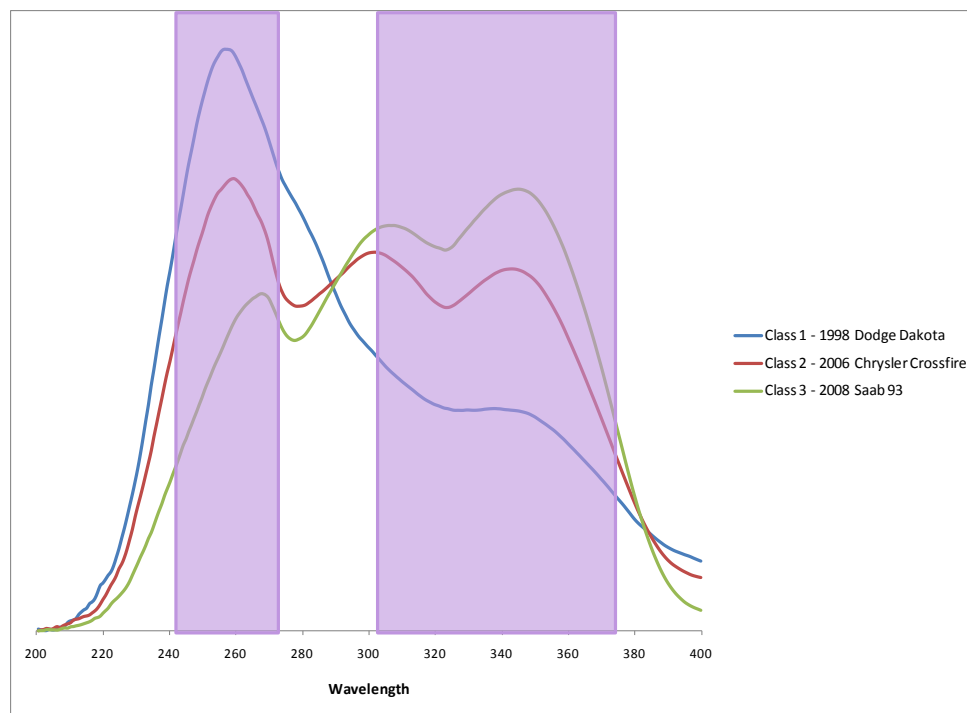


Figure 3.14 Class central objects with ANOVA regions highlighted.



### 3.3.2 External Validation

Thirty of the original samples were run a second time as a blind external validation study. The results are shown in Table 3.3. DA predicted which classes the additional samples should be grouped into, and the correct class was determined by the classification of the original sample. The bold numbers in green represent the number of samples that were correctly classified. The bold numbers in red indicate the numbers of samples that were incorrectly classified. Overall, the external validation correctly assigned 50% of the samples. This was a very poor result. In general, the spectra collected during the external validation were of poor quality for unknown reasons. In comparing the original and external validation spectra of the various samples, it becomes obvious that the additional noise in the external validation was enough to lead to incorrect classifications. Visually, many of the supplemental spectra were very similar to their original counterparts. Figure 3.15 shows one of the external validation samples that was incorrectly classified on the same axes as the original sample. However, some external validation samples were also correctly classified when their spectra did not resemble the original spectra at all. Figure 3.16 is an example of such a case. If better spectra had been collected, the external validation would likely have been much more successful.

Table 3.3 Confusion matrix for the external validation results of the supplemental data from DA.

From/To	1	2	3	Total	% correct
1	<b>4</b>	<b>5</b>	<b>1</b>	10	40.00%
2	0	<b>5</b>	<b>7</b>	12	41.67%
3	0	<b>1</b>	<b>5</b>	6	83.33%
Total	4	11	13	<b>28</b>	<b>50.00%</b>

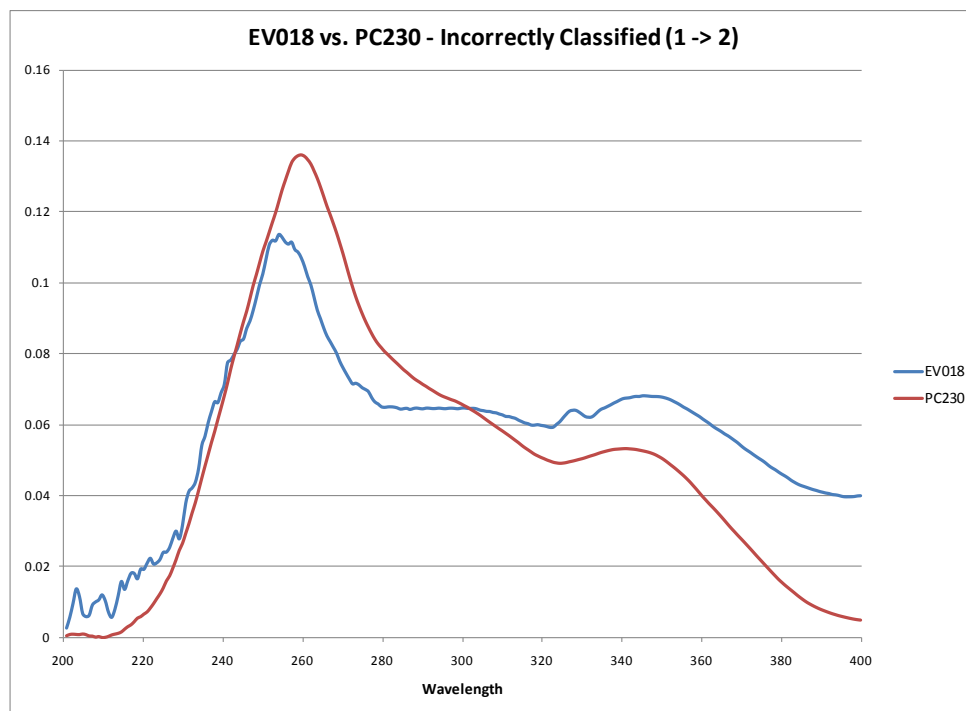


Figure 3.15 External validation sample EV018 compared to original sample PC230. EV018 was incorrectly classified from Class 1 to Class 2.

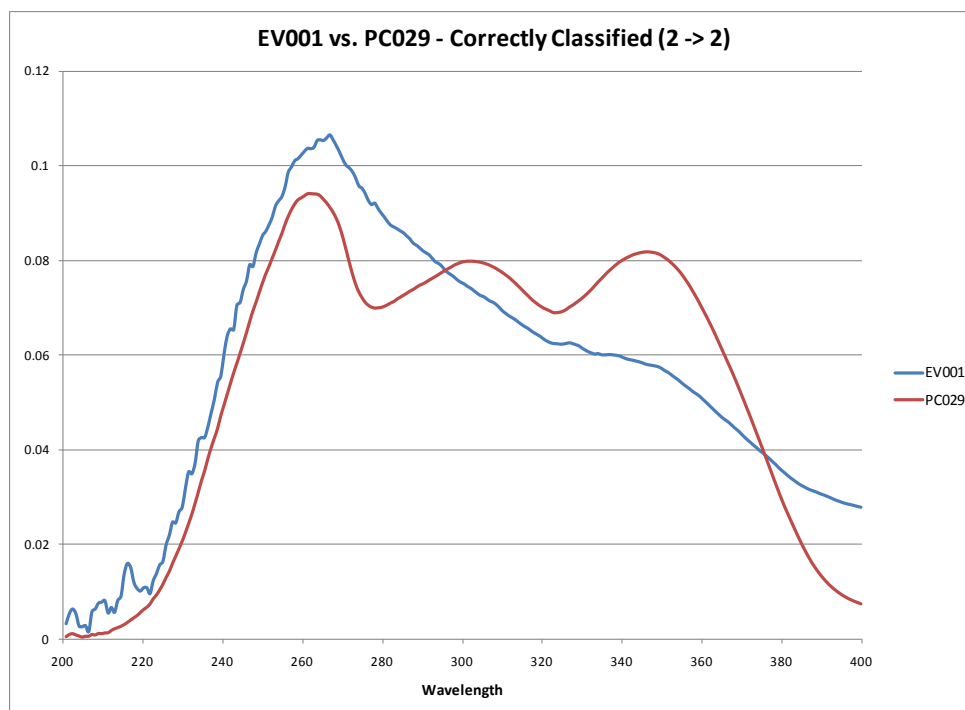


Figure 3.16 External validation sample EV001 compared to original sample PC029. EV001 was correctly classified from Class 2 to Class 2.

### 3.3.3 Formation of Classes

Using chemometric analysis, this study determined that three classes were formed with distinguishable spectra. The next phase of the analysis was to then determine whether make, model, and year of the vehicle affected the formation of these classes. To accomplish this, spectra of clear coats from the same make and model of vehicle but different years were examined.

Figure 3.17 shows two cars of the same make and model but different years that were sorted into different classes. Both vehicles were Ford Tauruses. Year 1996 was sorted into Class 1, while year 2001 was sorted into Class 2. Figure 3.18 shows two cars of the same make and model but different years that were sorted into the same class. The samples were Chevrolet Blazers, year 1996 and 2000, and were both sorted into Class 1. The spectra in Figure 3.17 are obviously quite different from one another, while the spectra in Figure 3.18 nearly overlap. These two figures show that year does not impact the formation of classes.

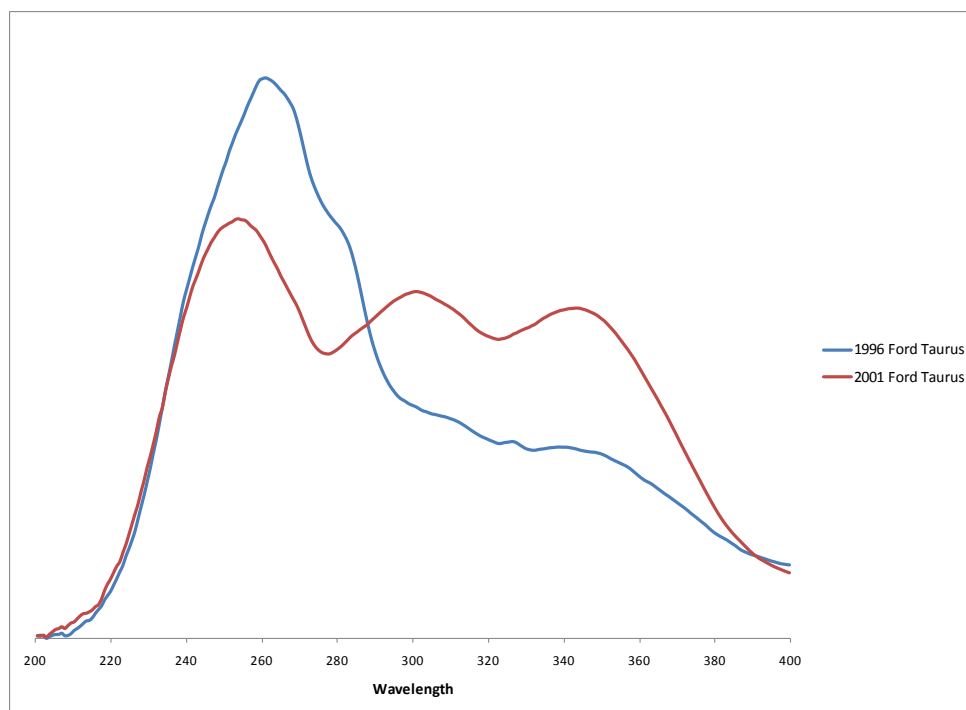


Figure 3.17 Samples of the same make and model but different year placed in different classes.

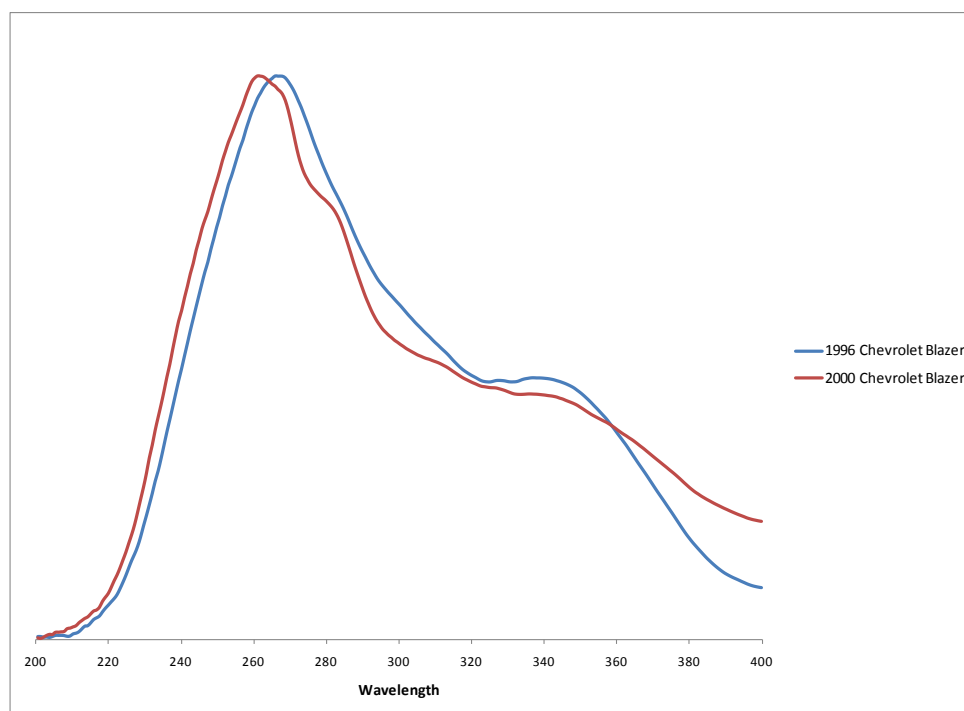


Figure 3.18 Samples of the same make and model but different year placed in the same class.

Figure 3.19 shows two vehicles of the same make, model, and year placed into the same class. The samples in this case were 2001 Hyundai Sonatas, and they were both sorted into Class 2. Figure 3.20 shows two vehicles of the same make, model, and year placed into different classes. The two samples were 1993 Ford Tauruses, and one was sorted into Class 2, while the other was sorted into Class 1. It becomes evident that make and model of vehicle also do not affect the classifications of automotive clear coats.

As with the Raman study, examining the types of vehicles in each class further proved that make, model, and year did not affect the classification of clear coats. Some models fell into multiple classes, such as the Ford Taurus. Many makes had vehicles in all three classes, such as Chrysler, GM, Honda, and Toyota. In general, it appears that no correlation exists between make, model, or year and classification of the clear coat's MSP spectrum.

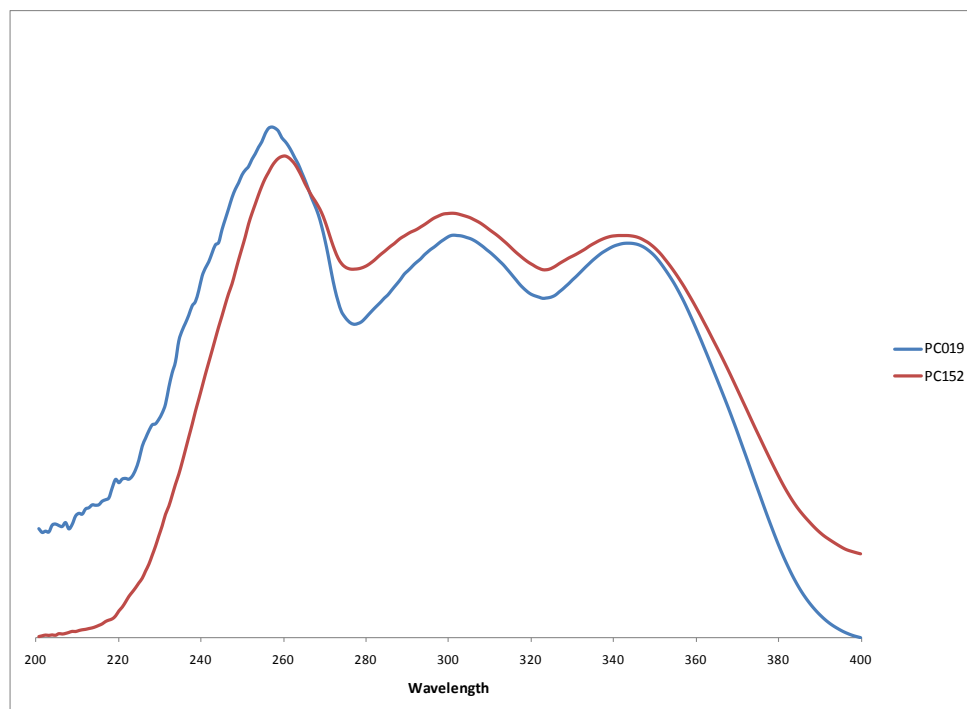


Figure 3.19 Samples of the same make, model, and year placed in the same class.

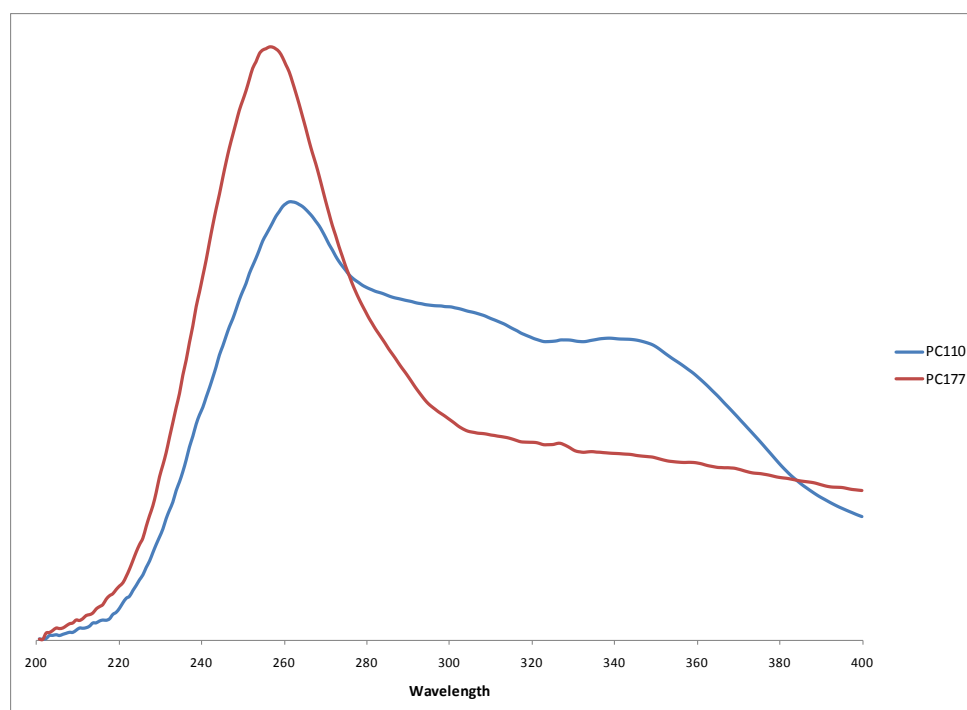


Figure 3.20 Samples of the same make, model, and year placed in different classes.

### 3.3.4 Known UV Absorbers

MSP spectra of three known UV absorbers are shown in Figure 3.21. Tinuvin 292 is shifted a bit more to the left than the peaks of most of the MSP spectra, but the peaks of the others are similar to the regions in which some of the class centroids' peaks appear, as seen in the grey regions of Figure 3.22. It is possible that 2,4-DHBP or 4-DD-2-HBP could be present in the clear coat samples. It is unlikely that Tinuvin 292 is present in the clear coat samples based on its spectrum.

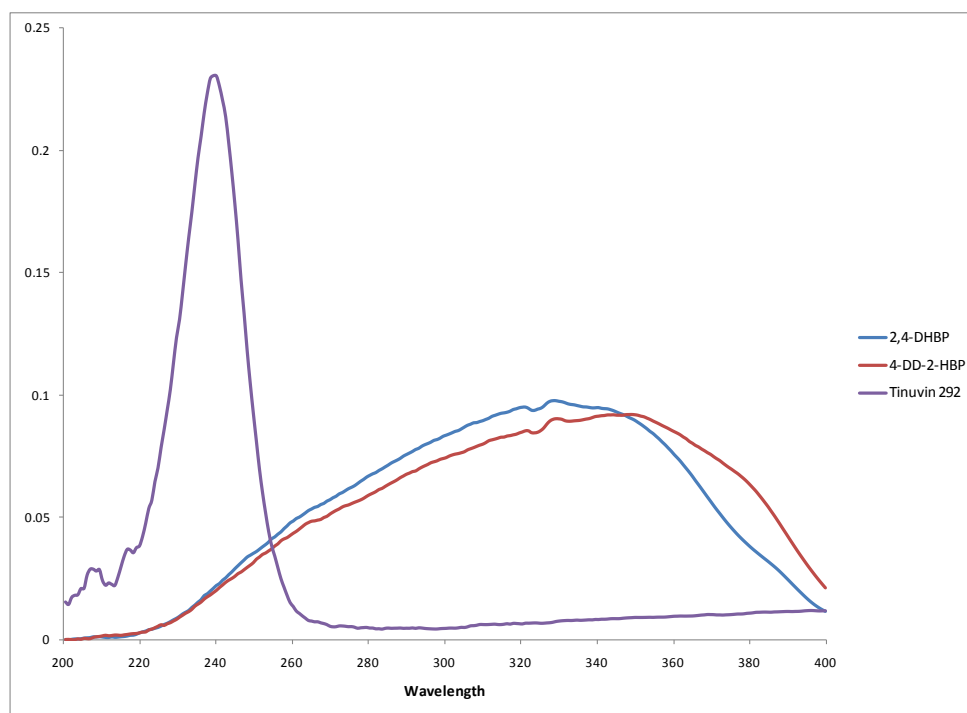


Figure 3.21 MSP spectra of known UV absorbers.

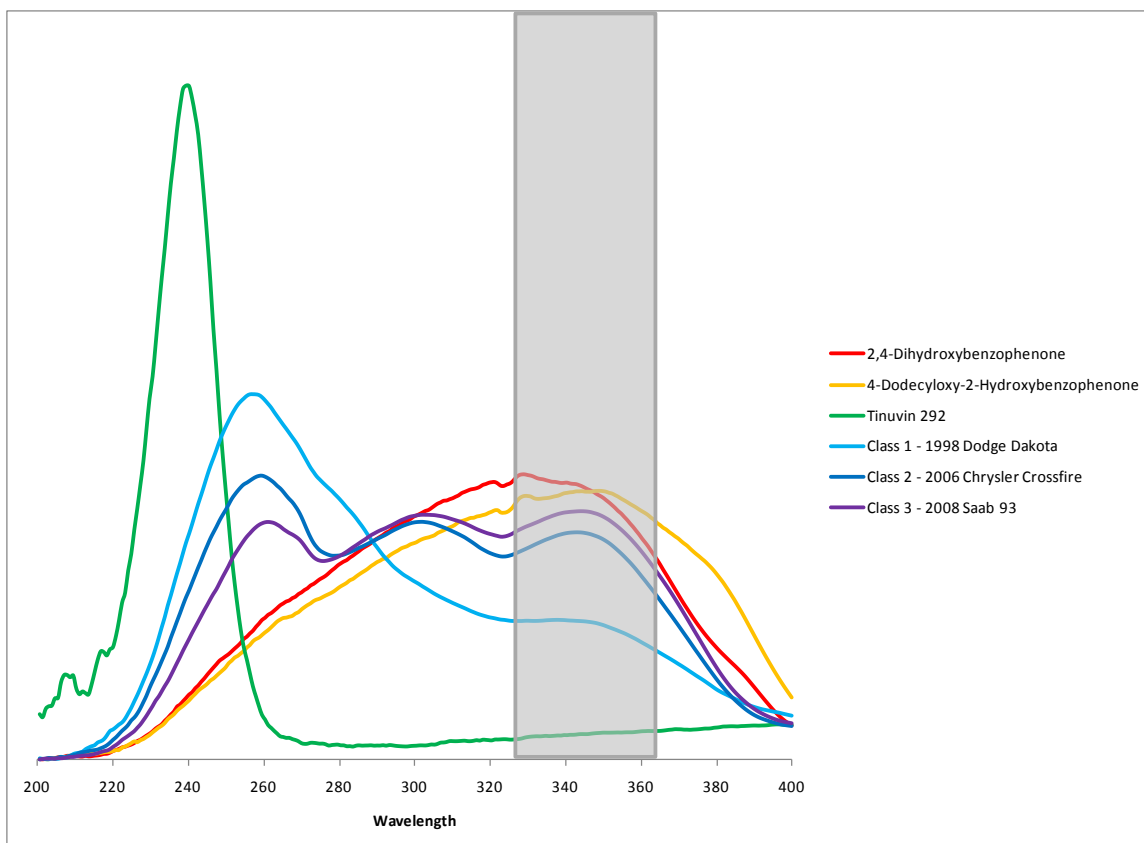


Figure 3.22 MSP spectra of known UV absorbers compared to class central objects.

### 3.3.5 Limitations of the Study

As many of the limitations of this study are not a result of the instrumental technique employed, rather due to the samples themselves, a discussion of the limitations is found in section 2.3.5.

### 3.4 Conclusions

MSP has been previously proven to be effective in the analysis of automotive clear coat samples.<sup>1</sup> Sample preparation is, as with Raman, minimal and easily accomplished.

Chemometric analysis of the clear coats using AHC, PCA, and DA resulted in several findings. Three distinct classes formed within the sample set. The central objects of these classes show that the areas of the spectra with the highest variability between the classes appear within the 300 – 370 nm region. These classes were accurately differentiated using cross-validation, but poor data resulted in a very poor external validation outcome. As in the Raman study, no correlations between make, model, and year were found.



#### CHAPTER 4. CONCLUSIONS OF THE STUDY











After all of the data was collected and analyzed in this study, it became important to determine whether the AHC groups for the Raman and MSP contained the same vehicles between the two methods. Table 4.1 shows the comparison of AHC groups between Raman and MSP. It appears that the groups for both instrumental techniques contain very different members. This could be useful in identifying clear coats in the future, especially if other instrumental techniques have still different groupings. Finding a clear coat that falls into, for example, Raman class 1 and MSP class 2 might limit the possible sources and give more weight to the evidentiary value of the clear coat sample.

The research conducted in this work demonstrates the behavior of a large and varied data set under both Raman and MSP. Although no correlations between vehicle make, model, and year and clear coat spectra were found, both instrumental techniques could be valuable in forensic case work. It would not be necessary for a lab to purchase either instrument, but if the instruments were available, their existing uses could be expanded to include clear coat analysis. While this work shows that a forensic paint examiner will not be able to attribute a clear coat back to a particular source on its own, Raman and MSP could assist with a questioned versus known analysis.

Table 4.1 Members of Raman and MSP AHC groups.

Raman							MSP								
1			2				3	1			2			3	
PC001	PC081	PC218	PC020	PC112	PC203	PC248	PC095	PC001	PC108	PC201	PC002	PC113	PC217	PC007	PC229
PC002	PC082	PC220	PC023	PC115	PC204	PC250	PC096	PC003	PC111	PC208	PC009	PC115	PC218	PC010	PC233
PC003	PC085	PC221	PC024	PC117	PC205	PC251	PC098	PC008	PC117	PC213	PC017	PC116	PC219	PC013	PC234
PC006	PC087	PC253	PC025	PC118	PC206	PC252	PC099	PC011	PC121	PC214	PC019	PC118	PC221	PC014	PC235
PC008	PC088		PC026	PC120	PC207	PC254	PC101	PC018	PC124	PC230	PC021	PC131	PC222	PC015	PC236
PC009	PC091		PC027	PC121	PC208	PC257	PC102	PC020	PC125	PC257	PC022	PC133	PC223	PC016	PC237
PC010	PC092		PC028	PC126	PC209	PC258	PC103	PC023	PC126	PC264	PC026	PC134	PC224	PC027	PC238
PC011	PC093		PC029	PC128	PC210	PC259	PC132	PC024	PC127	PC265	PC029	PC138	PC231	PC028	PC239
PC013	PC104		PC030	PC130	PC211	PC260	PC133	PC025	PC128	PC266	PC033	PC140	PC232	PC032	PC240
PC016	PC107		PC032	PC131	PC212	PC261	PC134	PC030	PC129		PC035	PC141	PC241	PC041	PC242
PC017	PC110		PC035	PC149	PC213	PC263	PC135	PC031	PC130		PC037	PC145	PC243	PC043	PC246
PC018	PC111		PC036	PC150	PC214	PC264	PC136	PC034	PC132		PC038	PC146	PC244	PC075	PC248
PC019	PC113		PC037	PC151	PC216	PC265	PC138	PC036	PC135		PC042	PC148	PC245	PC077	PC251
PC021	PC116		PC043	PC152	PC219	PC266	PC139	PC039	PC136		PC046	PC150	PC247	PC078	PC254
PC022	PC122		PC044	PC167	PC222	PC267	PC140	PC040	PC143		PC048	PC152	PC250	PC091	PC258
PC031	PC124		PC046	PC171	PC223	PC268	PC141	PC044	PC144		PC049	PC153	PC252	PC120	PC259
PC033	PC125		PC048	PC172	PC224		PC142	PC052	PC147		PC050	PC154	PC253	PC122	PC261
PC034	PC127		PC053	PC173	PC226		PC153	PC053	PC149		PC054	PC159	PC260	PC139	PC267
PC038	PC129		PC055	PC174	PC227		PC154	PC055	PC151		PC057	PC163	PC263	PC142	
PC039	PC143		PC057	PC176	PC229		PC155	PC056	PC155		PC058	PC164	PC268	PC165	
PC040	PC144		PC058	PC178	PC230		PC156	PC061	PC156		PC060	PC170		PC166	
PC042	PC145		PC059	PC179	PC231		PC157	PC062	PC157		PC068	PC173		PC168	
PC049	PC146		PC060	PC181	PC232		PC158	PC063	PC158		PC070	PC179		PC172	
PC050	PC147		PC061	PC182	PC233		PC159	PC065	PC160		PC072	PC182		PC175	
PC052	PC148		PC062	PC183	PC234		PC160	PC066	PC161		PC082	PC183		PC185	
PC054	PC166		PC065	PC185	PC235		PC161	PC067	PC162		PC086	PC188		PC186	
PC056	PC168		PC068	PC186	PC236		PC162	PC069	PC167		PC092	PC189		PC187	
PC063	PC169		PC074	PC187	PC237		PC163	PC080	PC169		PC093	PC190		PC192	
PC066	PC170		PC080	PC189	PC238		PC164	PC081	PC171		PC094	PC191		PC195	
PC067	PC175		PC083	PC192	PC239		PC165	PC083	PC174		PC099	PC194		PC197	
PC069	PC177		PC086	PC193	PC240			PC087	PC176		PC100	PC202		PC200	
PC070	PC180		PC094	PC194	PC241			PC095	PC177		PC102	PC203		PC205	
PC072	PC188		PC097	PC195	PC242			PC096	PC178		PC103	PC204		PC206	
PC075	PC190		PC100	PC198	PC243			PC097	PC180		PC105	PC207		PC209	
PC076	PC191		PC105	PC199	PC244			PC098	PC181		PC107	PC211		PC210	
PC077	PC197		PC106	PC200	PC245			PC101	PC193		PC109	PC212		PC220	
PC078	PC215		PC108	PC201	PC246			PC104	PC198		PC110	PC215		PC226	
PC079	PC217		PC109	PC202	PC247			PC106	PC199		PC112	PC216		PC227	

Legend:

									
Raman 1	Raman 1	Raman 1	Raman 2	Raman 2	Raman 2	Raman 3	Raman 3	Raman 3	
MSP 1	MSP 2	MSP 3	MSP 1	MSP 2	MSP 3	MSP 1	MSP 2	MSP 3	

## CHAPTER 5. FUTURE DIRECTIONS

The work in this research has been both a basis for future research and an expansion on past research. Analysis of clear coats by Raman and MSP has only been conducted on a very limited scale previously. In the future, the investigation of clear coats should be expanded to other instrumental techniques, such as Py-GC-MS, FTIR, and DESI, to find out if the chemometric groupings remain the same. FTIR research is being currently conducted. With these same samples analyzed by multiple methods, it should be determined whether the classes are the same over all of the methods (i.e., whether they contain the same samples).

It might be interesting as well to see if surface-enhanced Raman scattering (SERS) yields any more information in the spectra of clear coats. The fluorescence and signal intensity issues that SERS aims to correct were not issues in this study, however, so unless a significant amount of new information is available with SERS analysis, it may prove to be unnecessary. Some available SERS substrates are silver or copper foils etched with nitric acid,<sup>41</sup> or glass slides etched in chromic acid and covered with island films of silver.<sup>42</sup> The clear coats themselves may need to be dissolved in some sort of solvent, such as dimethylformamide (DMF)<sup>41</sup> or ethanol,<sup>42</sup> then deposited on the substrate.

It would also be important to investigate why the classes form in the manner that they do. Some of the potential factors could include the types and concentrations of UV absorbers and binders present in the various samples,<sup>3</sup> and the effects of weathering and migration on these over time. However, in order to accomplish some of this, clear coat and/or automobile manufacturers would need to provide information

about their UV absorbers in order to obtain a larger sample of clear coat components to run on the various instruments. Raman peak assignments might also prove useful in discovering which molecular components of the clear coats seem to be most important in classifying the clear coat samples. Correlating spectra with UV absorbers and identifying the absorbers in each class for each analytical method would also be useful in this determination.

It would be useful to know the impact, if any, of vehicle color on the spectra of the clear coats. This could be performed using the Raman and MSP data from this work and the general color classifications of each vehicle used in the study. The vehicles could also be segregated based on their color and chemometrics could be performed on all of the samples of a single color. This would address the fact that, in the course of normal casework, a clear coat from a red vehicle would not be compared to a clear coat from a silver vehicle if the vehicles' base coats were present. The two would be unlikely to come from the same source. A study of this type could later be expanded to include the other instrumental techniques that might be used.

A comparison of smoothing methods might be conducted on at least the Raman data to determine whether smoothing negatively impacted the classification of the clear coats during both the construction of the classification model and the external validations phases of the study.

A more comprehensive time study could also be completed to attempt to more adequately determine the effects of actual wear and weathering on the clear coats. If possible, this could include making paint peels directly from vehicles over the course of many months.

The external validation study should be redone in order to determine the sources of excess noise in the spectra. For example, the clear coat peels should be redone using microscalpels that have been used fewer times. Using the microscalpels more than 10 times should perhaps be avoided, especially in the case of MSP analysis.

Finally, actual forensic procedures for clear coat analysis should be established. For instance, if an analyst were using both Raman spectroscopy and MSP in casework,

which method should be done first? How many replicates should be run from the known and unknown? Should chemometric methods be used on real cases? If so, which ones?

## LIST OF REFERENCES

## LIST OF REFERENCES

1. Liszewski, E.A., et al. Characterization of automotive paint clear coats by ultraviolet absorption microspectrophotometry with subsequent chemometric analysis. *Applied Spectroscopy* 2010, 64 (10), 1122 – 1125.
2. Ryland, S., et al. Discrimination of 1990s original automotive paint system: a collaborative study of black nonmetallic base coat/clear coat finishes using infrared spectroscopy. *Journal of Forensic Sciences* 2001, 46 (1), 31 – 45.
3. Stoecklein, W., and Fujiwara, H. The examination of UV-absorbers in 2-coat metallic and non-metallic automotive paints. *Science & Justice* 1999, 39 (3), 118 – 195.
4. Edmonstone, G., et al. An assessment of the evidential value of automotive paint comparisons. *Canadian Society of Forensic Sciences Journal* 2004, 37 (3), 147 – 153.
5. Scientific Working Group on Materials Analysis (SWGMAT). Forensic Paint Analysis and Comparison Guidelines. In *Forensic Science Communications*. 1999, 1 (2).
6. De Gelder, J., et al. Forensic analysis of automotive paints by Raman spectroscopy. *Journal of Raman Spectroscopy* 2005, 36 (11), 1059 – 1067.
7. Giang, Y., et al. Two complementary approaches to the full identification of automobile paints. *Proceedings of the 27<sup>th</sup> Annual IEEE International Carnahan Conference on Security Technology, Ottawa, Canada, Oct. 13-15<sup>th</sup>, 1993*. 259 – 262.
8. Kuptsov, A.H. Applications of Fourier Transform Raman Spectroscopy in Forensic Science. *Journal of Forensic Sciences* 1994, 39 (2), 305 – 318.
9. Wheeler, B. P.; Wilson, L. J., UV-Visible-NIR Microspectrophotometry. In *Practical Forensic Microscopy: A Laboratory Manual*. John Wiley & Sons, Ltd: New York, 2008.

10. Cousins, D.R., et al. The use of microspectrophotometry for the identification of pigments in small paint samples. *Forensic Science International* 1984, 24, 183 – 196.
11. Kopchick, K.A., et al. Color analysis of apparently achromatic automotive paints by visible microspectrophotometry. *Journal of Forensic Sciences* 2006, 51 (2), 340 – 343.
12. Morgan, S.L., and Bartick, E.G. Discrimination of forensic analytical chemical data using multivariate statistics. In: Blackledge, R.D., ed. *Forensic Analysis on the Cutting Edge: New Methods for Trace Evidence Analysis*. John Wiley & Sons, Inc.: New York, 2007.
13. Brereton, R.G. *Chemometrics: Applications of Mathematics and Statistics to Laboratory Systems*. Ellis Horwood Limited: Chichester, England, 1990.
14. National Research Council. *Strengthening Forensic Science in the United States: a path forward*. National Academies Press: Washington, DC, 2009.
15. Johnson, R., and Wichern, D. *Applied Multivariate Statistical Analysis*. Prentice Hall: Englewood Cliffs, NJ, 1982.
16. Brereton, R.G. *Chemometrics: Data Analysis for the Laboratory and Chemical Plant*. John Wiley & Sons, Inc.: Chichester, England, 2003.
17. Beebe, K.R., et al. *Chemometrics: A Practical Guide*. John Wiley & Sons, Inc.: New York, 1998.
18. Kramer, R. *Chemometric Techniques for Quantitative Analysis*. Marcel Dekker, Inc.: New York, 1998.
19. Thanasoulas, N.C., et al. Multivariate chemometrics for the forensic determination of blue ball-point pen inks based on their Vis spectra. *Forensic Science International* 2003, 138 (1 – 3), 75 – 84.
20. Thanasoulas, N.C., et al. Application of multivariate chemometrics in forensic soil discrimination based on the UV-Vis spectrum of the acid fraction of humus. *Forensic Science International* 2002, 130 (2 – 3), 73 – 82.
21. Goodpaster, J.V., et al. Identification and comparison of electrical tapes using instrumental and statistical techniques: I. Microscopic surface texture and elemental composition. *Journal of Forensic Sciences* 2007, 52 (3), 610 – 629.



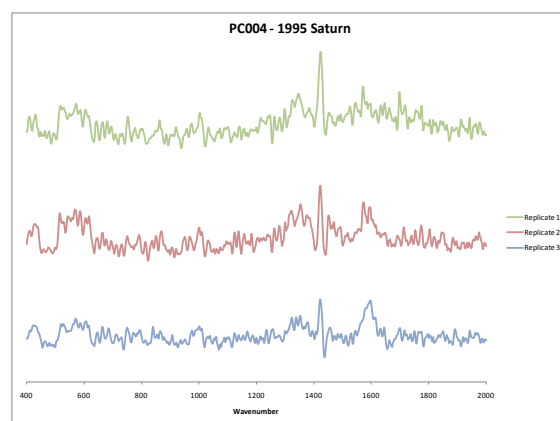
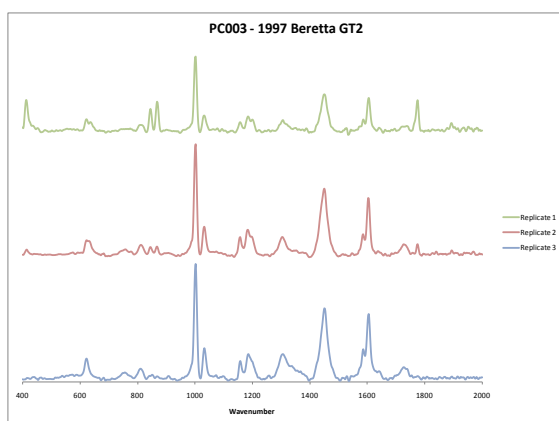
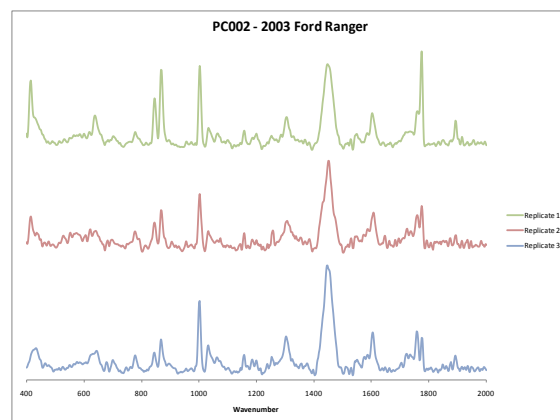
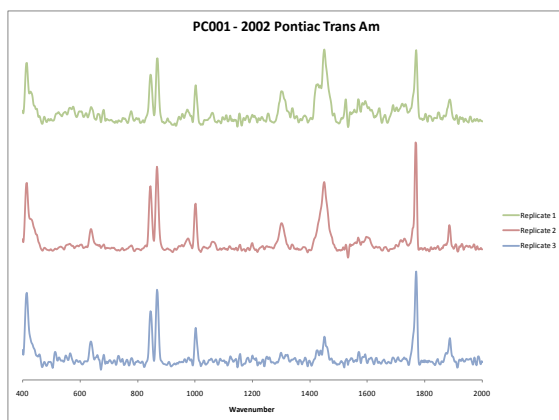
22. Goodpaster, J.V., et al. Identification and comparison of electrical tapes using instrumental and statistical techniques: II. Organic composition of the tape backing and adhesive. *Journal of Forensic Sciences* 2009, 54 (2), 328 – 338.
23. Mat Desa, W.N.S., et al. Application of unsupervised chemometric analysis and self-organizing feature map (SOFM) for the classification of lighter fuels. *Analytical Chemistry* 2010, 82, 6395 – 6400.
24. Klemenc, S. In common batch searching of illicit heroin samples – evaluation of data by chemometric methods. *Forensic Science International* 2001, 115, 43 – 52.
25. StatSoft, Inc. Principal Components and Factor Analysis. In: *Electronic Statistics Textbook*. StatSoft: Tulsa, OK, 2011. WEB: <http://www.statsoft.com/textbook/>.
26. Miller, J.C., and Miller, J.N. *Statistics for Analytical Chemistry*. 2<sup>nd</sup> ed. Ellis Horwood Limited: Chichester, England, 1988.
27. Primera-Pedrozo, O.M., et al. High explosives mixtures detection using fiber optics coupled: grazing angle probe/Fourier transform reflection absorption infrared spectroscopy. *Sensing and Imaging* 2008, 9, 27 – 40.
28. May, C.D., and Watling, R.J. The development of analytical and interpretational protocols to facilitate the provenance establishment of polycarbonate headlamp lens material. *Journal of Forensic Sciences* 2011, 56 (S1), S47 – S57.
29. Barrett, J.A., et al. Forensic discrimination of dyed hair color: II. Multivariate statistical analysis. *Journal of Forensic Sciences* 2011, 56 (1), 95 – 101.
30. StatSoft, Inc. ANOVA/MANOVA. In: *Electronic Statistics Textbook*. StatSoft: Tulsa, OK, 2011. WEB: <http://www.statsoft.com/textbook/>.
31. Anderson, R.L. *Practical Statistics for Analytical Chemists*. Van Nostrand Reinhold: New York, 1987.
32. Bell, S.E.J., et al. Composition profiling of seized ecstasy tablets by Raman spectroscopy. *Analyst* 2000, 125, 1811 – 1815.
33. Buchanan, H.A.S., et al. Role of five synthetic reaction conditions on the stable isotopic composition of 3,4-methylenedioxymethamphetamine. *Analytical Chemistry* 2010, 82, 5484 – 5489.

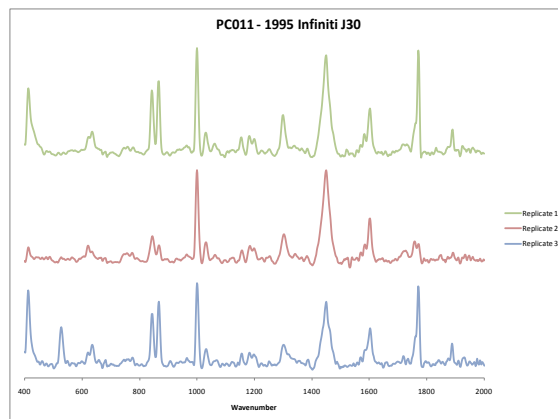
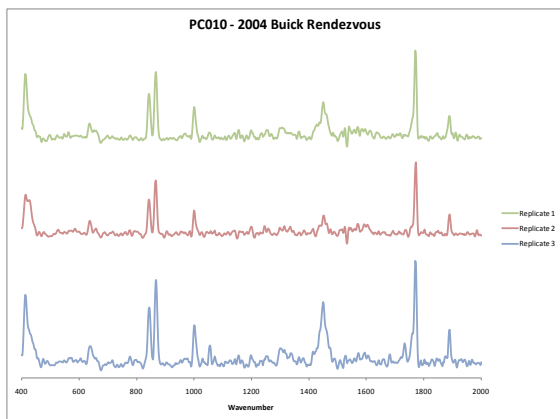
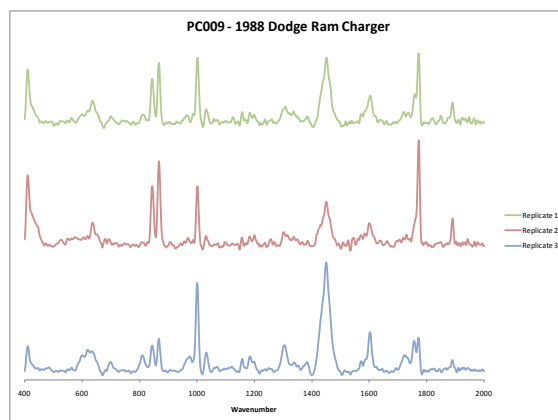
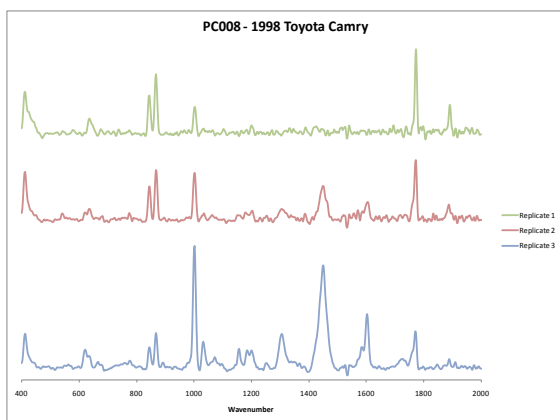
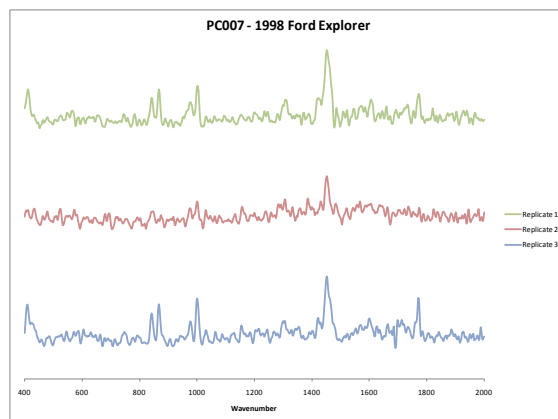
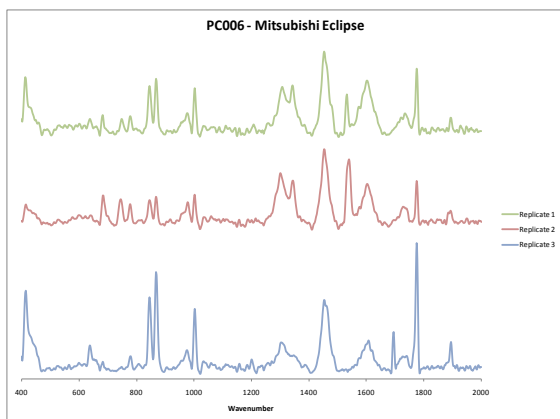
34. McGaw, E.A., et al. Determination of trace elemental concentrations in document papers for forensic comparison using inductively coupled plasma-mass spectrometry. *Journal of Forensic Sciences* 2009, 54 (5), 1163 – 1170.
35. Sahajpal, V., et al. Microscopic hair characteristics of a few bovid species listed under Schedule-I of Wildlife (Protection) Act 1972 of India. *Forensic Science International* 2009, 189, 34 – 45.
36. Barnett, N. W., et al. *Industrial Analysis with Vibrational Spectroscopy*. The Royal Society of Chemistry: Cambridge, UK, 1997.
37. Bell, S. *Forensic Chemistry*. Prentice Hall: Upper Saddle River, NJ, 2005.
38. Linstrom, P. J. and Mallard, W. G., Eds. *NIST Chemistry WebBook, NIST Standard Reference Database Number 69*. National Institute of Standards and Technology: Gaithersburg, MD, 2011. WEB: <http://webbook.nist.gov/chemistry/>.
39. Ciba Specialty Chemicals. Ciba™ Tinuvin 292 MSDS. Ciba Specialty Chemicals: Basel, Switzerland, 2000. WEB: <http://talasonline.com/photos/instructions/tinuvin292.pdf>.
40. Socrates, G. *Infrared and Raman Characteristic Group Frequencies: Tables and Charts*. 3<sup>rd</sup> ed. John Wiley & Sons, Ltd.: Chichester, England, 2001.
41. Xue, G. et al. Surface-enhanced Raman scattering study of polymer on metals. III. Chemisorbed polybenzimidazole and its corrosion-inhibiting properties at high temperature. *Journal of Polymer Science: Part B: Polymer Physics* 1992, 30, 1097 – 1102.
42. Roth, P. G. and Boerio, F. J. Surface-enhanced Raman scattering from poly(4-vinyl pyridine). *Journal of Polymer Science: Part B: Polymer Physics* 1987, 25, 1923 – 1933.

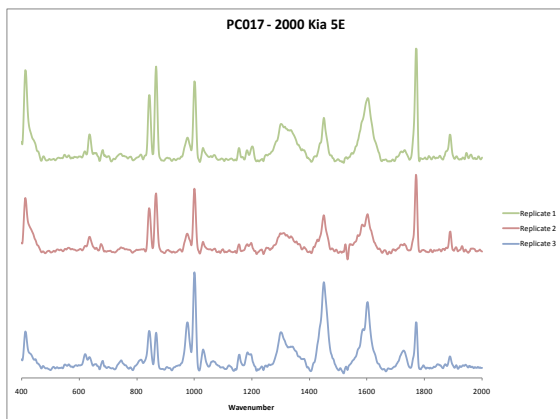
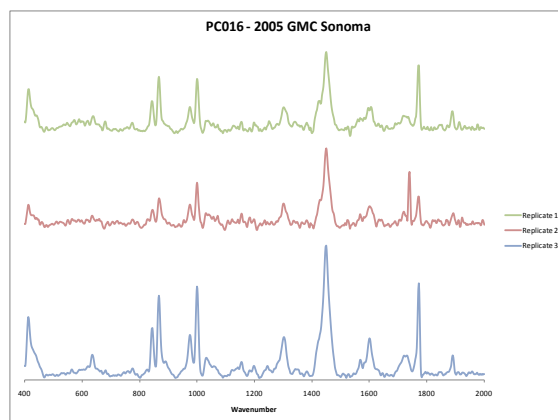
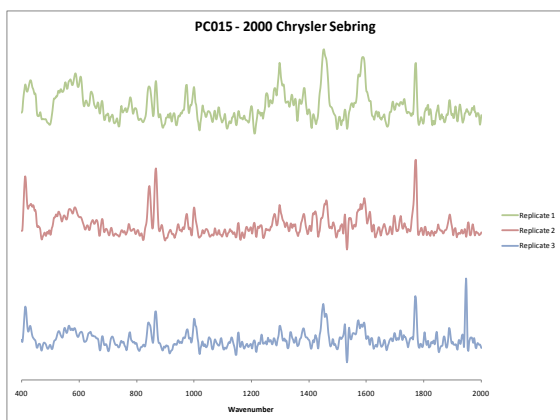
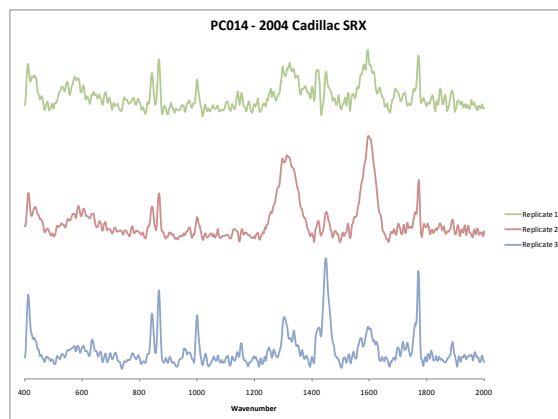
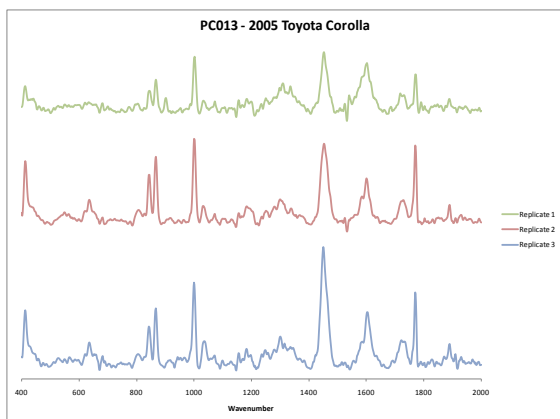
## APPENDICES

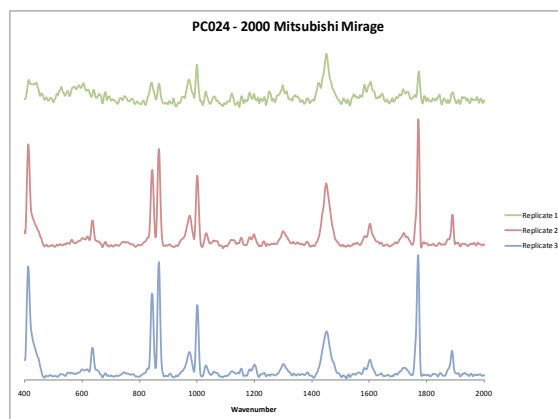
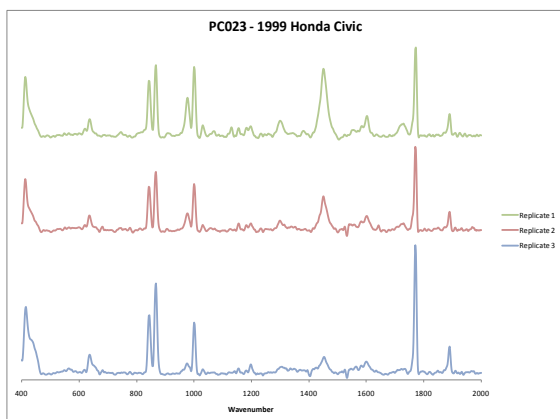
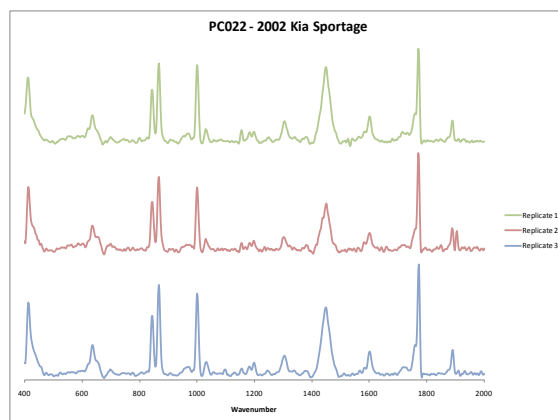
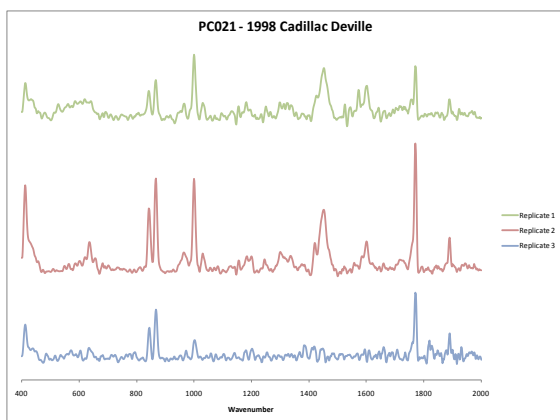
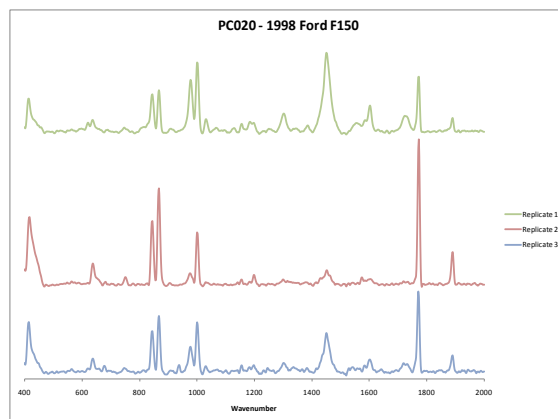
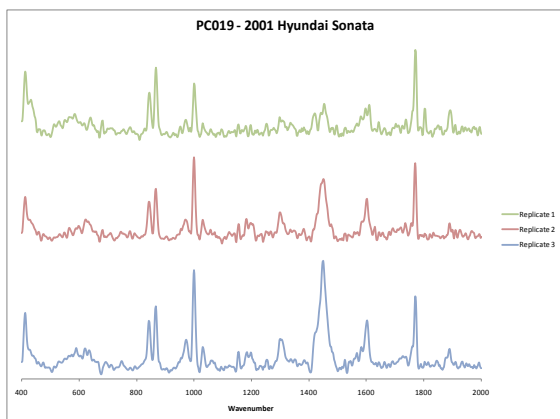
## Appendix A. Clear Coat Spectra by Raman Spectroscopy

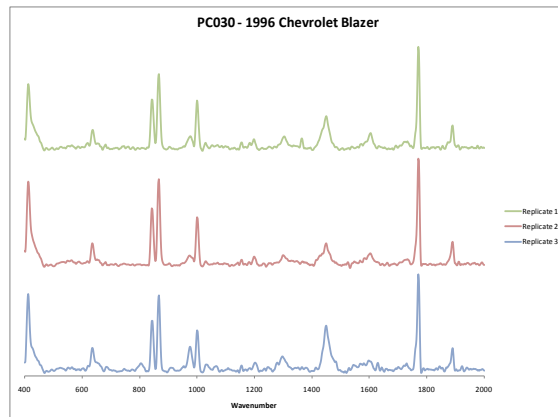
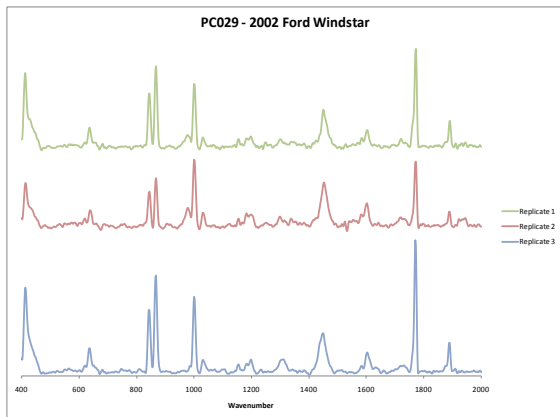
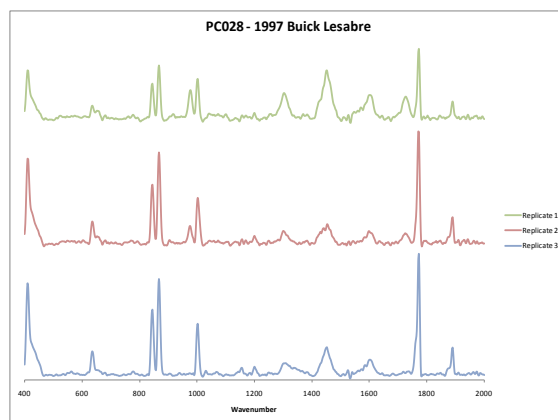
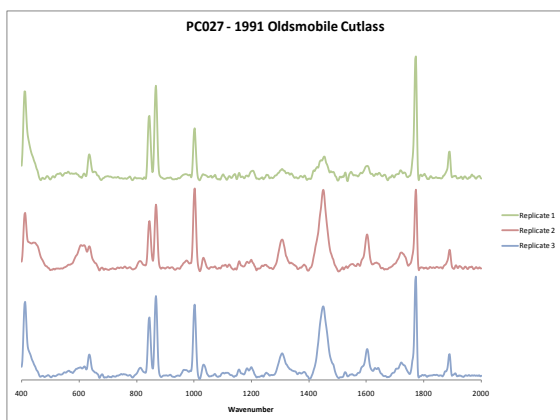
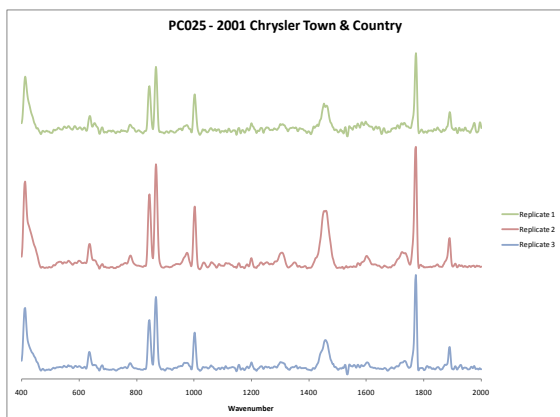
### A.1 Training Samples



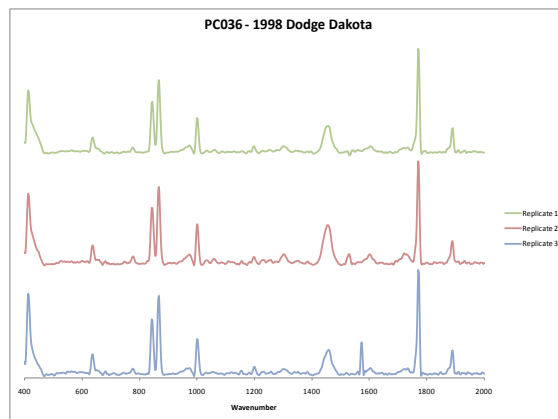
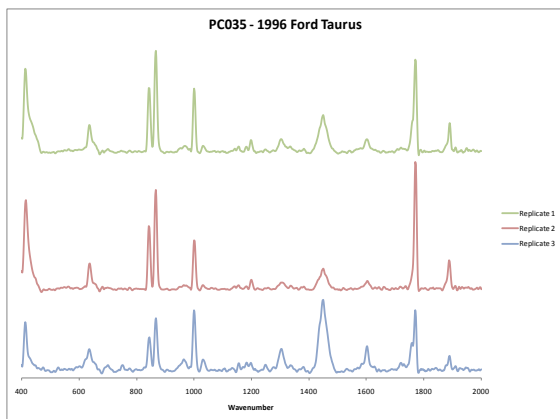
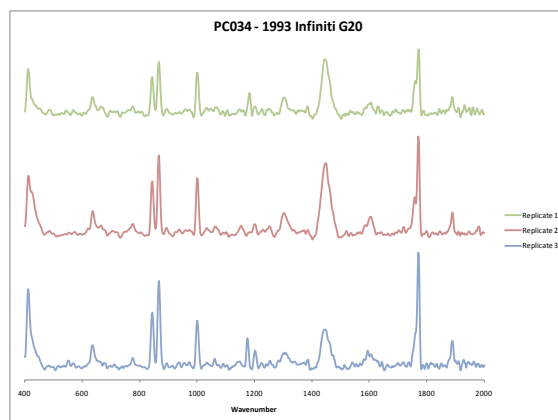
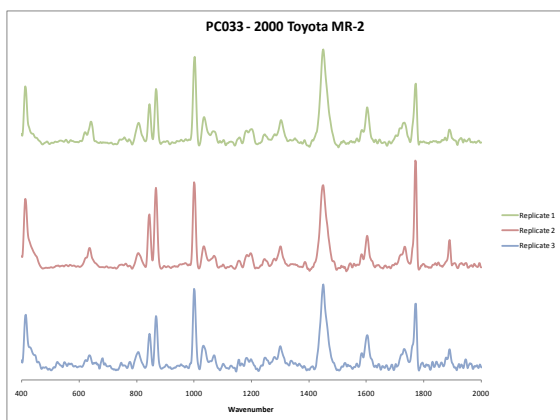
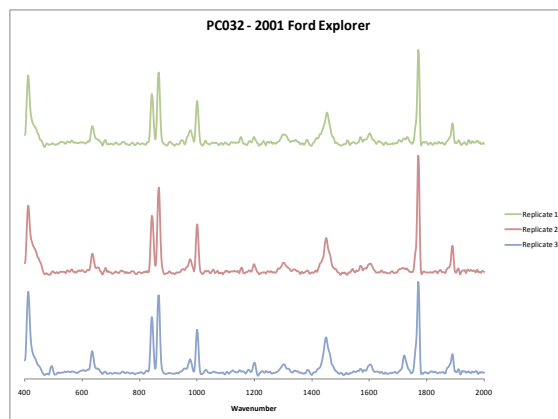
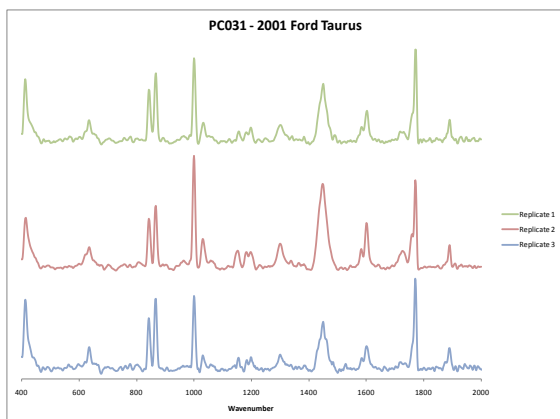


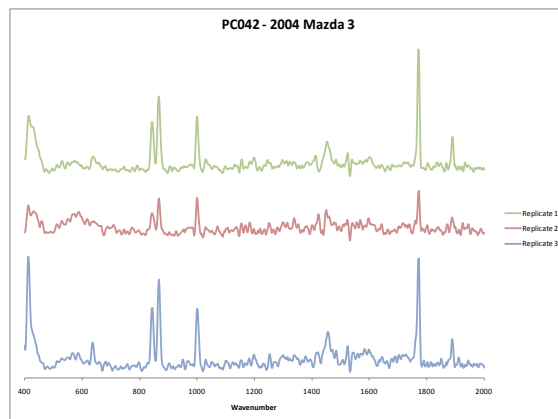
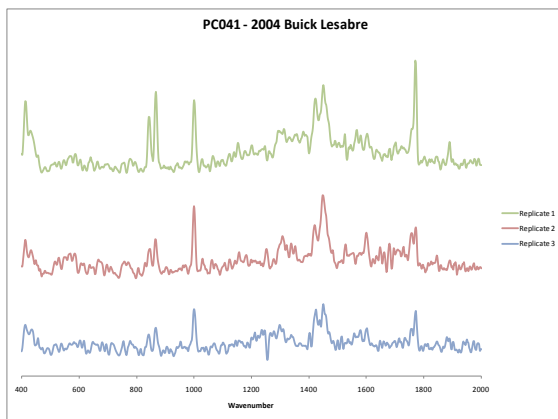
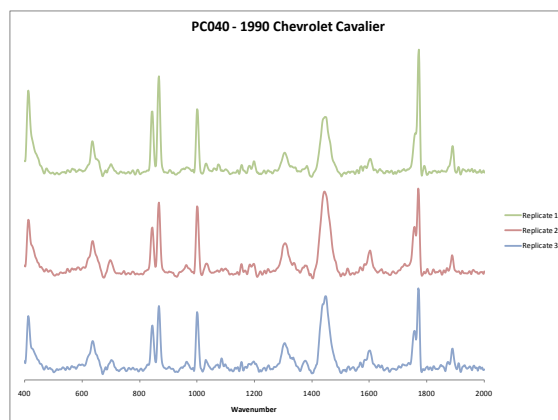
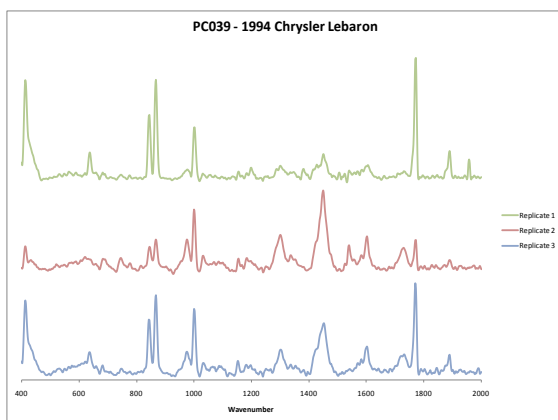
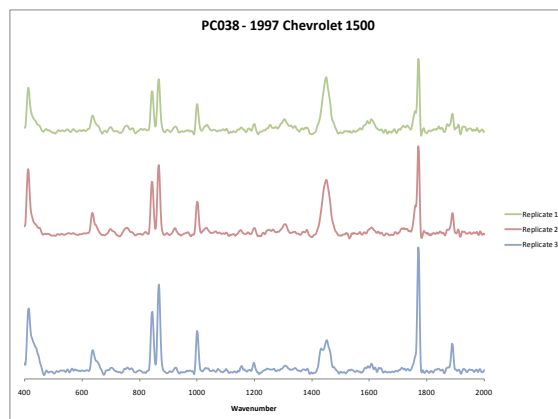
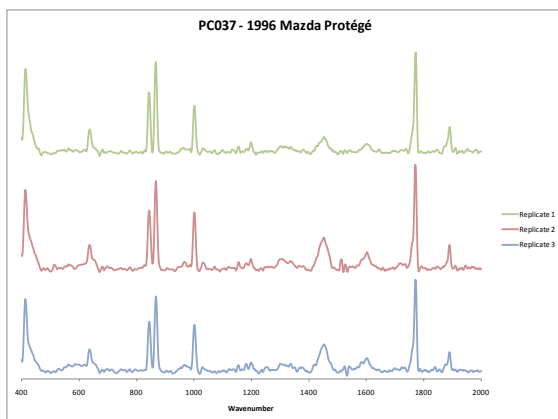


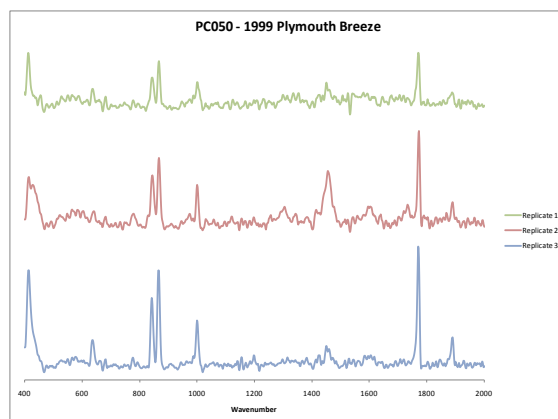
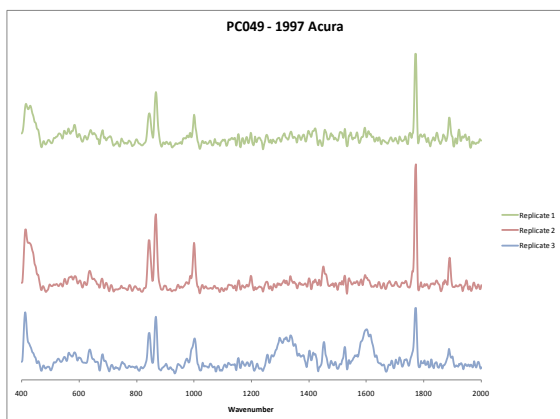
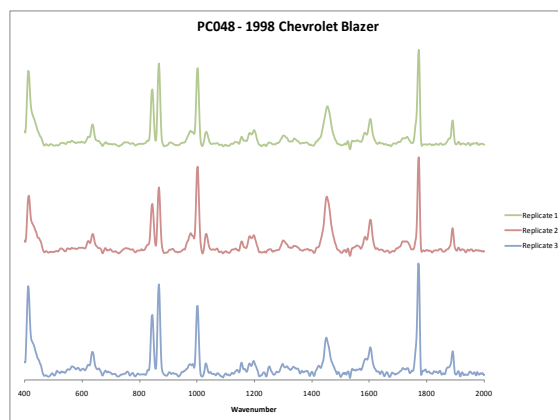
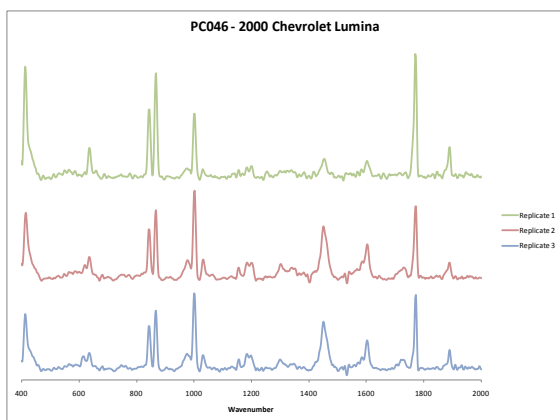
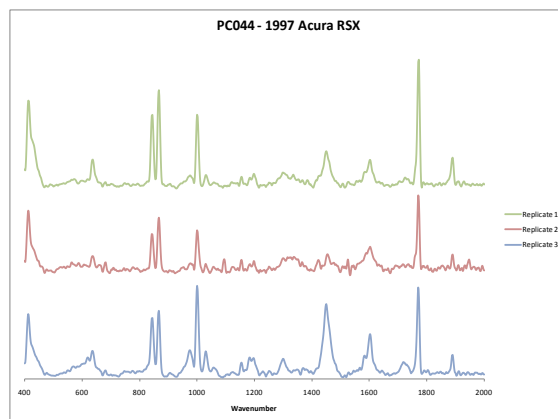
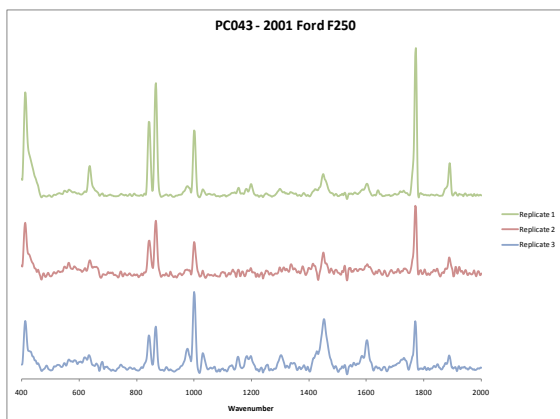


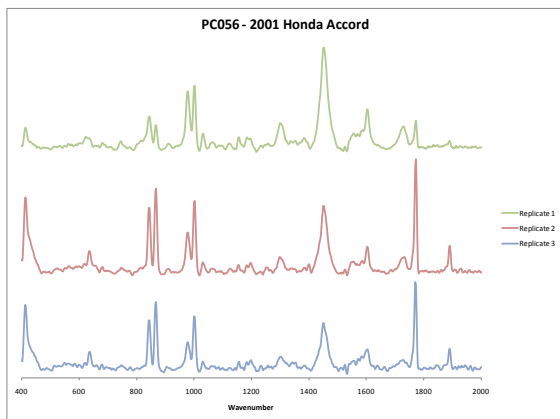
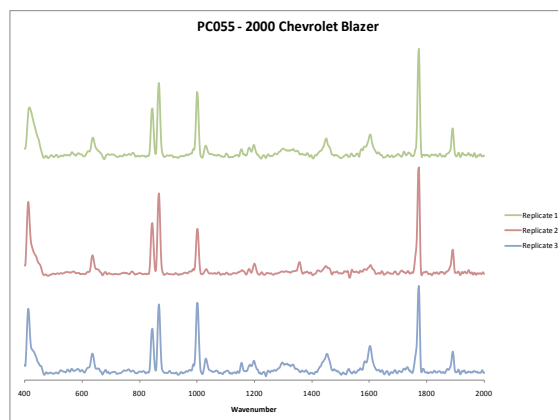
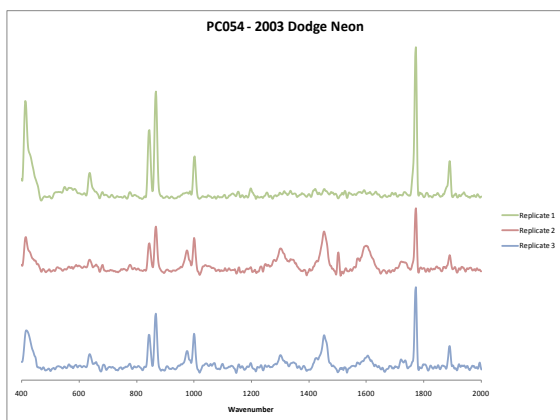
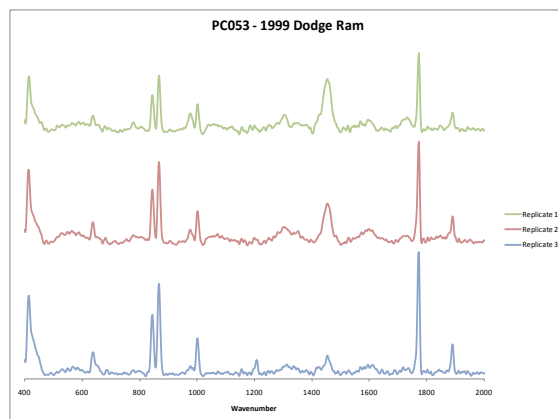
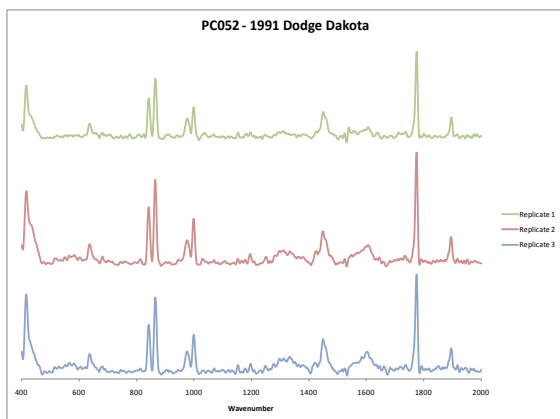


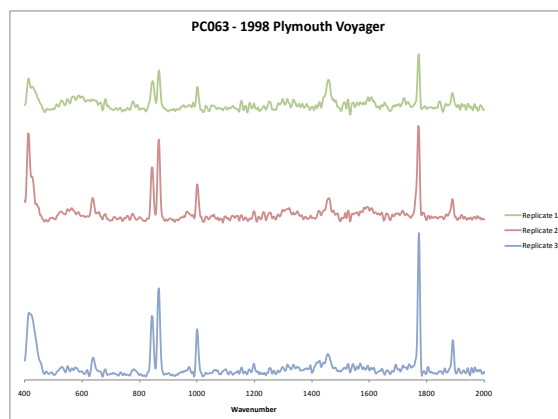
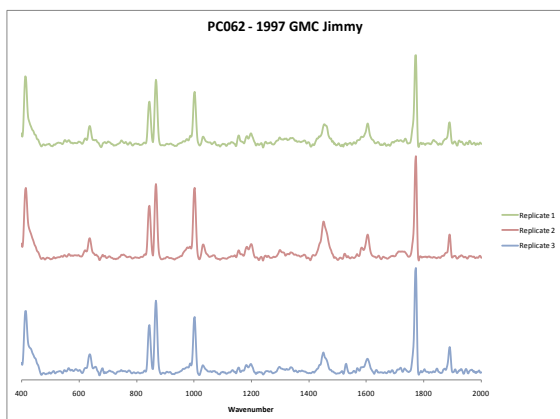
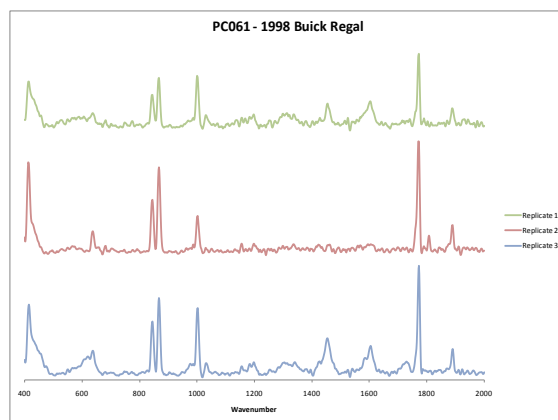
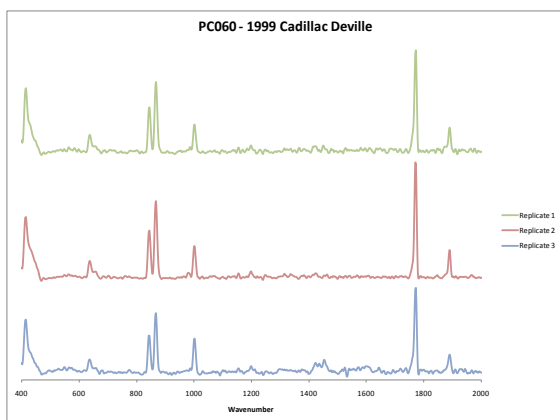
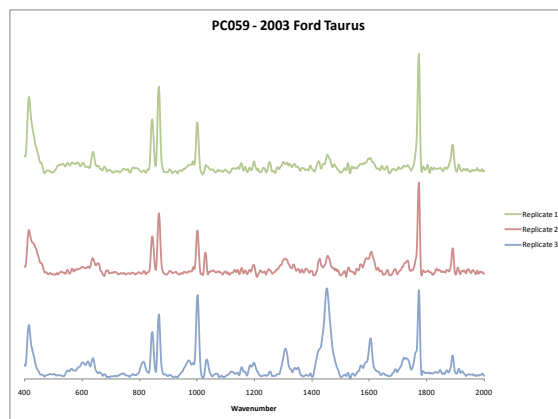
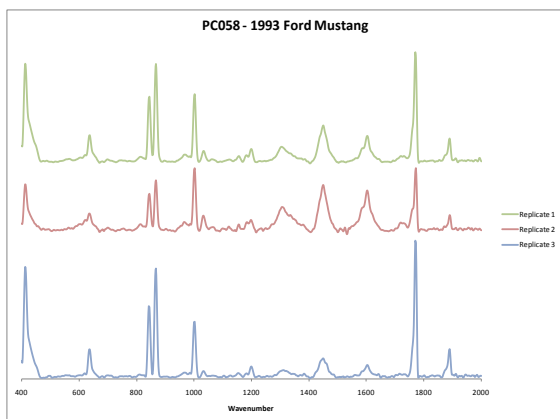


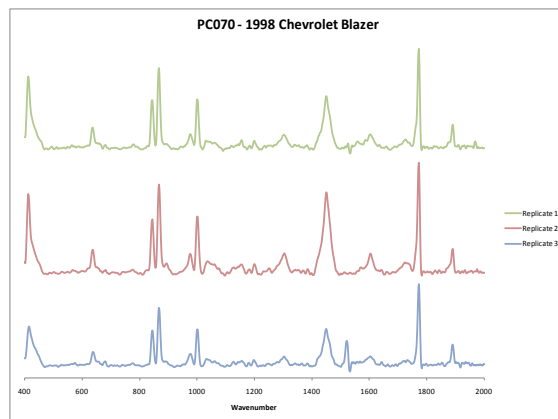
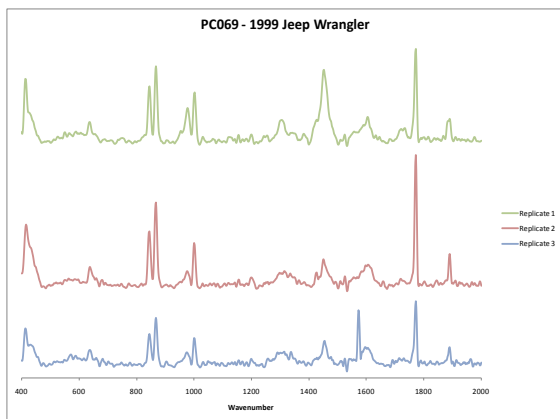
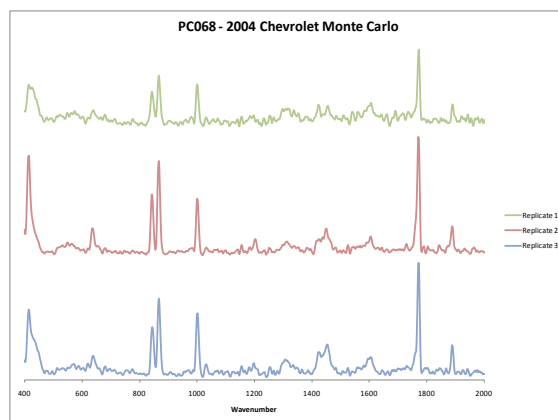
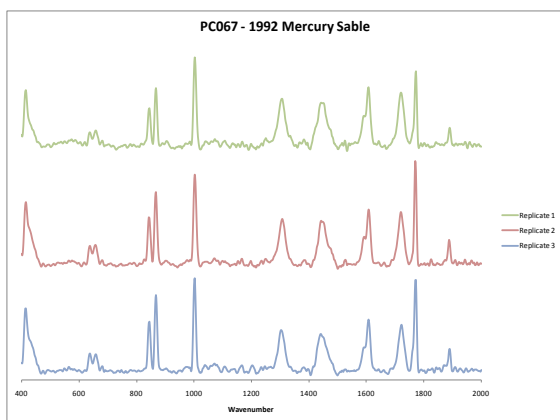
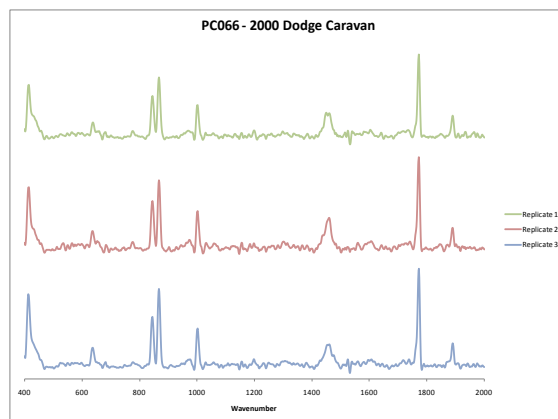
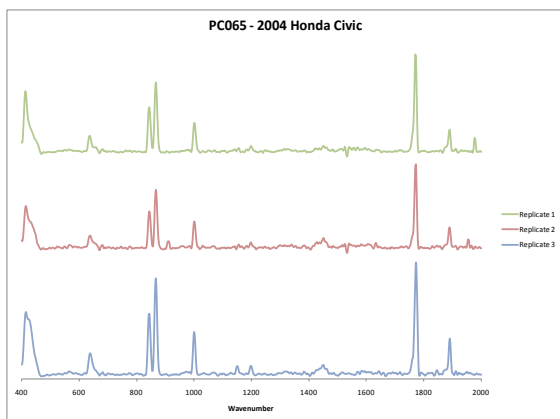


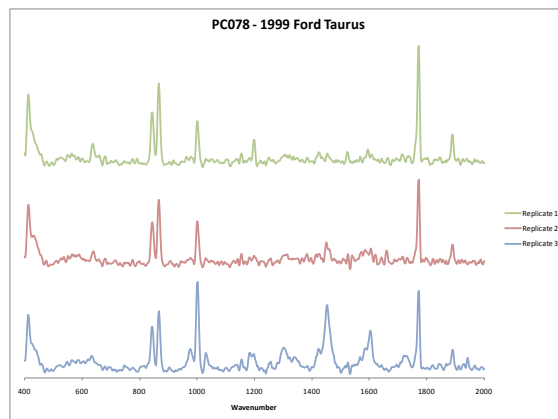
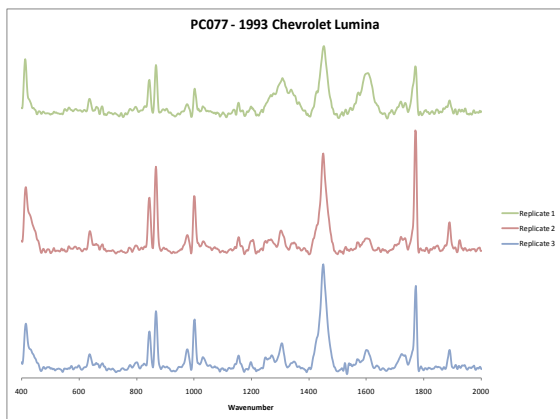
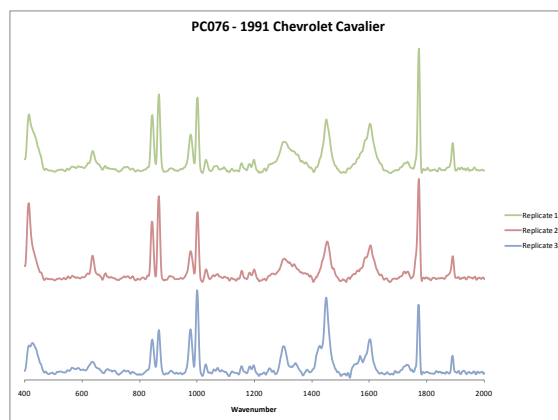
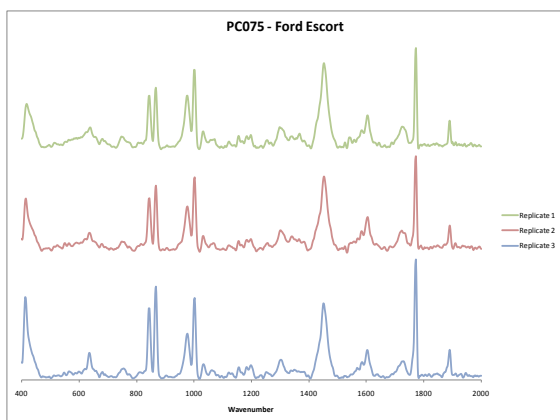
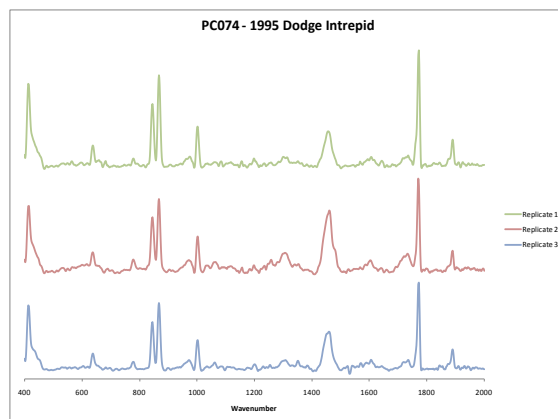
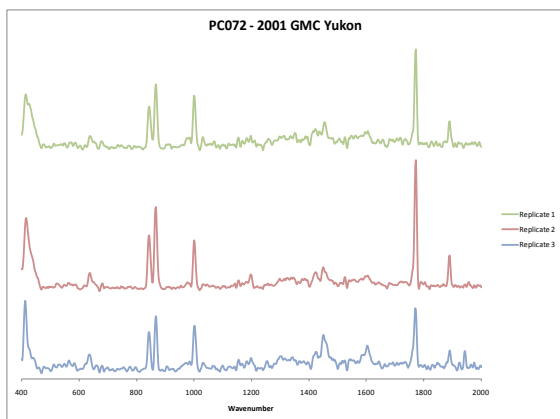


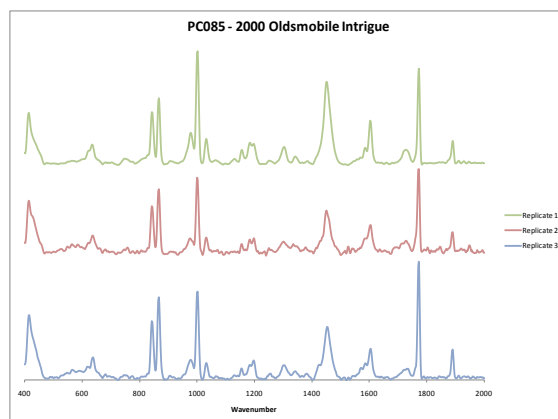
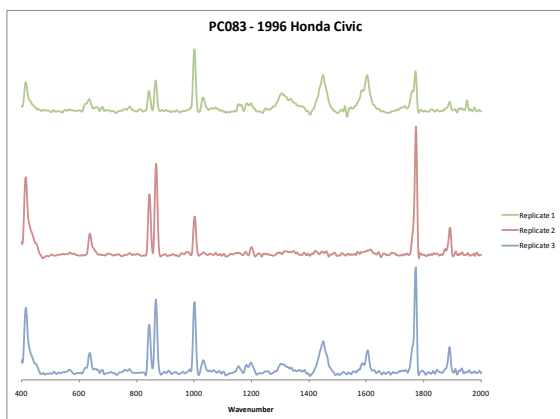
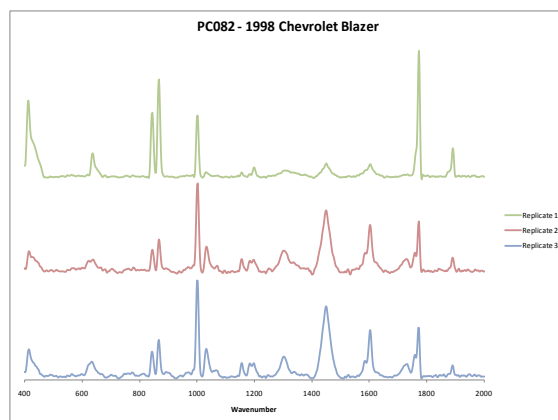
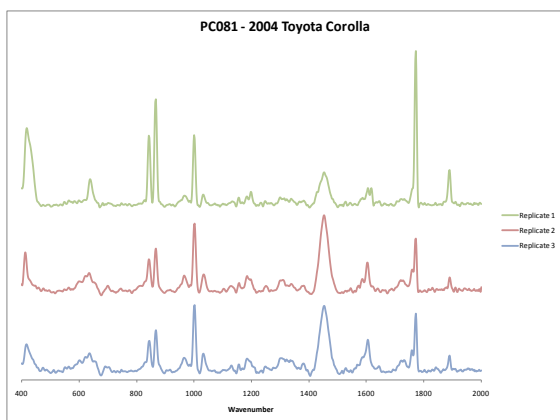
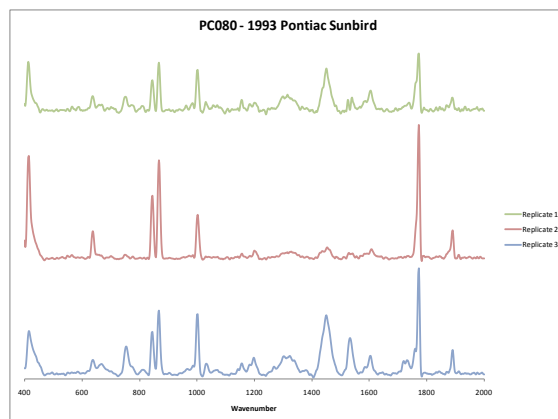
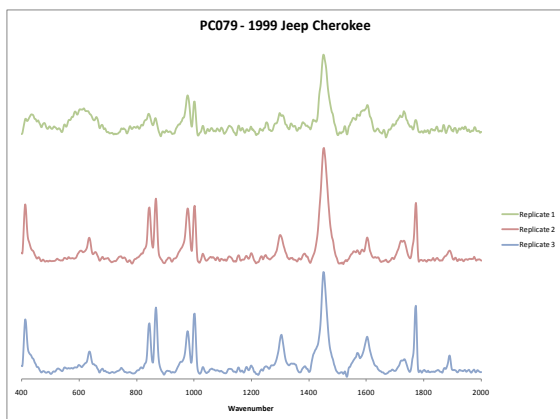




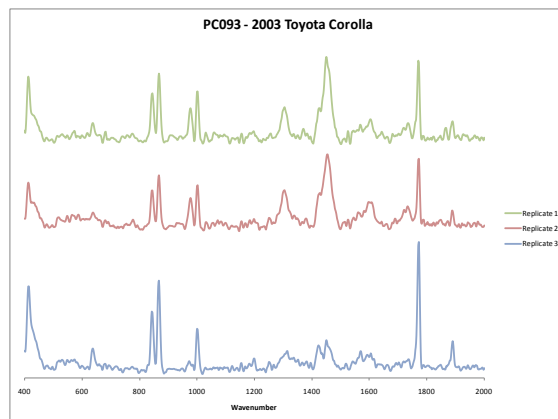
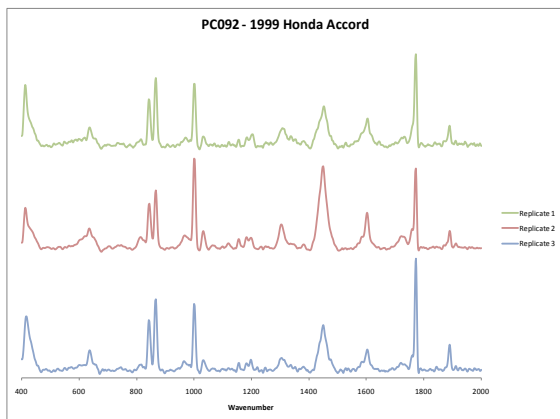
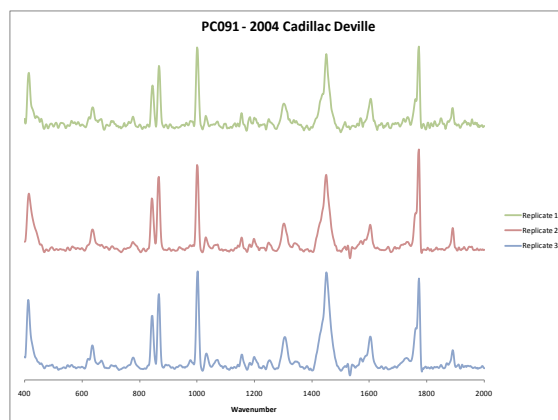
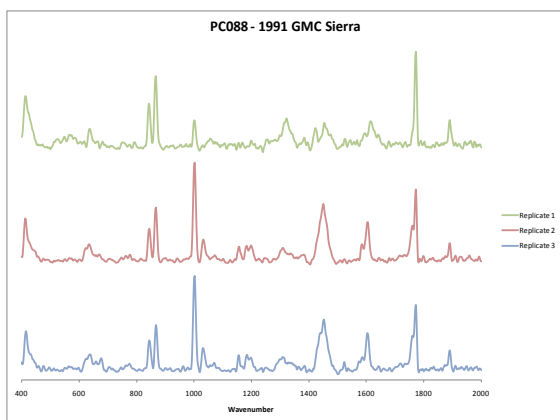
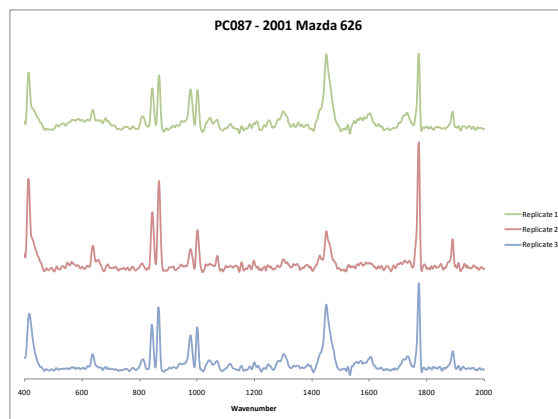
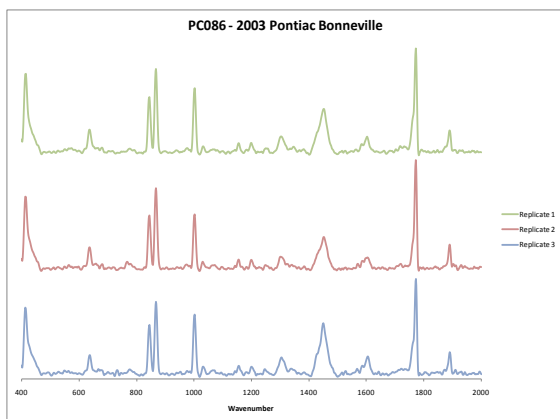


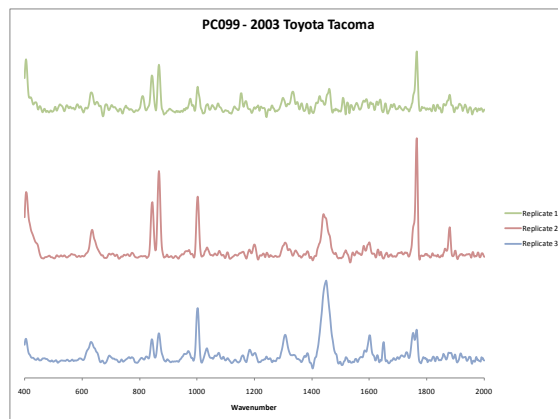
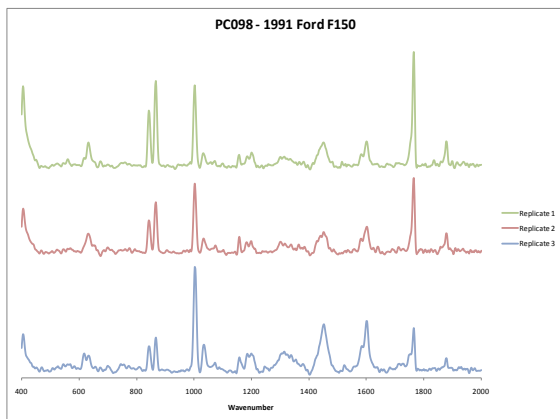
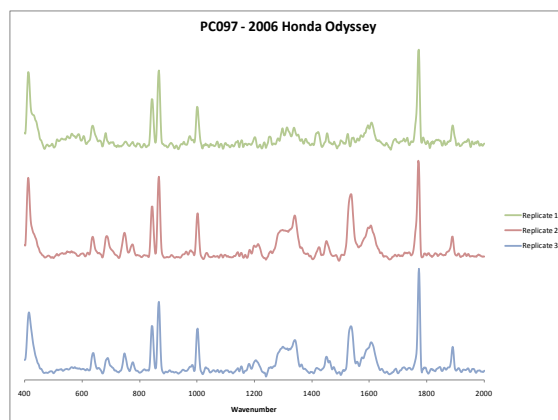
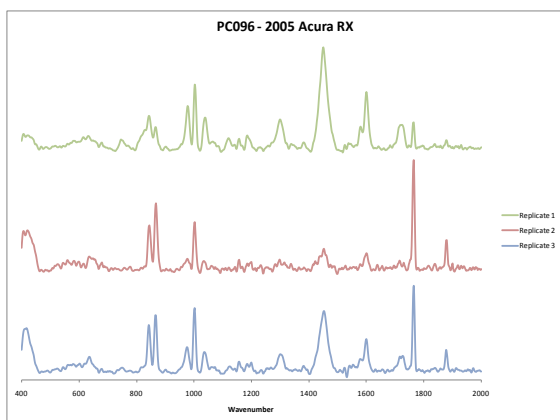
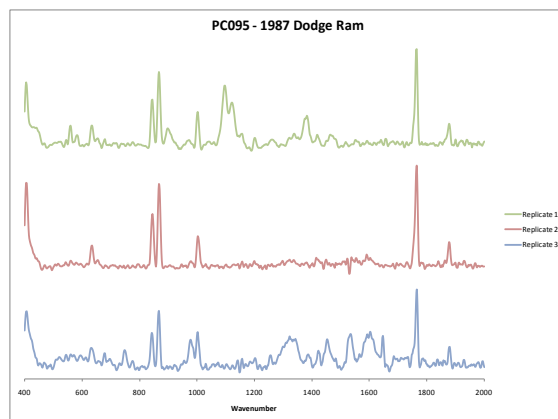
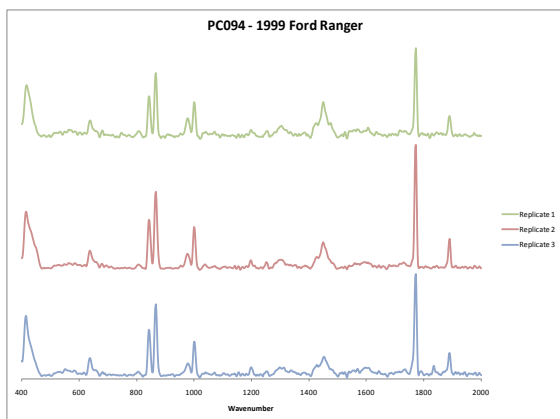


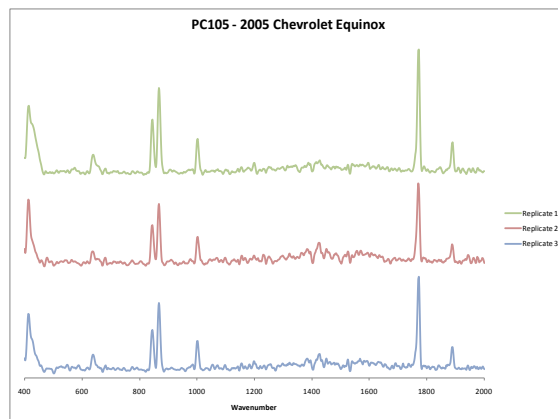
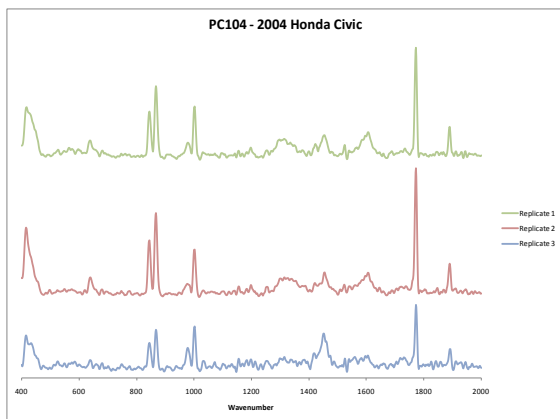
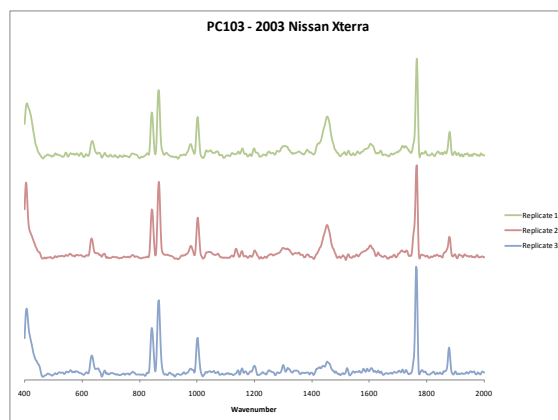
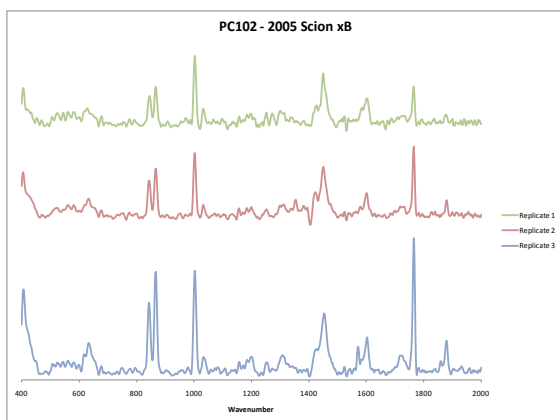
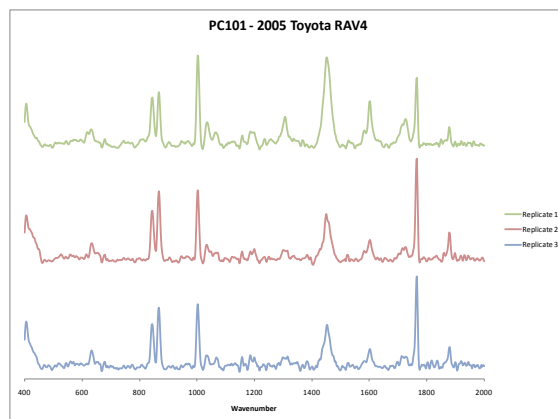
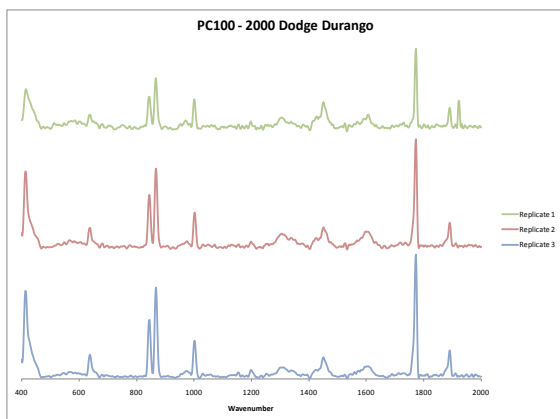


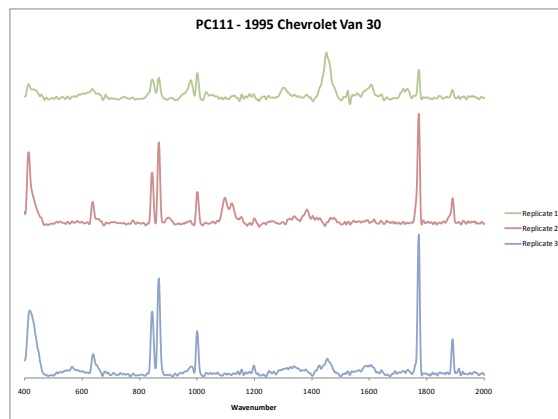
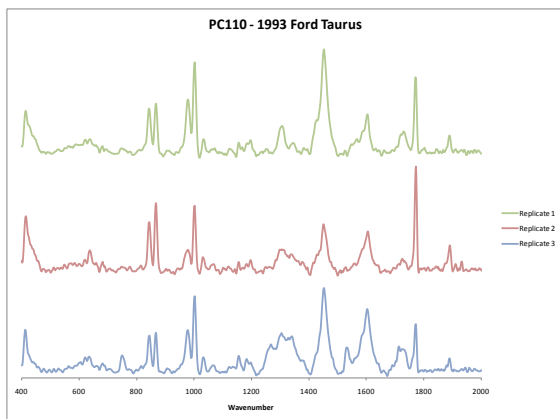
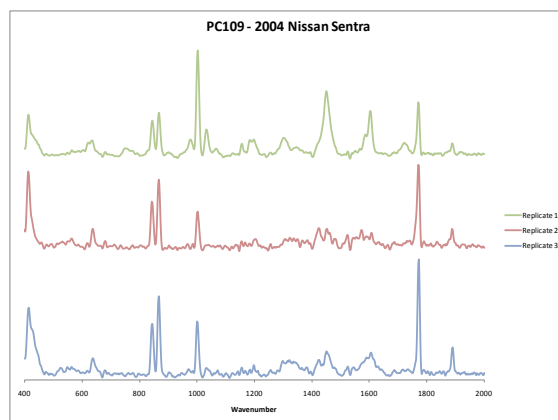
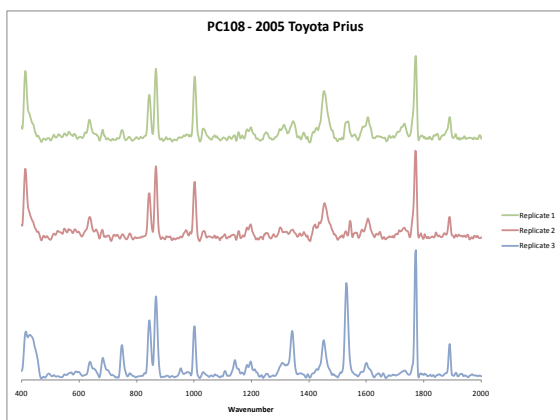
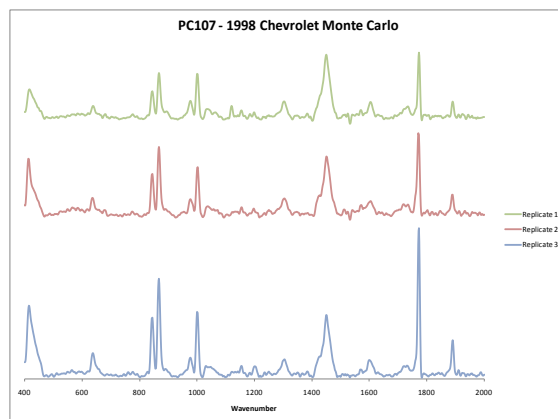
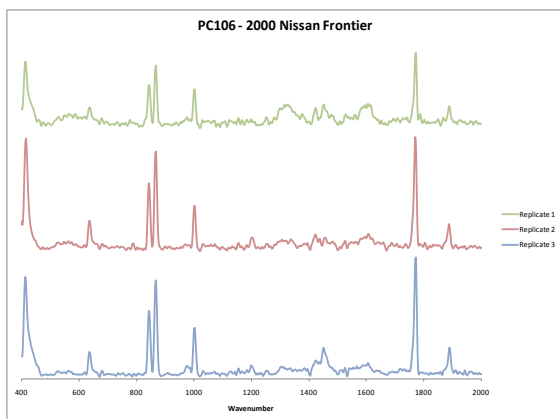


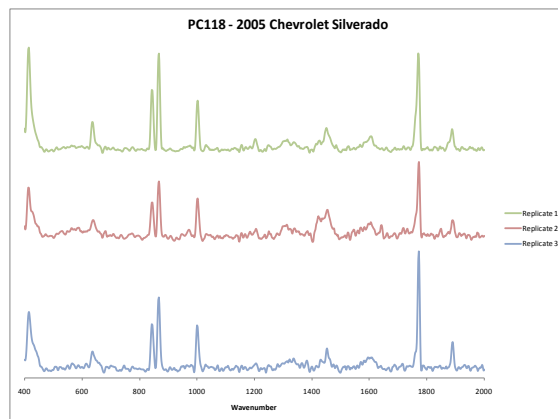
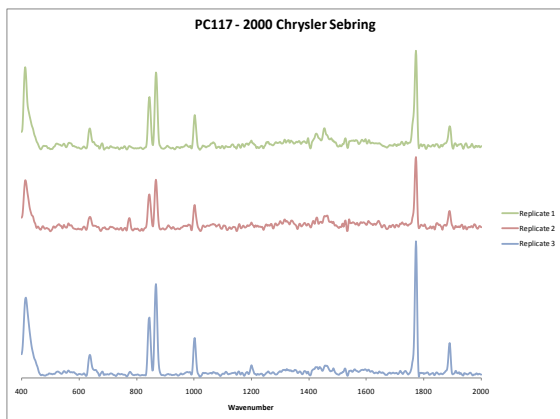
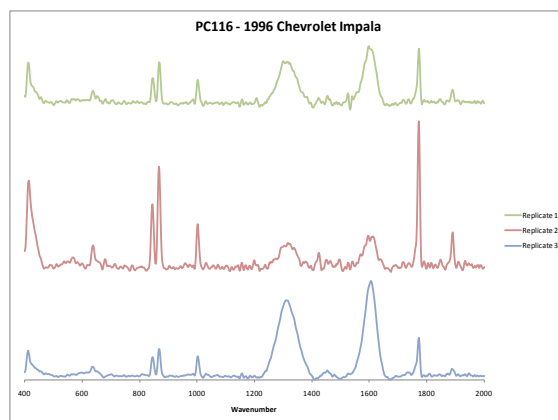
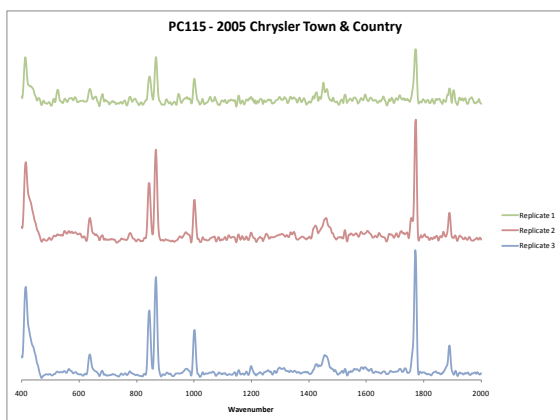
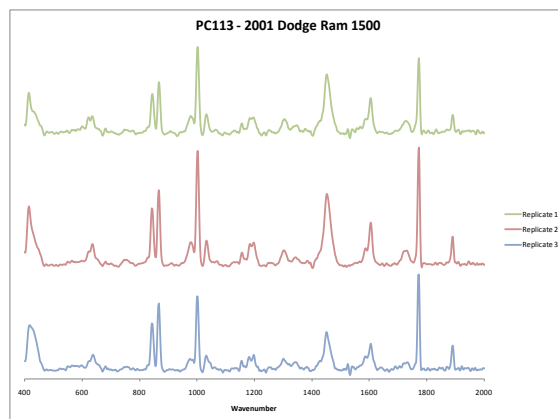
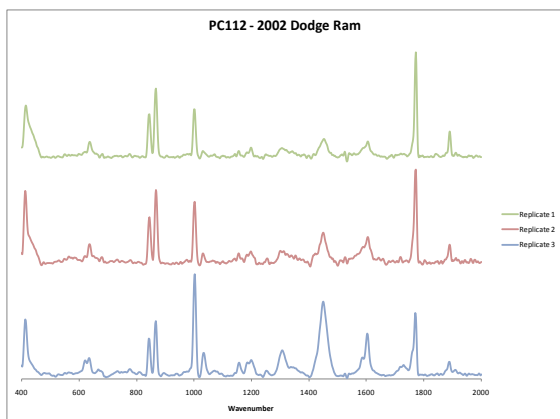


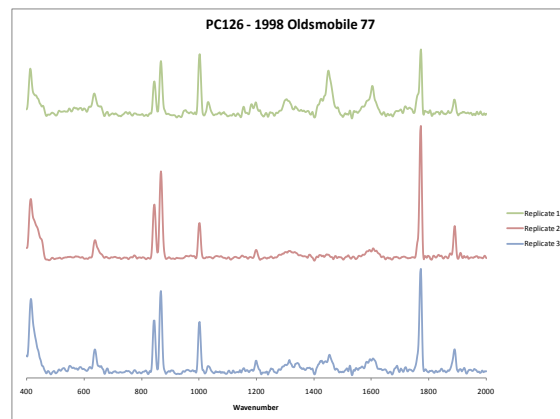
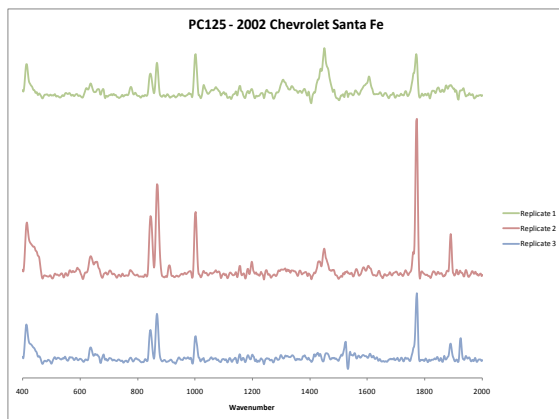
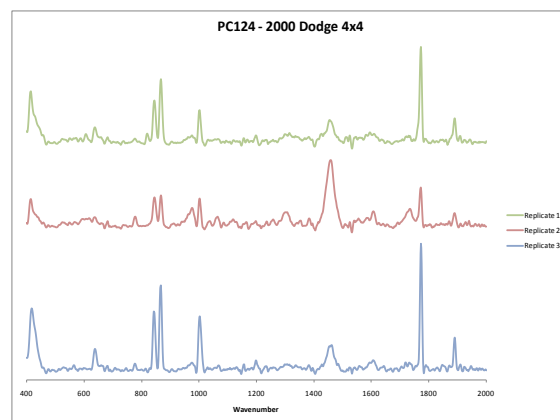
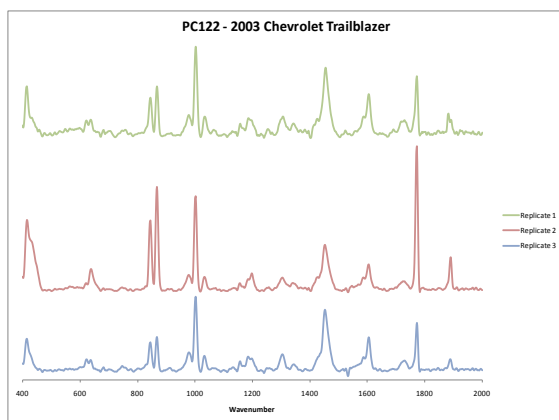
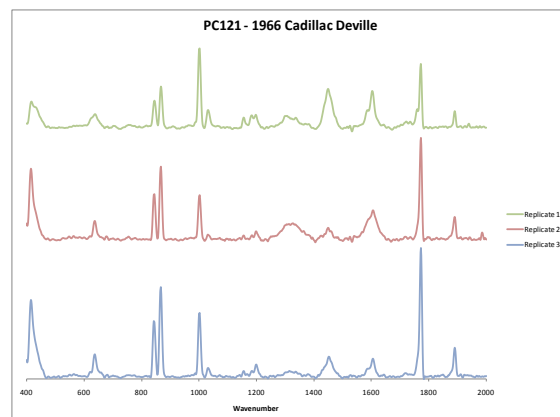
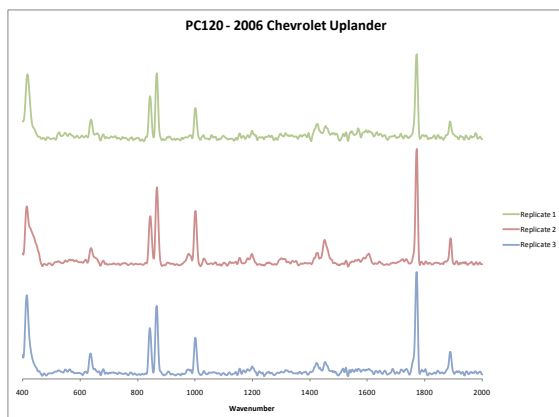


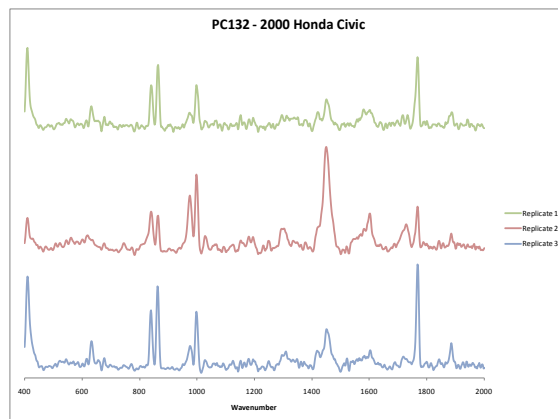
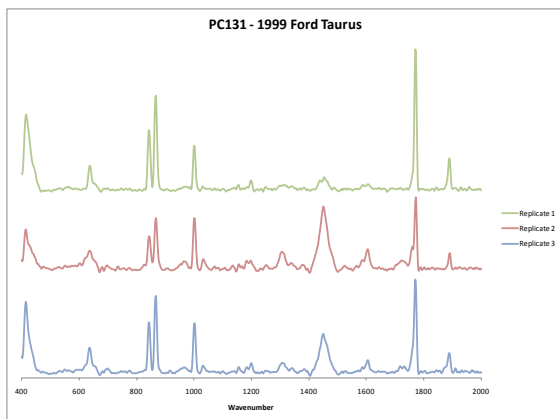
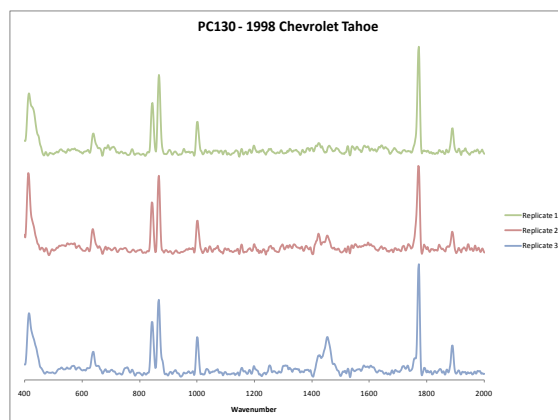
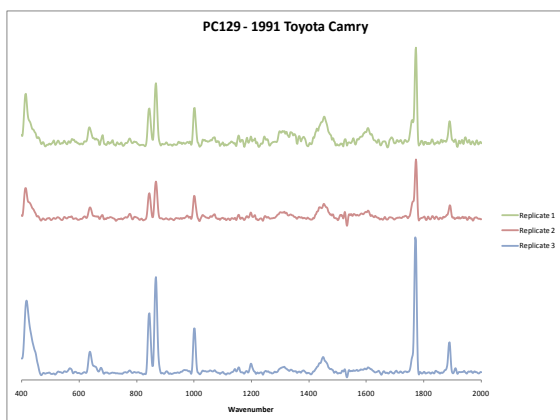
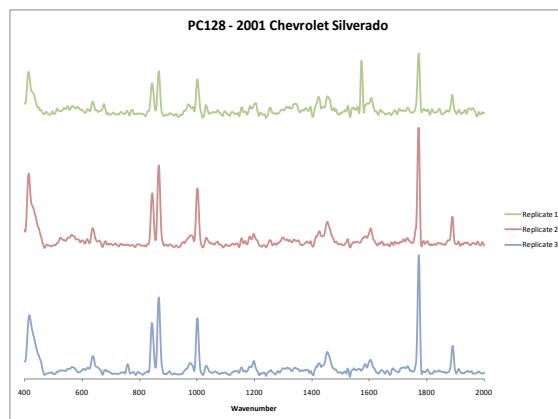
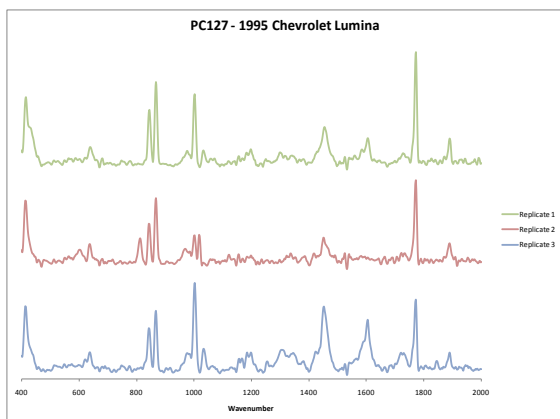


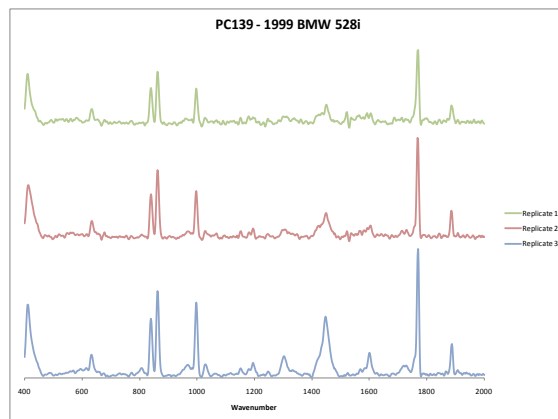
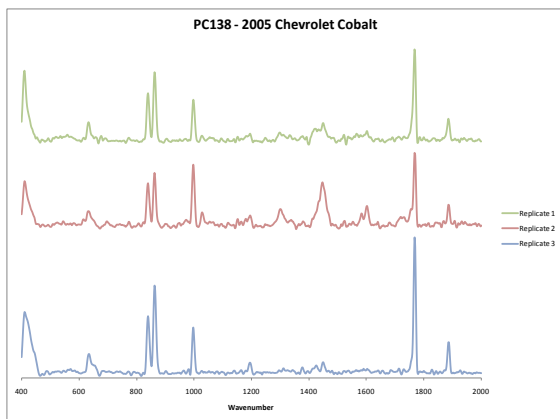
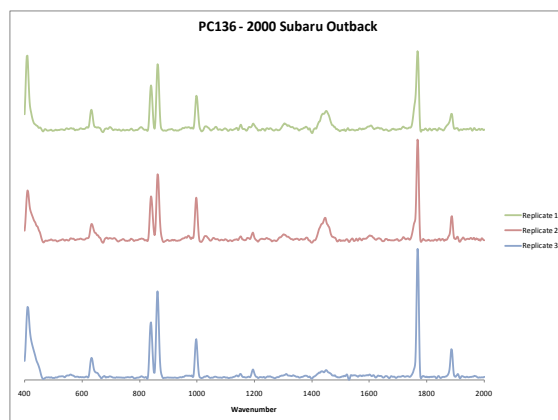
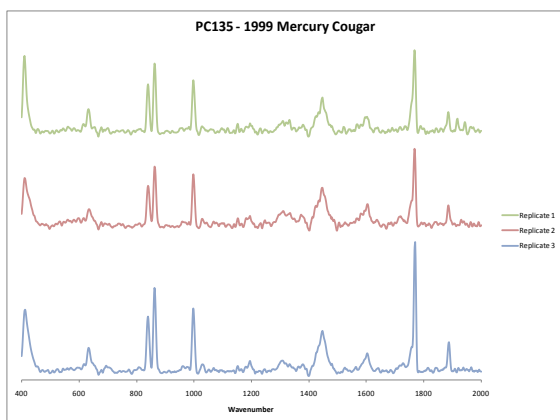
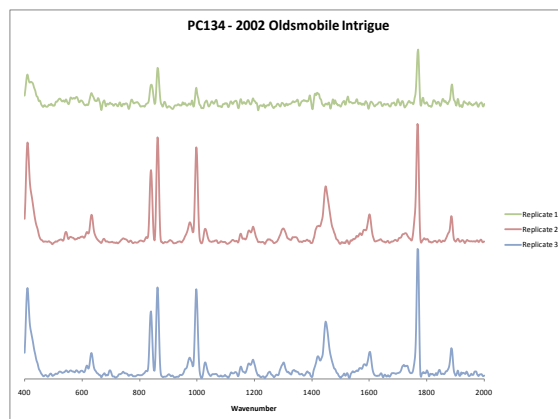
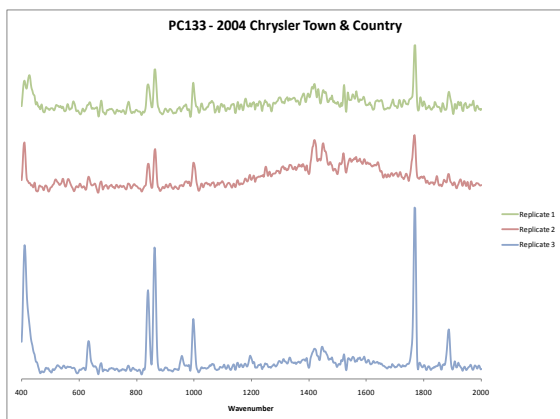




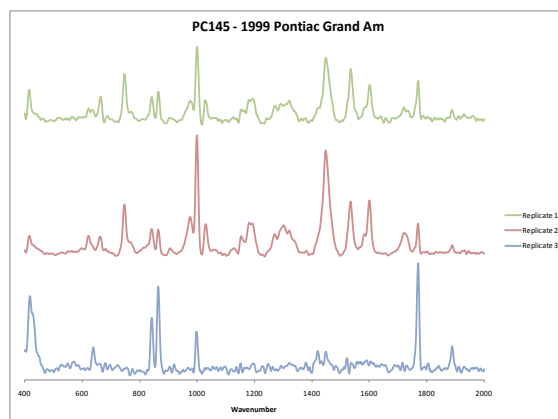
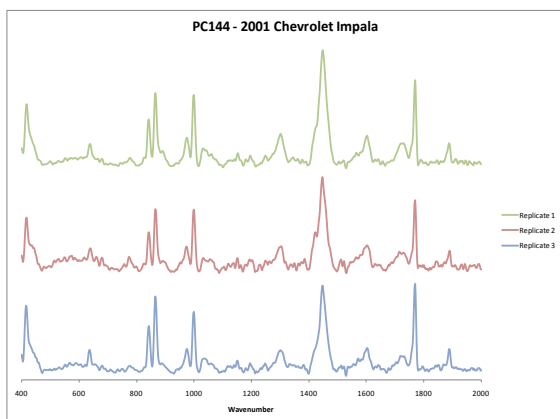
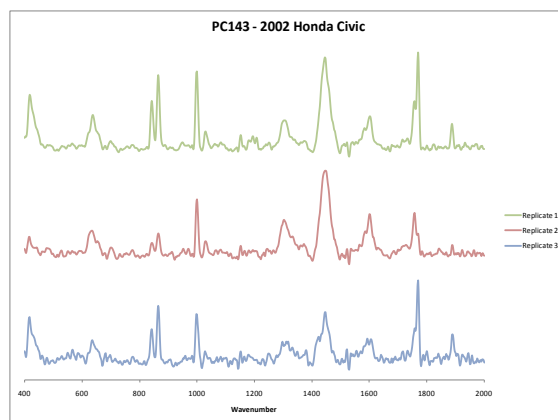
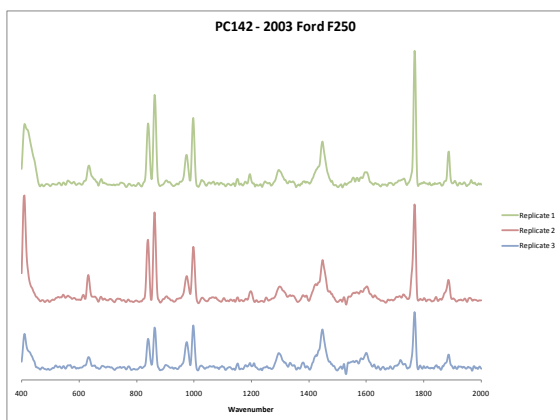
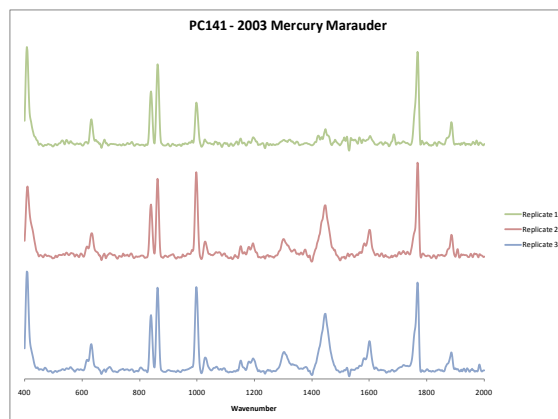
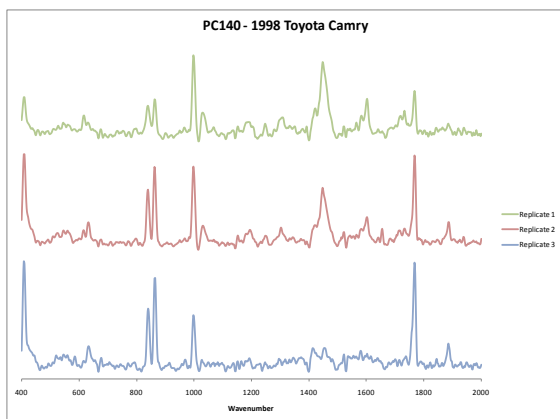


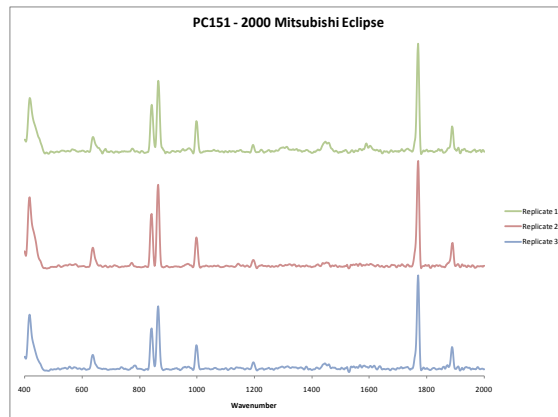
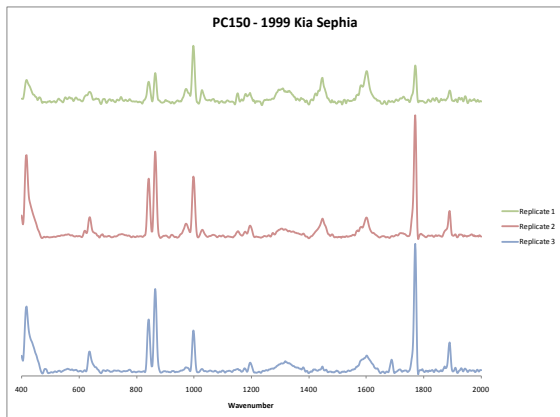
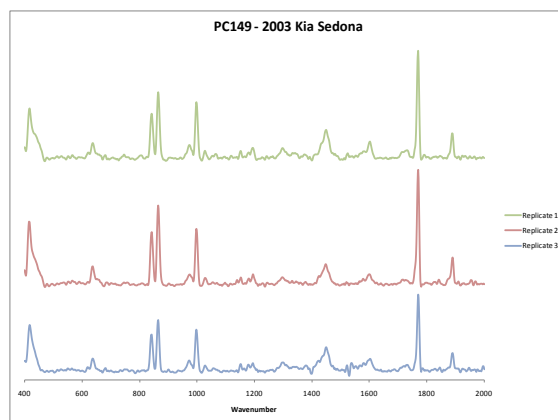
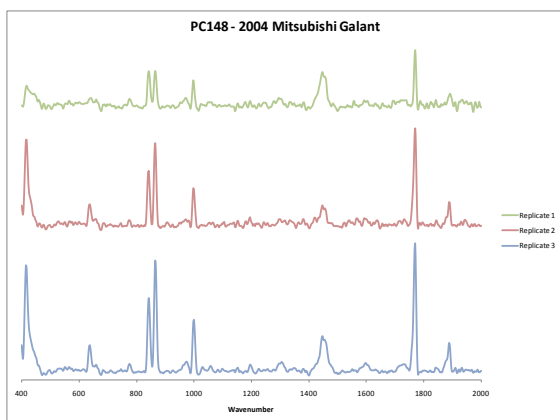
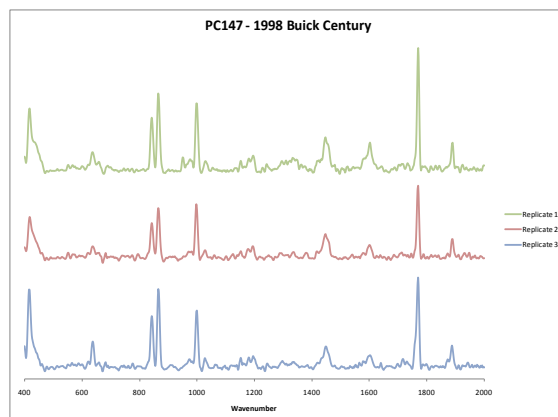
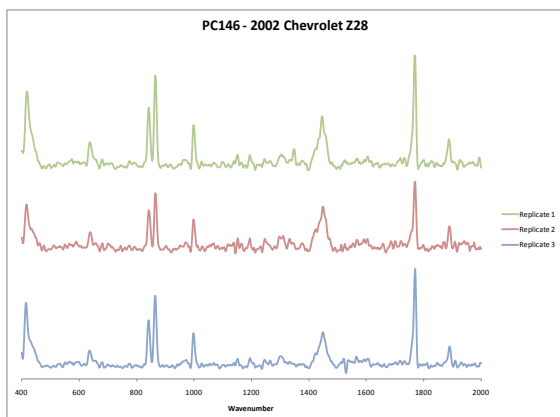


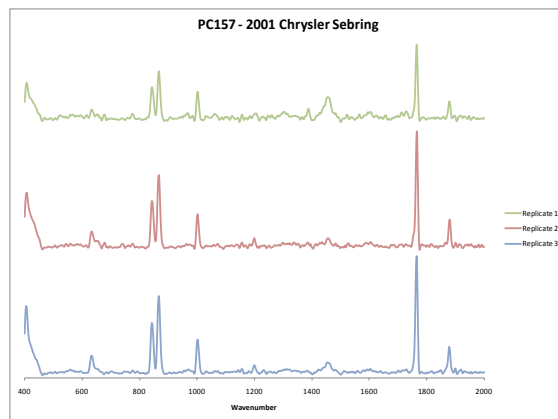
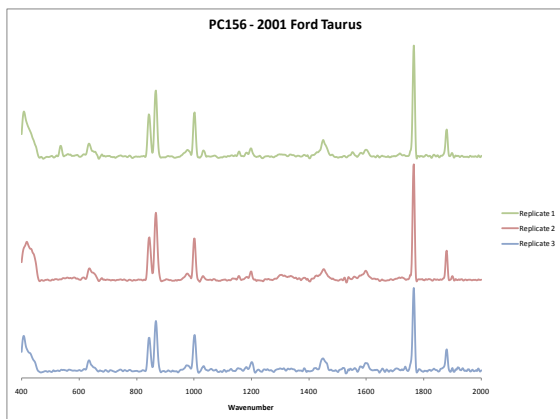
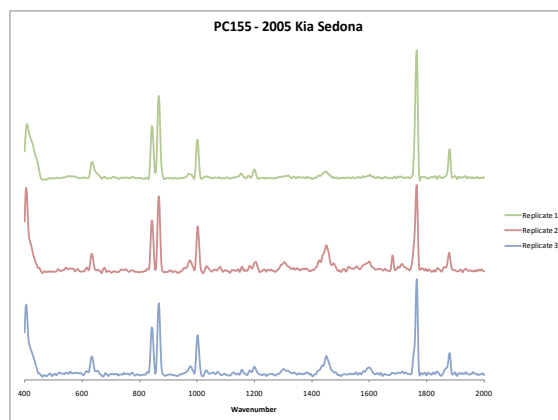
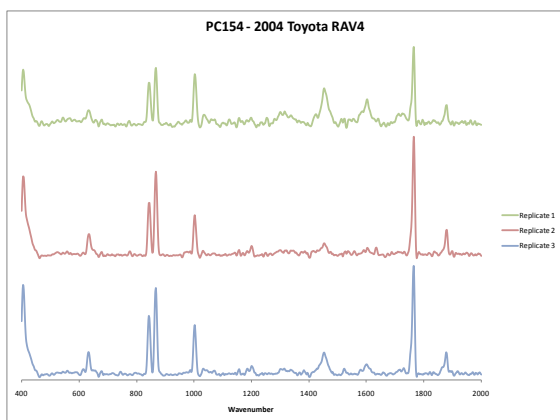
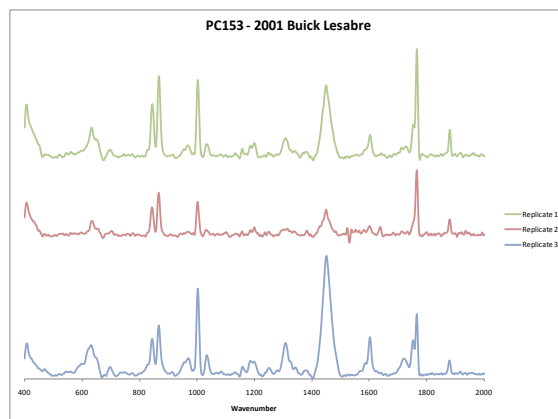
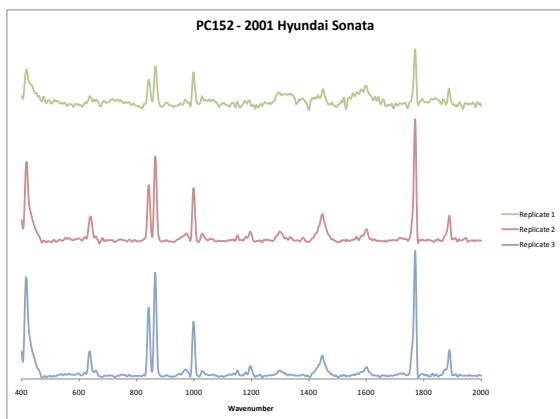


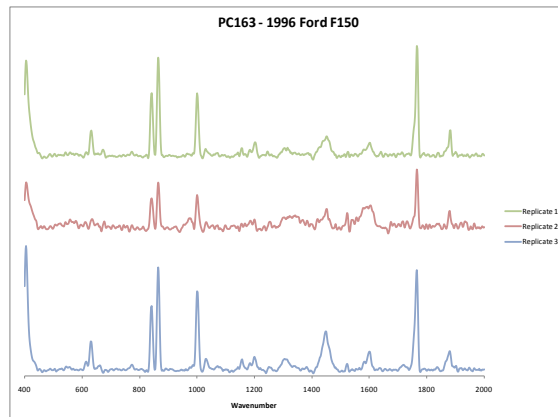
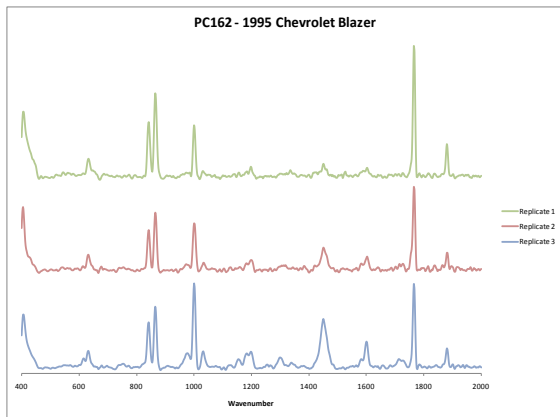
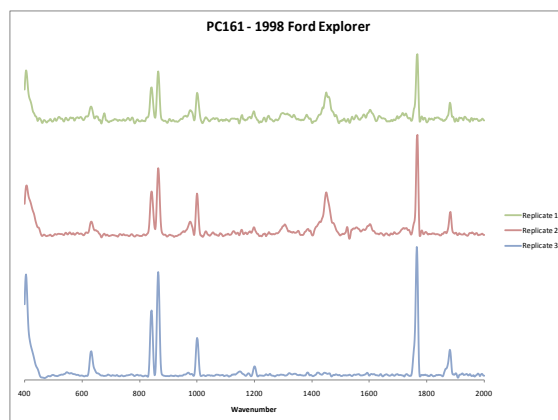
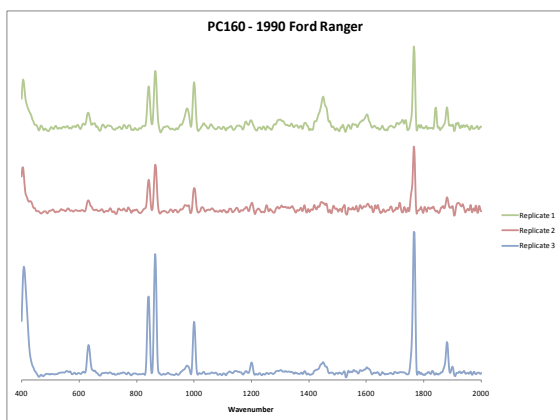
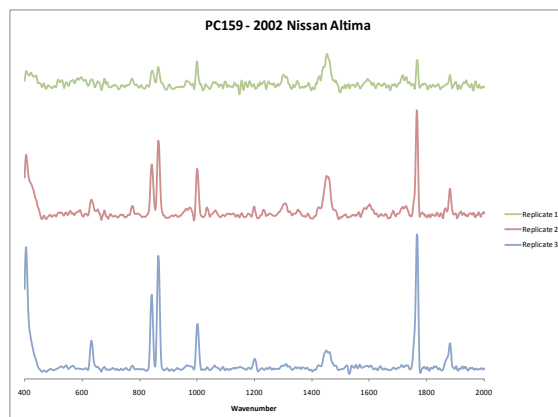
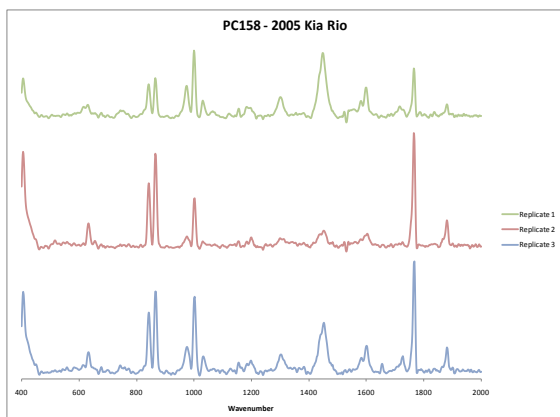


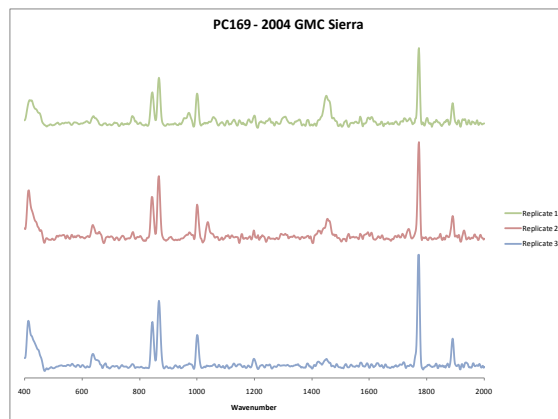
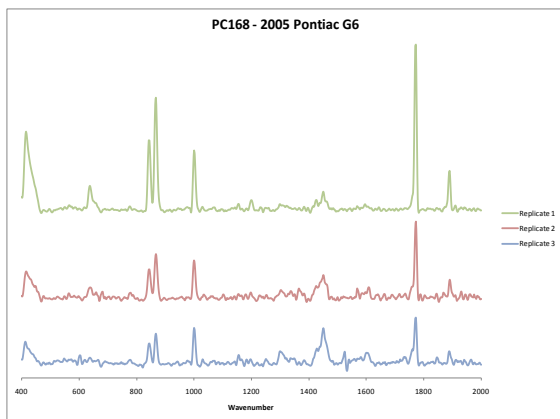
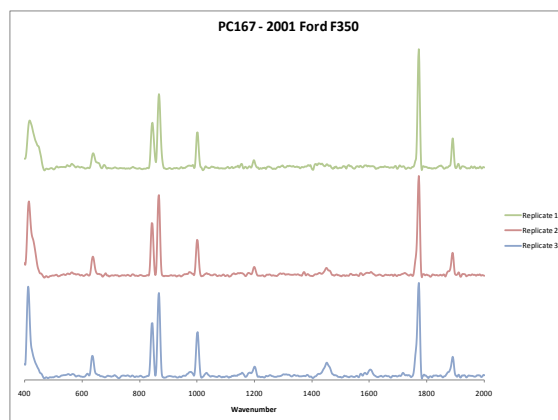
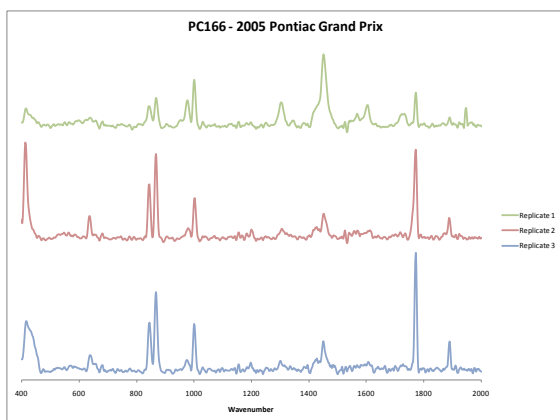
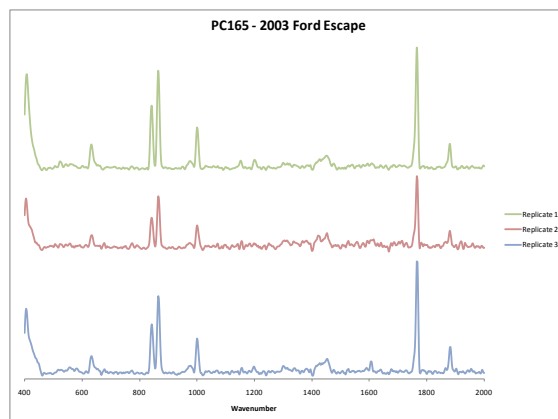
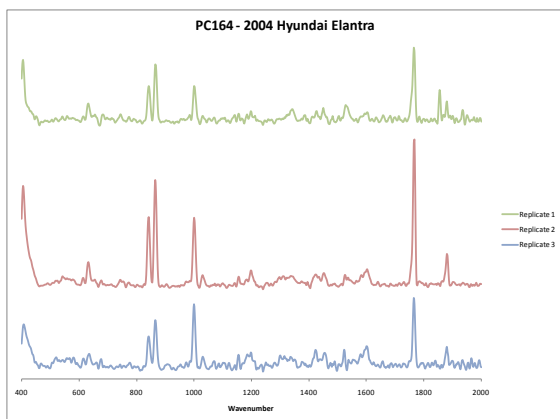


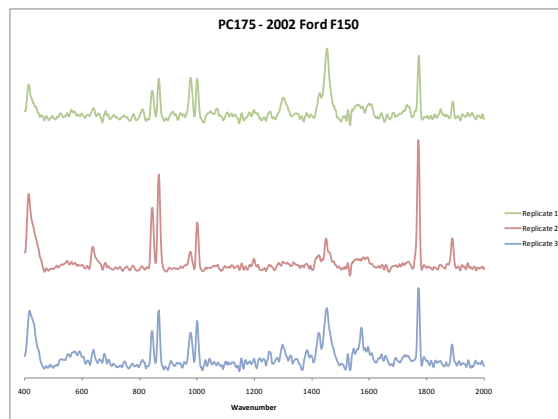
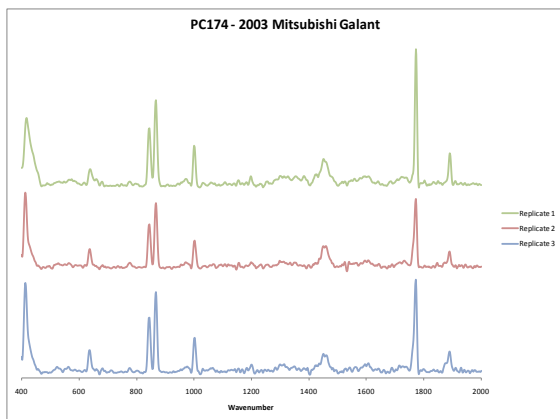
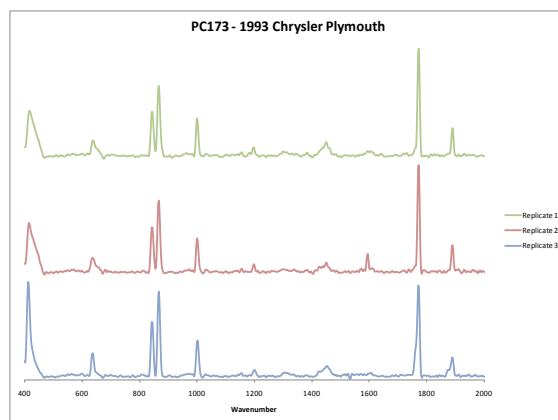
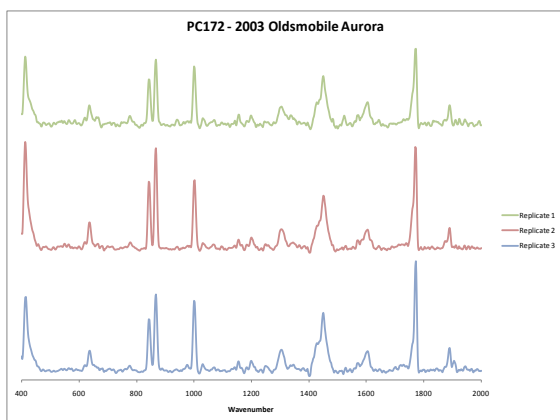
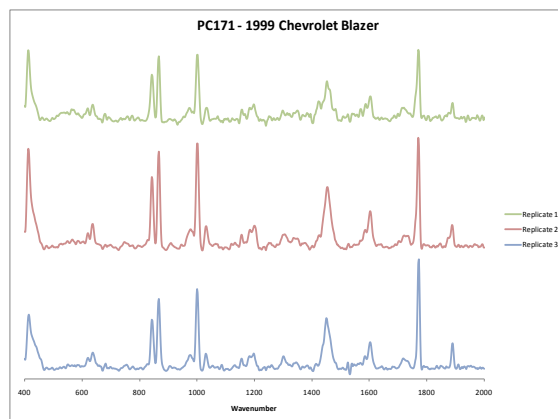
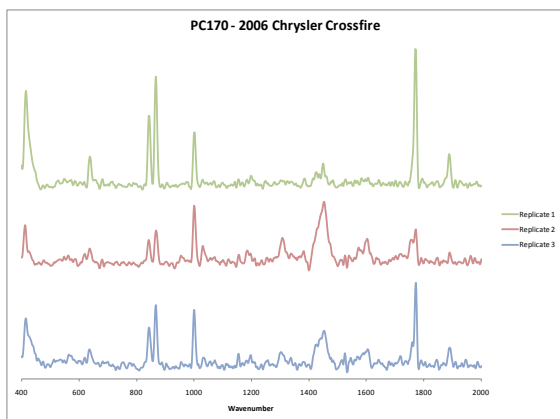


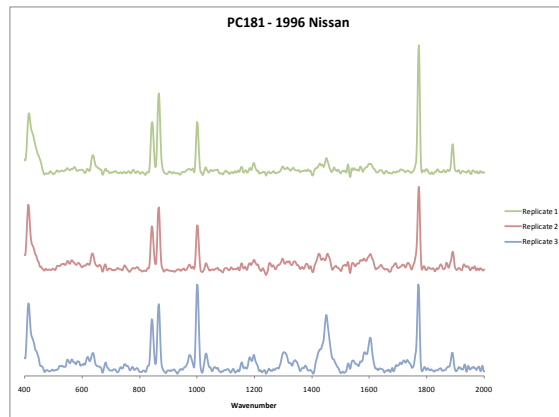
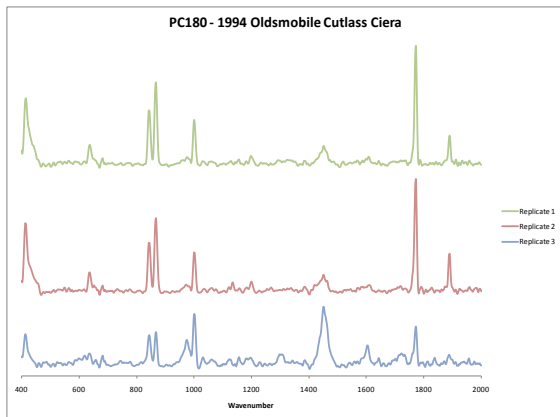
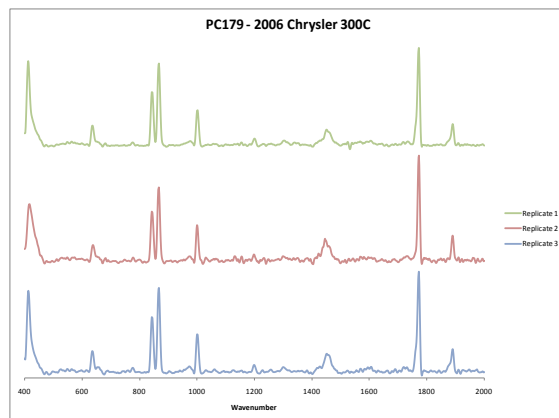
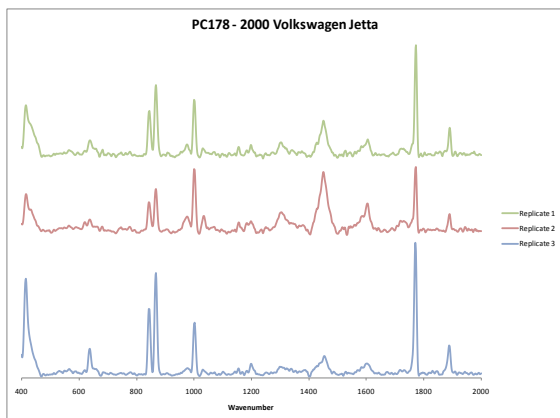
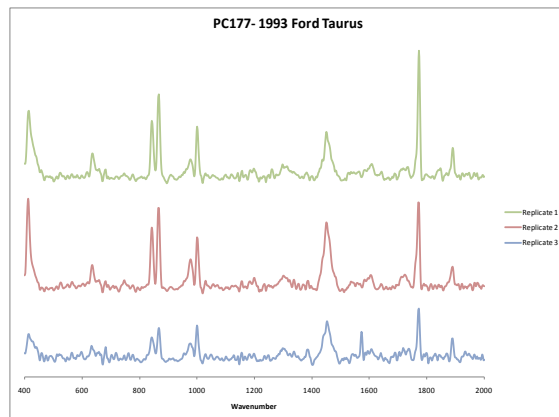
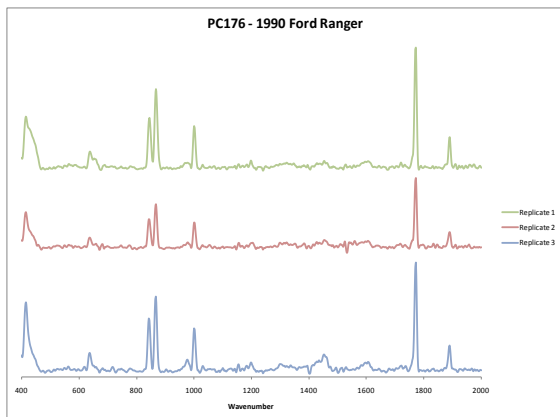


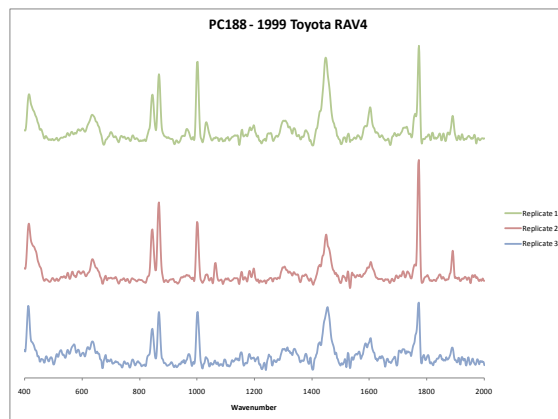
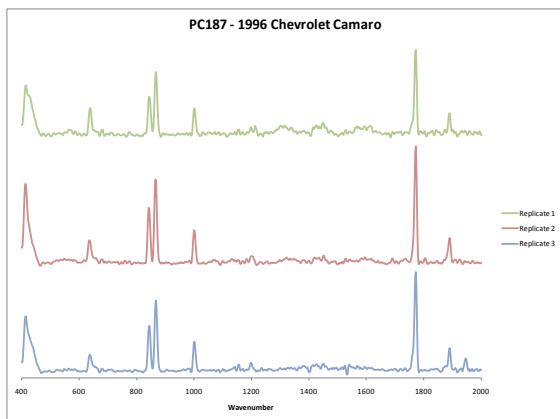
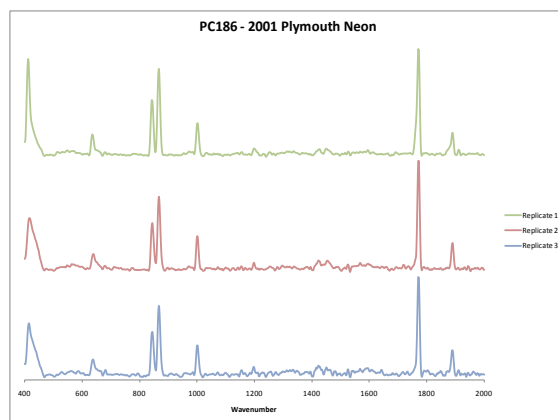
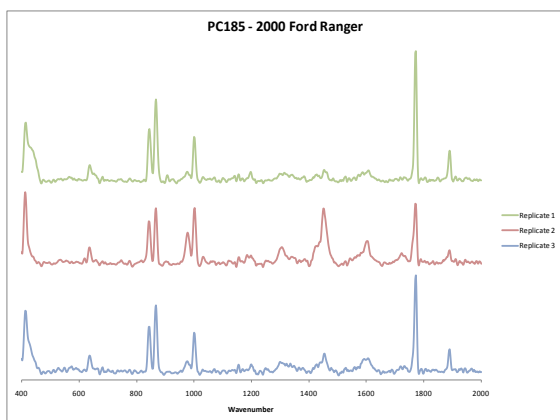
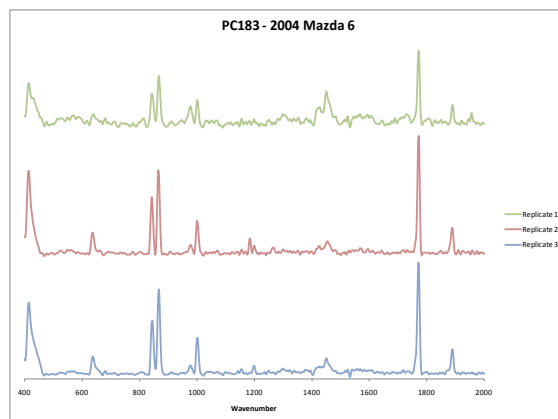
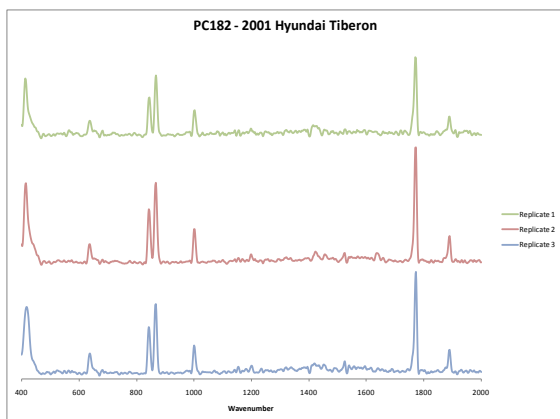




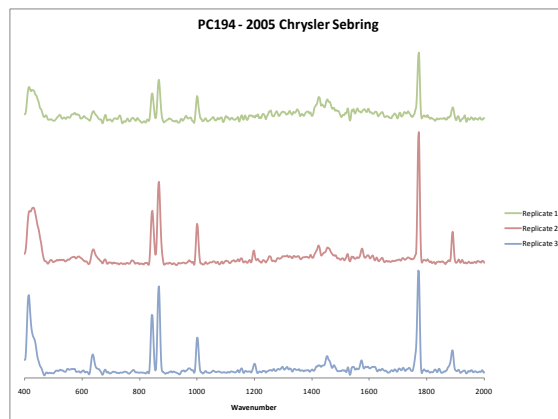
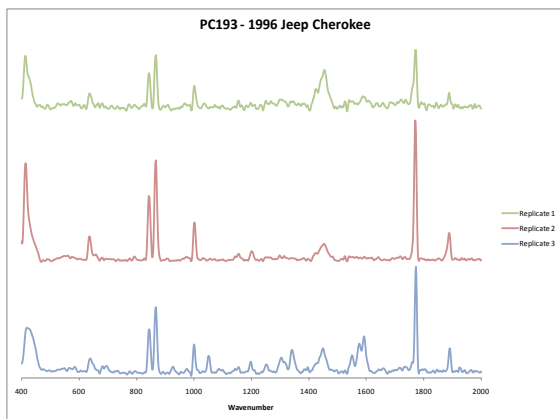
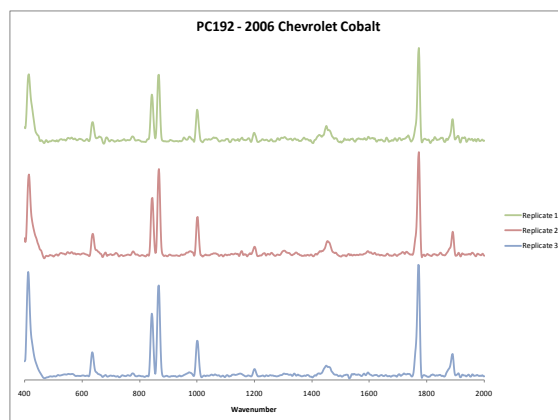
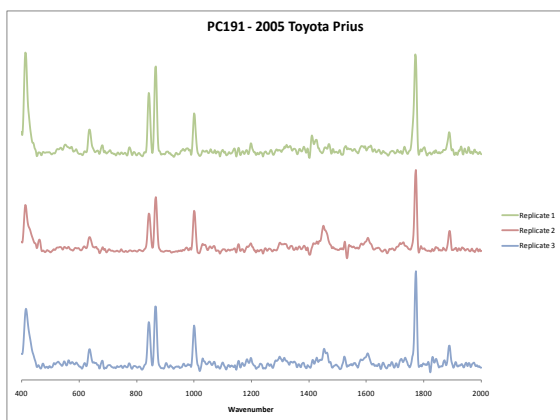
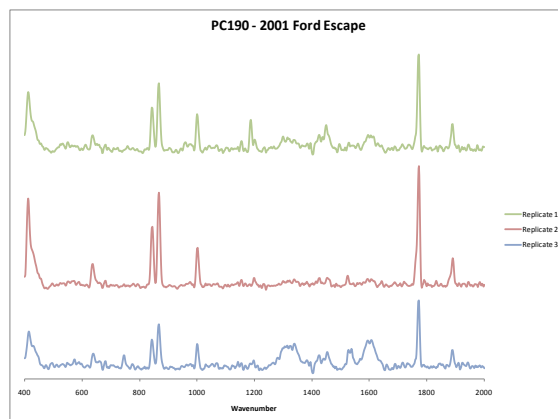
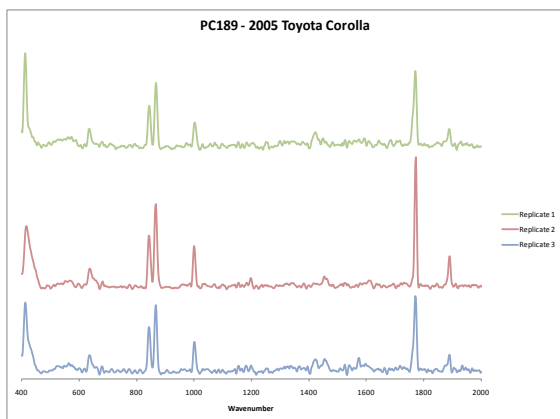


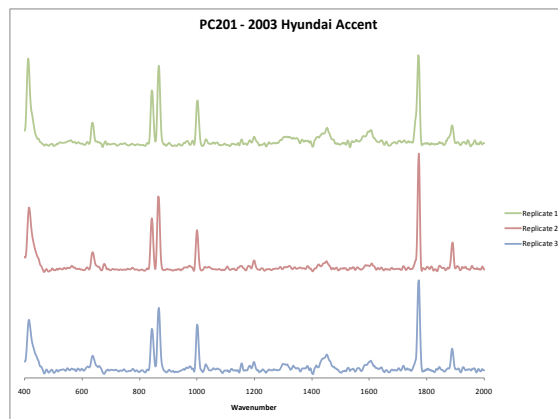
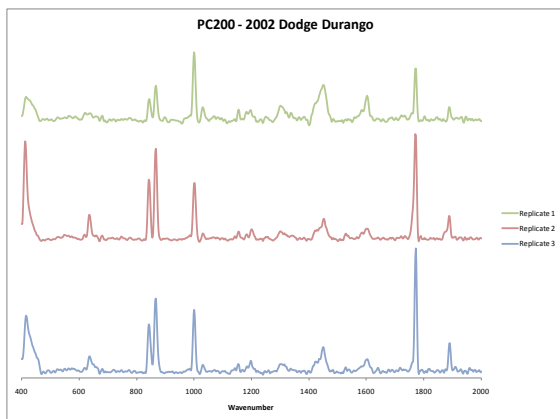
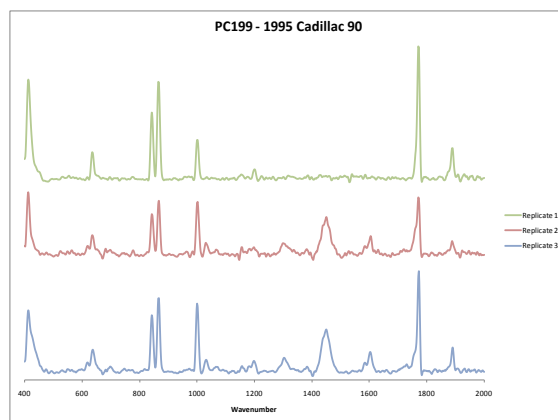
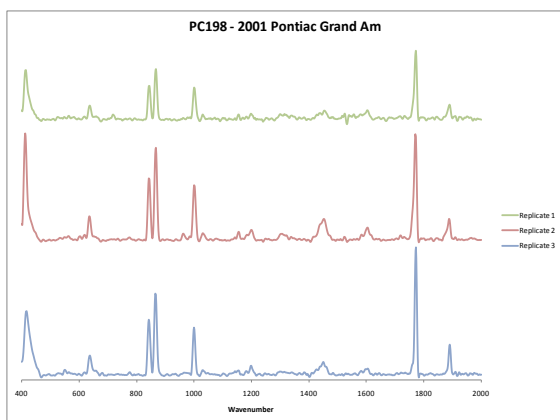
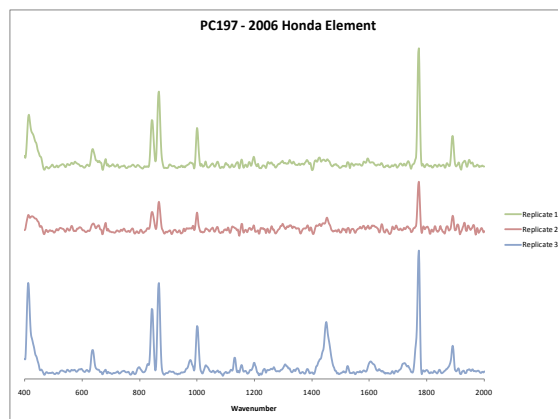
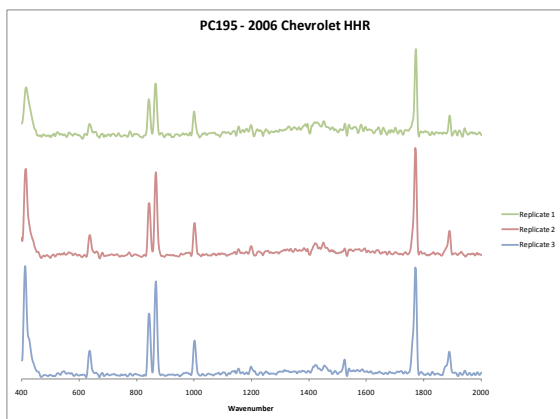


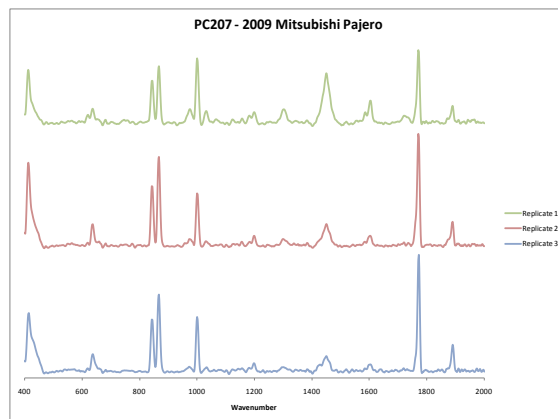
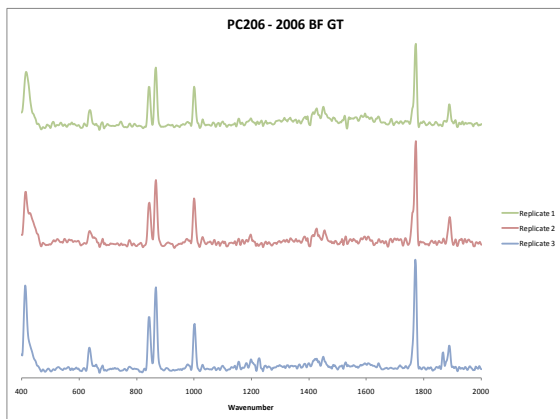
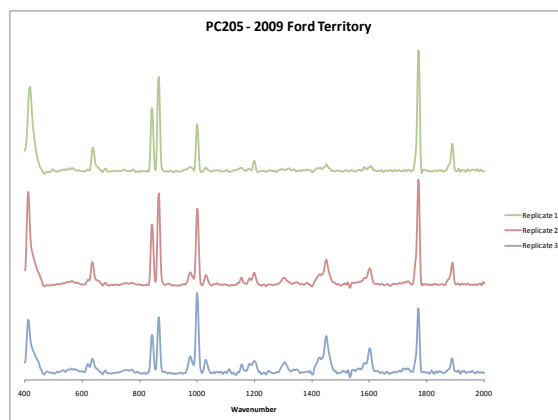
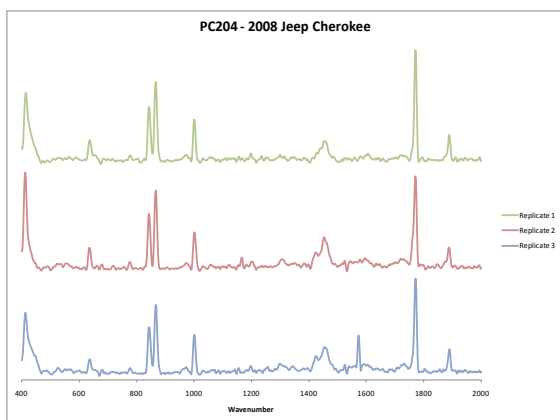
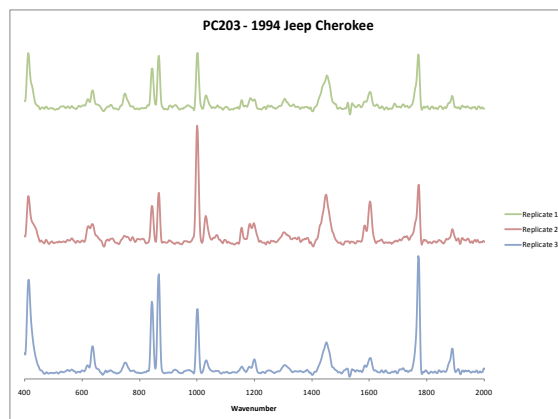
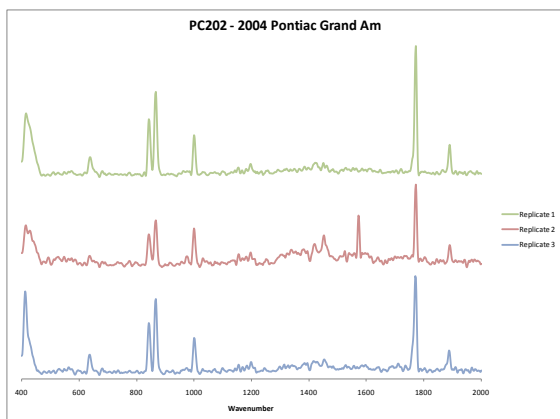


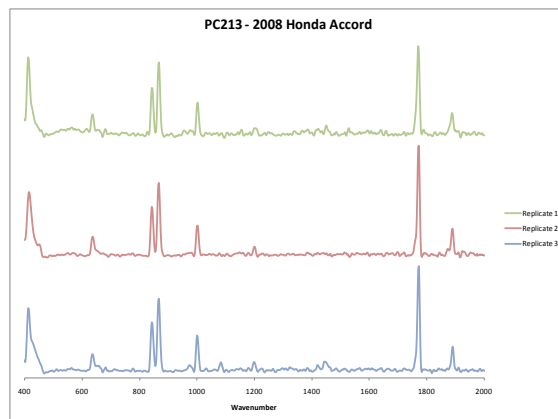
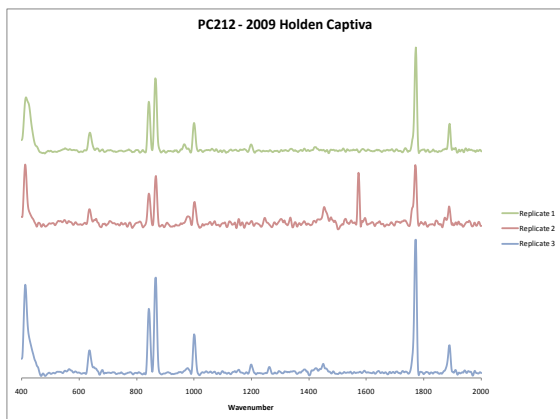
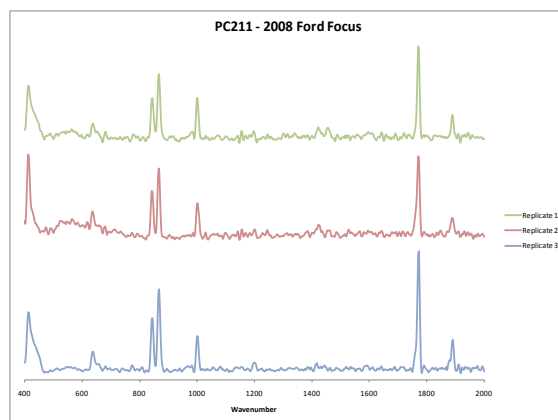
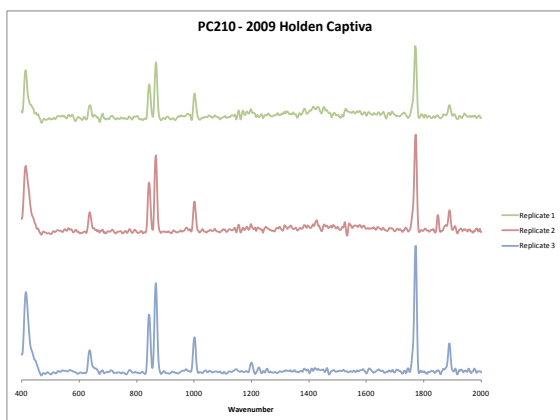
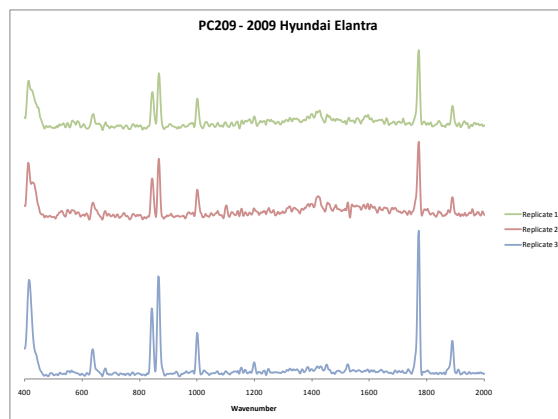
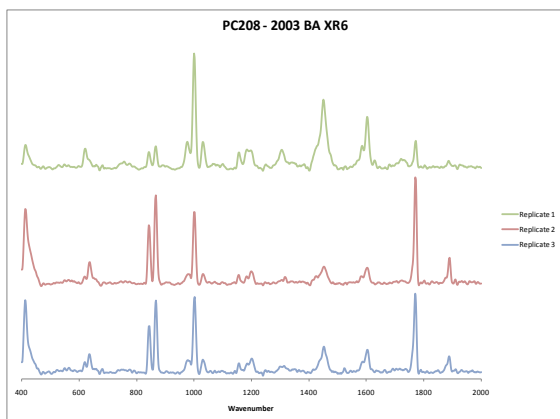


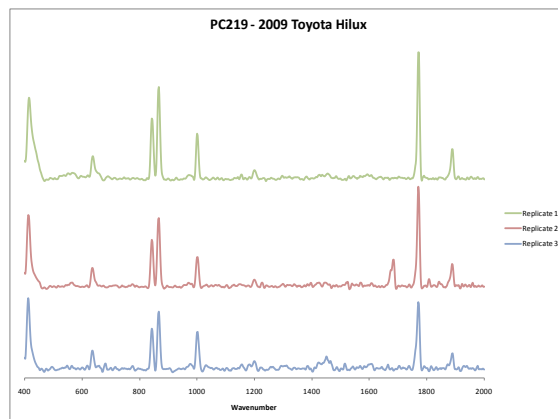
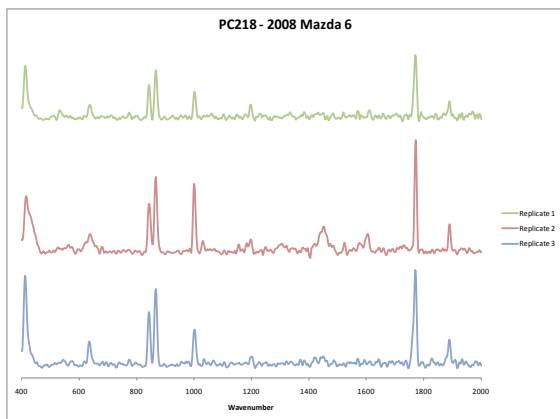
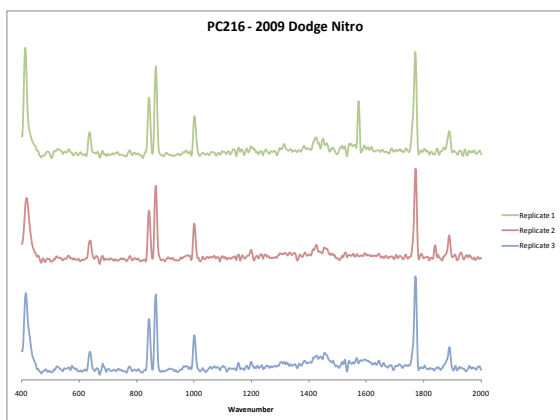
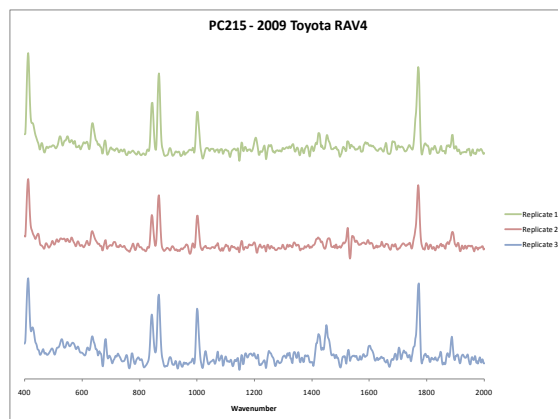
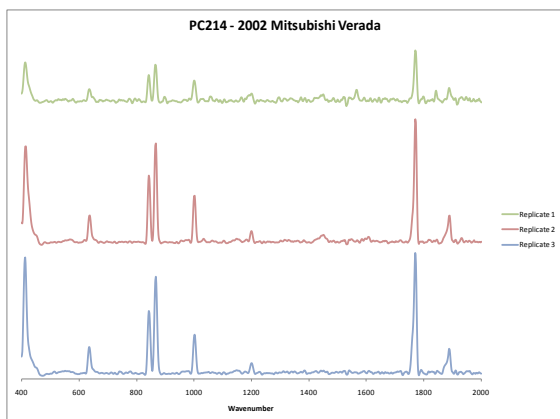


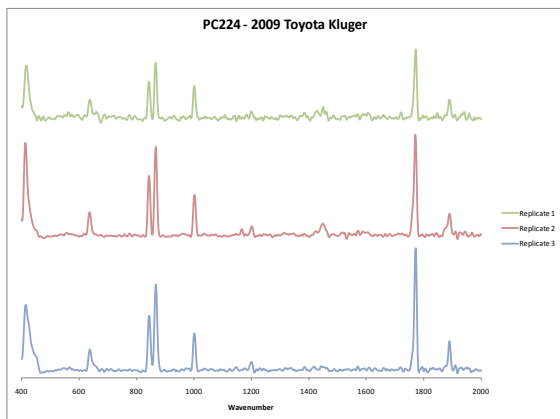
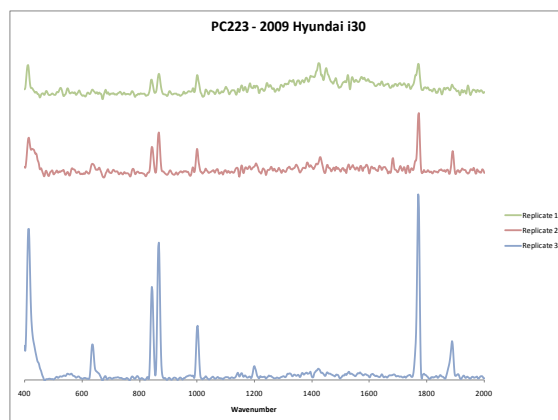
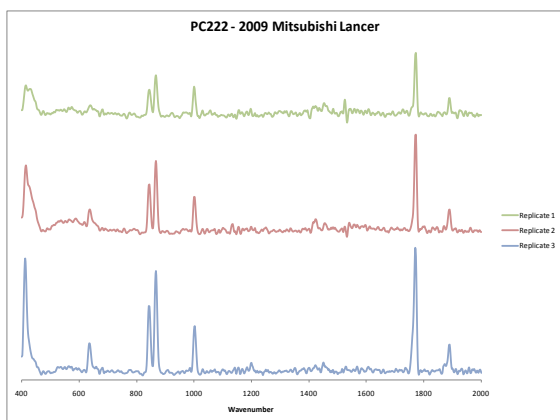
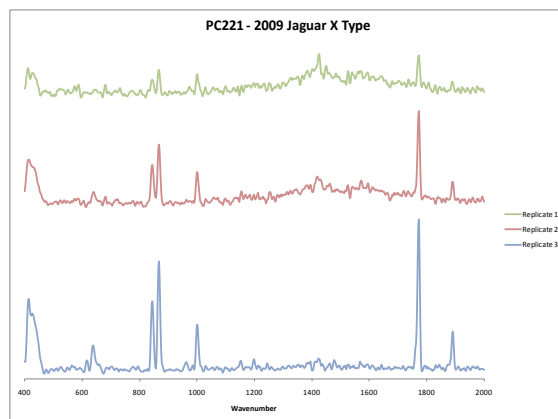
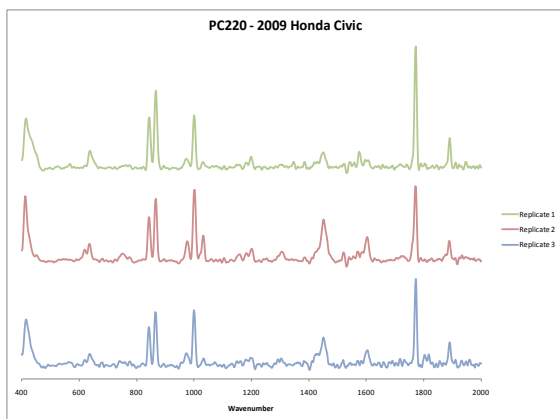


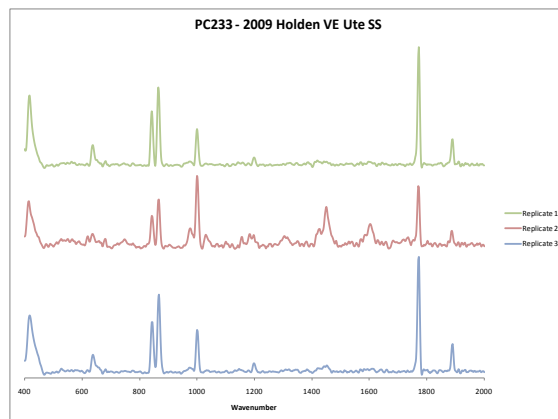
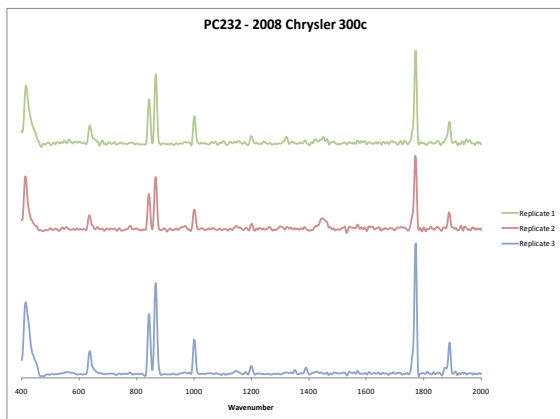
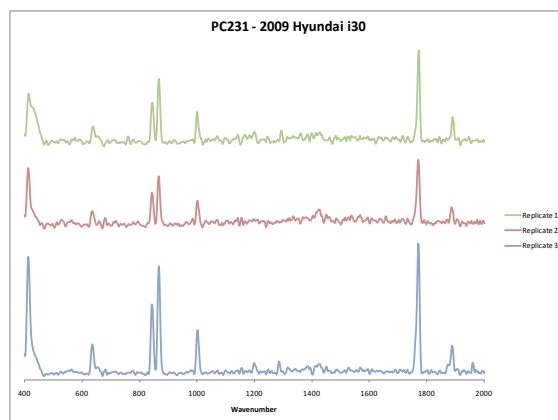
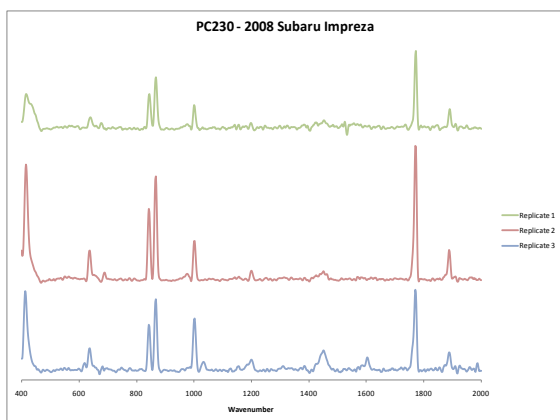
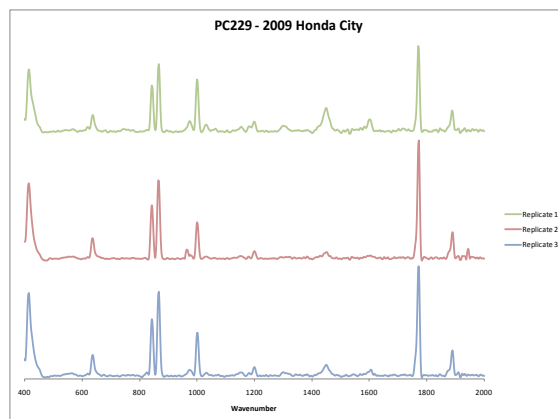
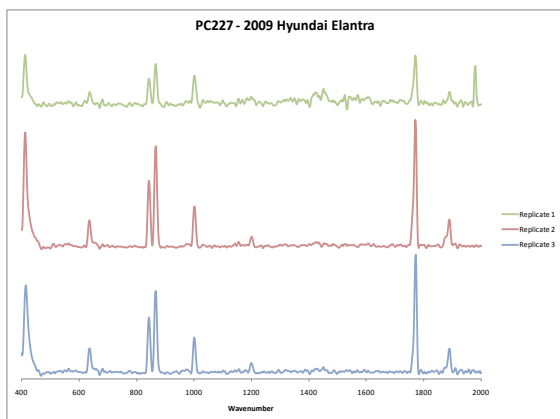


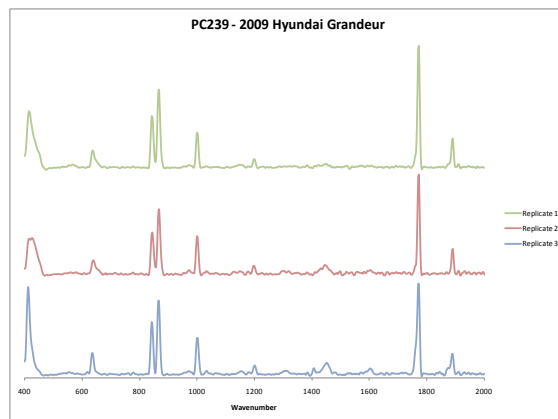
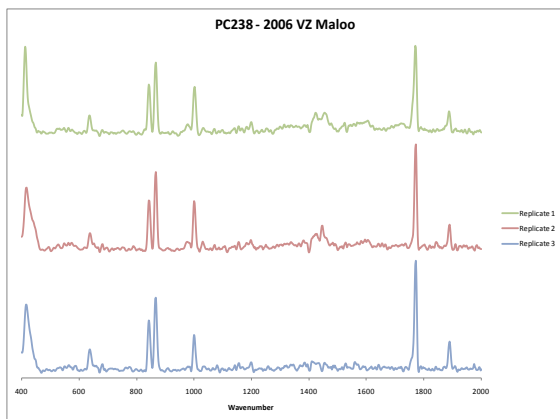
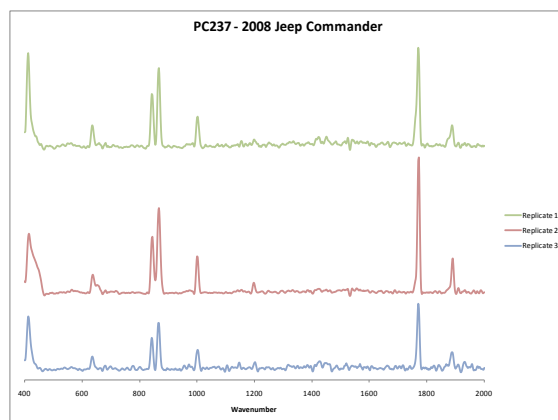
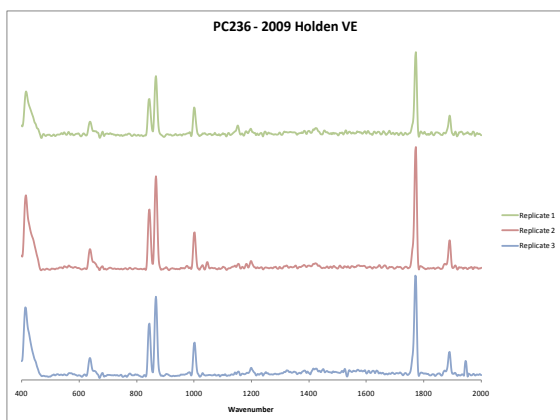
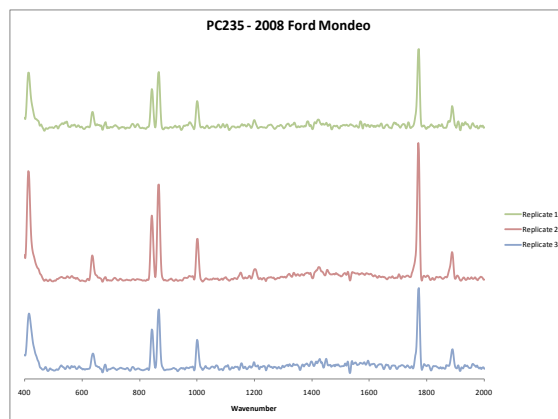
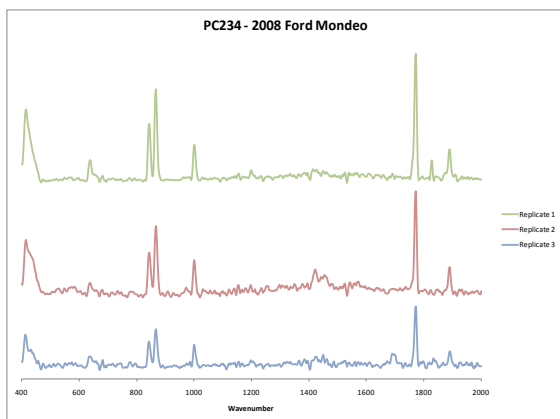




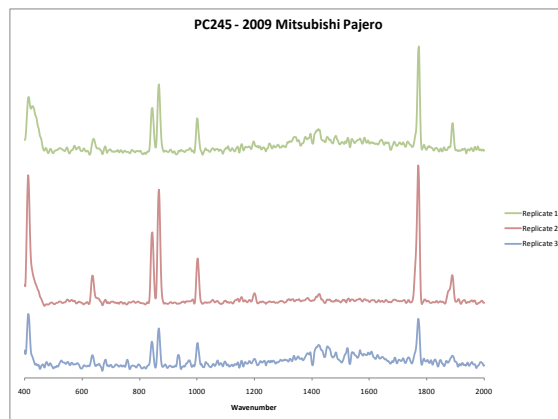
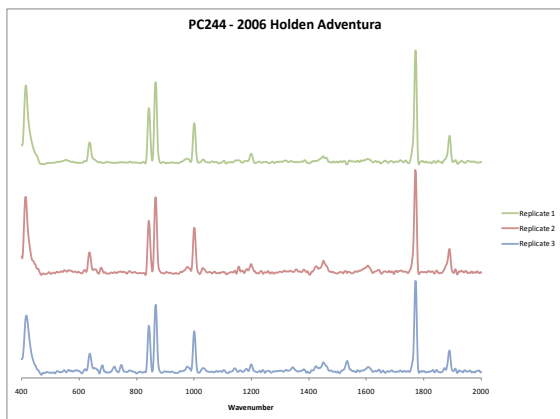
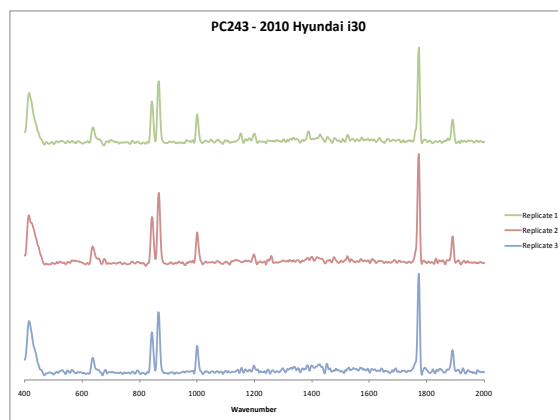
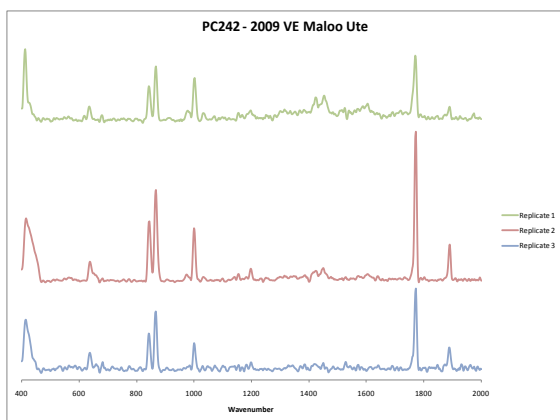
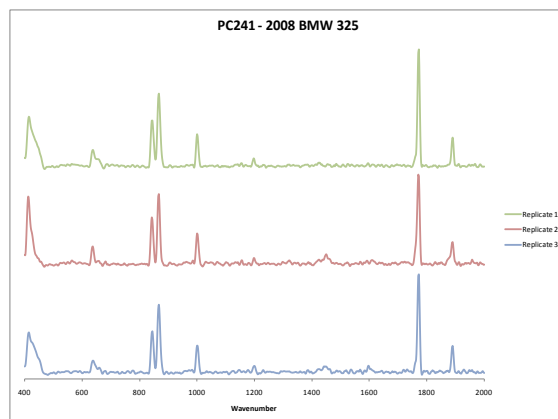
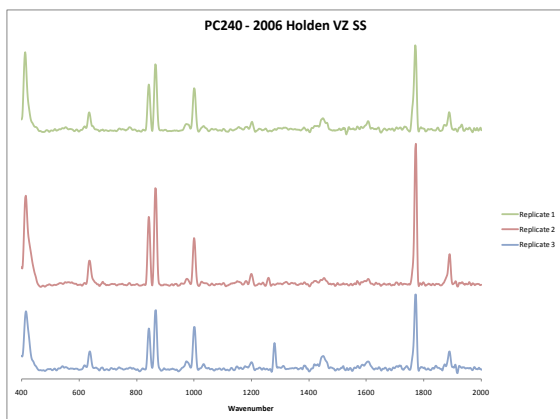


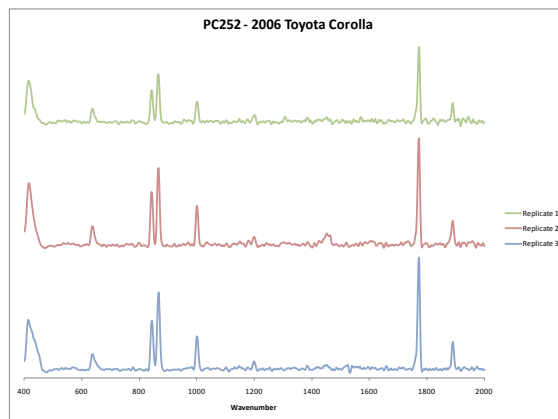
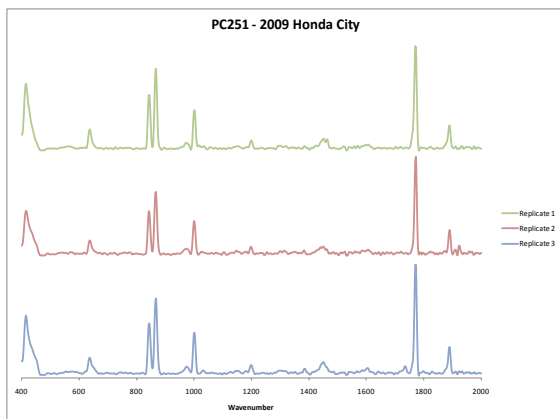
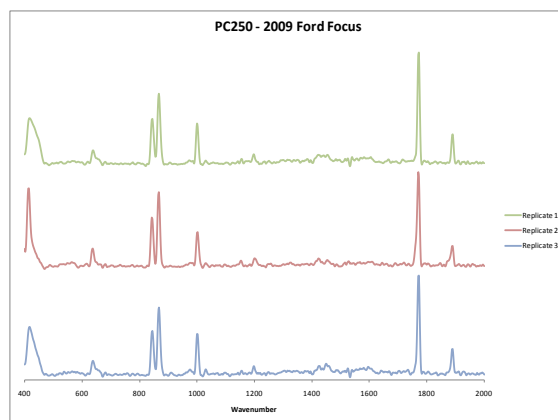
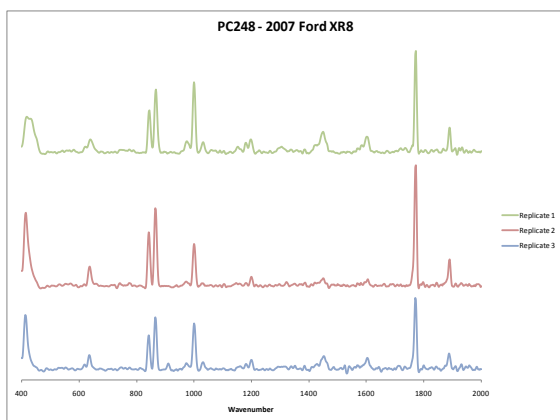
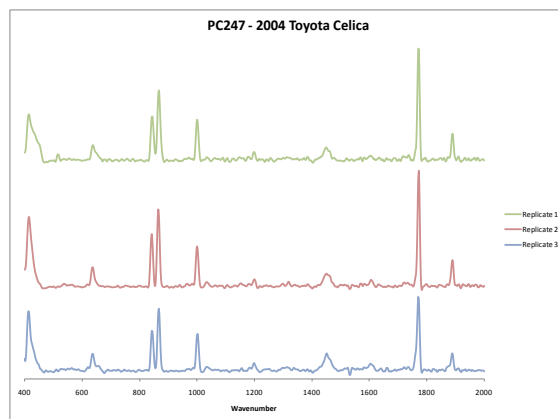
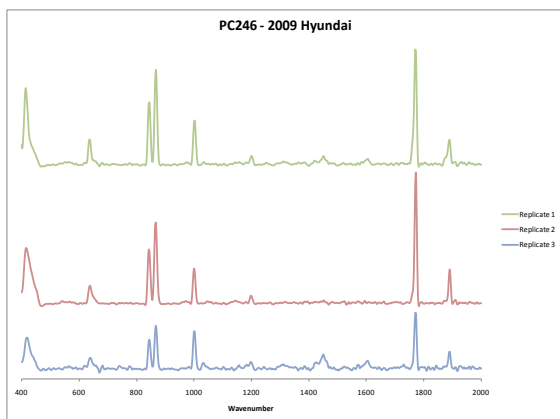


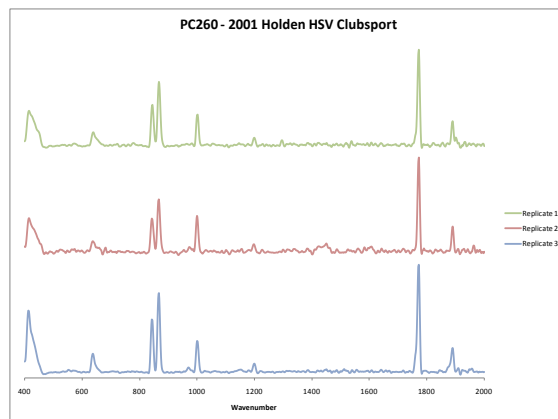
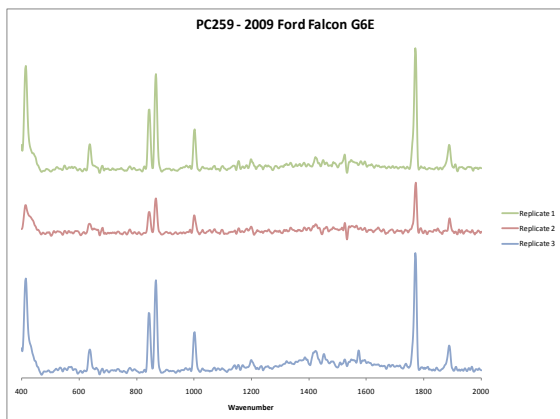
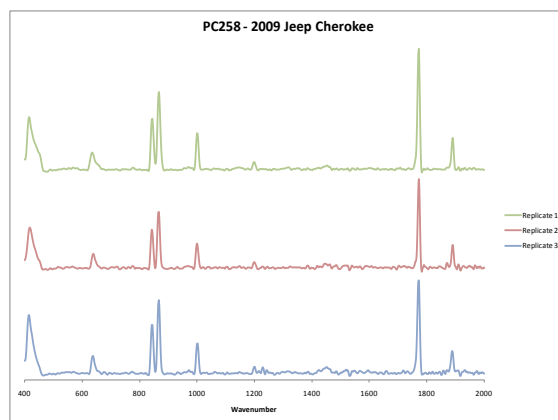
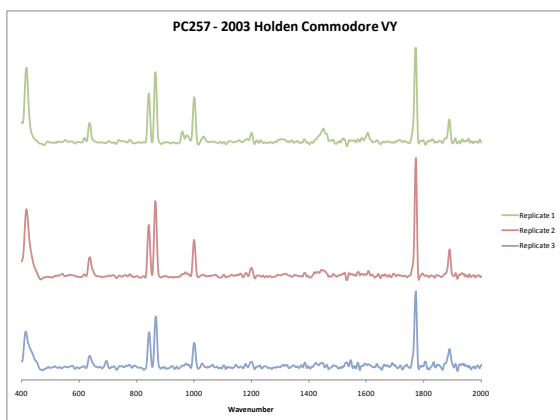
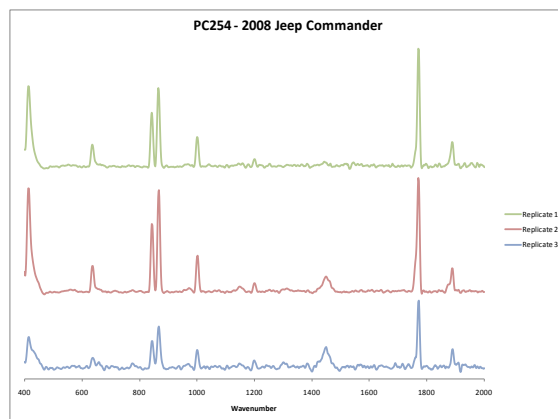
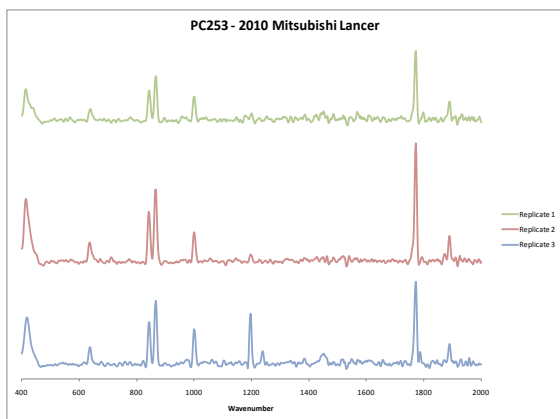


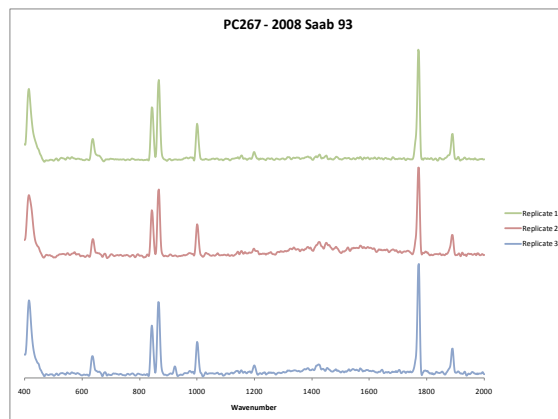
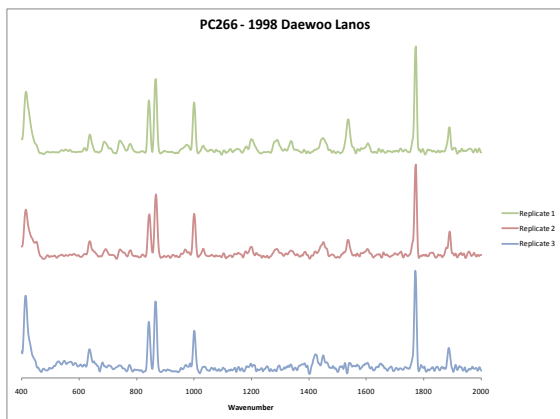
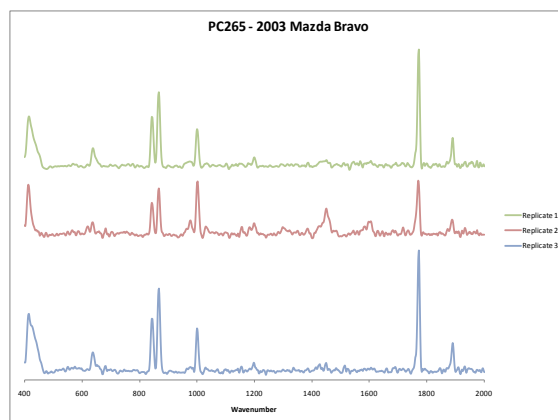
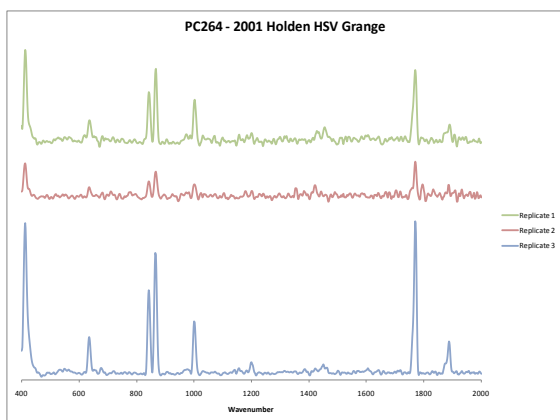
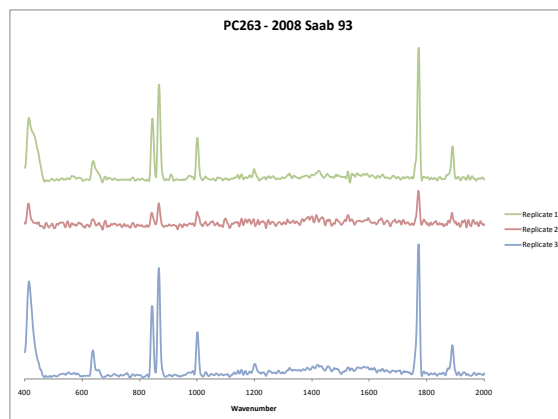
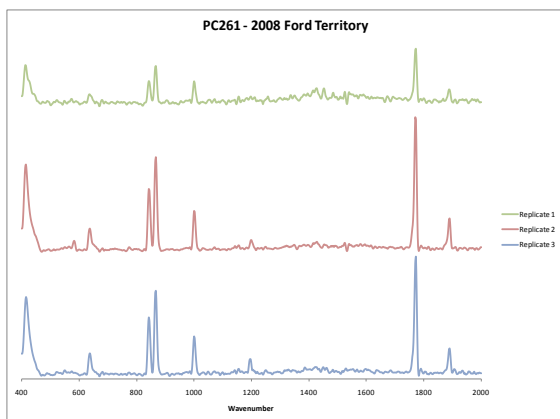


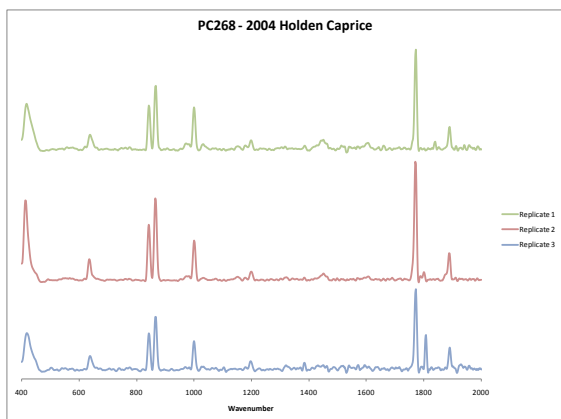






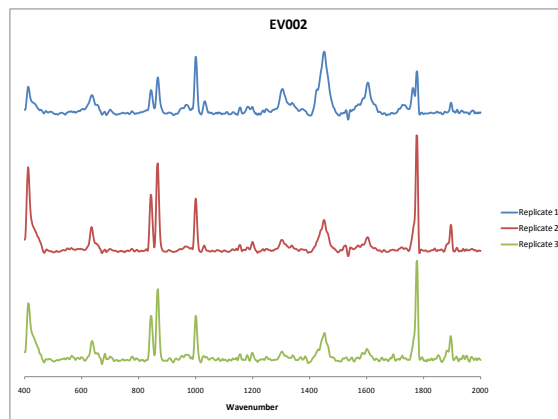
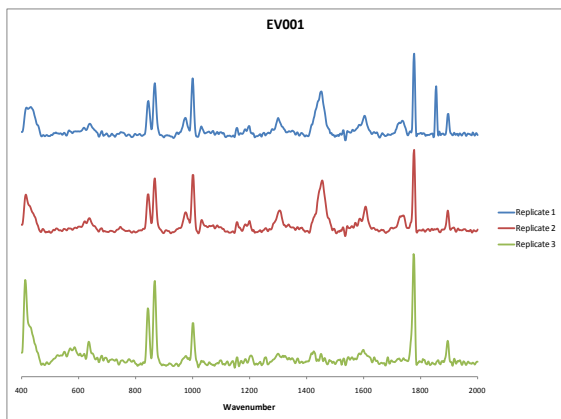


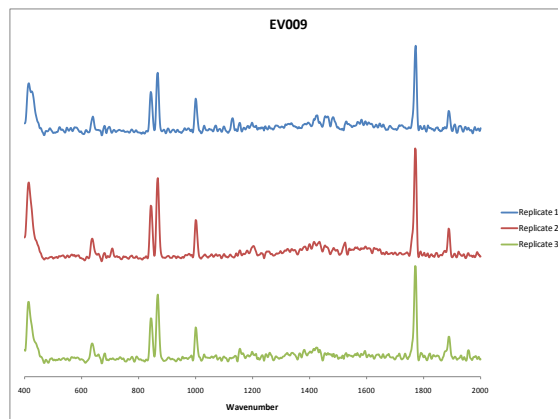
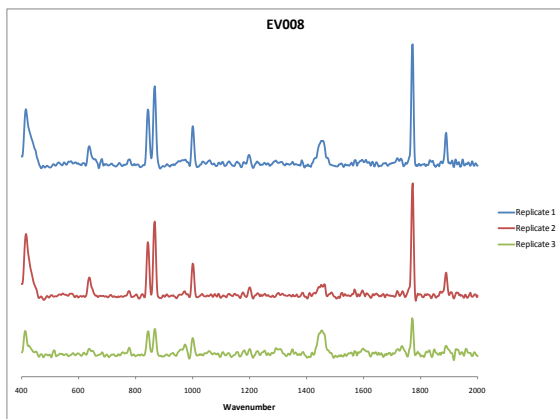
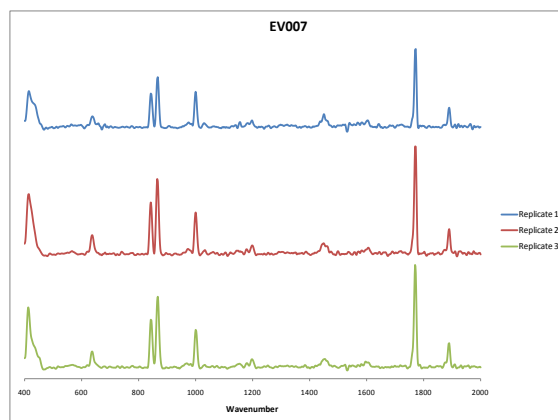
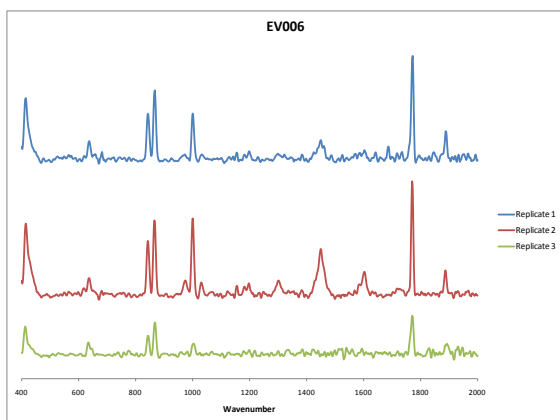
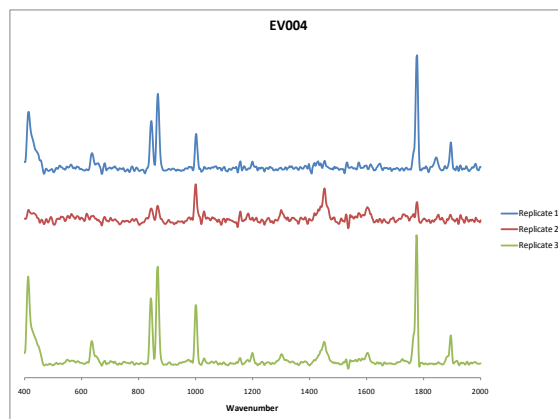
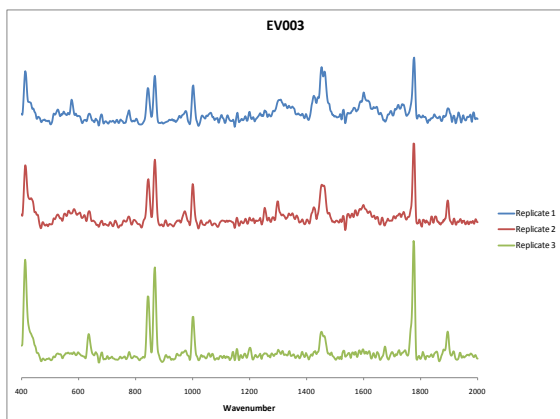


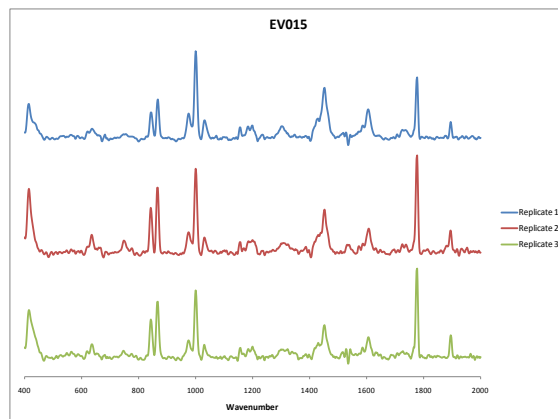
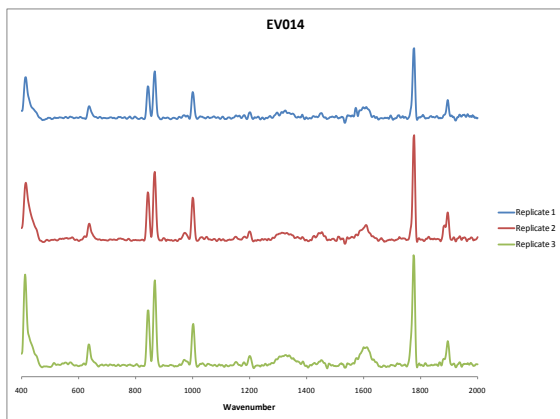
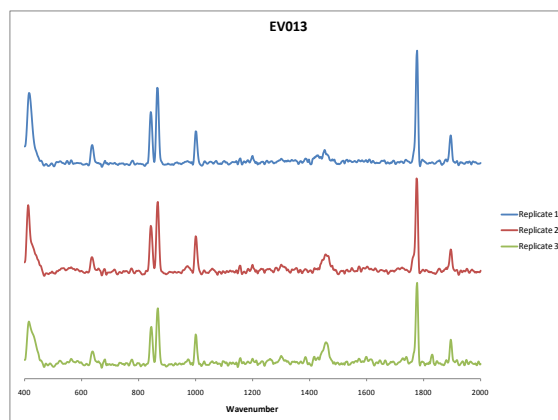
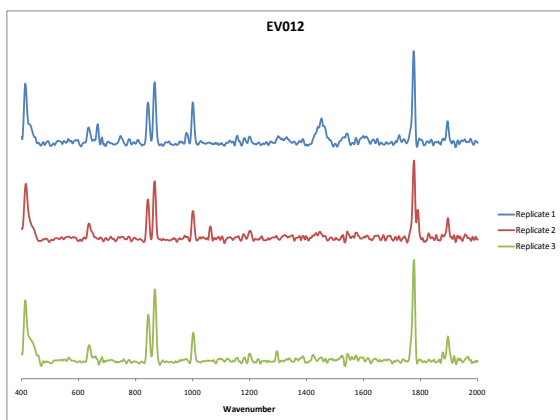
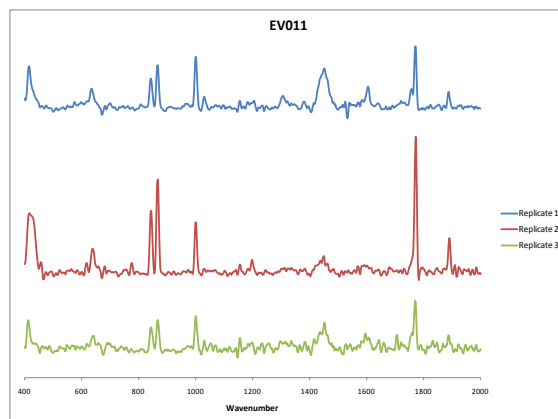
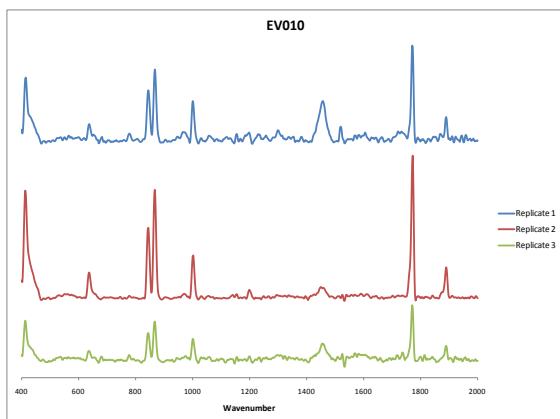


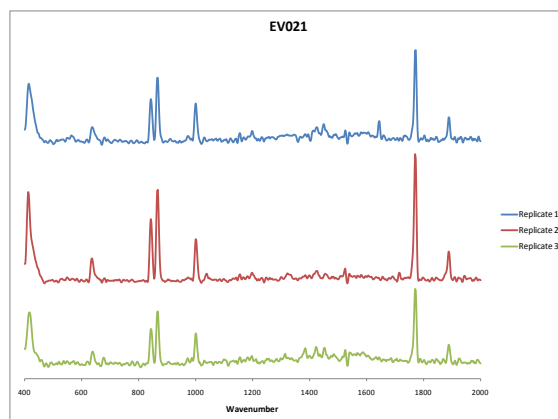
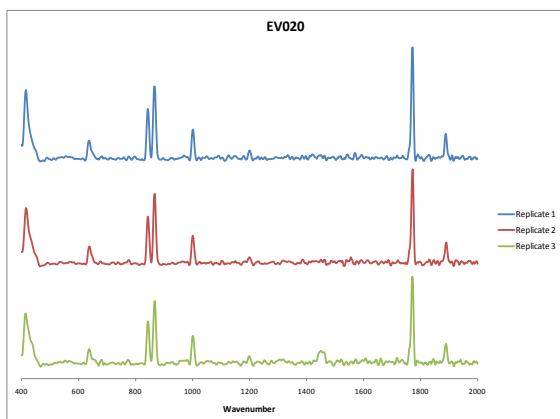
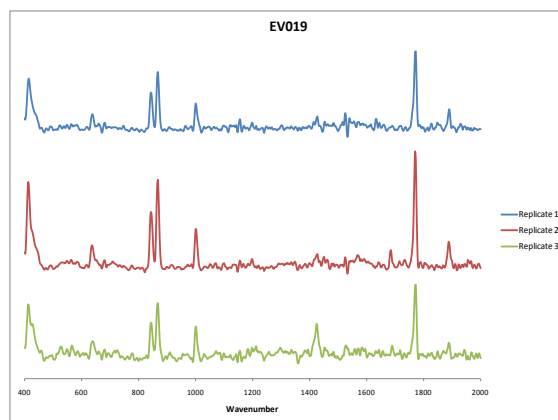
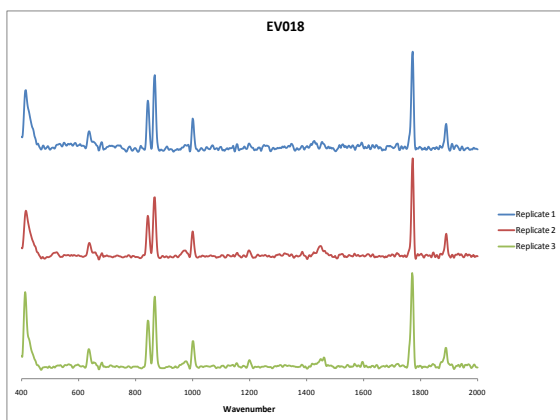
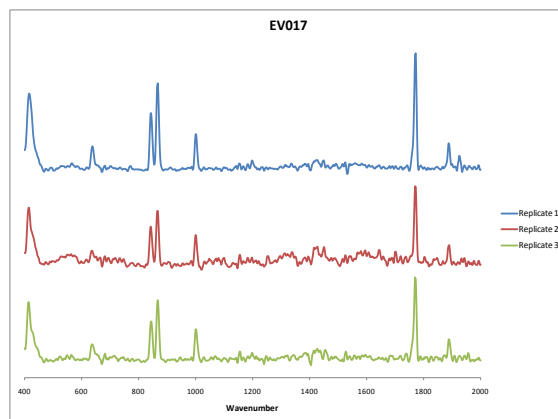
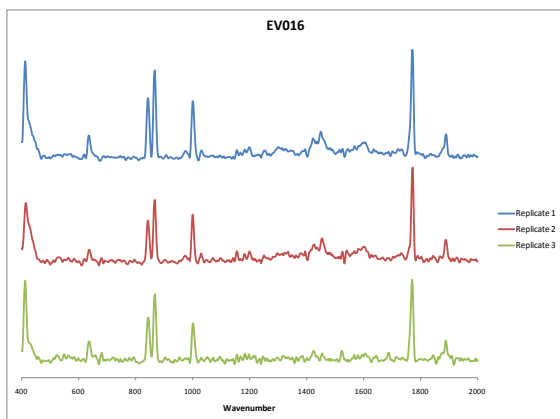
## A.2 External Validation Samples

### A.2.1 External Validation Spectra

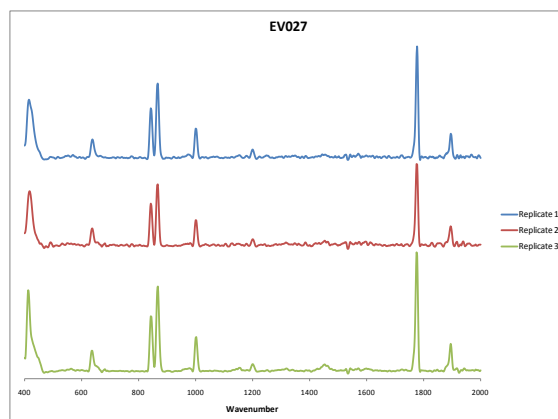
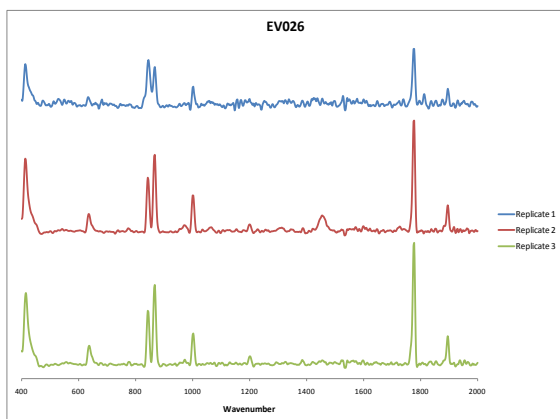
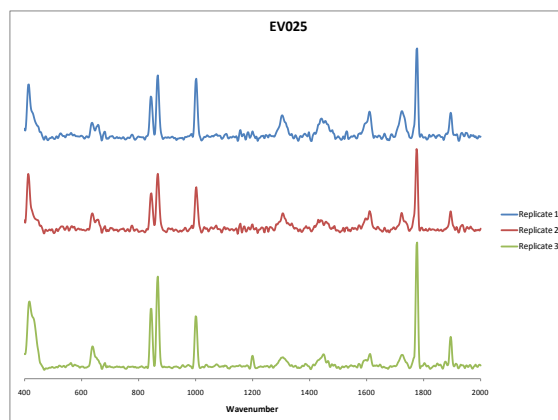
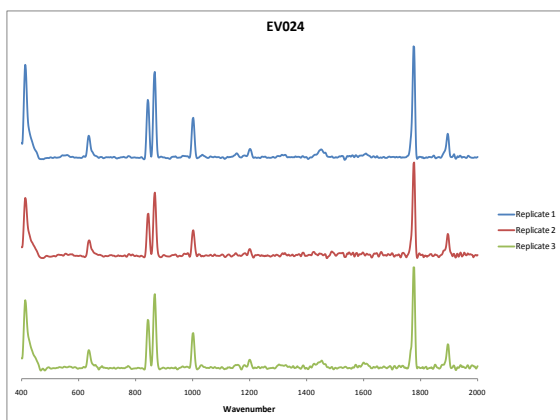
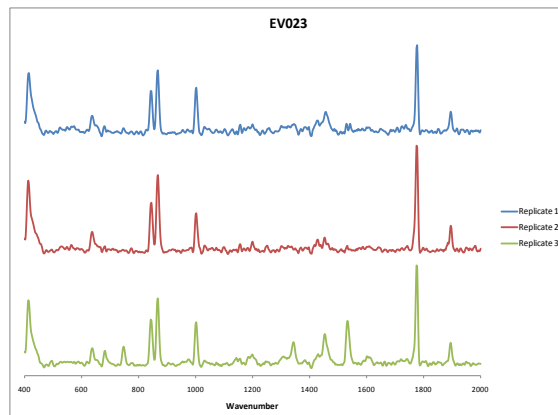
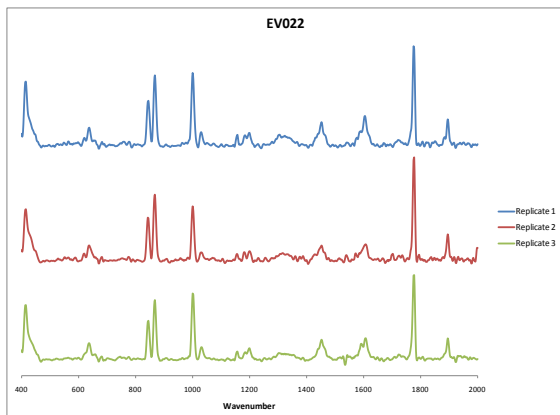


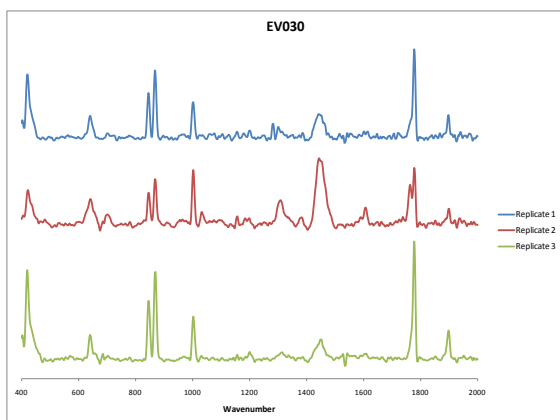
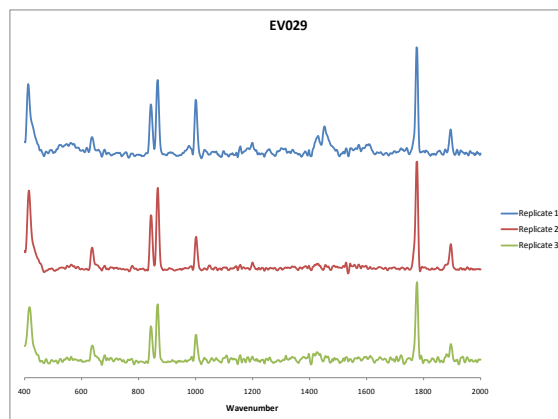
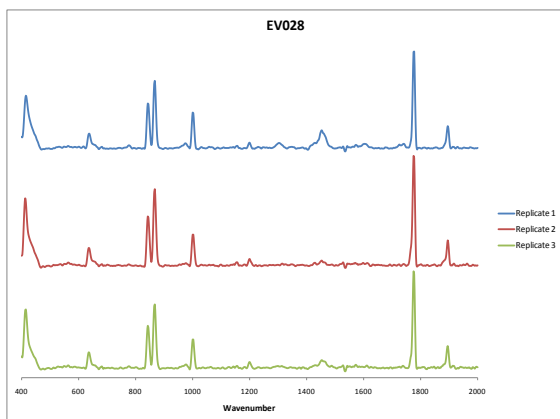




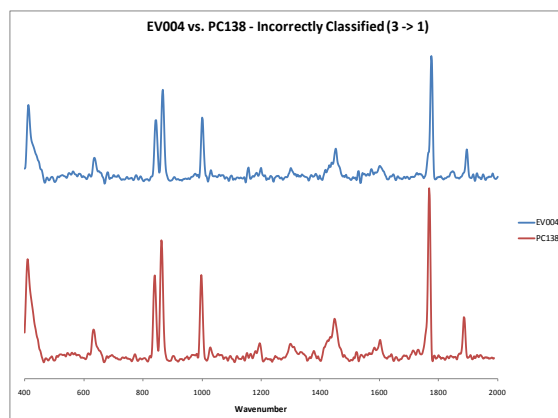
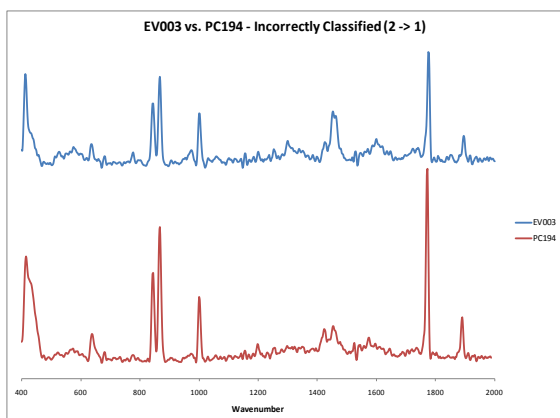
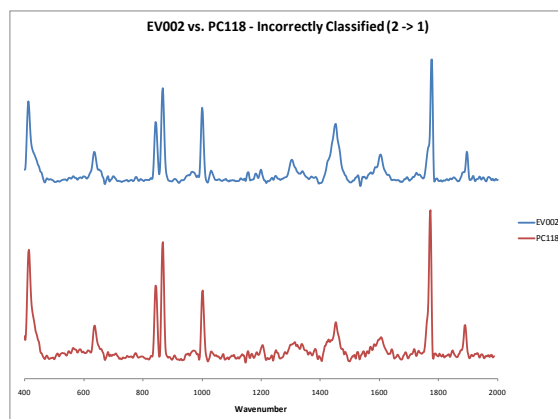
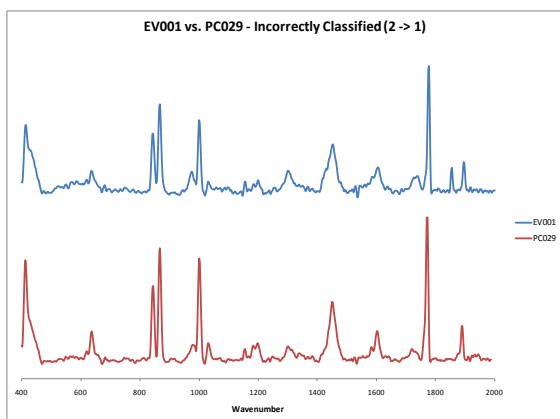


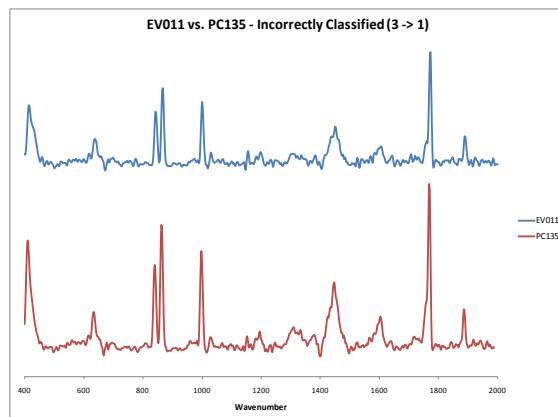
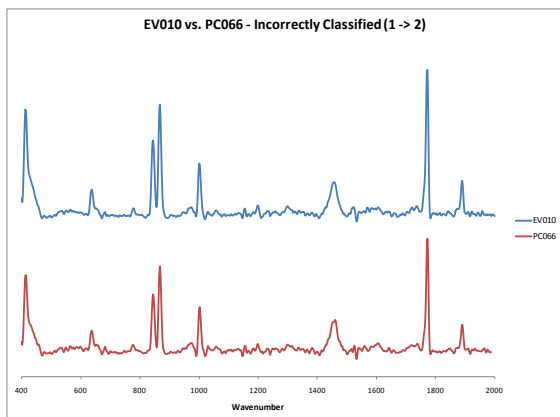
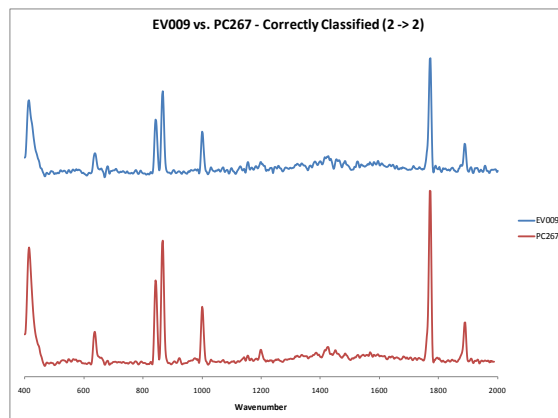
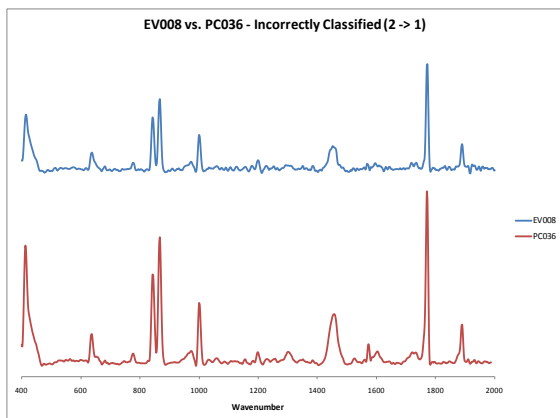
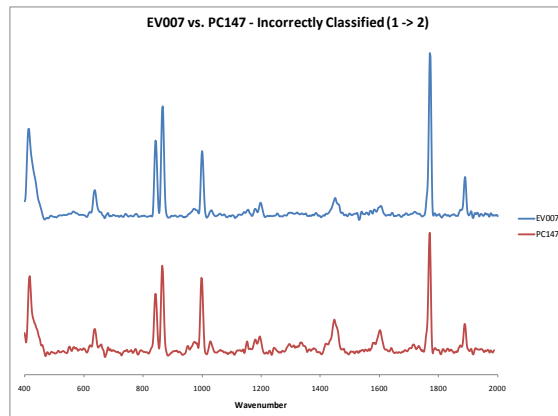
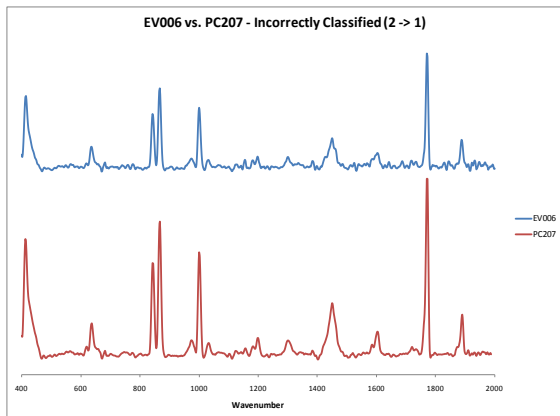


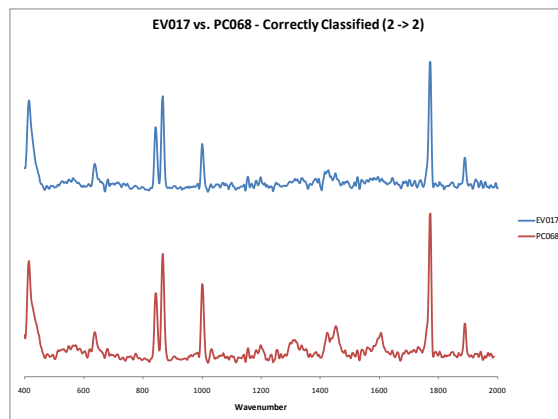
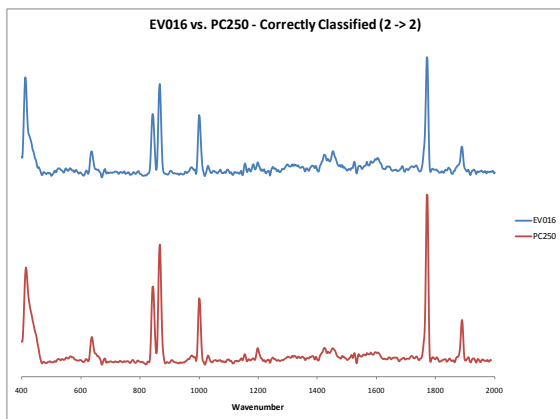
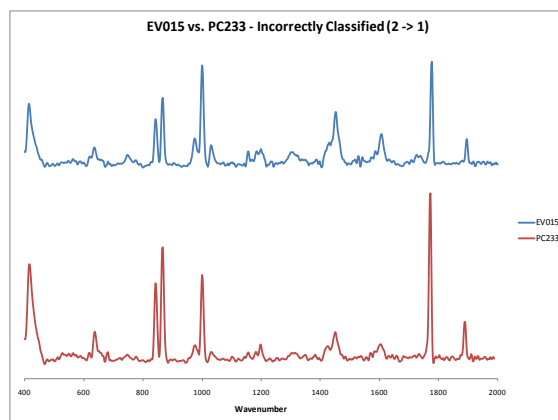
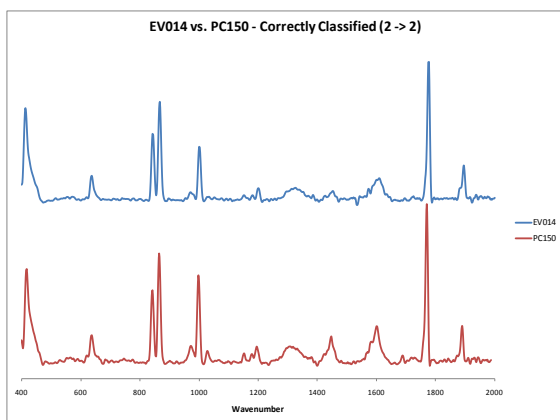
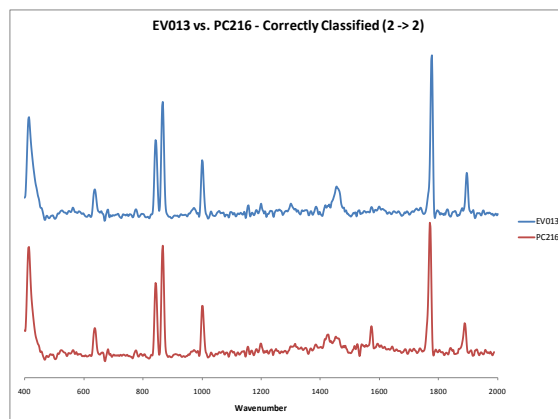
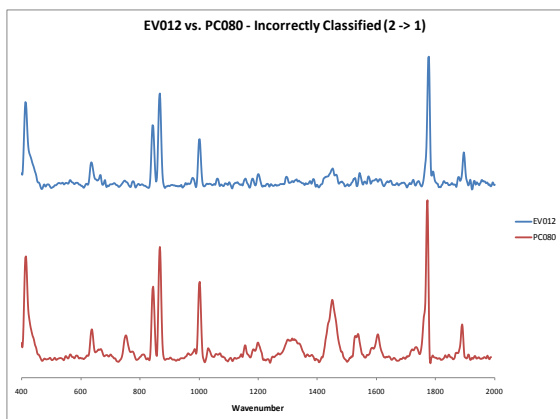


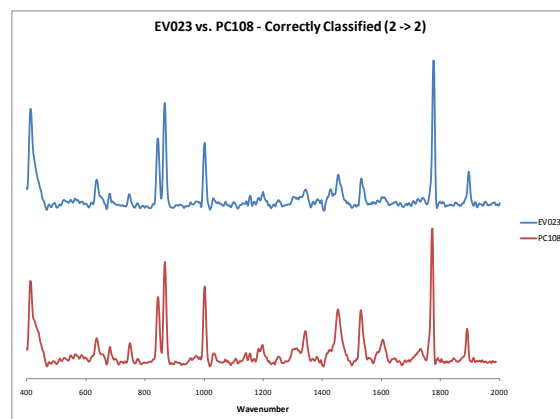
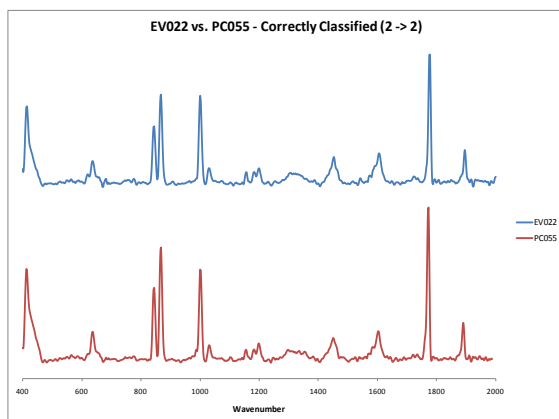
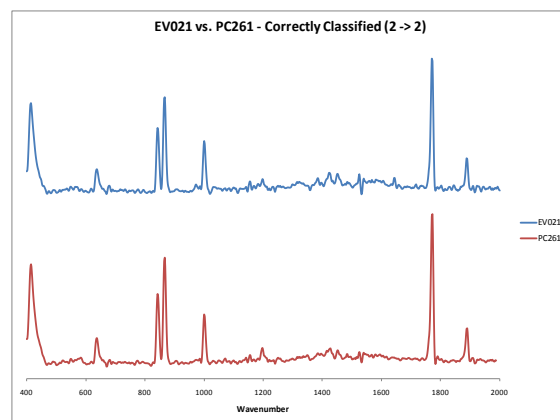
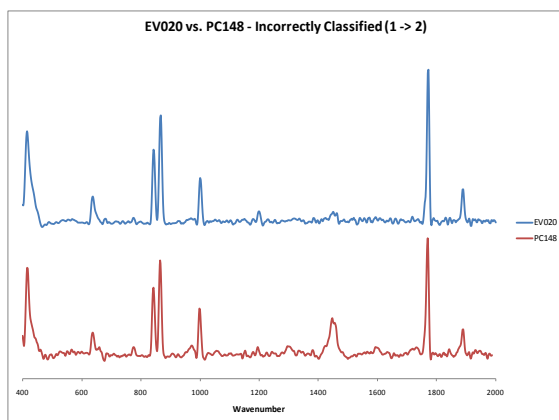
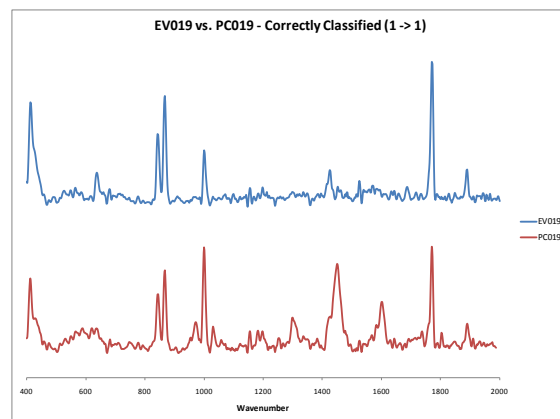
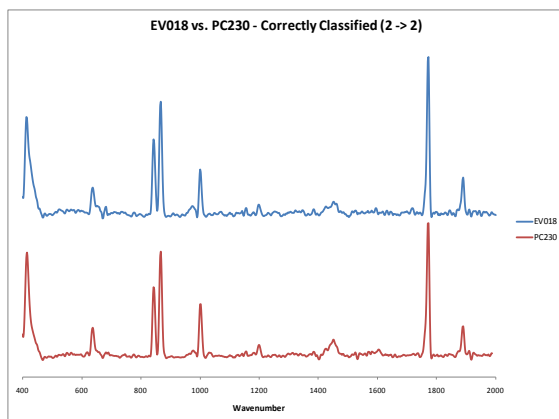


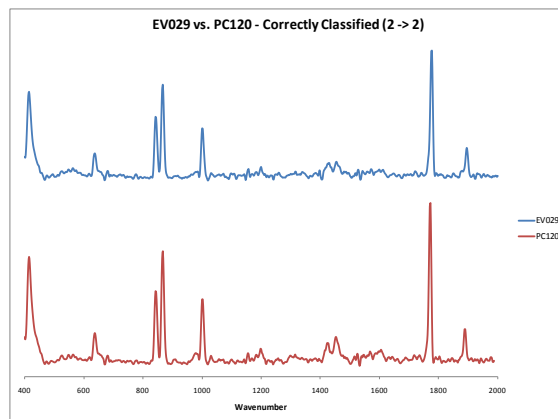
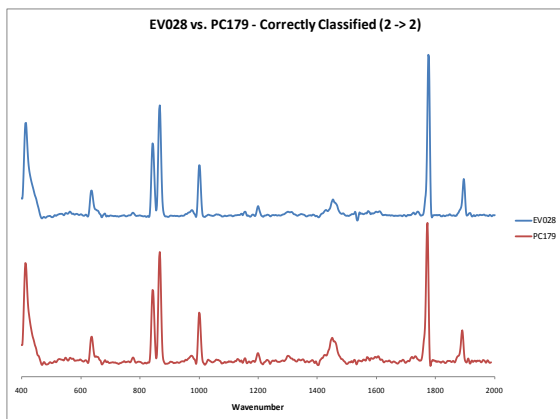
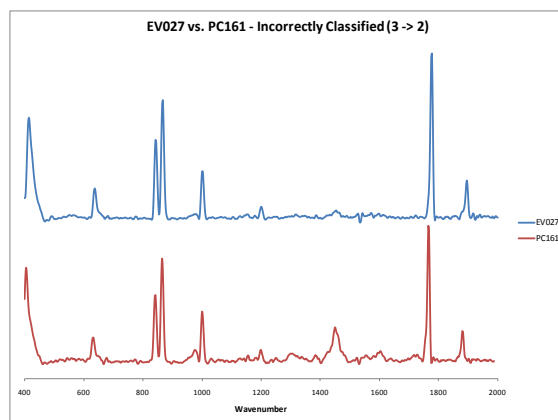
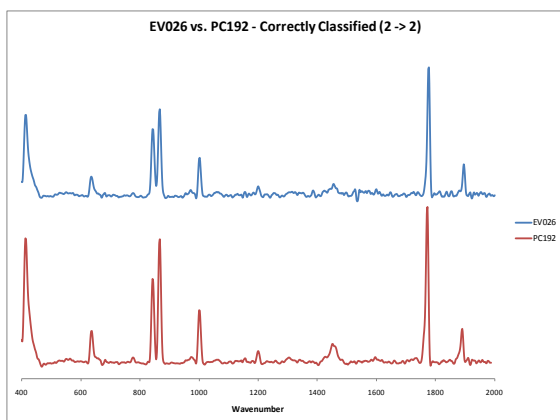
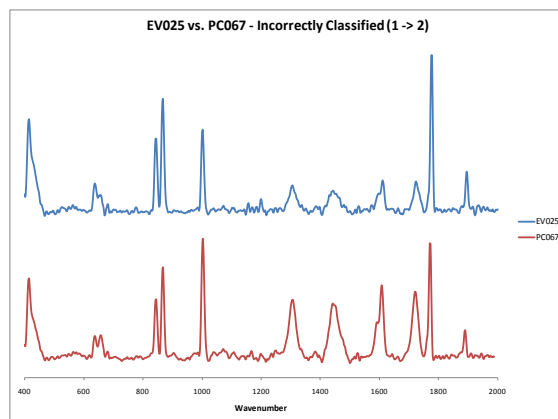
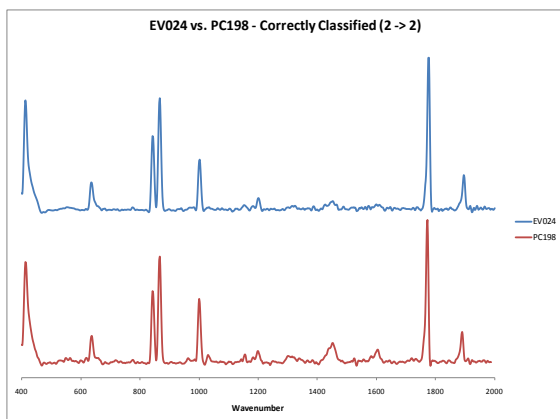
## A.2.2 Comparison of External Validation and Training Set (averaged spectra)

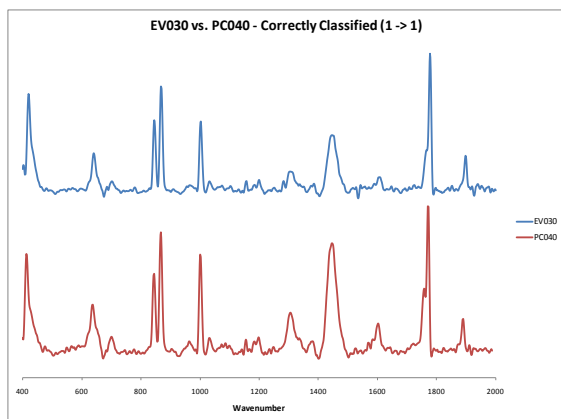








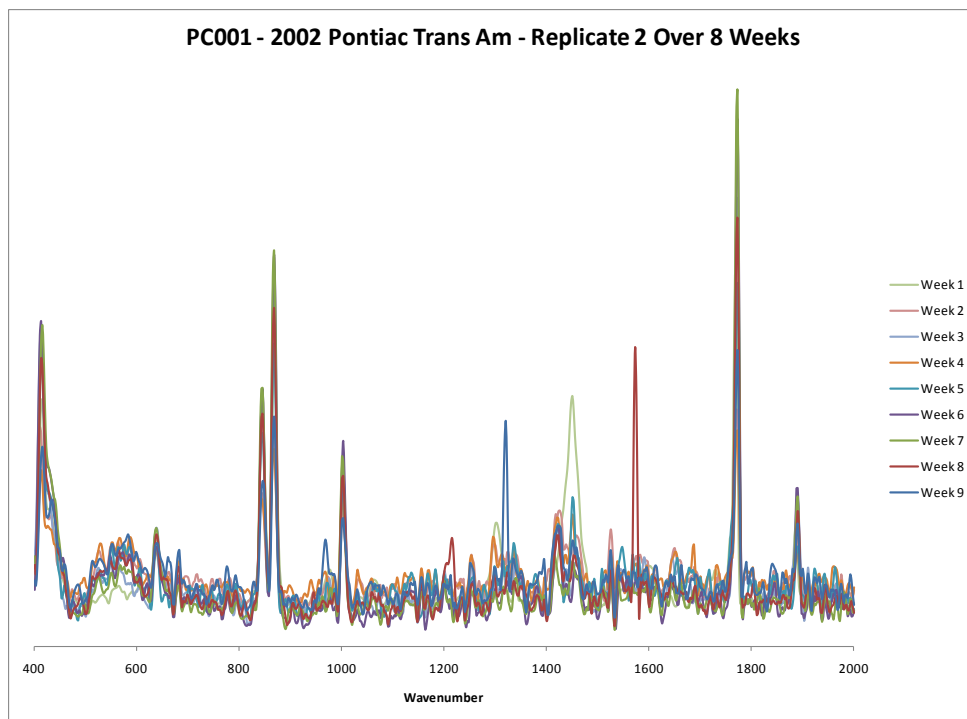
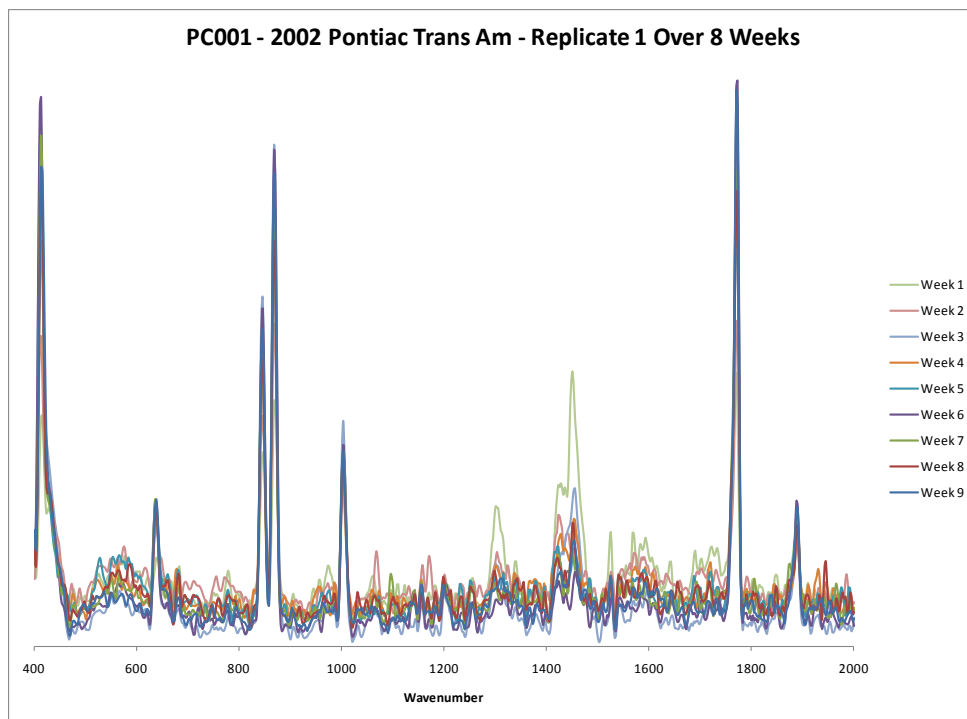


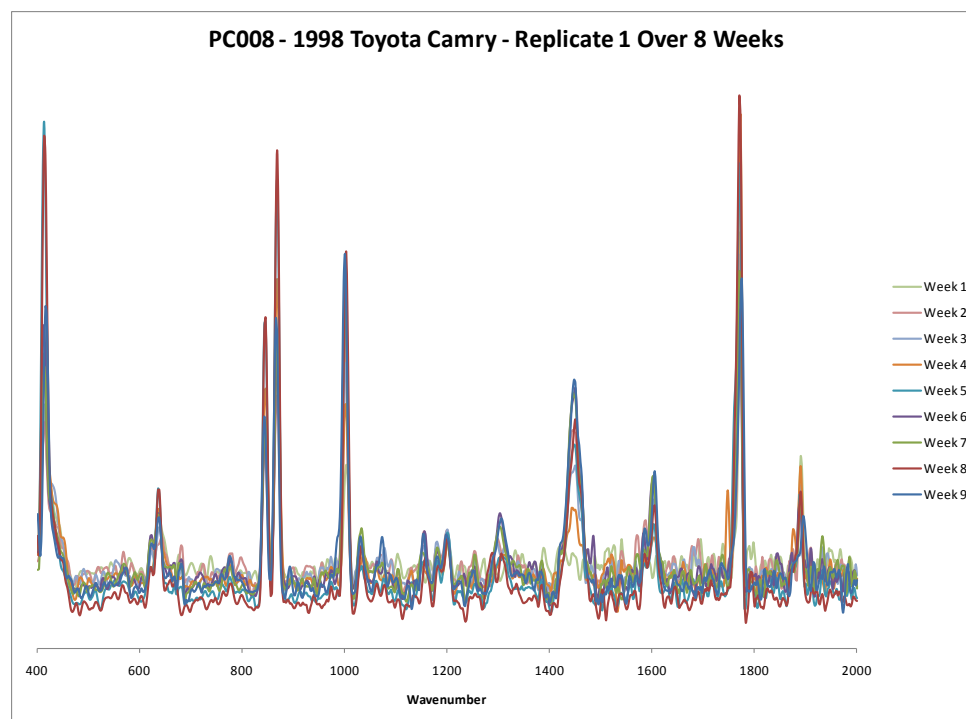
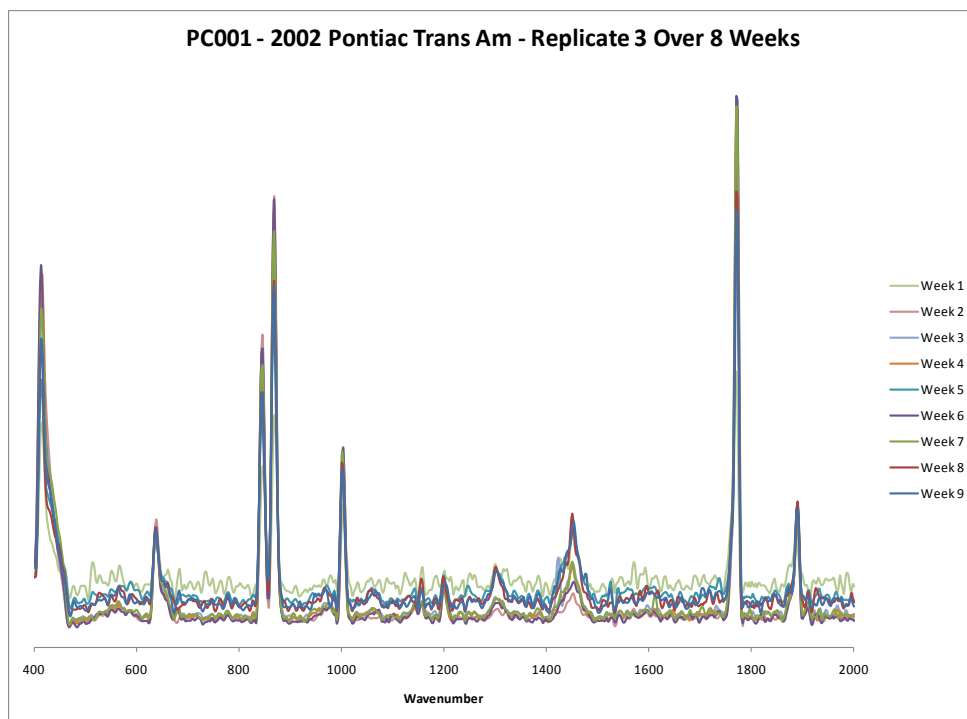


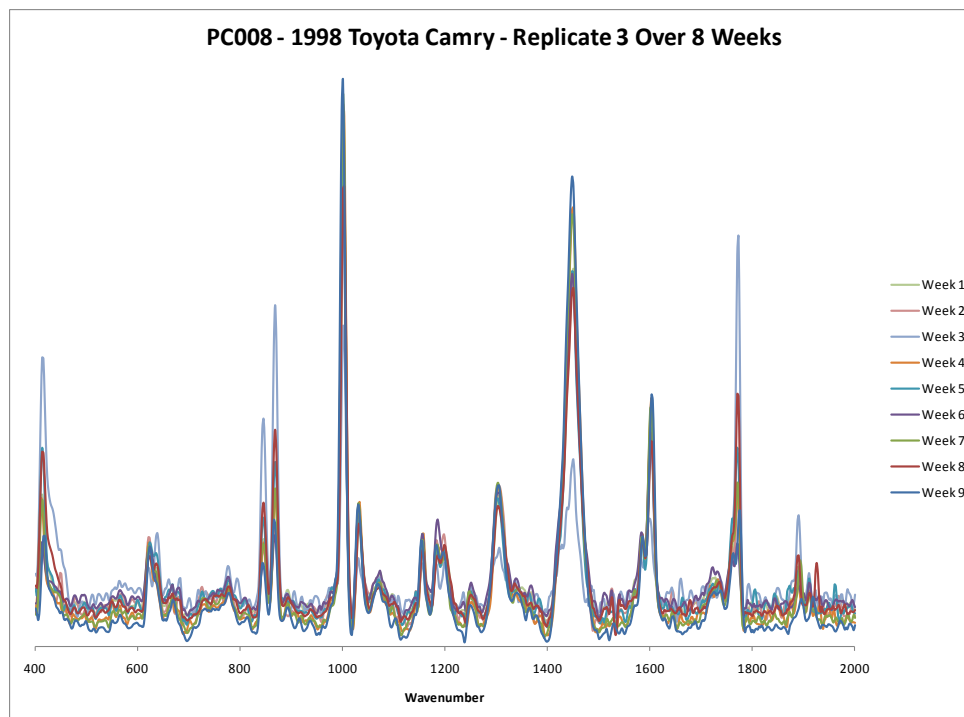
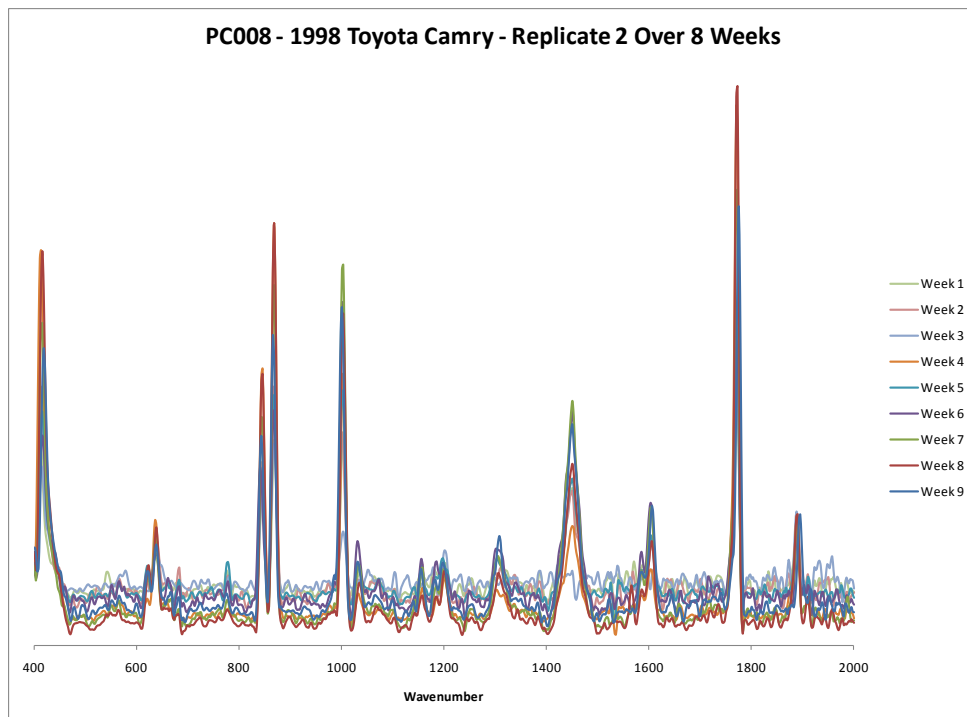


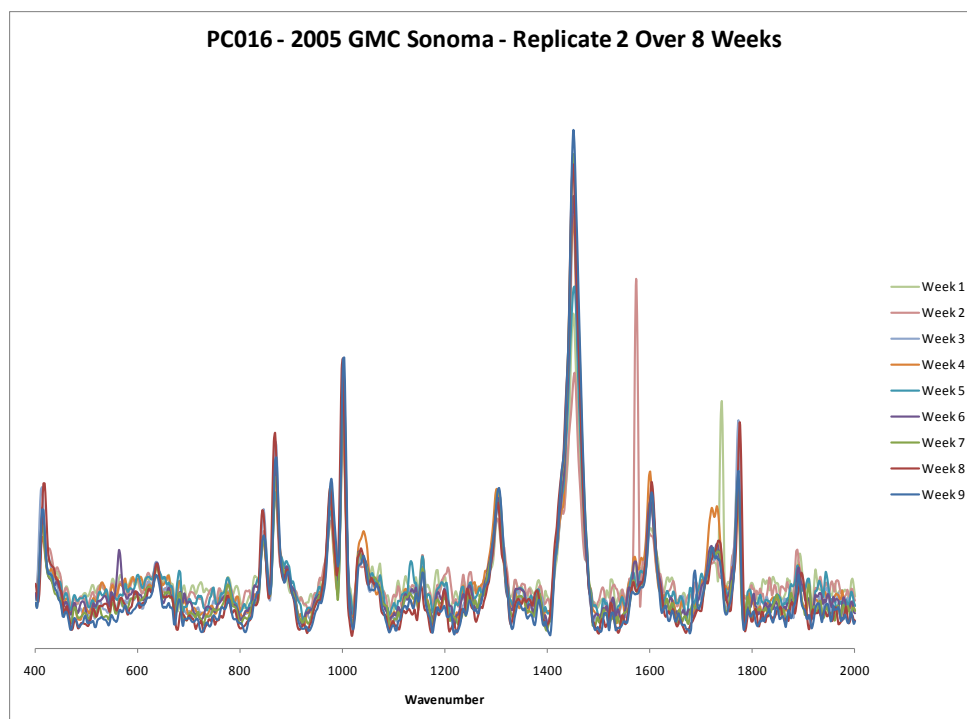
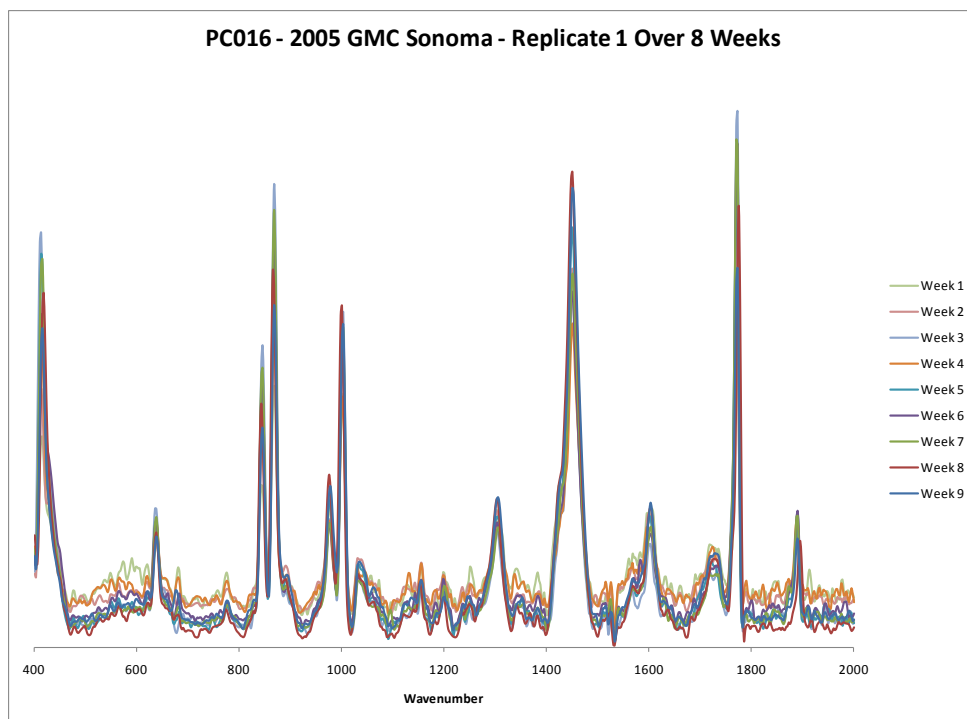
## Appendix B. Clear Coat Spectra by Raman Spectroscopy: Time Study

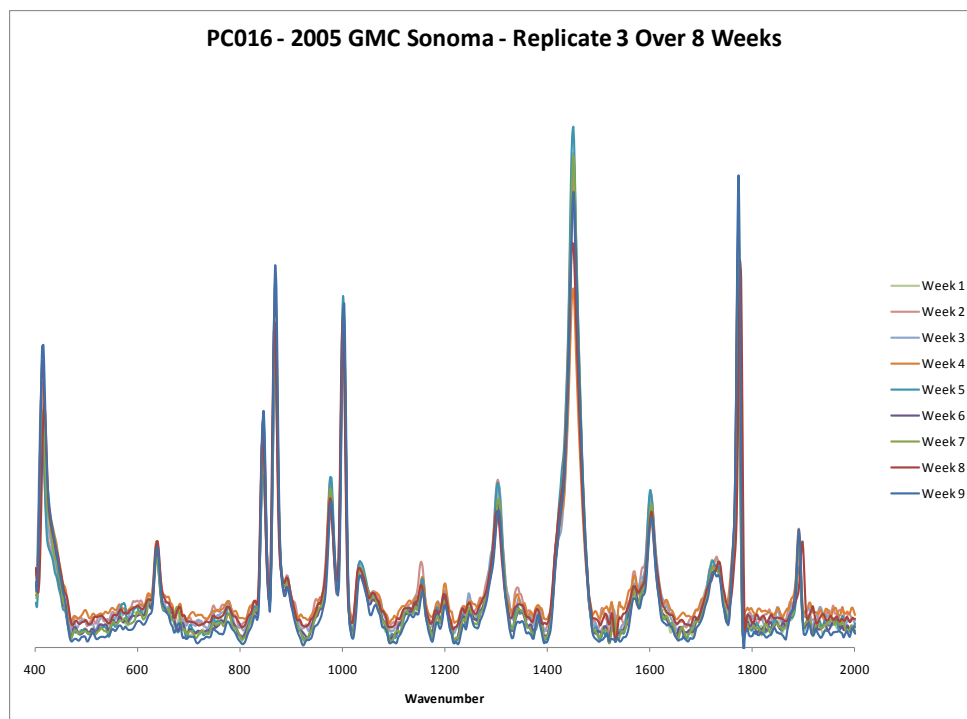
### B.1 Samples Stored in a Dark Cabinet



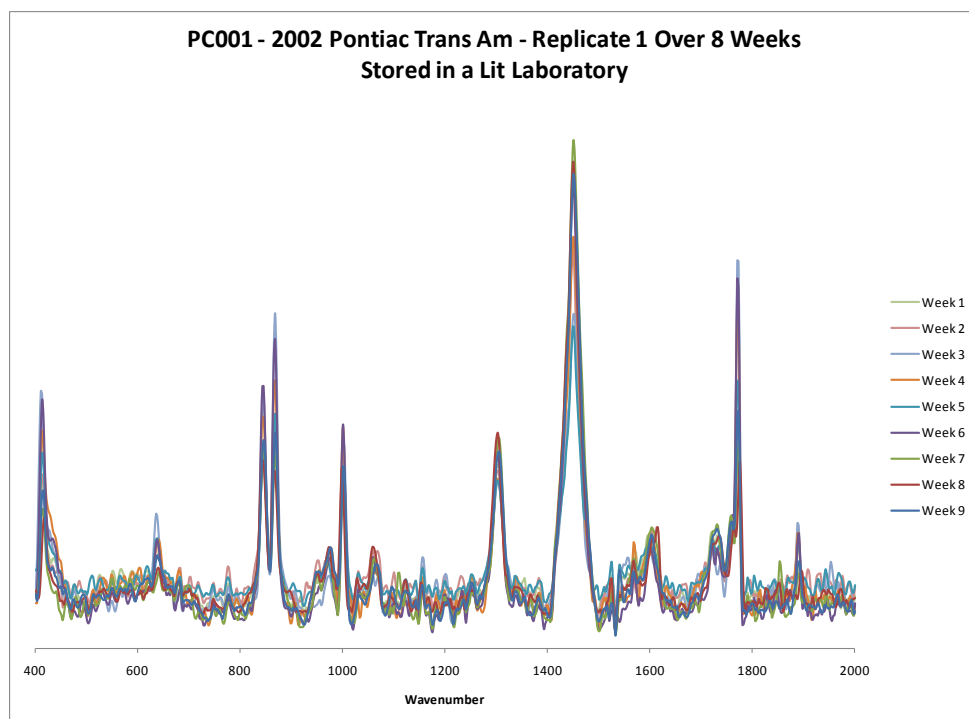


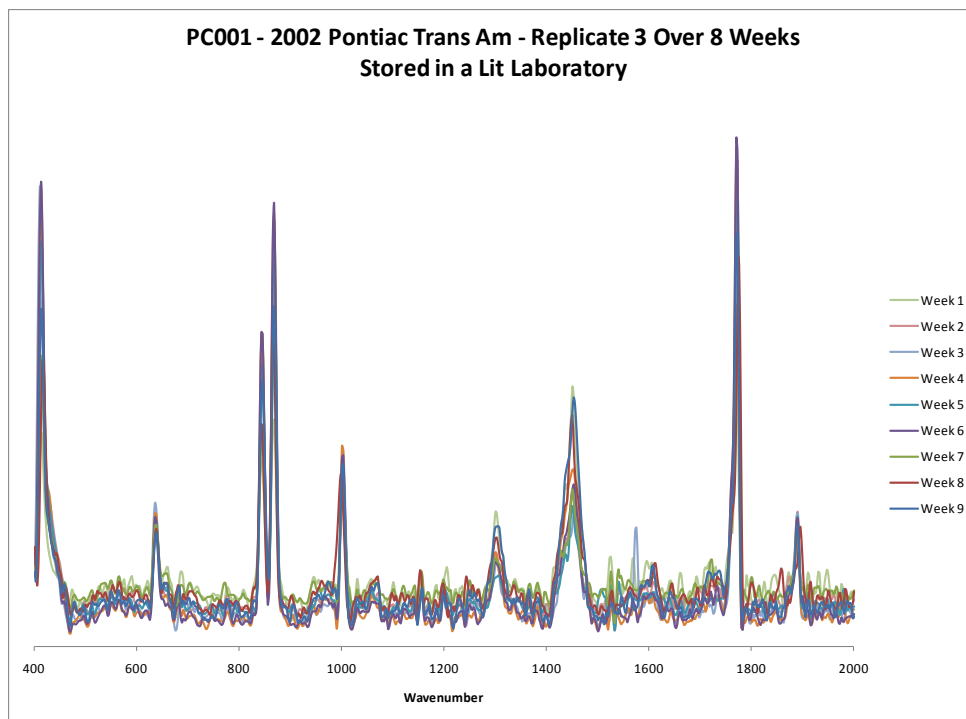
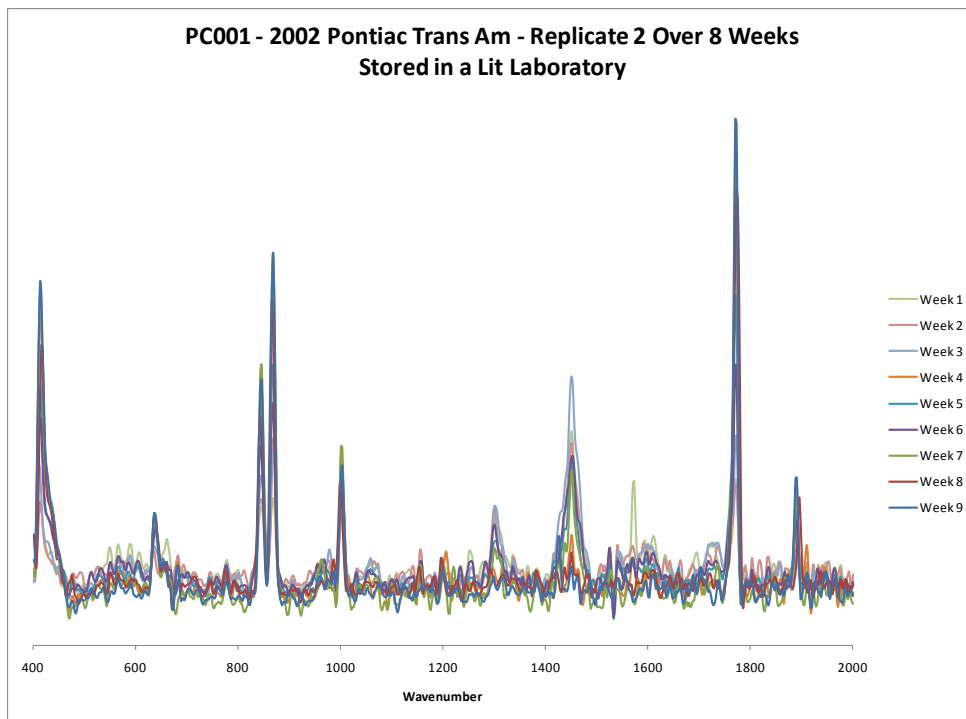


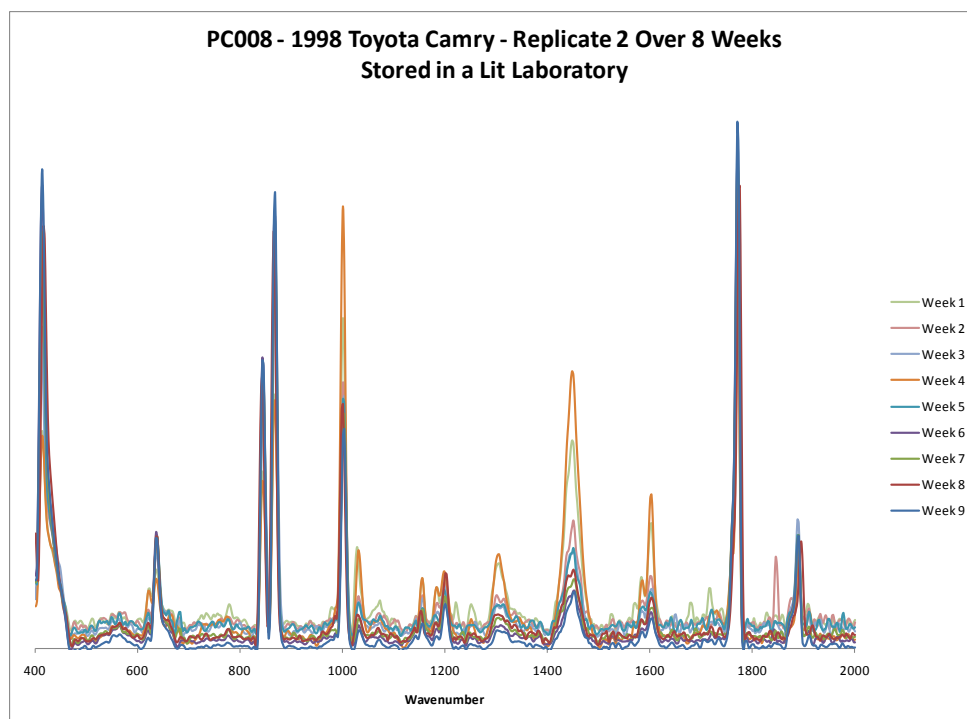
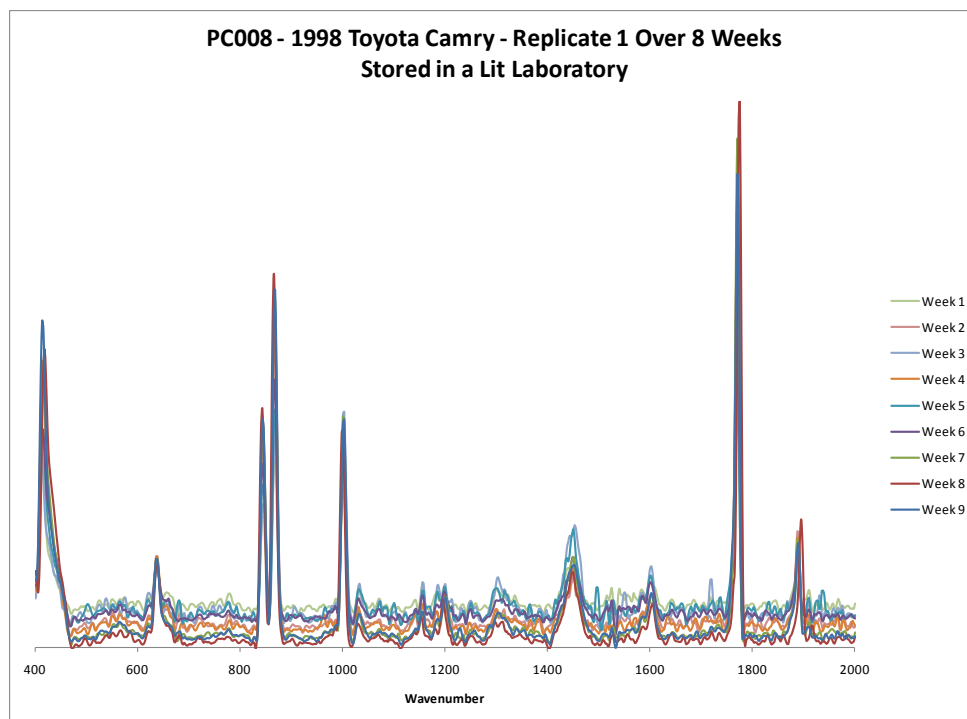


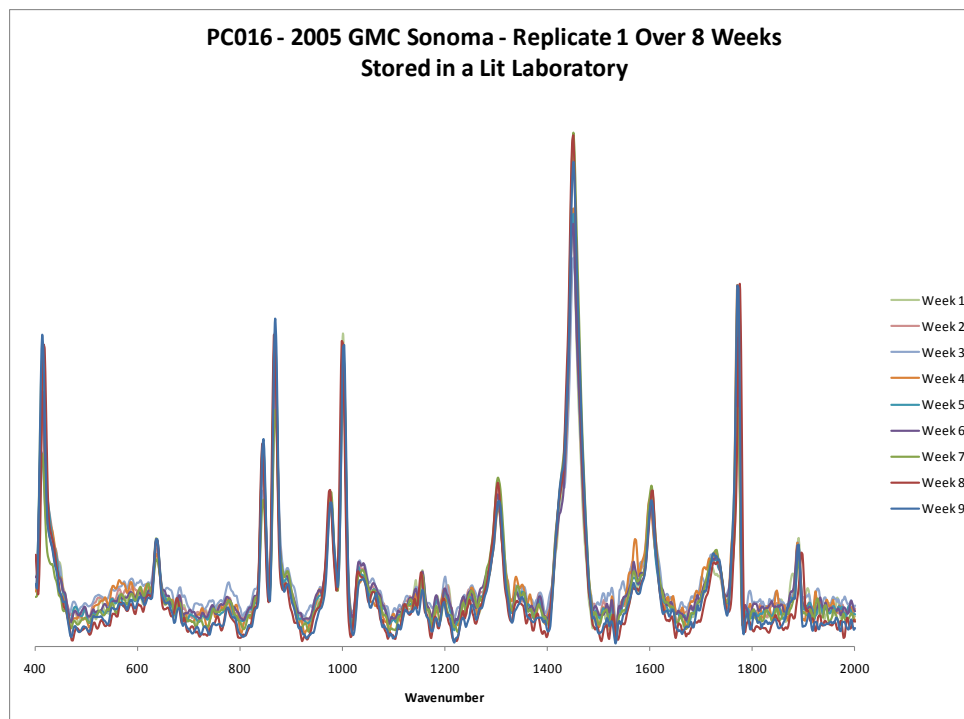
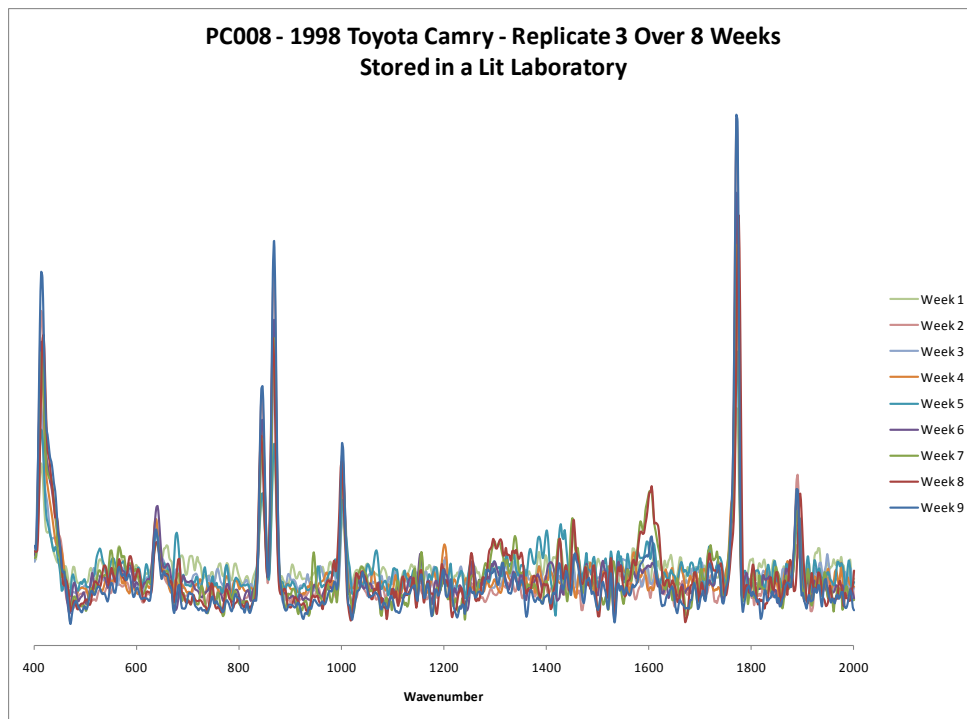


## B.2 Samples Stored in a Lit Laboratory

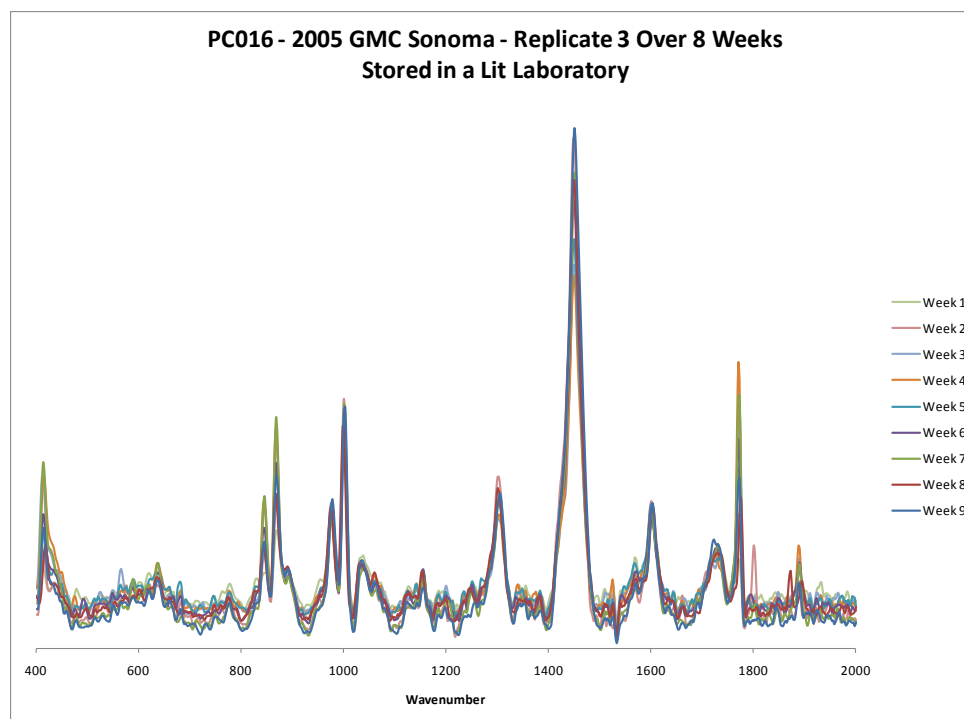
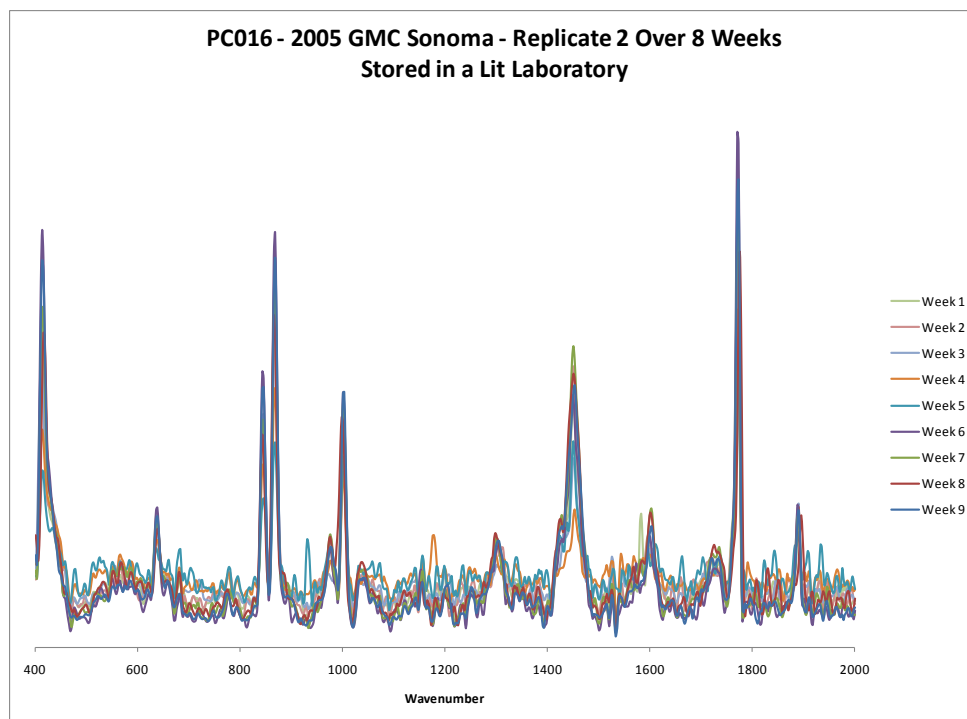






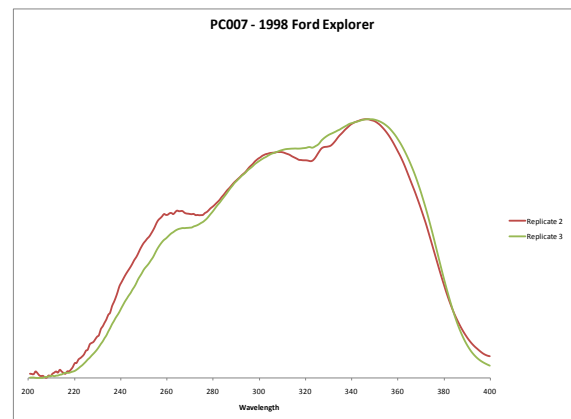
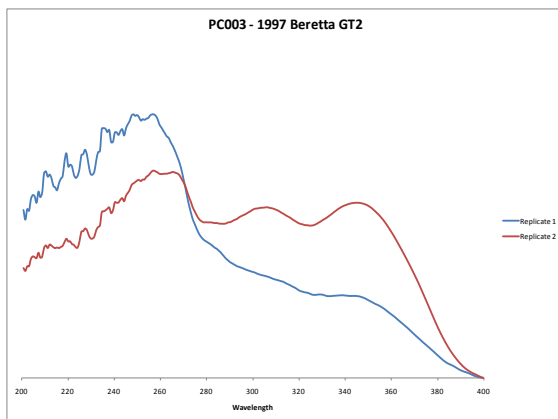
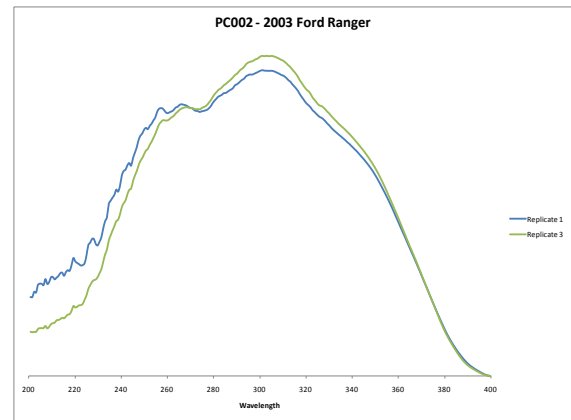
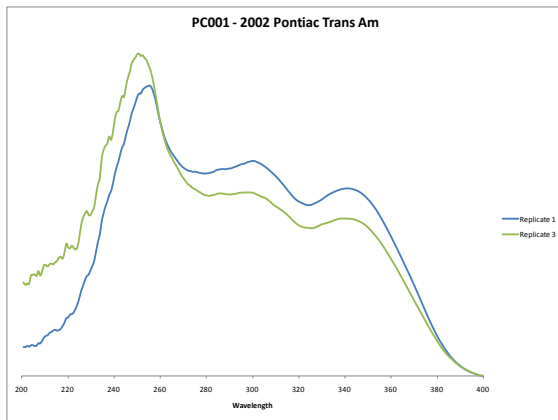


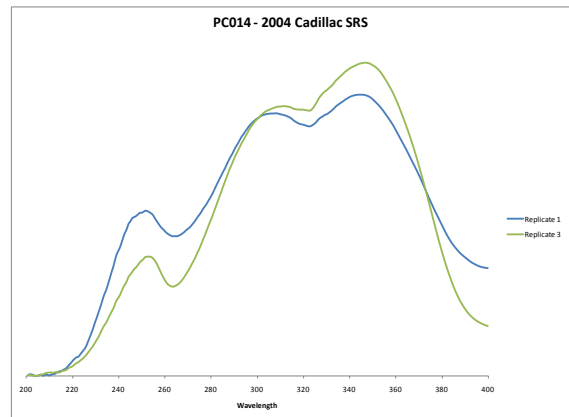
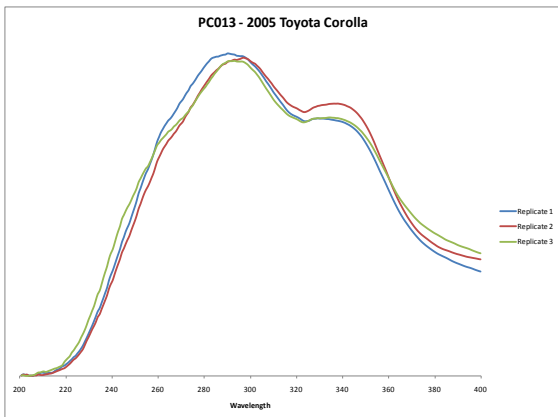
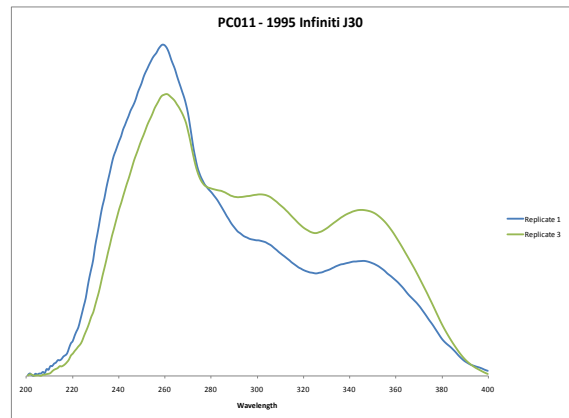
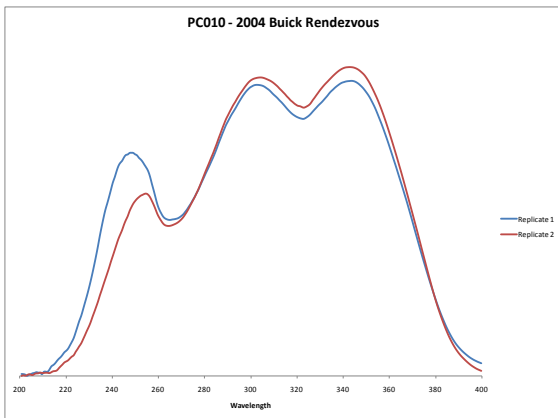
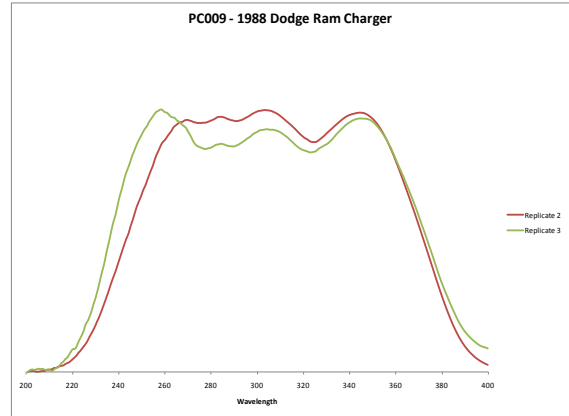
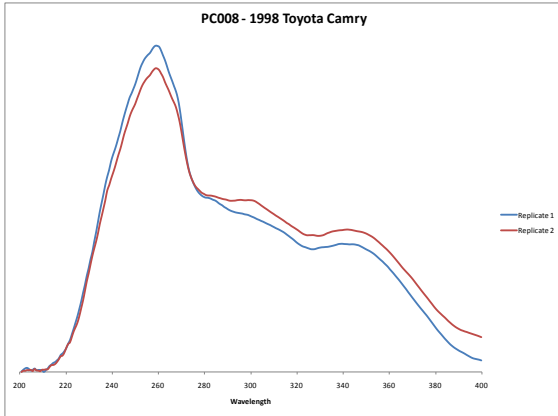


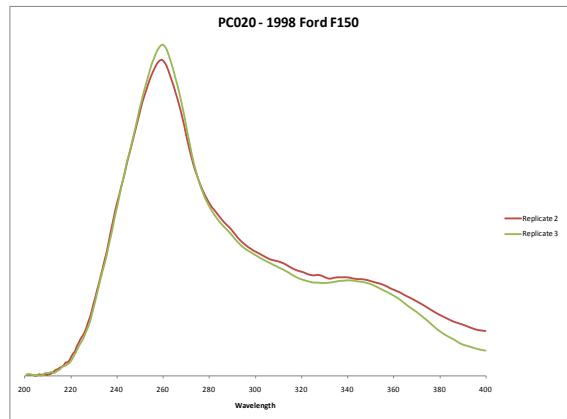
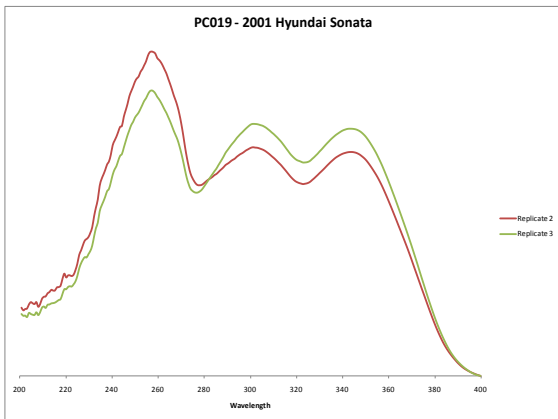
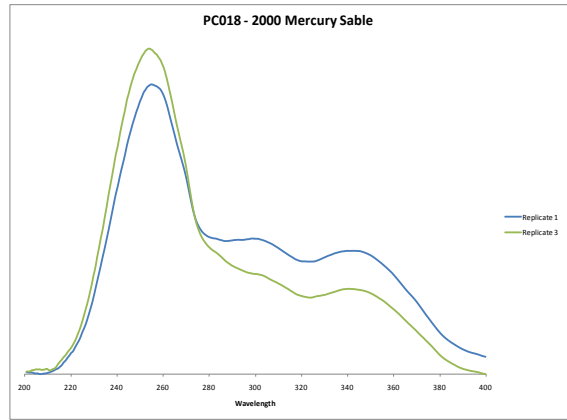
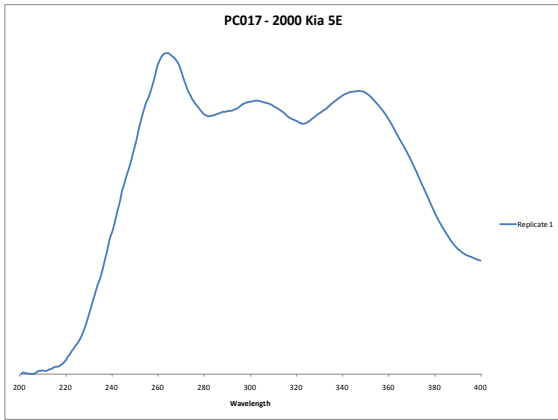
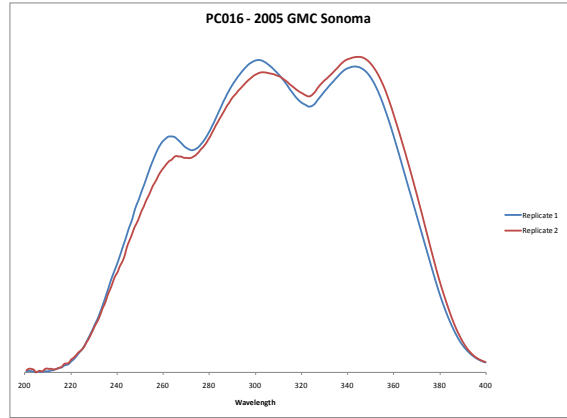
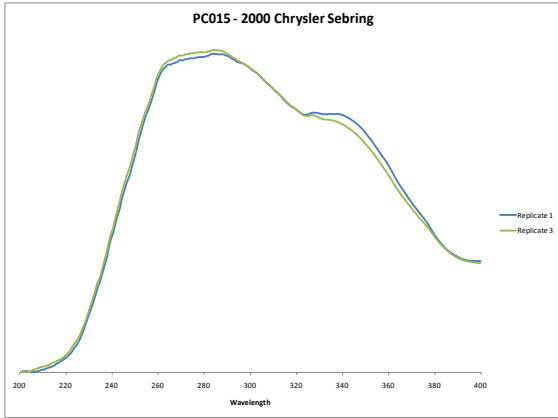


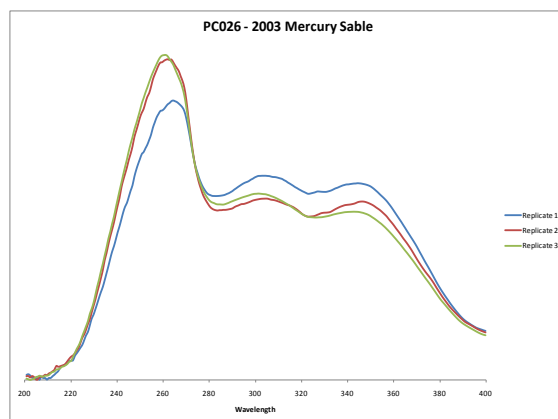
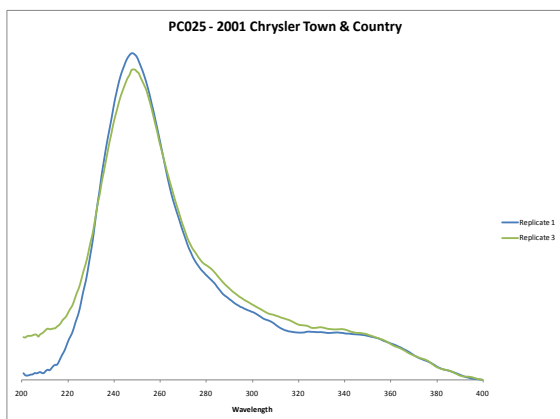
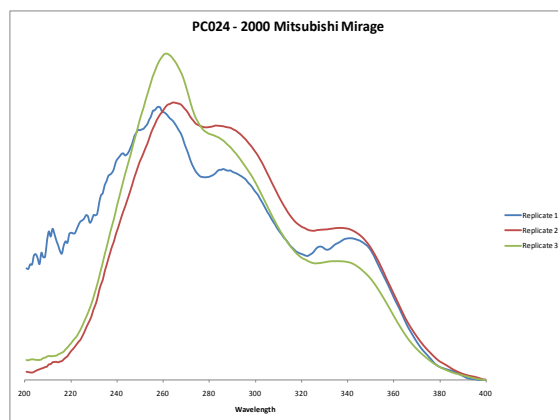
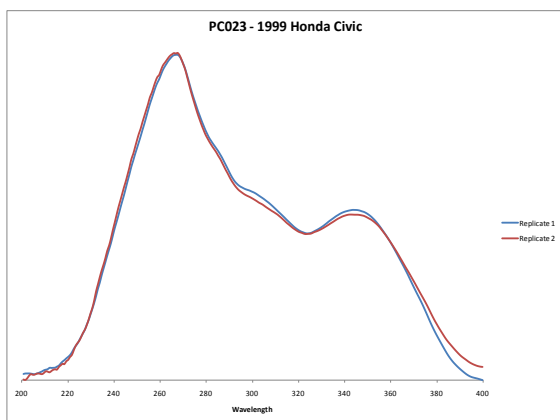
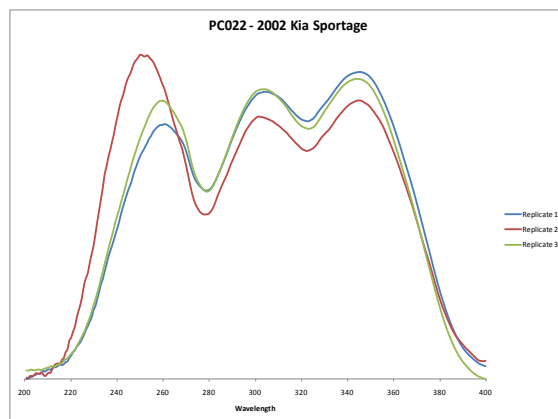
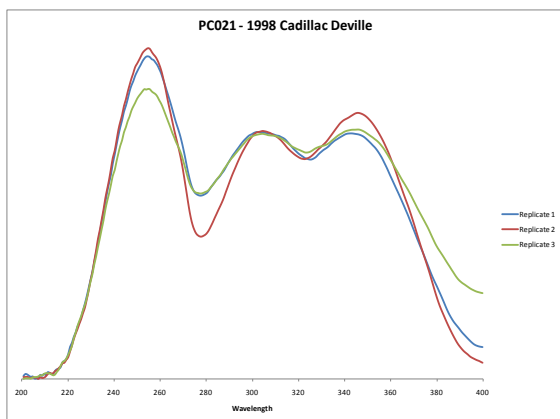
## Appendix C. Clear Coat Spectra by Microspectrophotometry

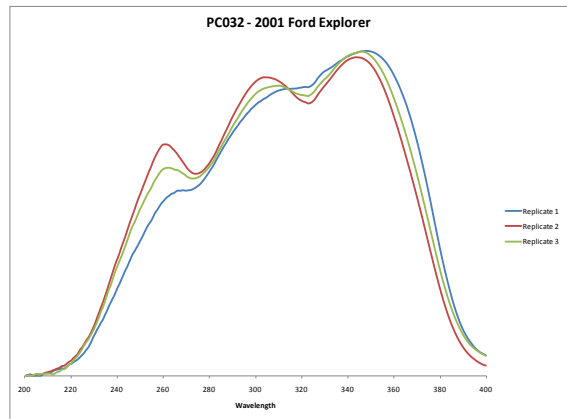
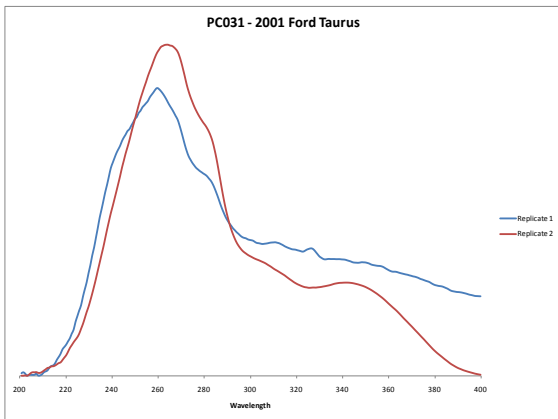
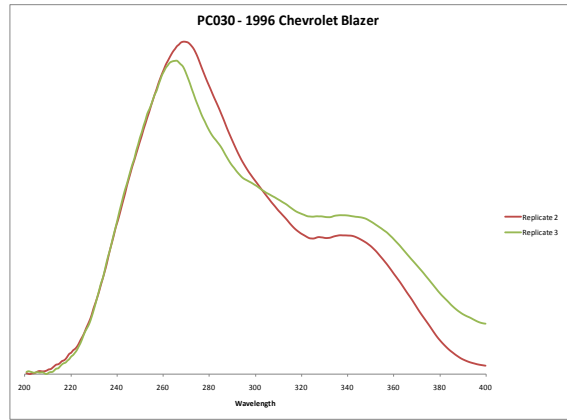
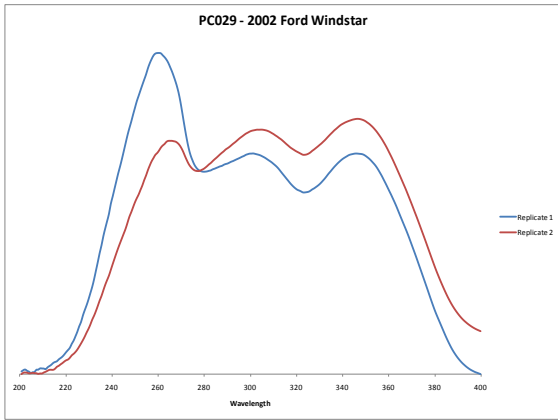
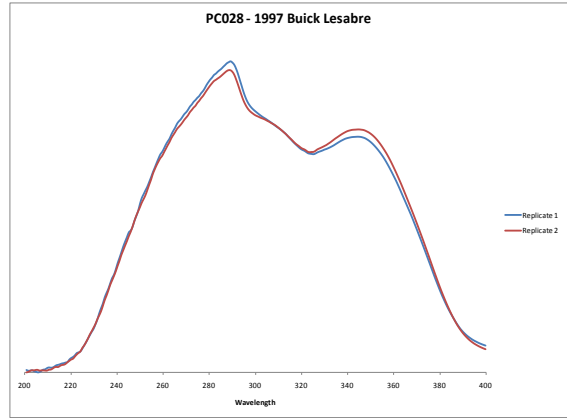
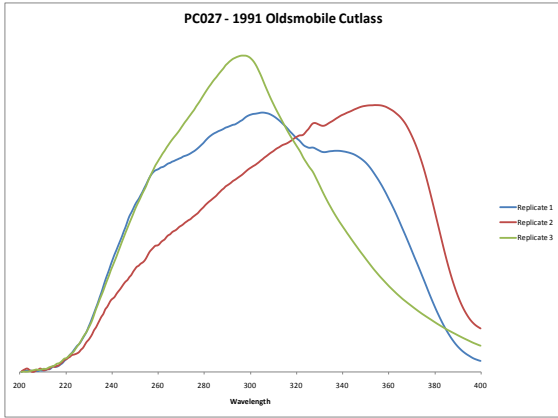
### C.1 Training Samples

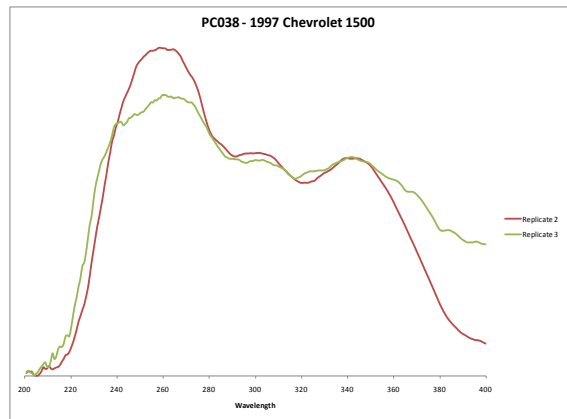
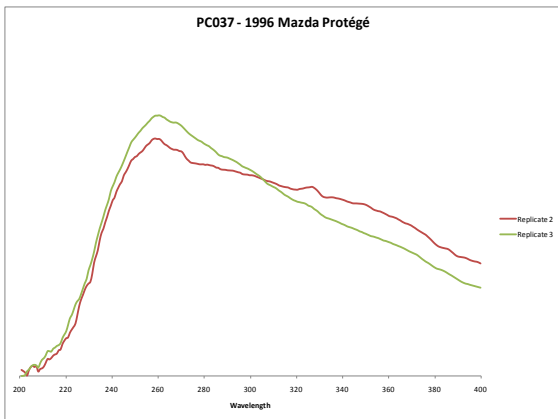
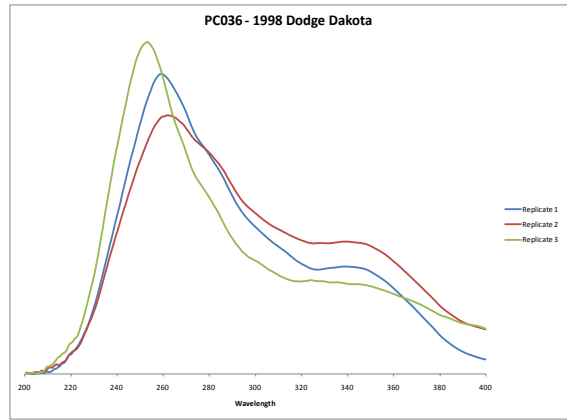
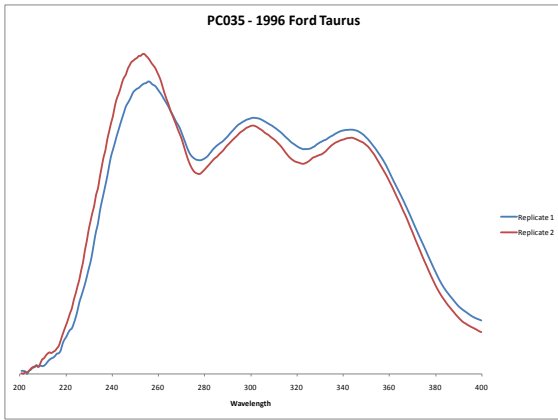
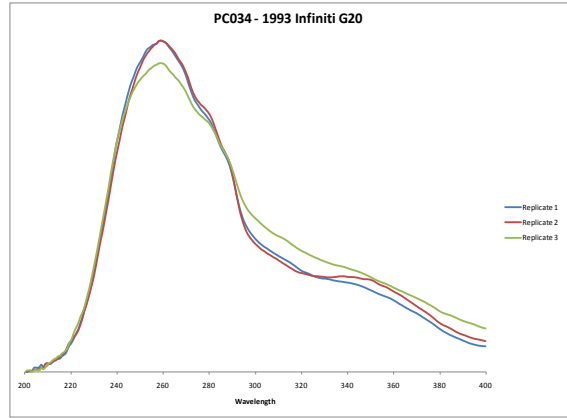
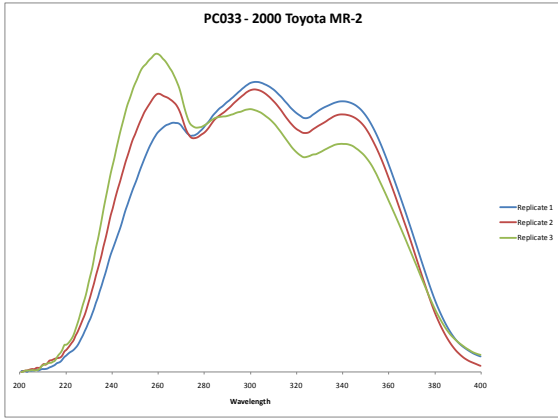


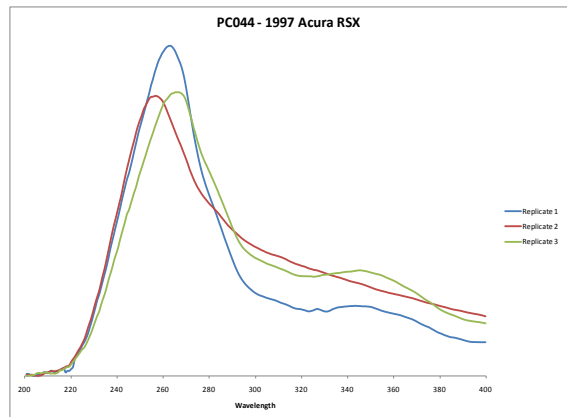
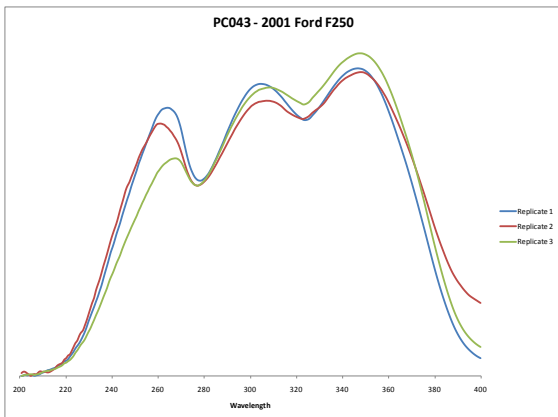
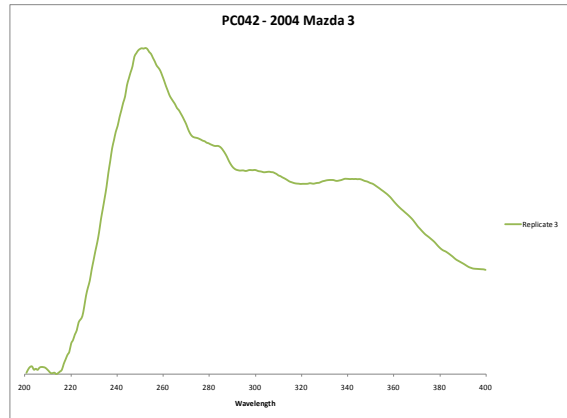
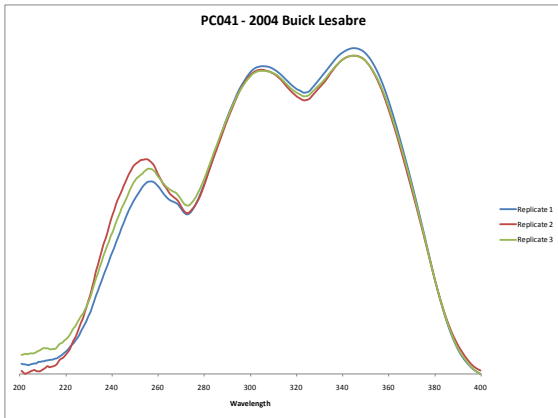
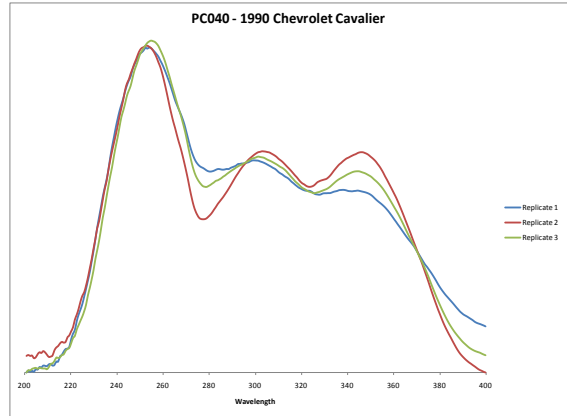
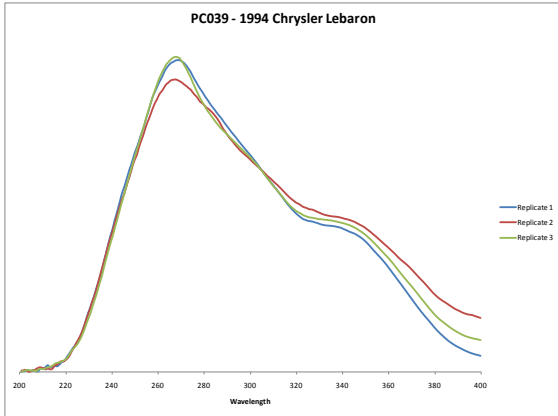




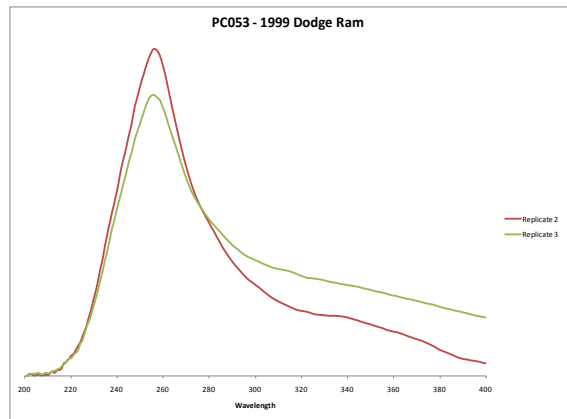
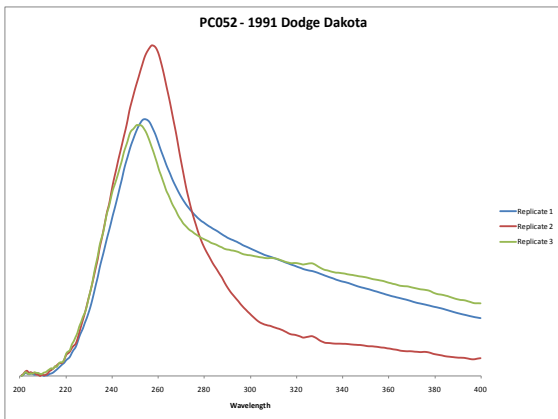
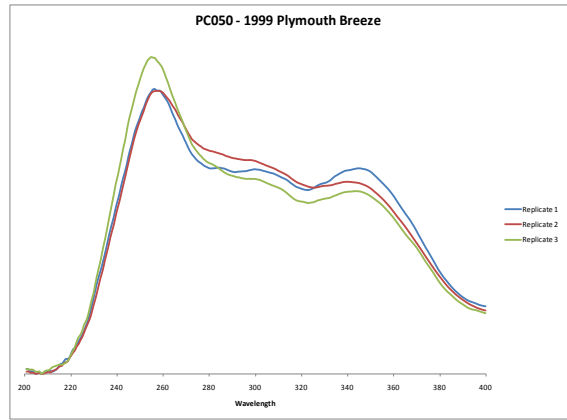
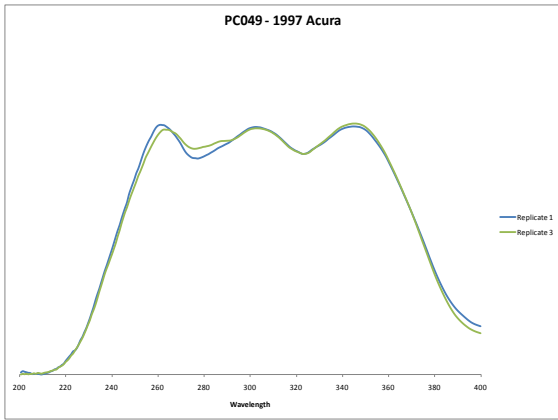
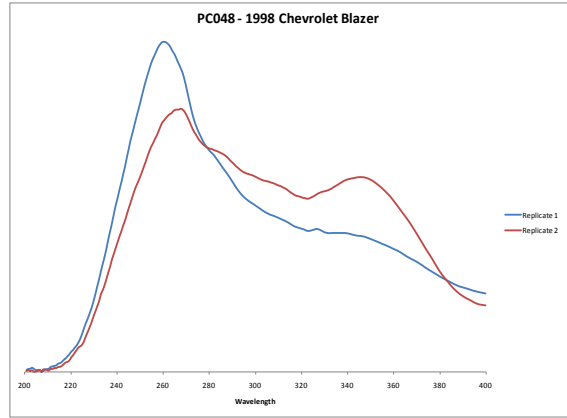
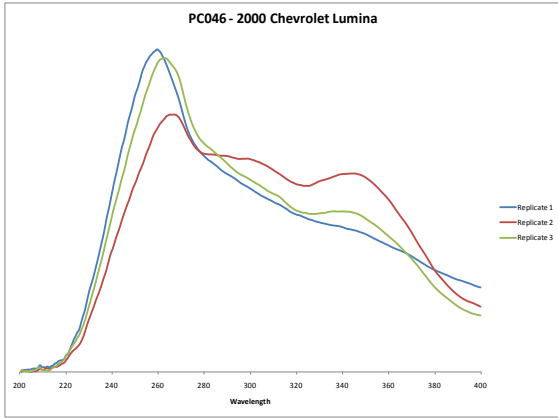


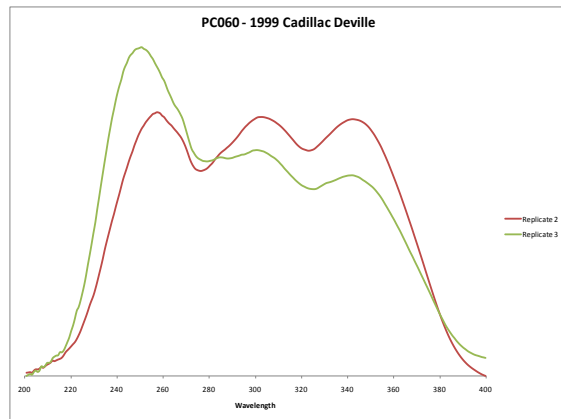
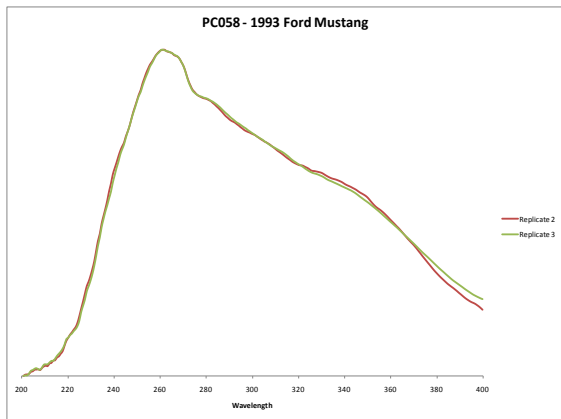
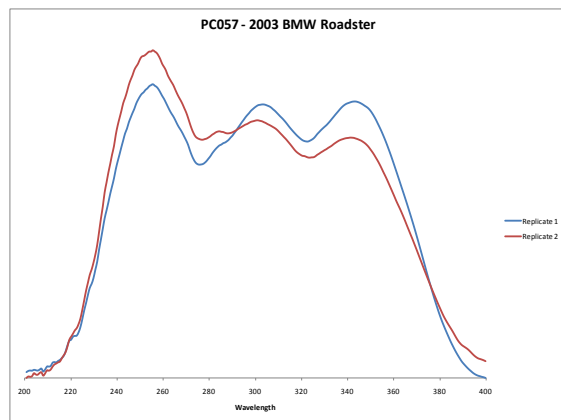
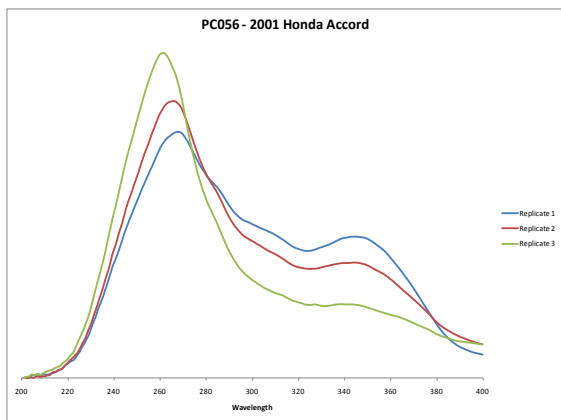
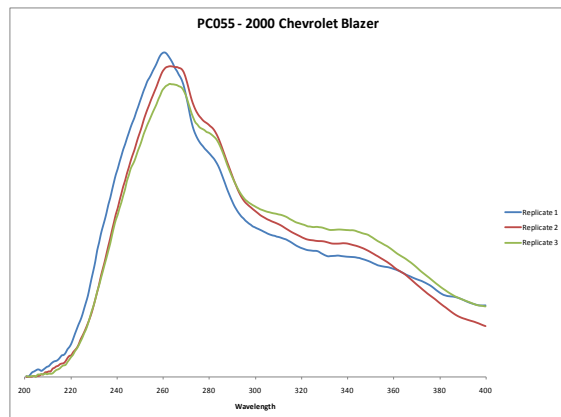
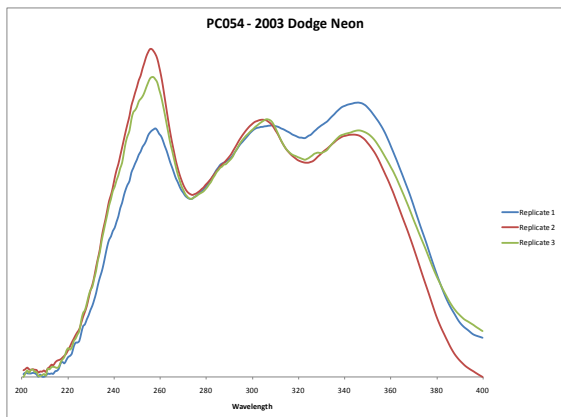


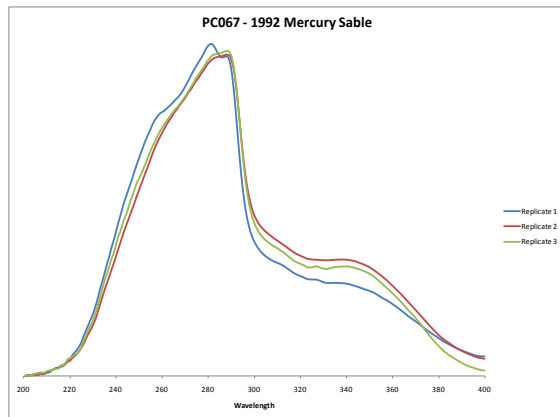
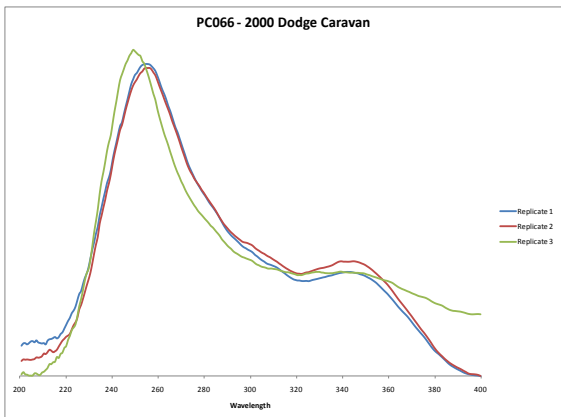
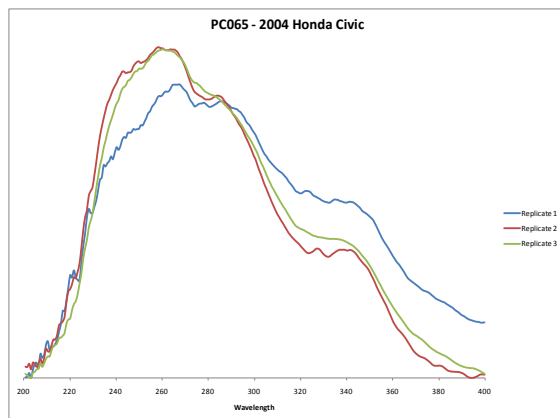
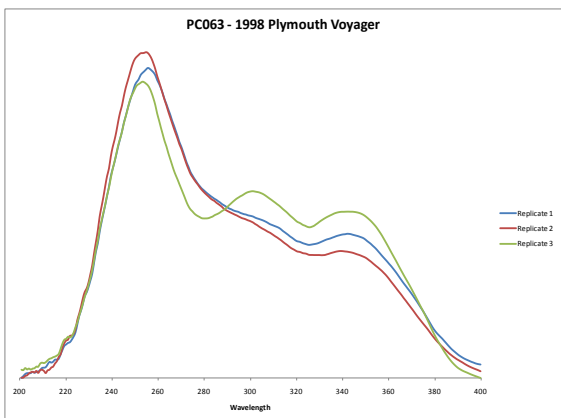
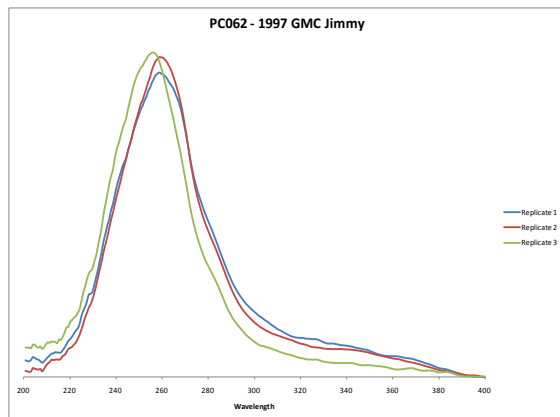
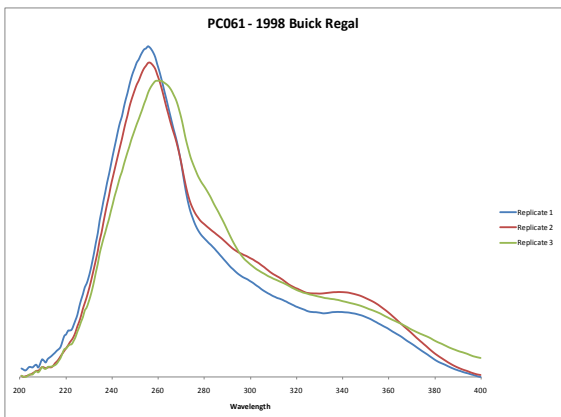


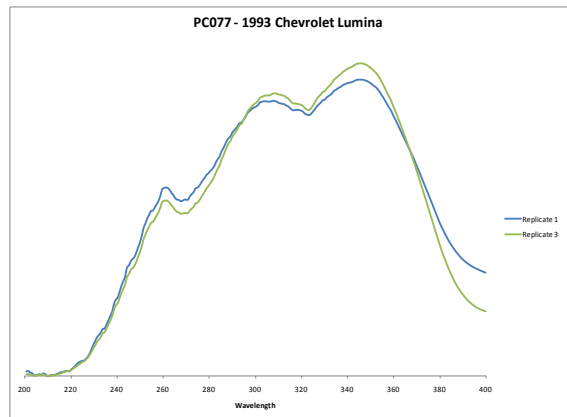
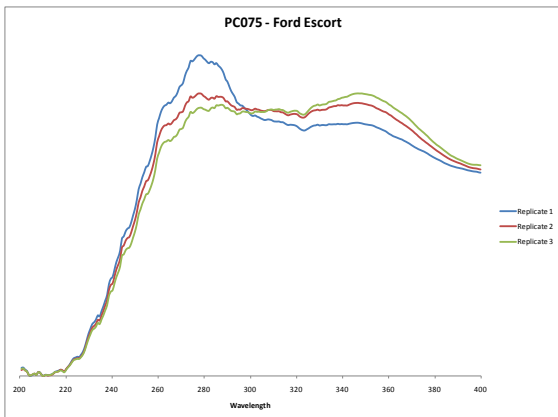
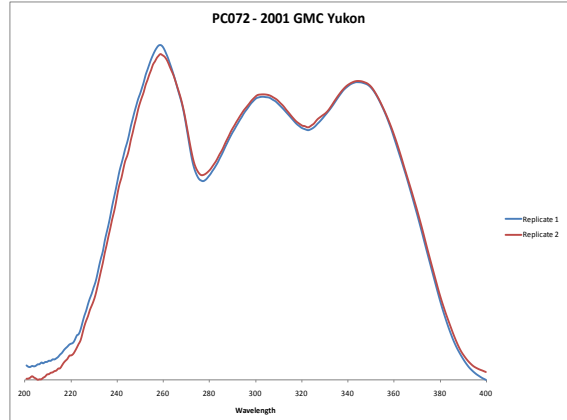
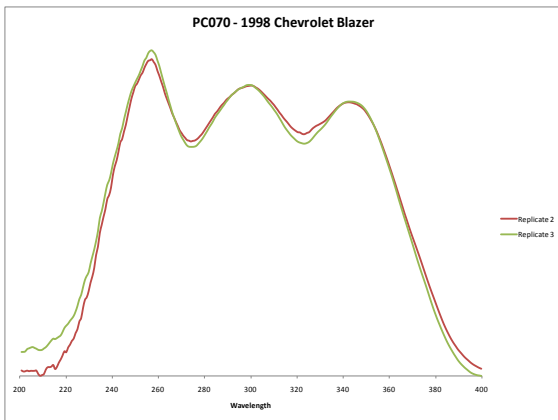
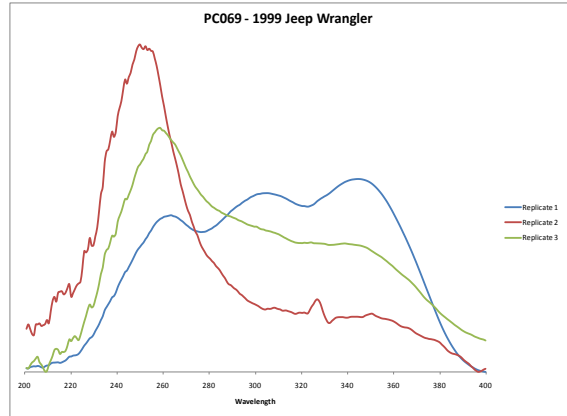
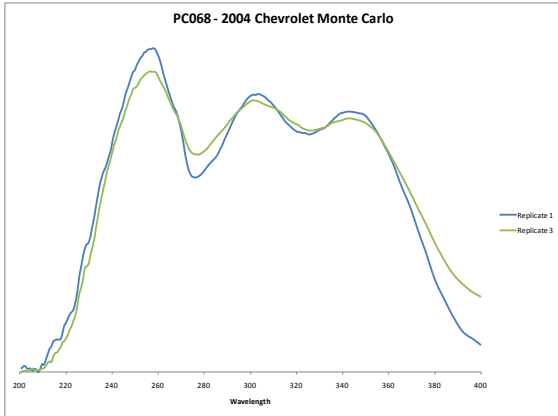


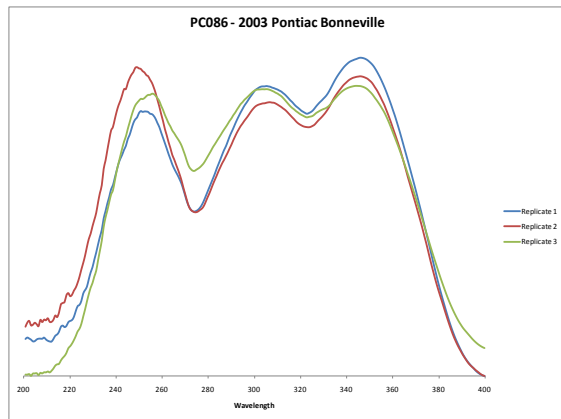
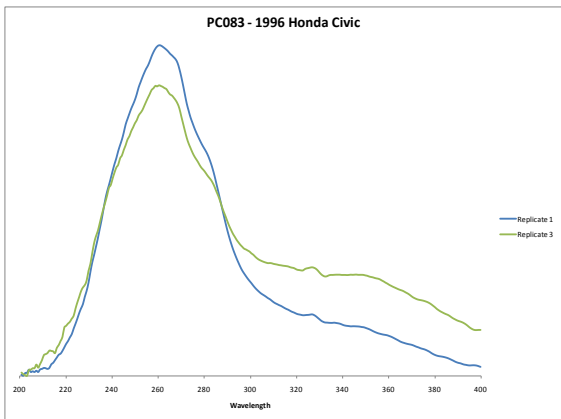
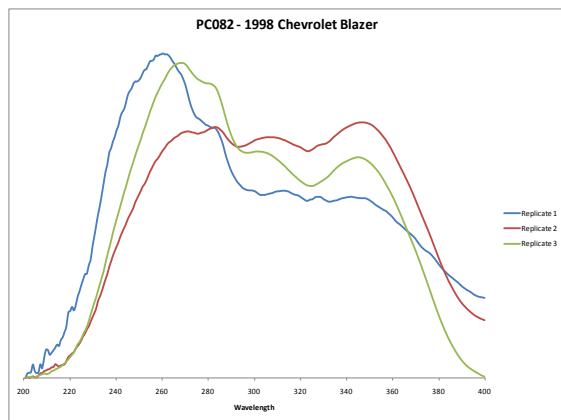
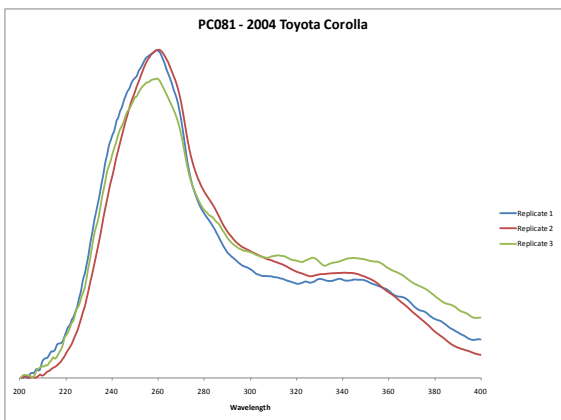
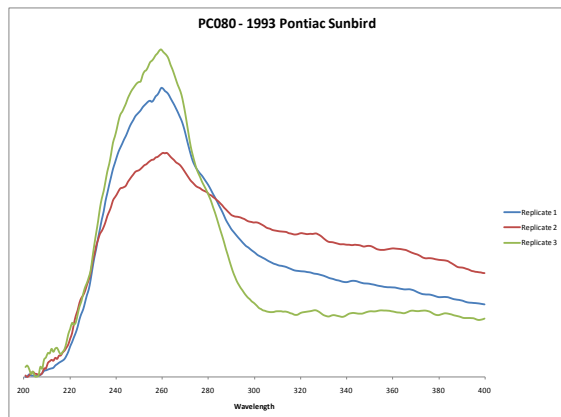
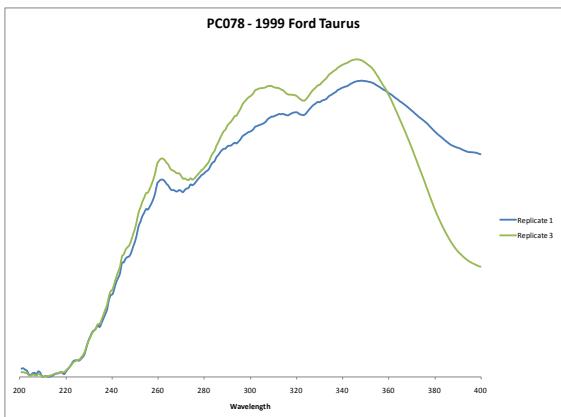


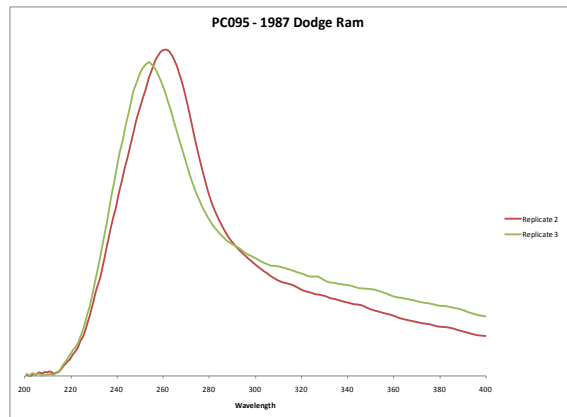
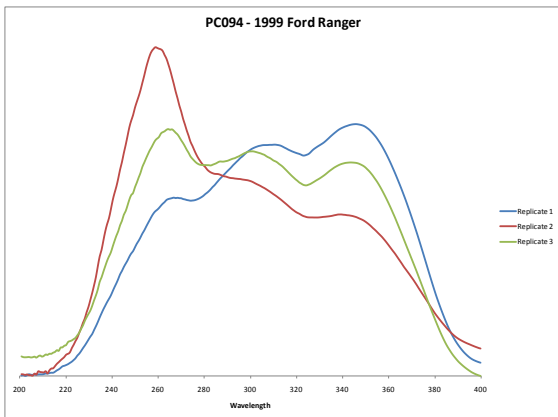
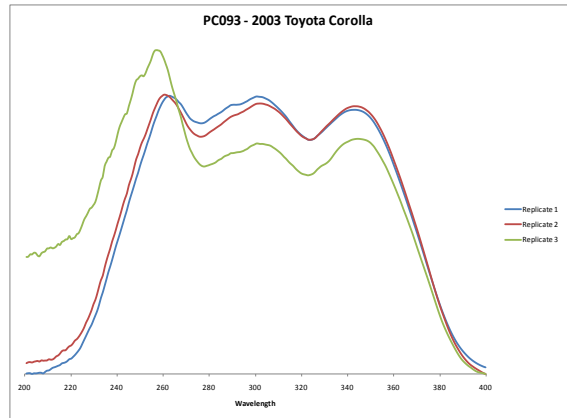
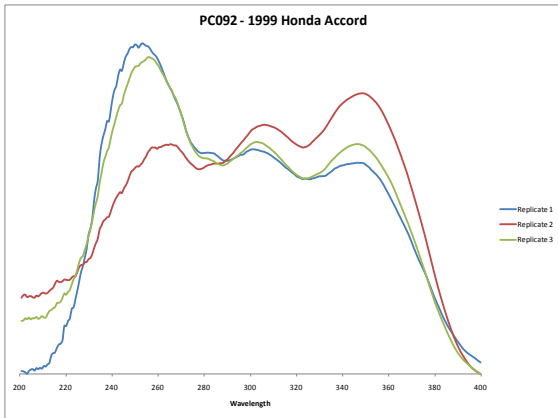
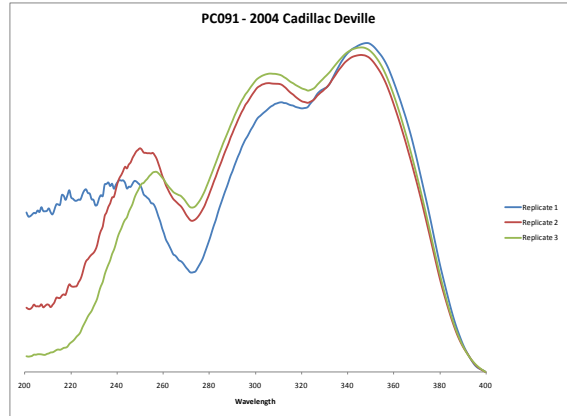
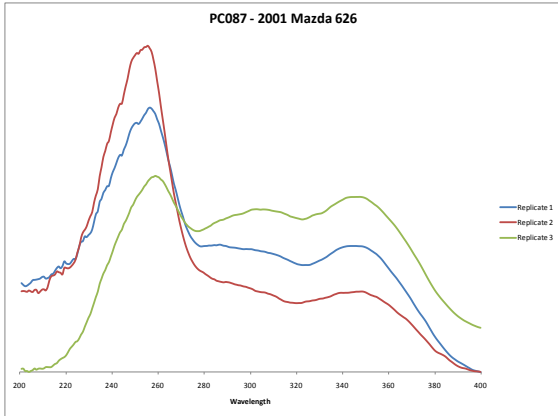


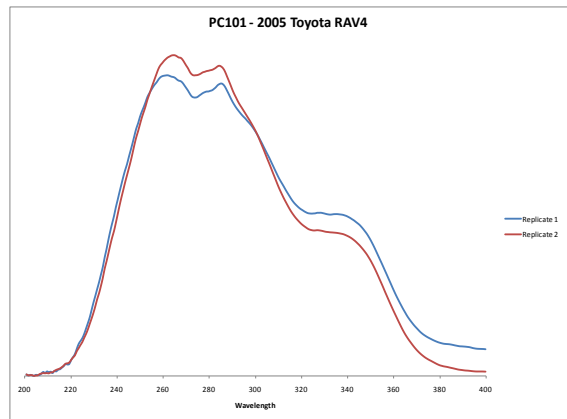
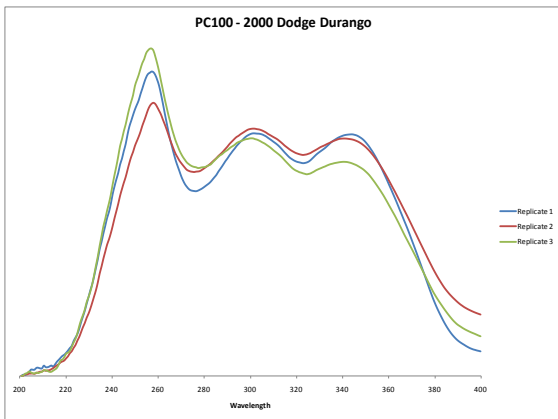
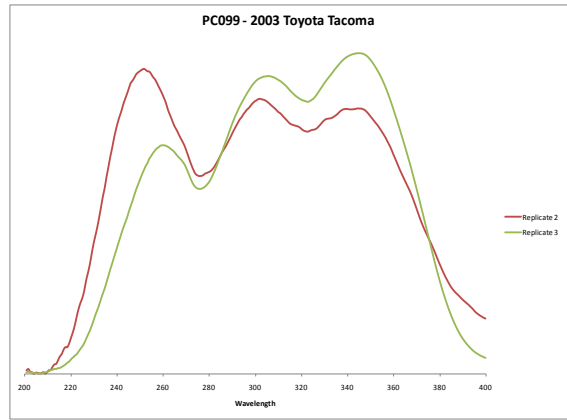
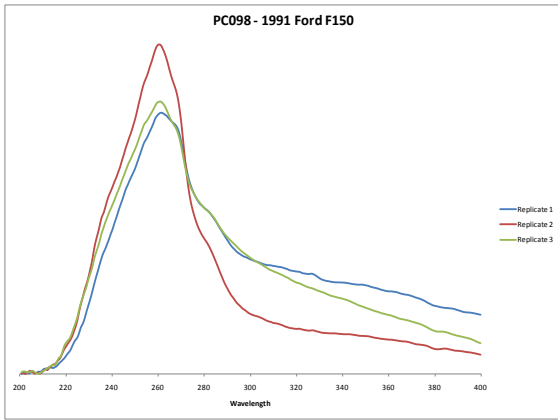
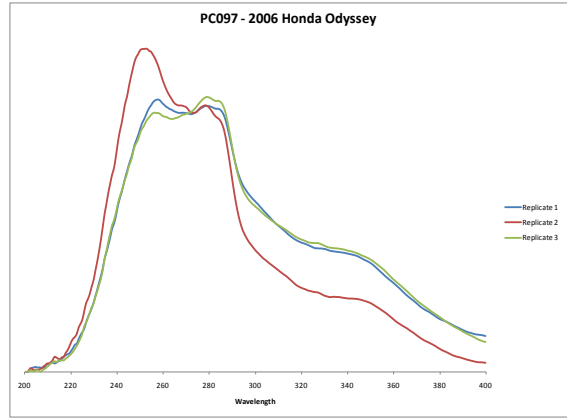
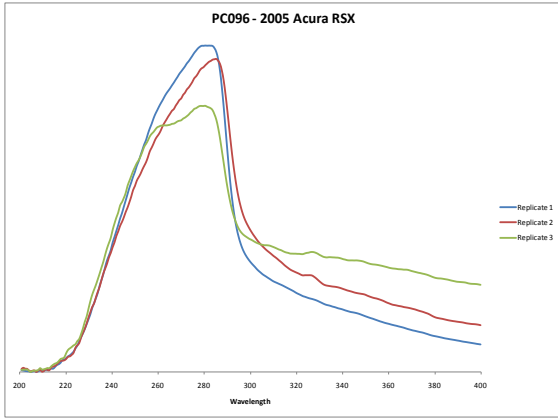


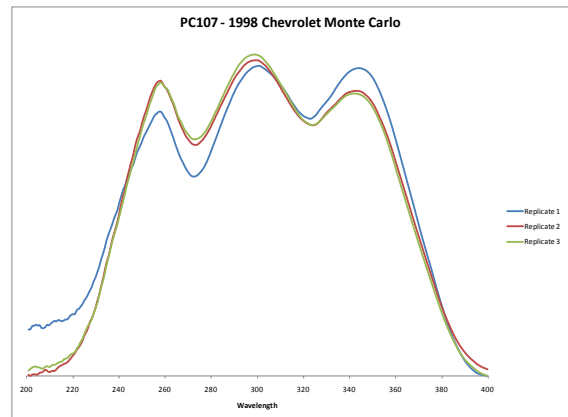
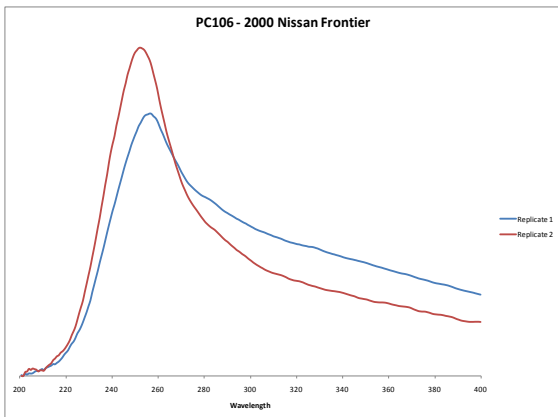
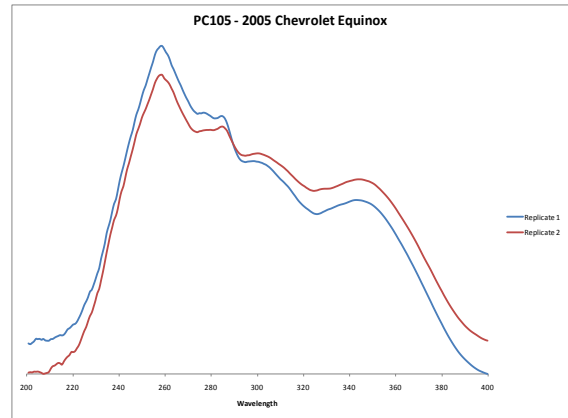
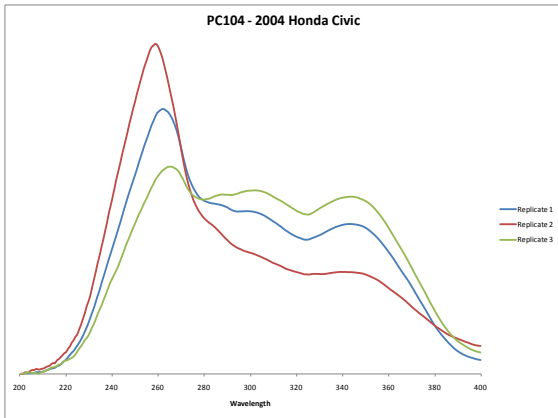
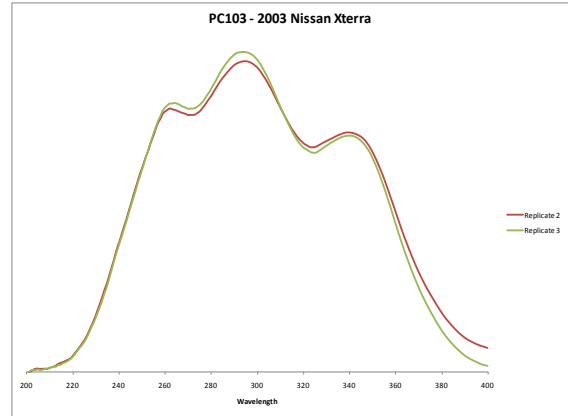
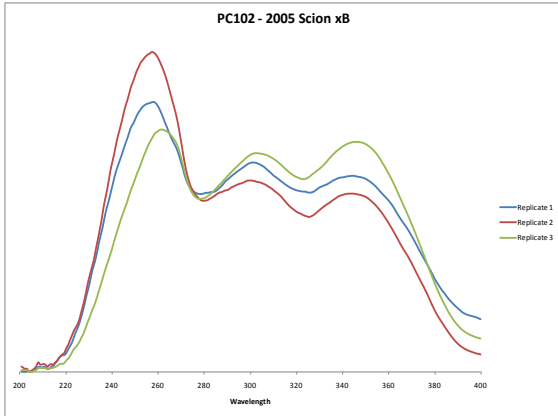




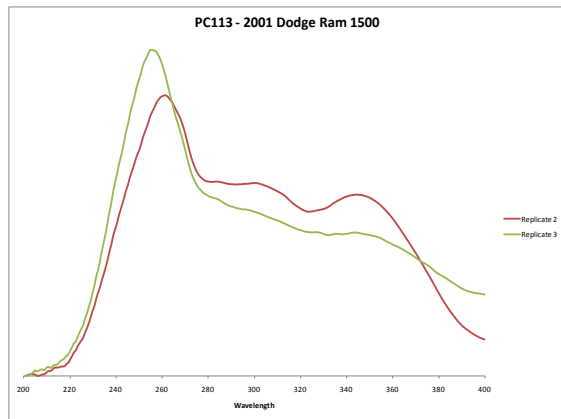
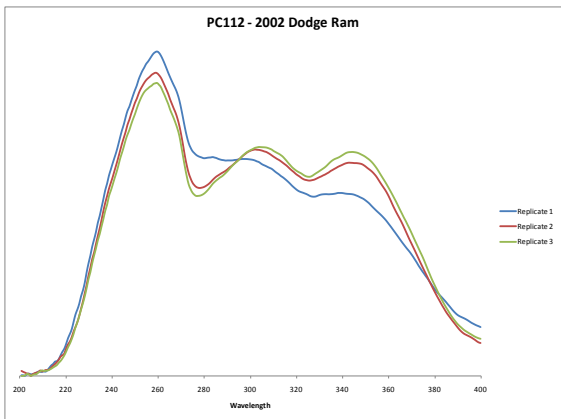
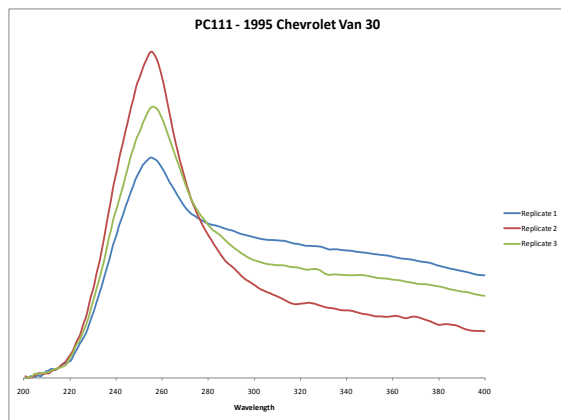
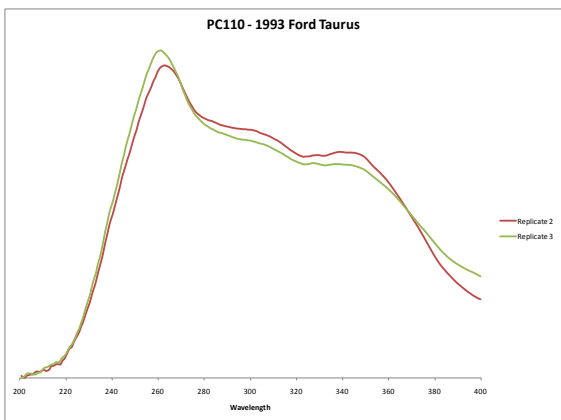
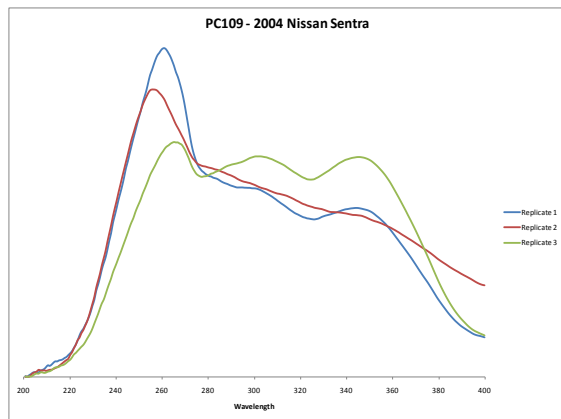
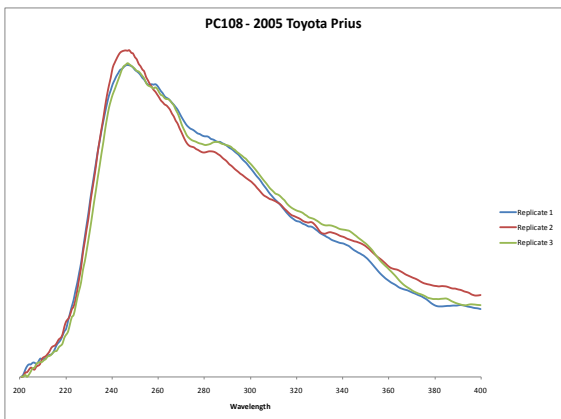


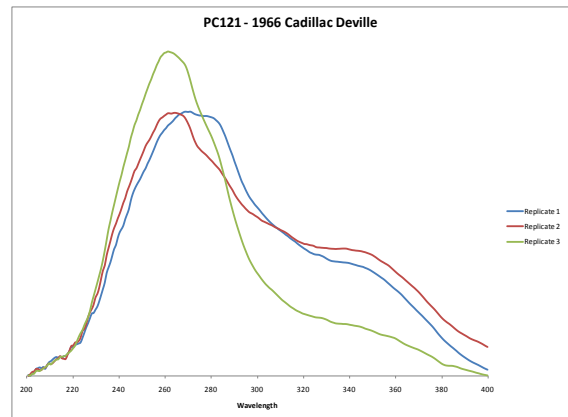
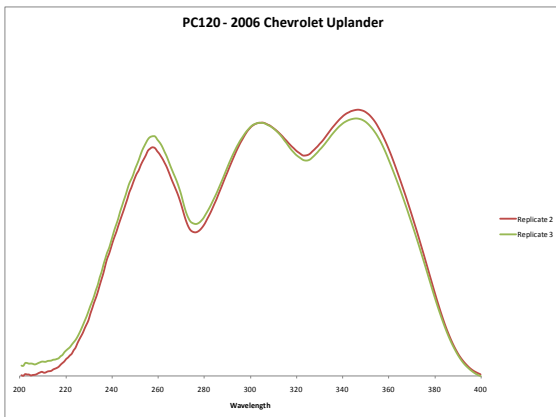
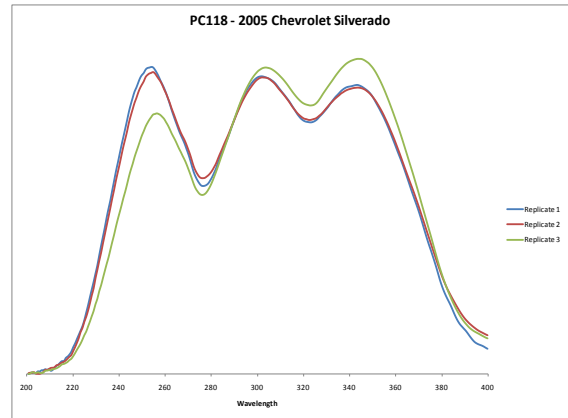
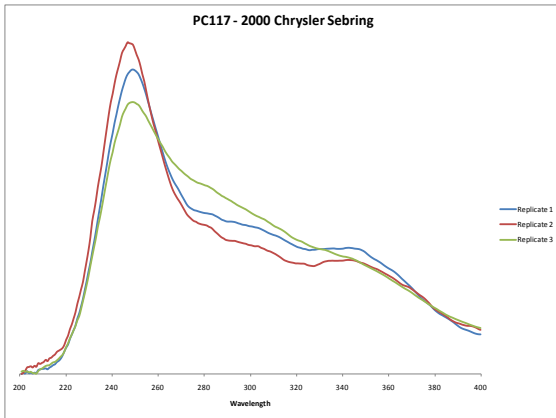
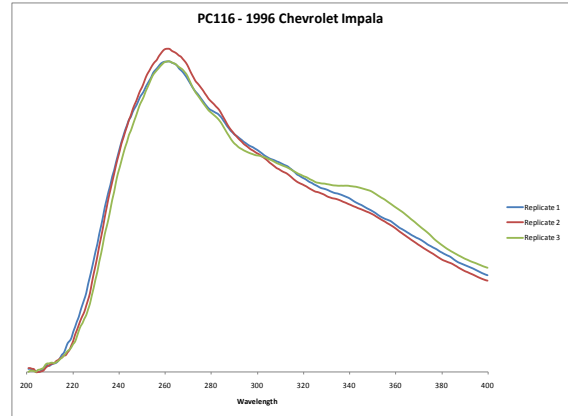
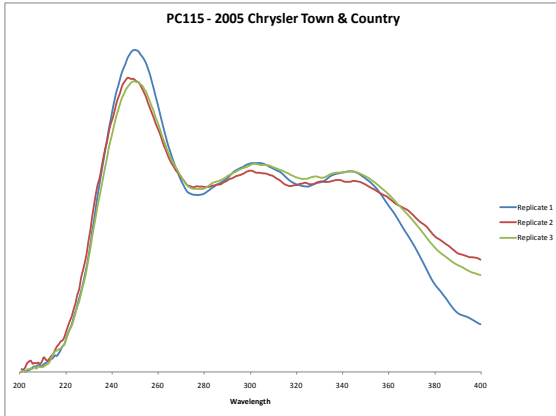


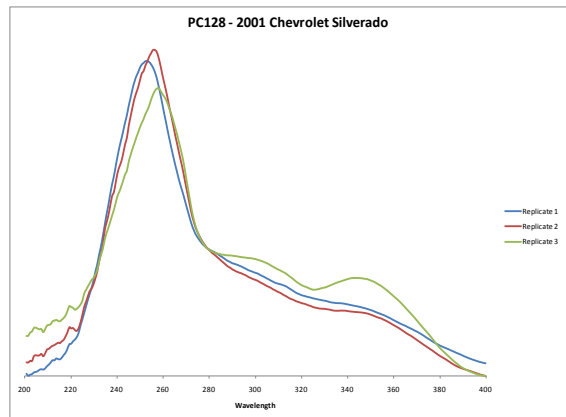
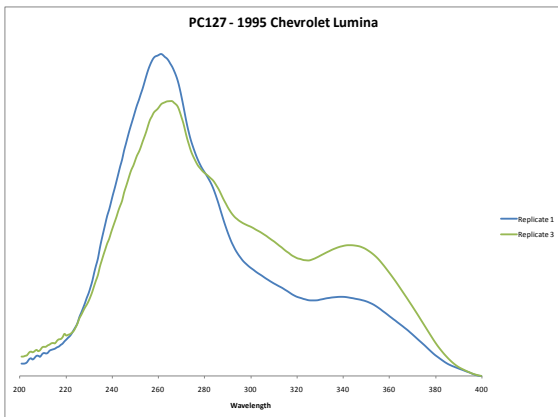
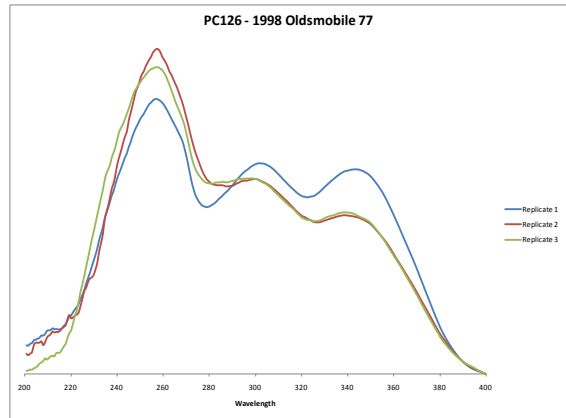
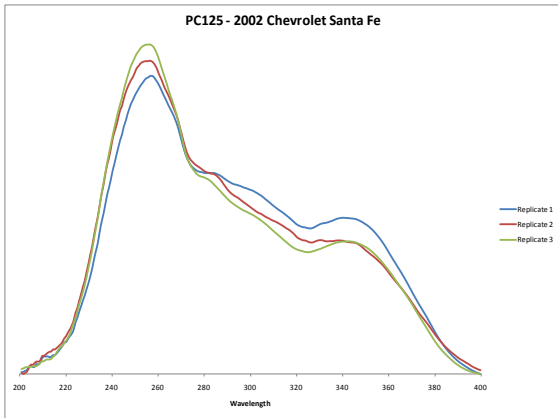
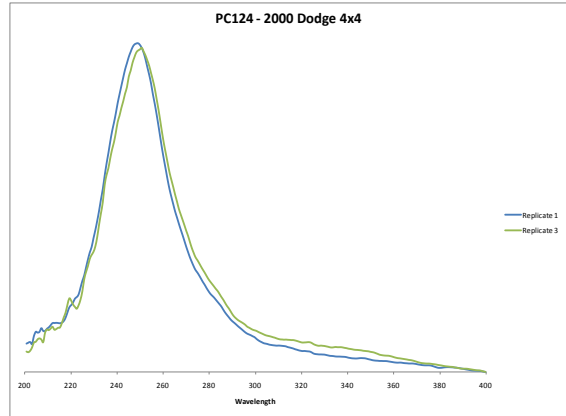
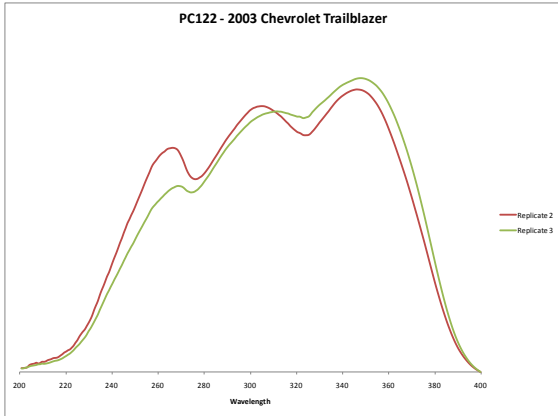


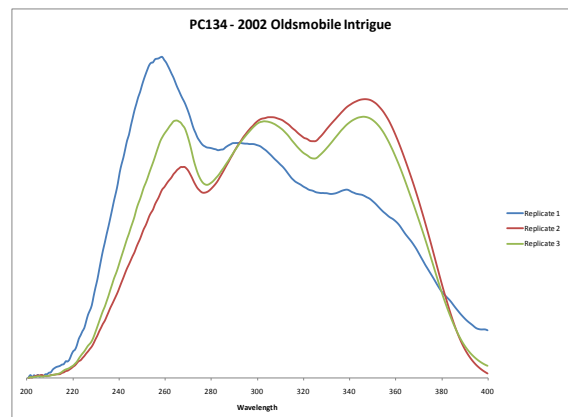
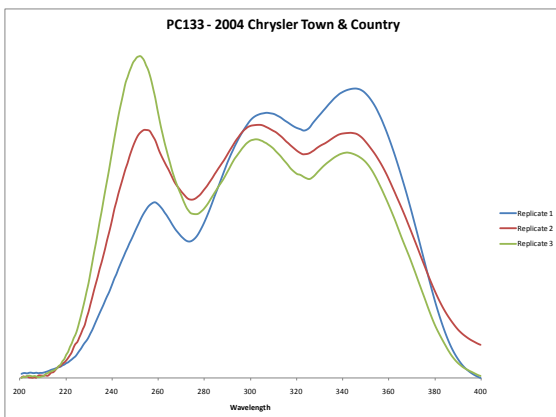
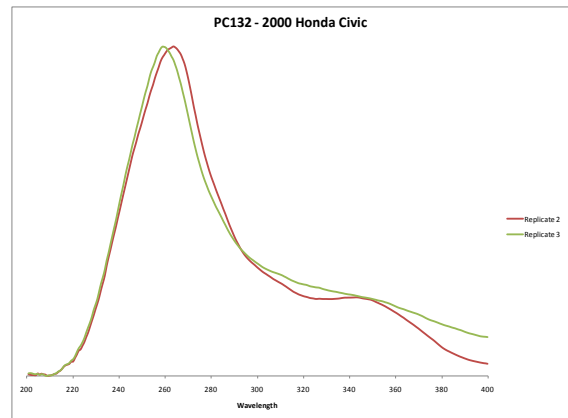
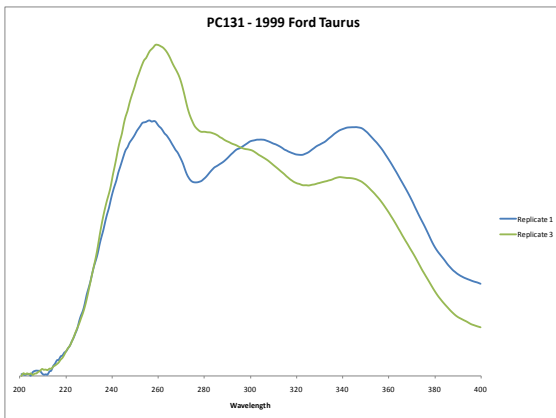
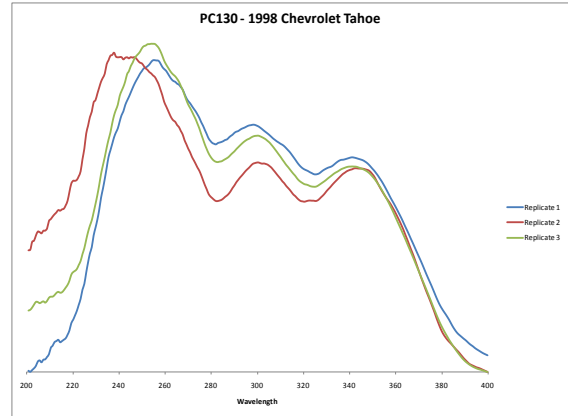
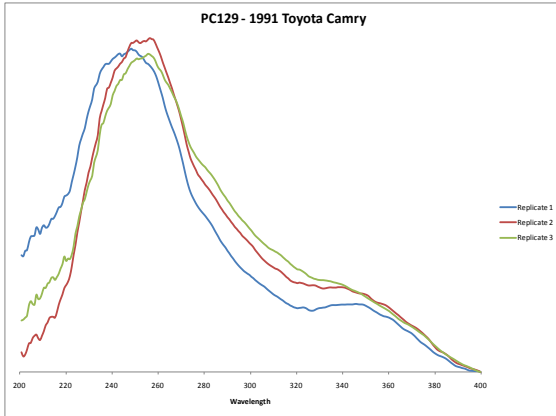


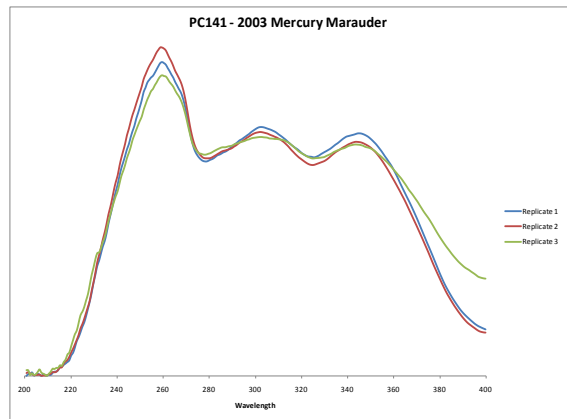
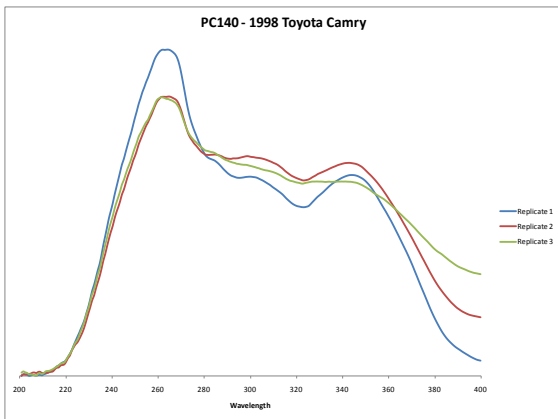
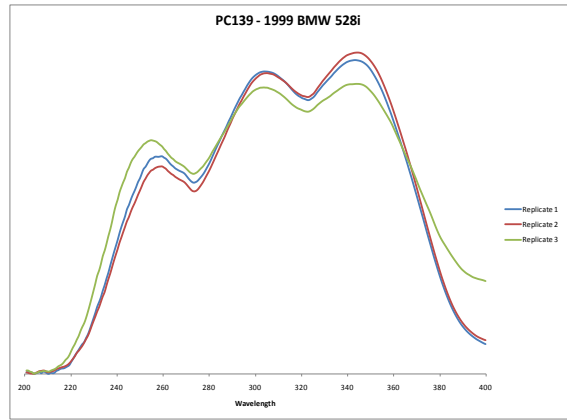
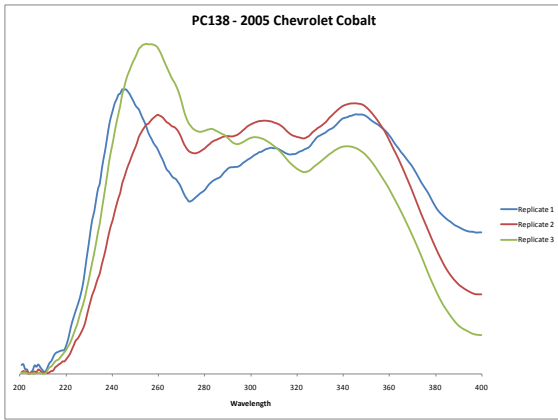
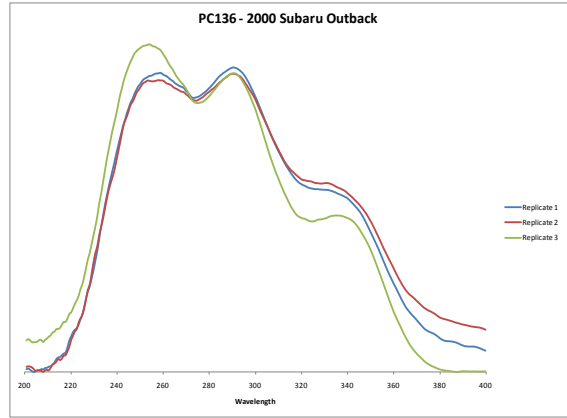
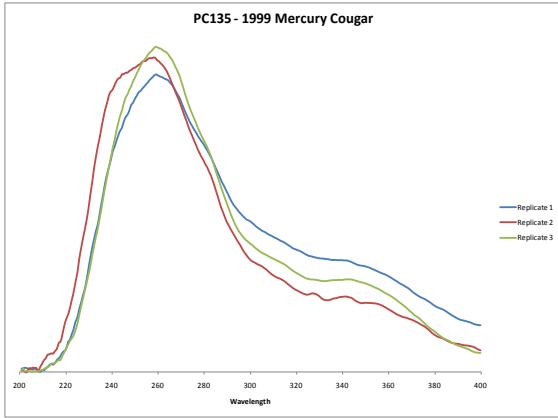


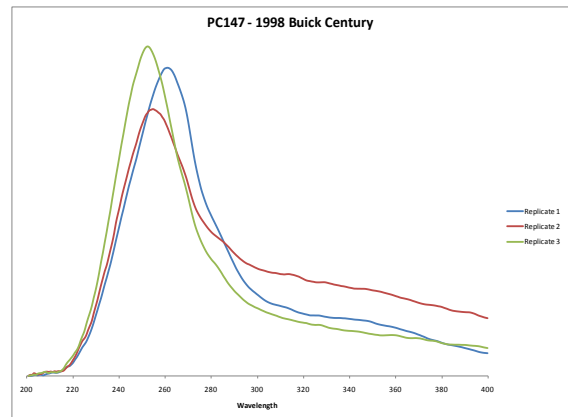
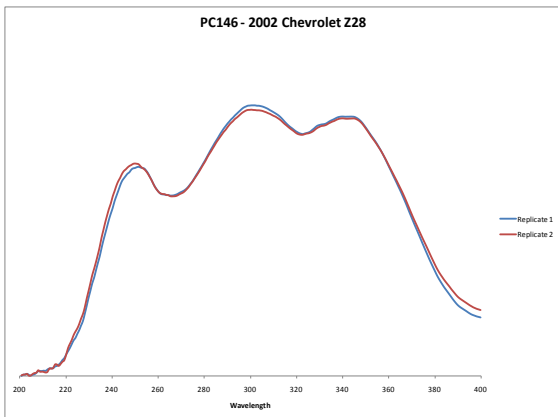
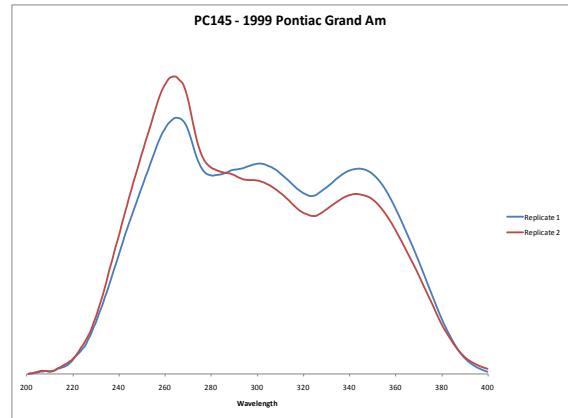
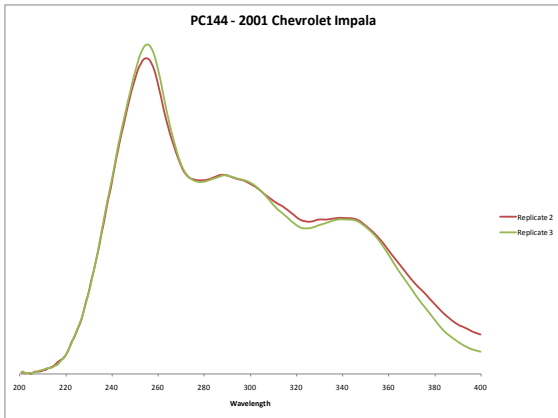
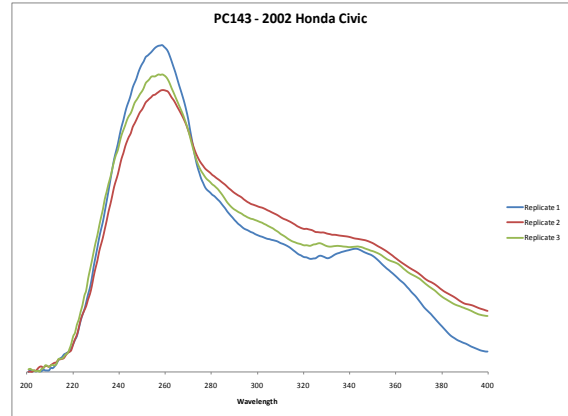
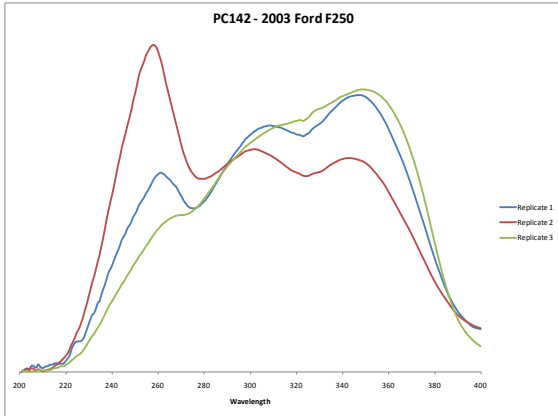


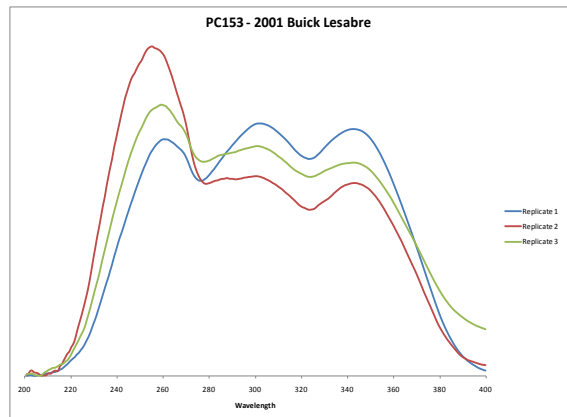
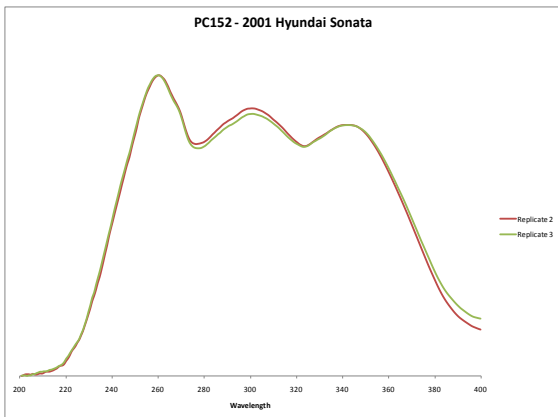
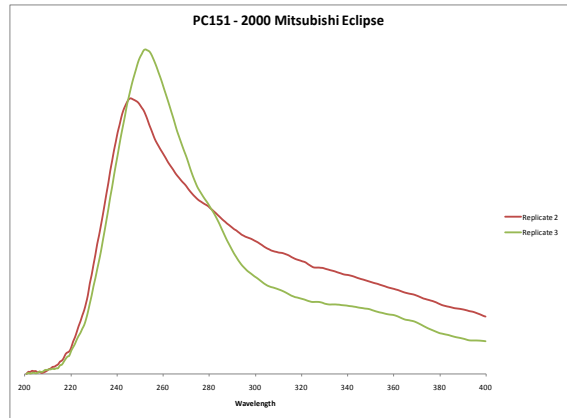
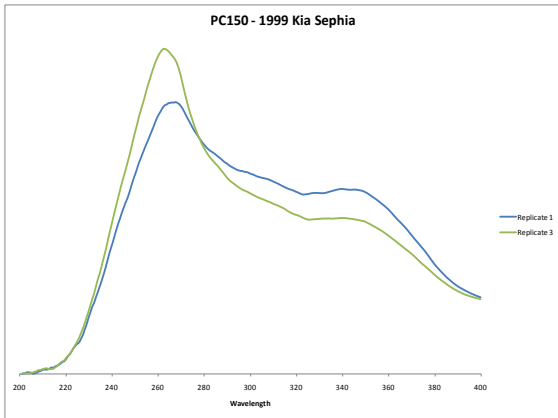
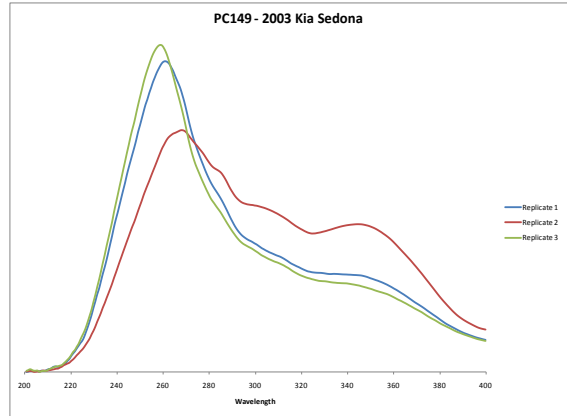
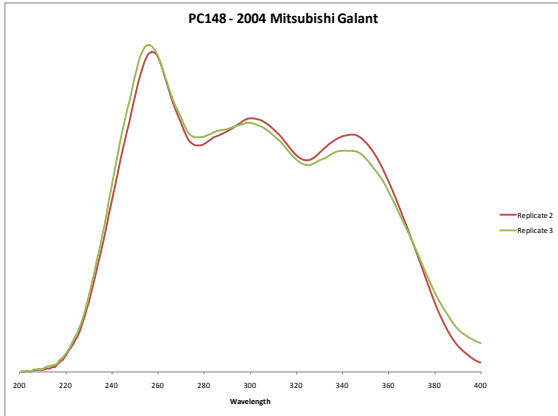


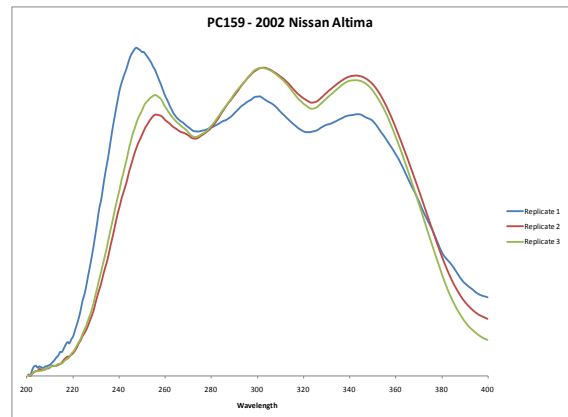
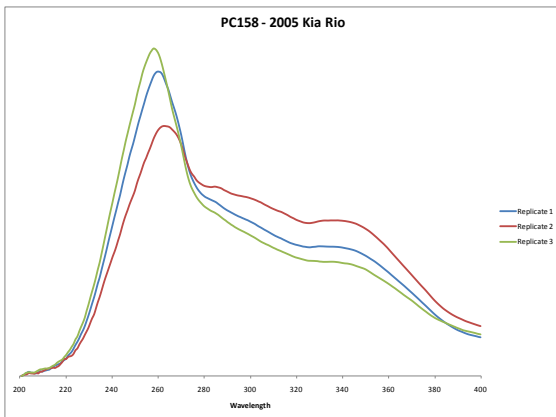
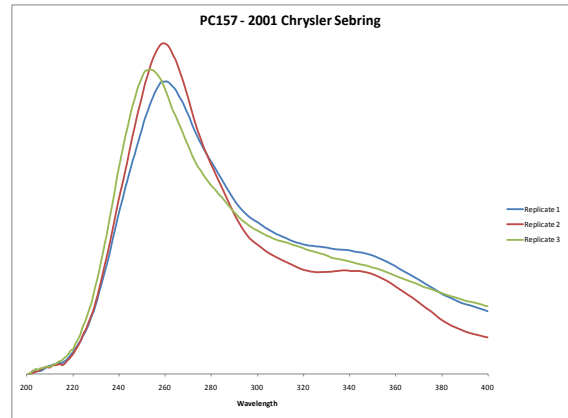
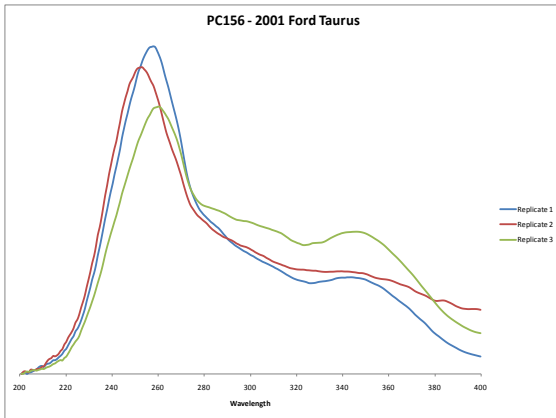
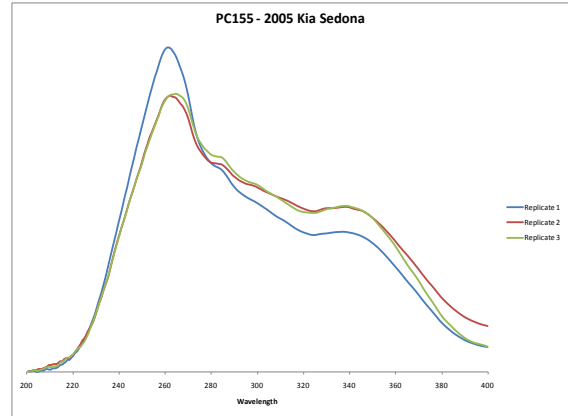
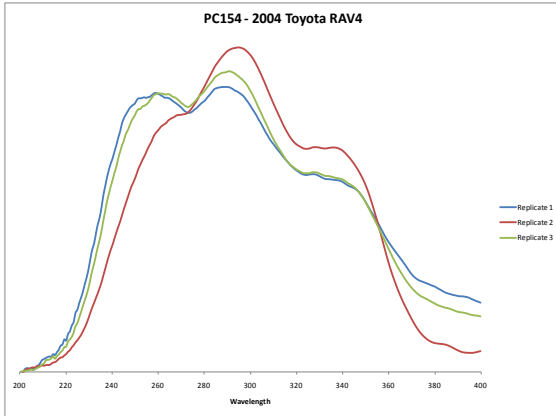




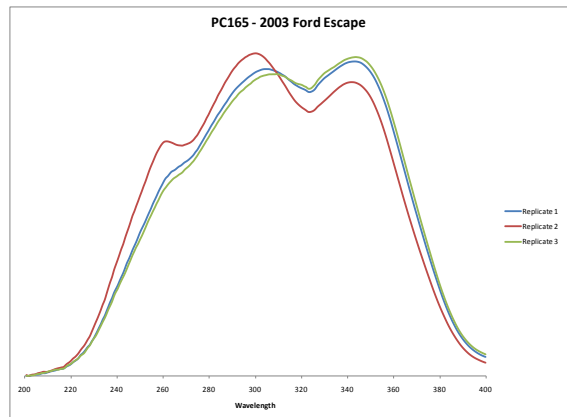
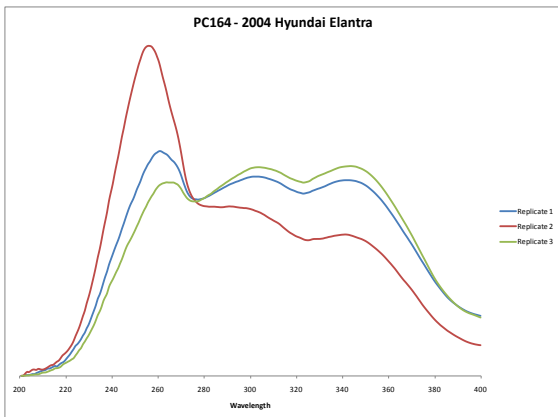
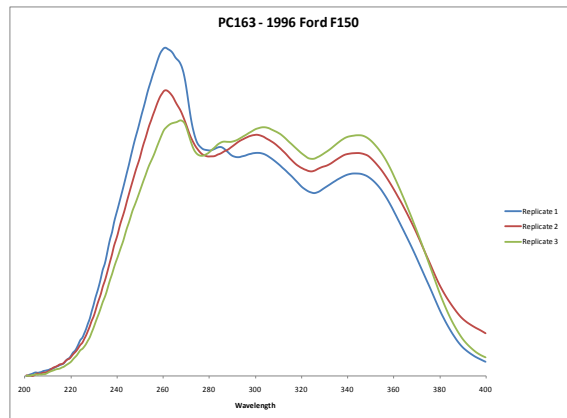
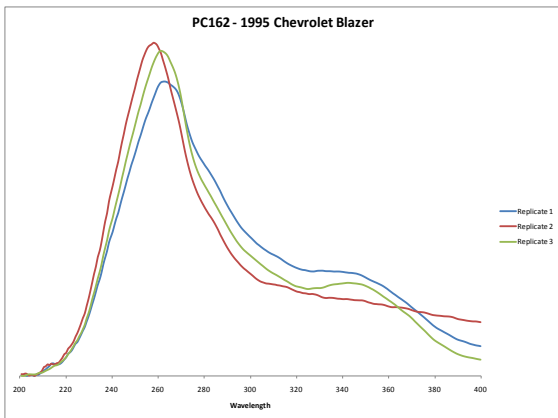
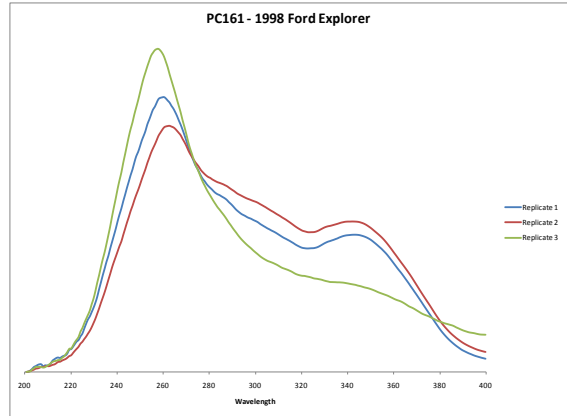
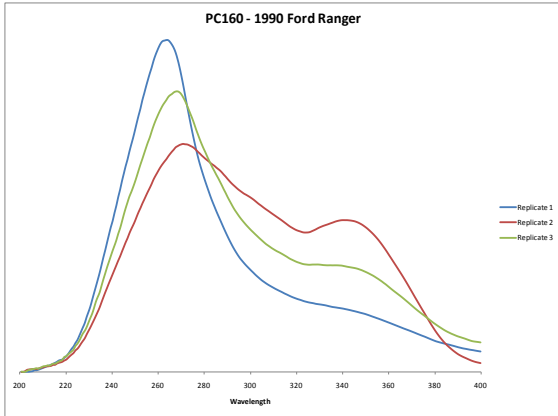


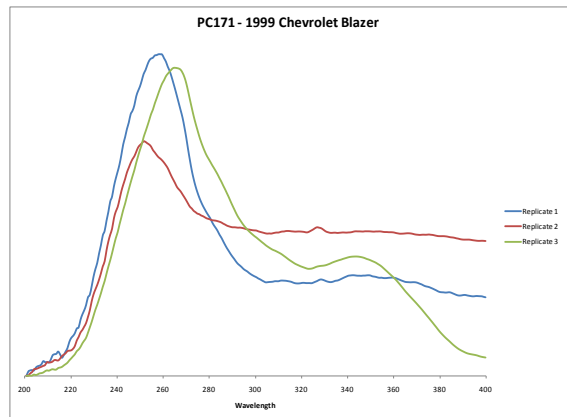
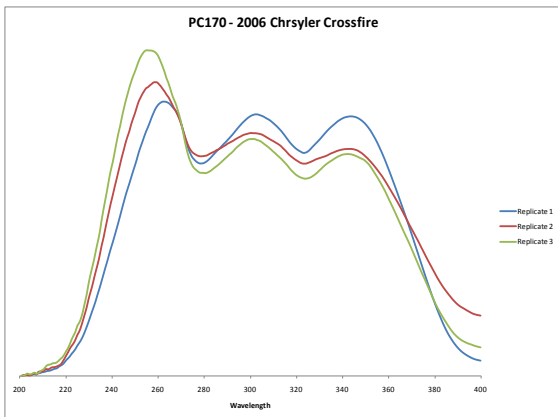
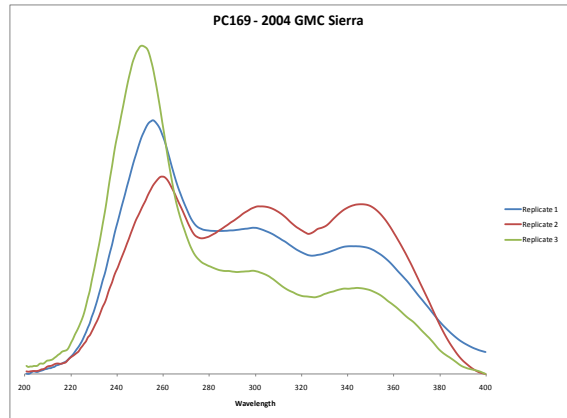
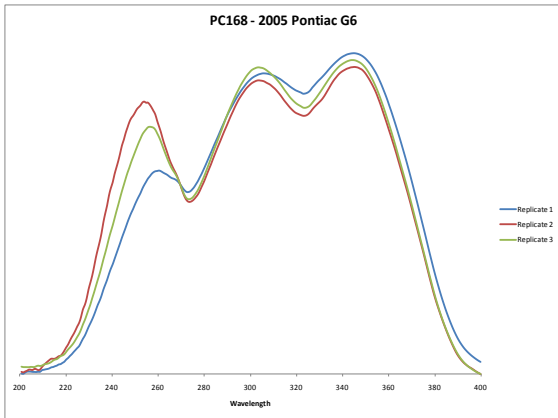
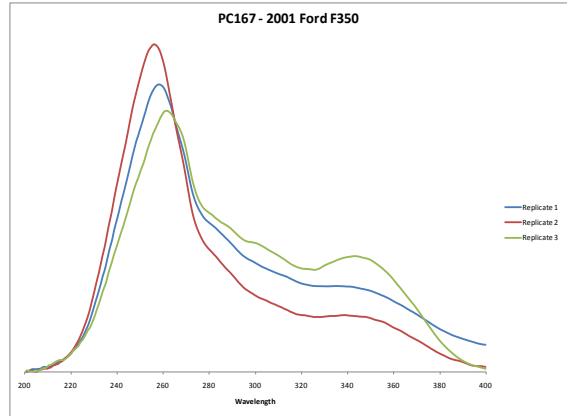
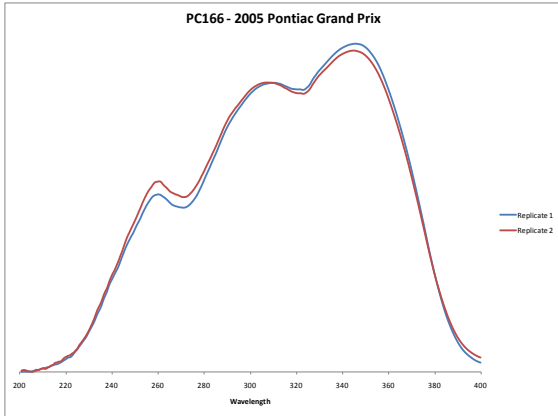


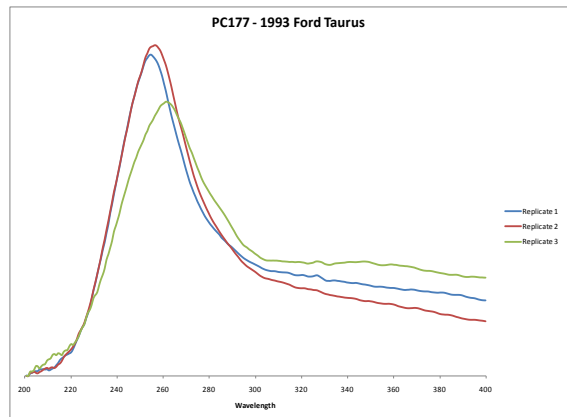
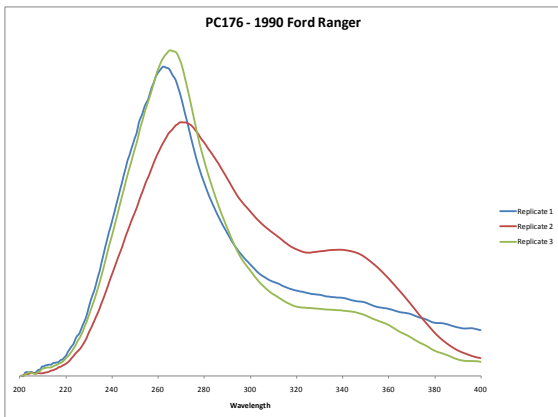
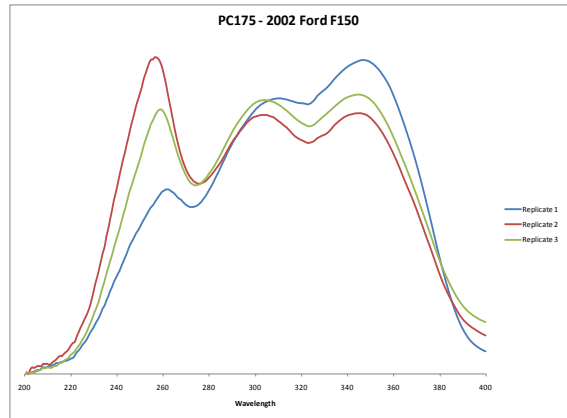
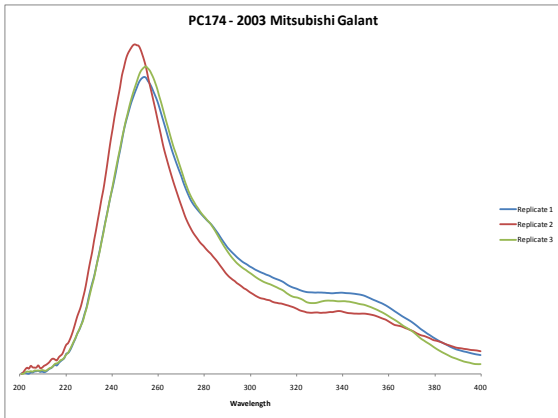
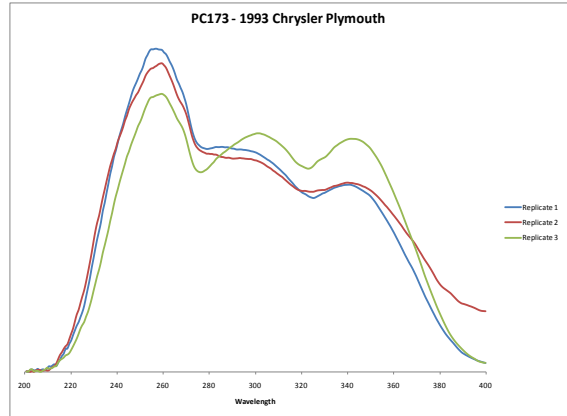
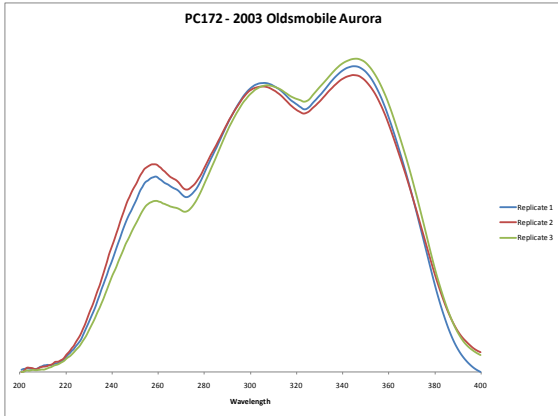


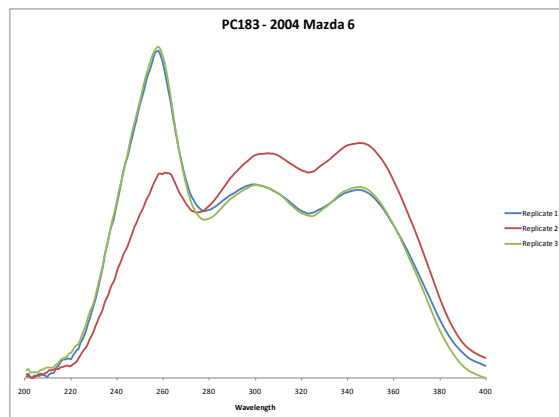
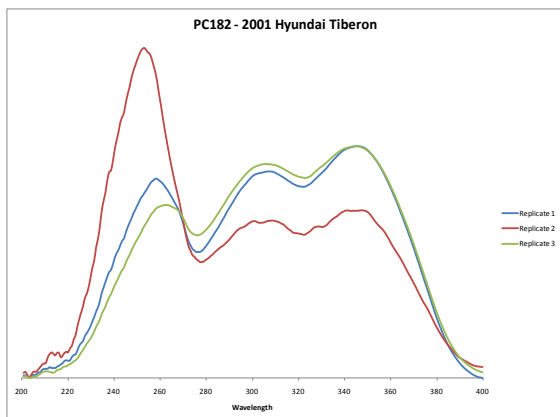
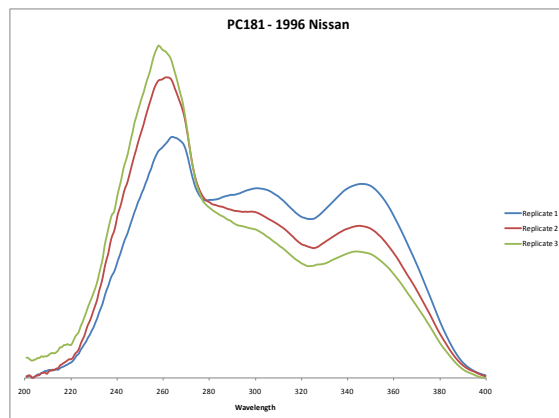
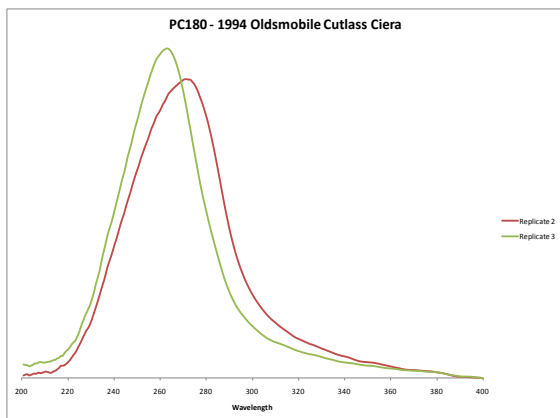
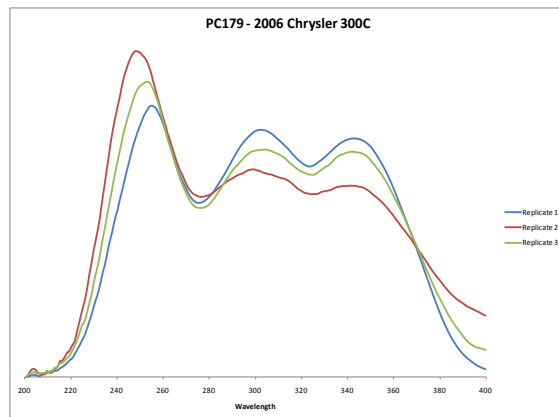
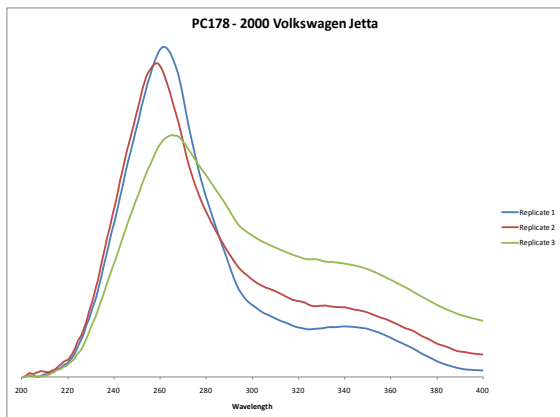


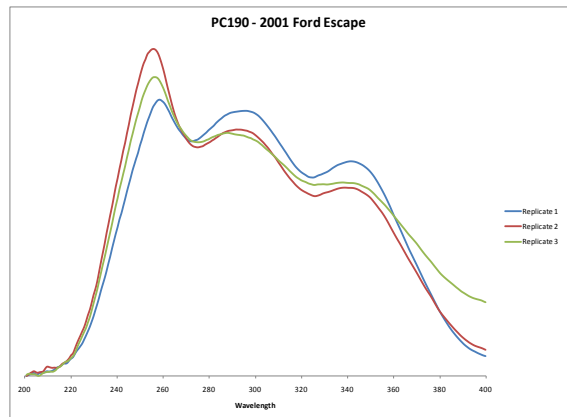
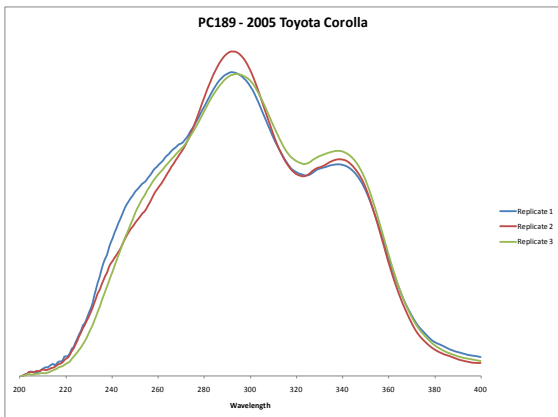
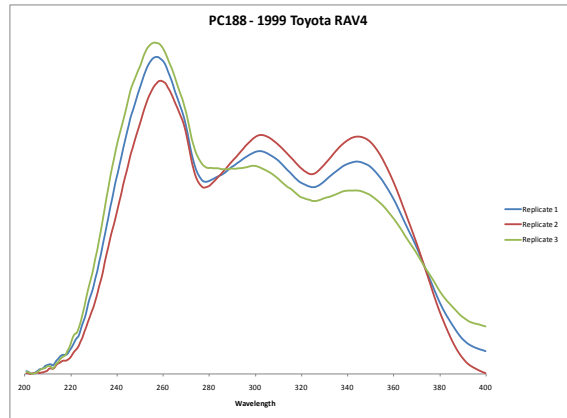
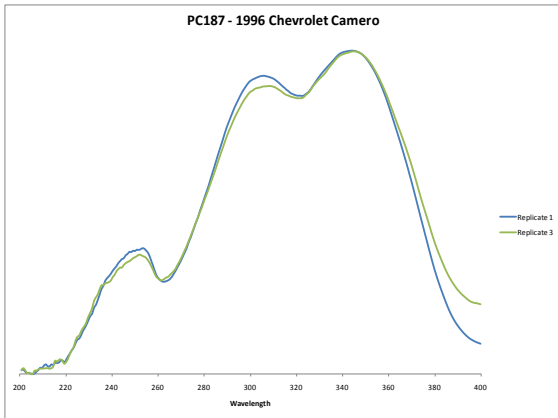
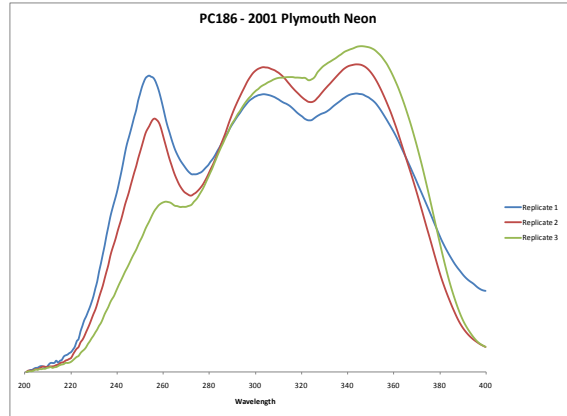
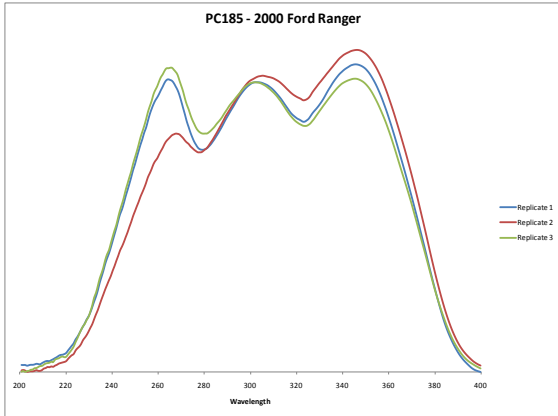


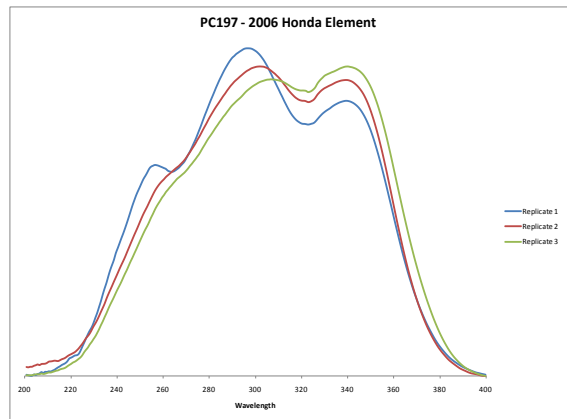
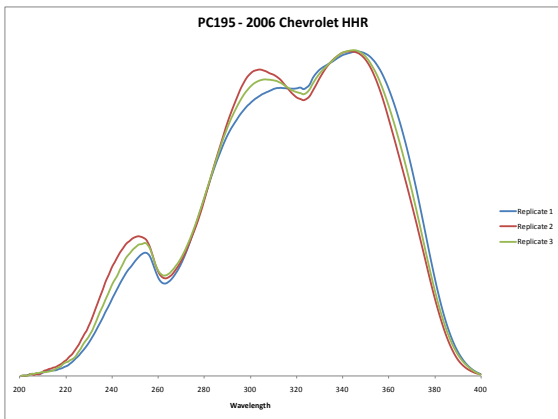
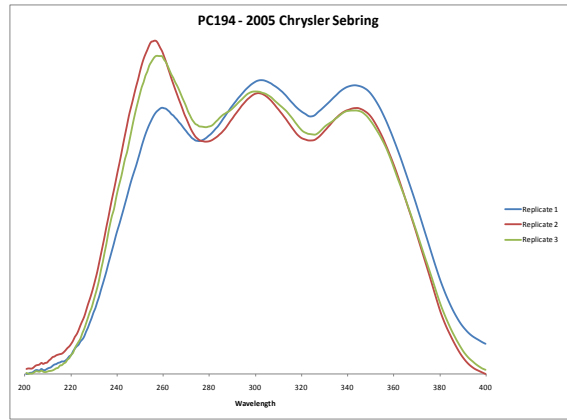
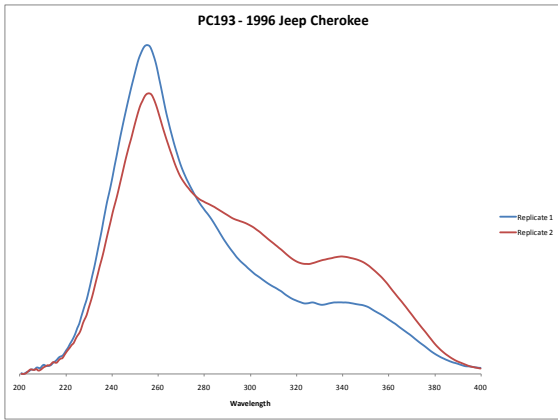
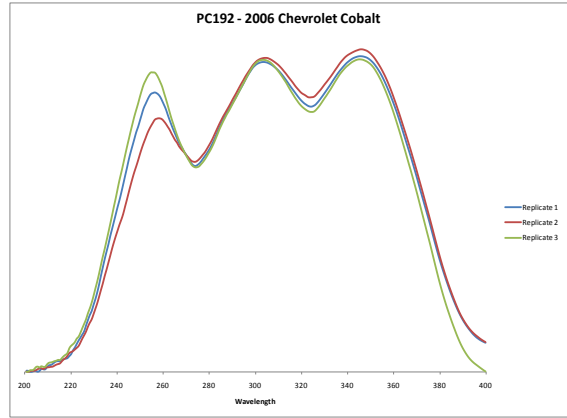
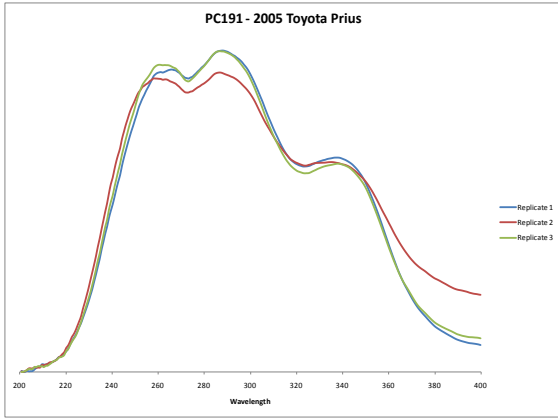


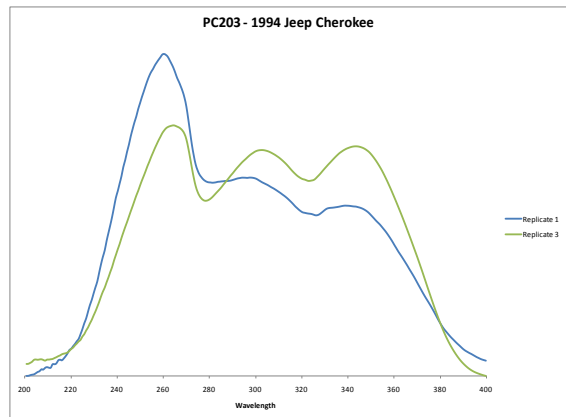
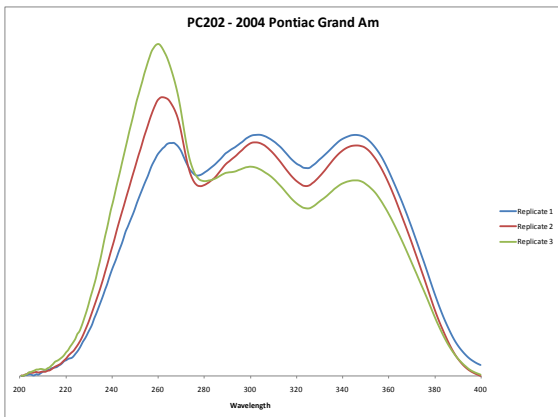
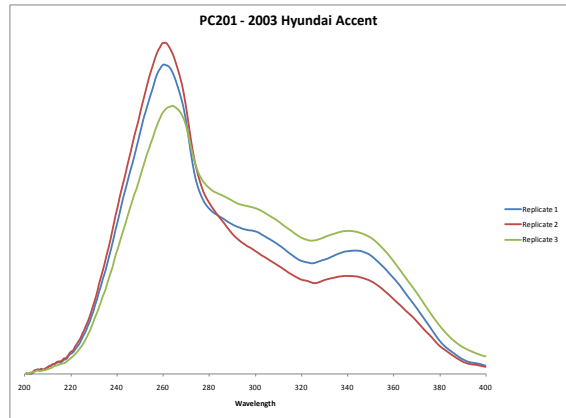
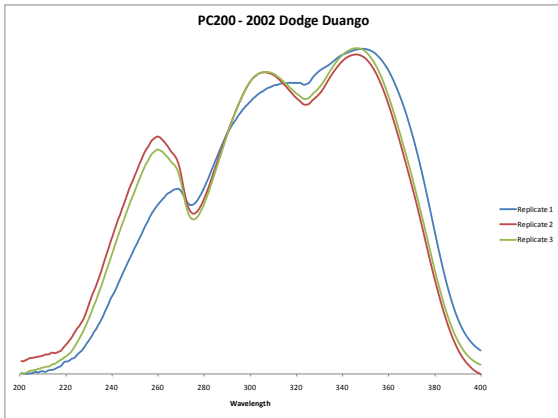
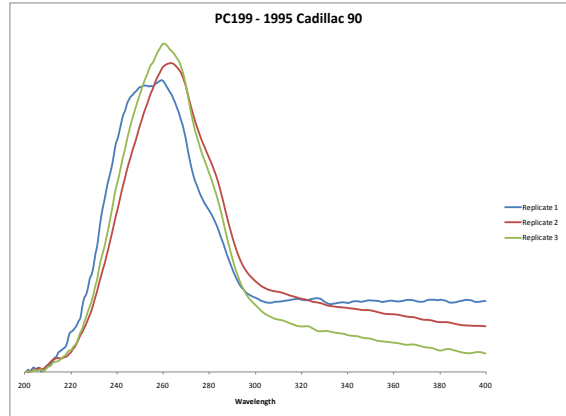
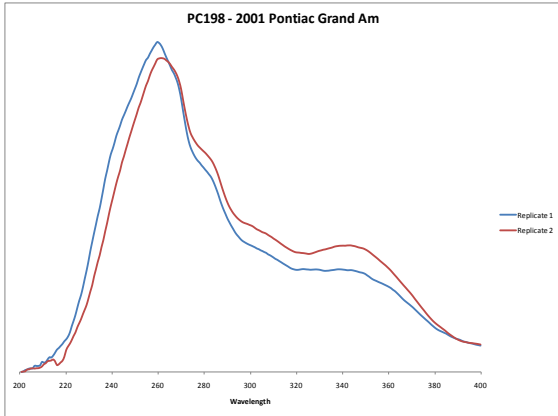


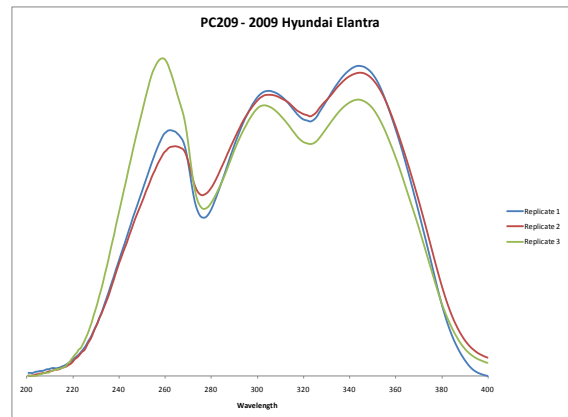
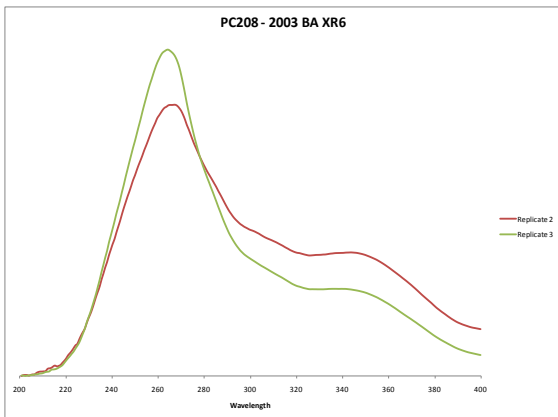
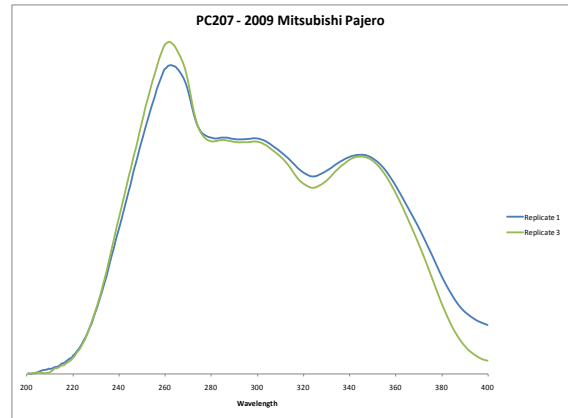
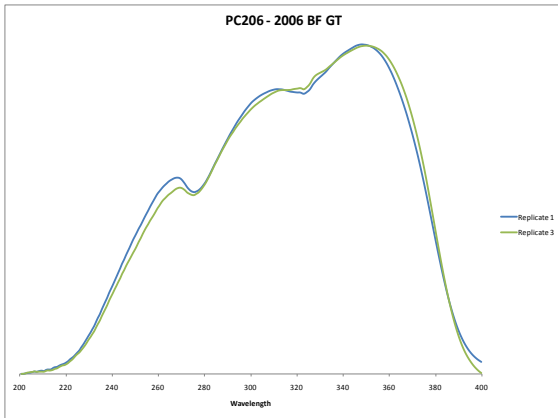
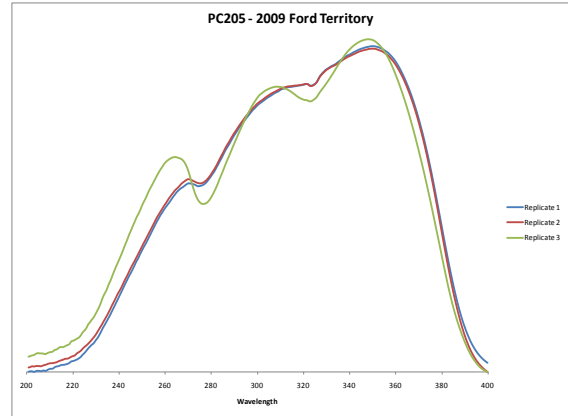
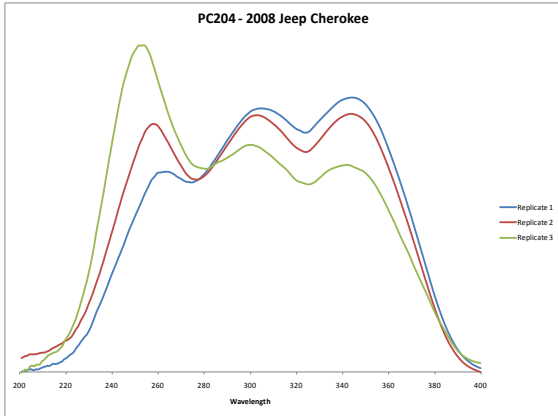




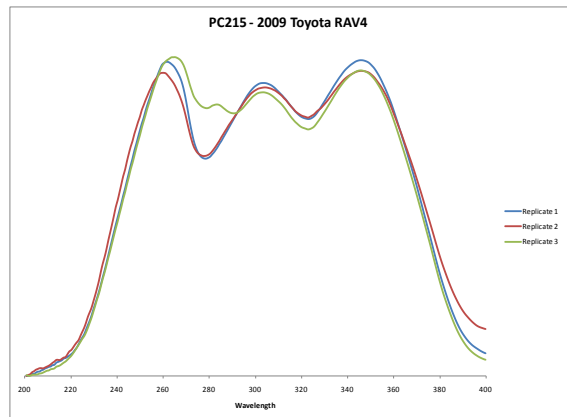
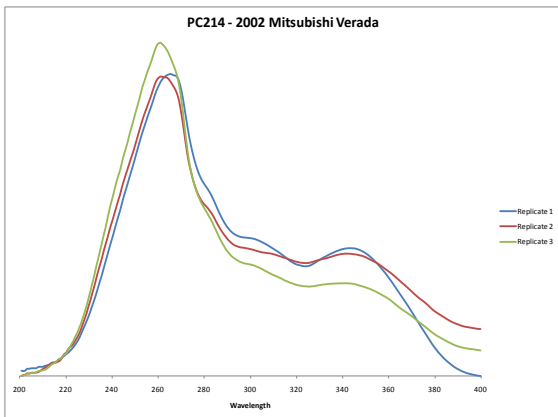
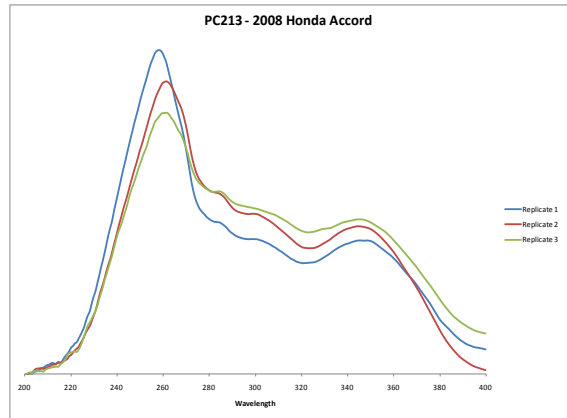
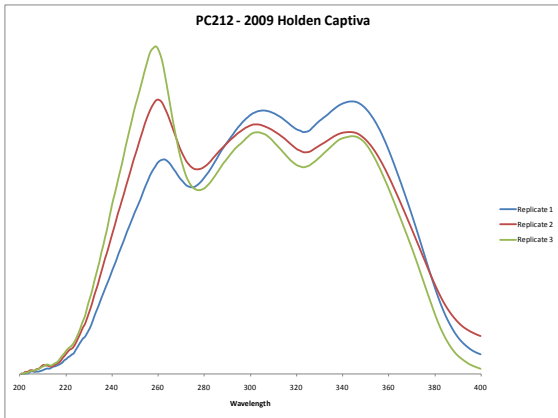
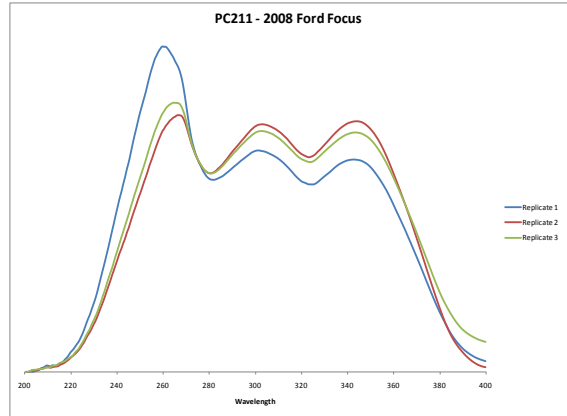
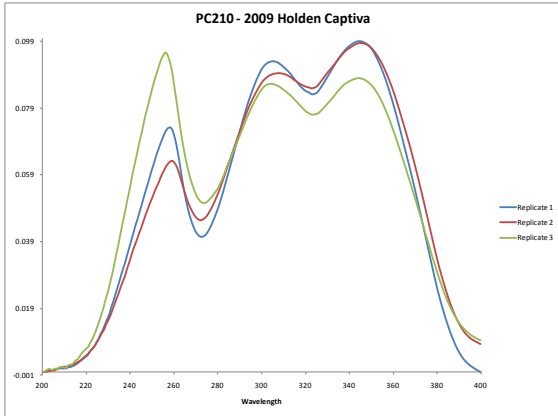


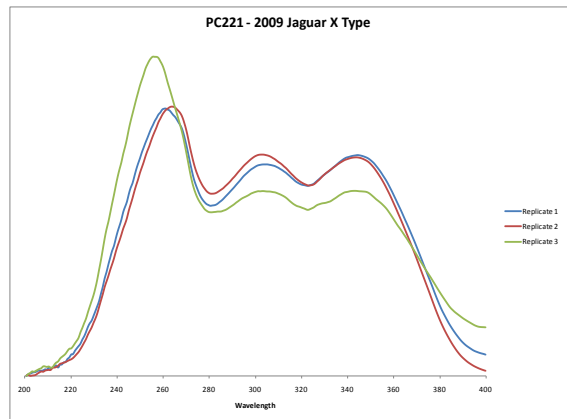
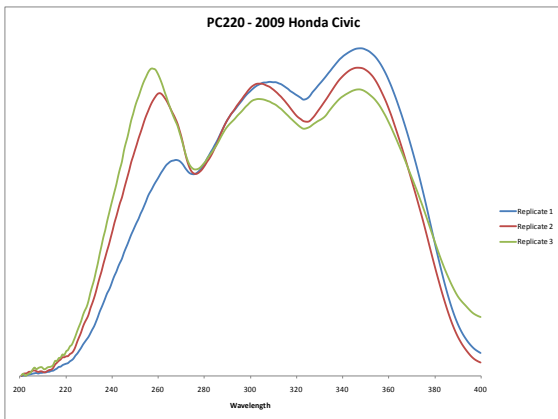
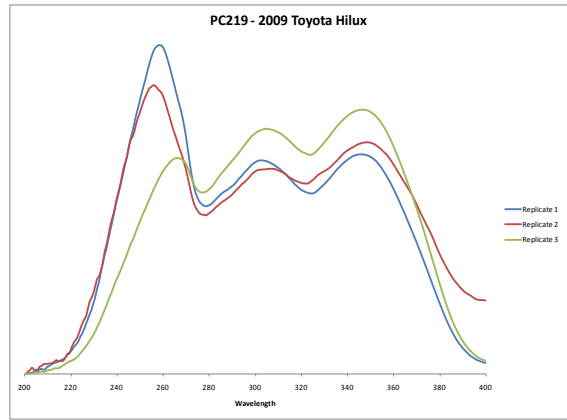
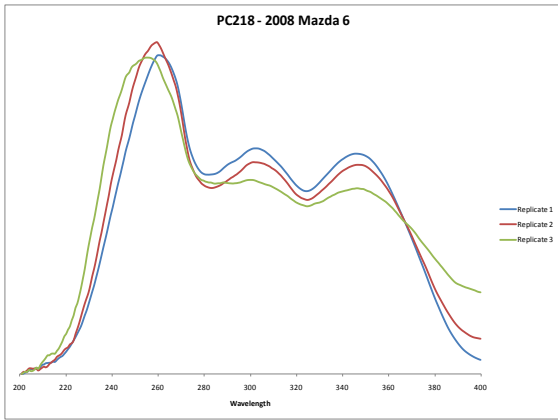
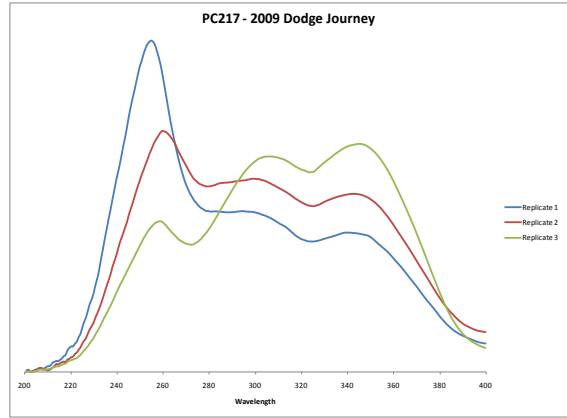
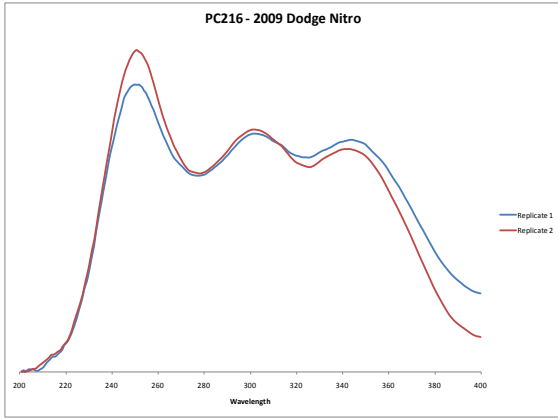


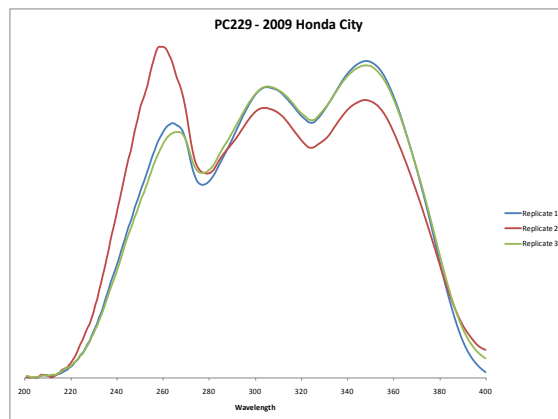
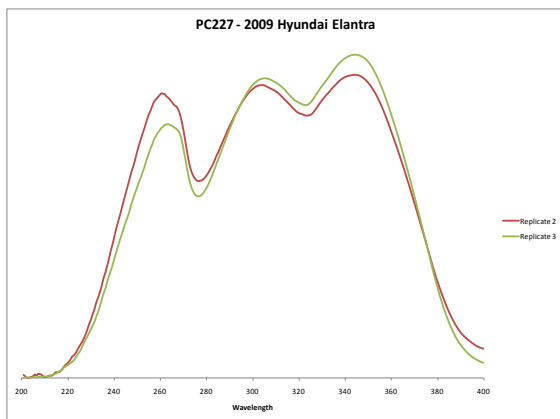
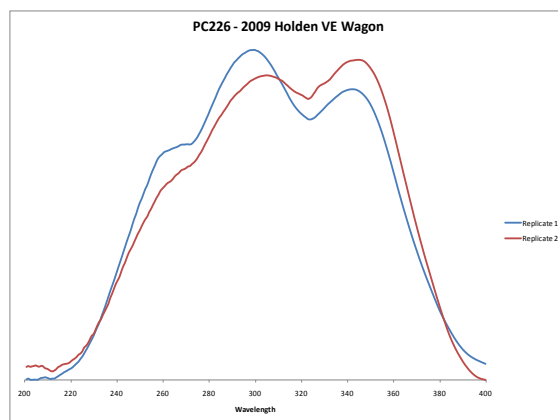
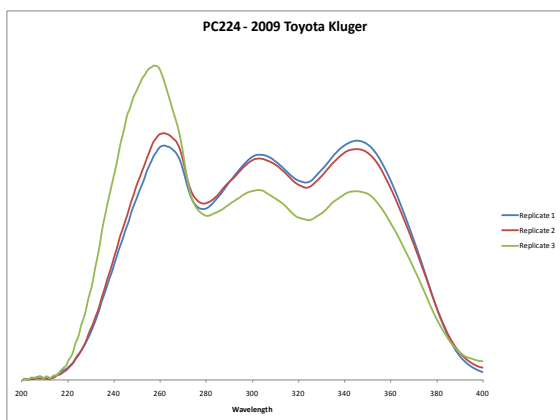
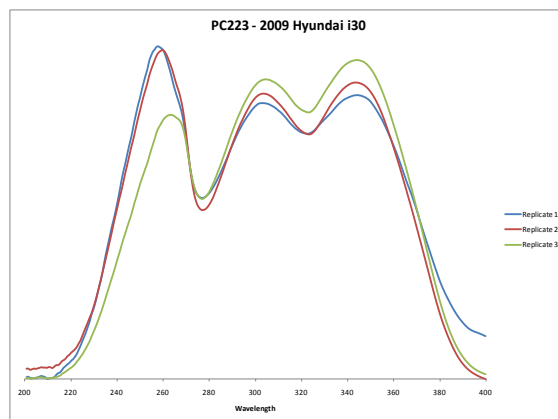
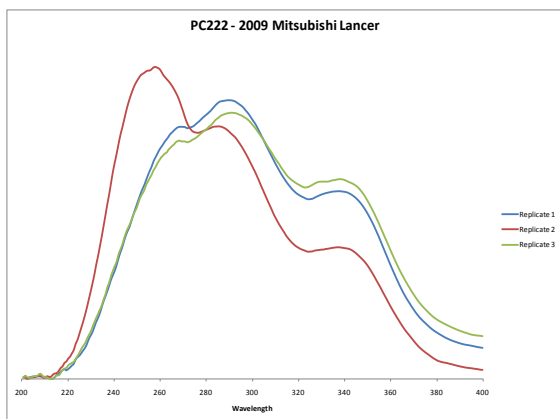


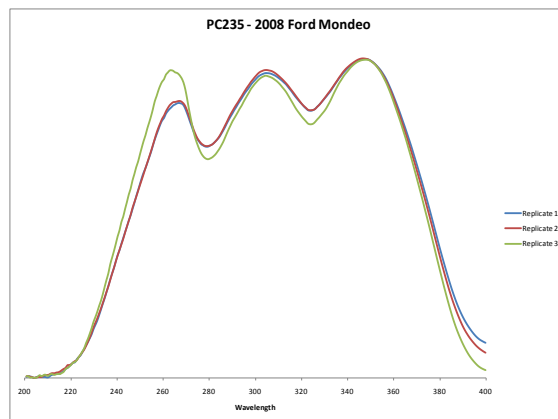
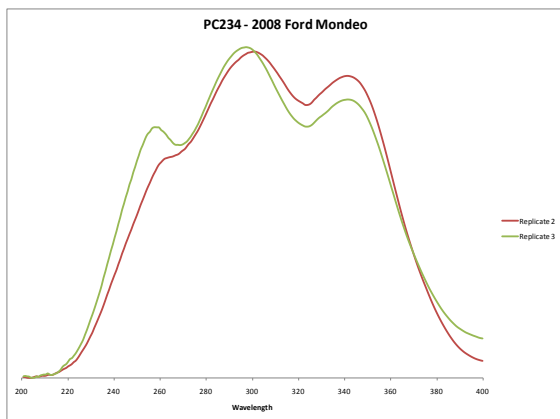
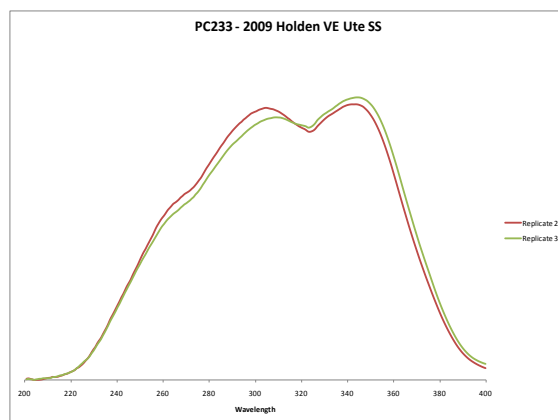
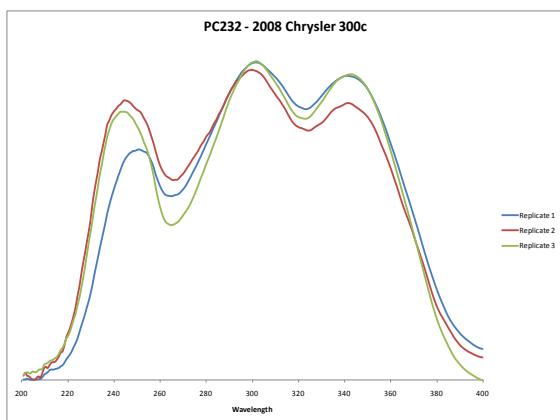
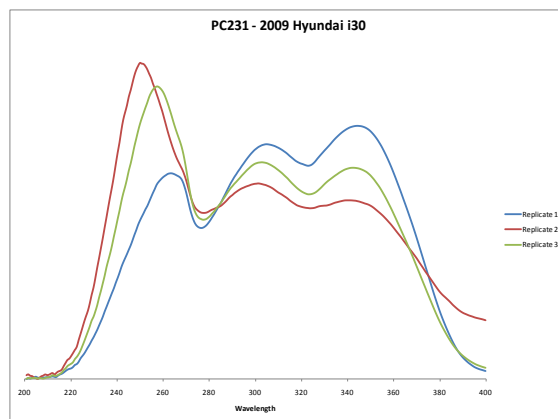
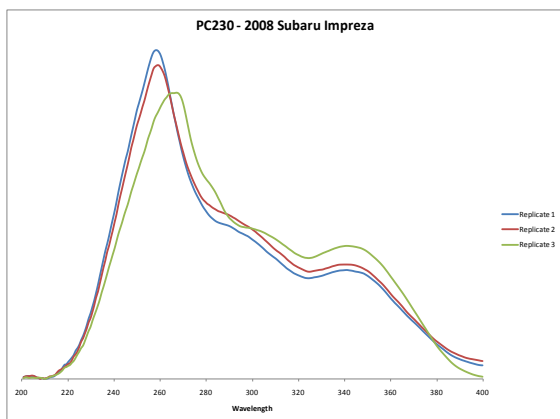


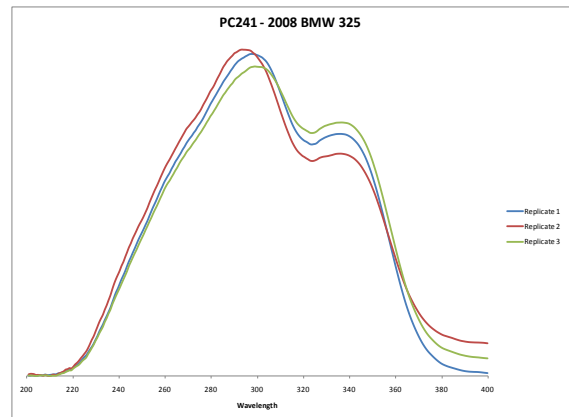
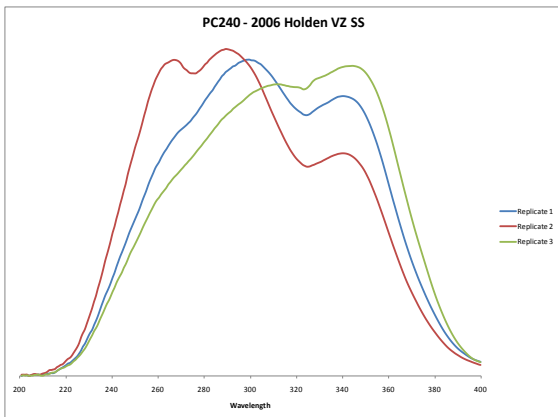
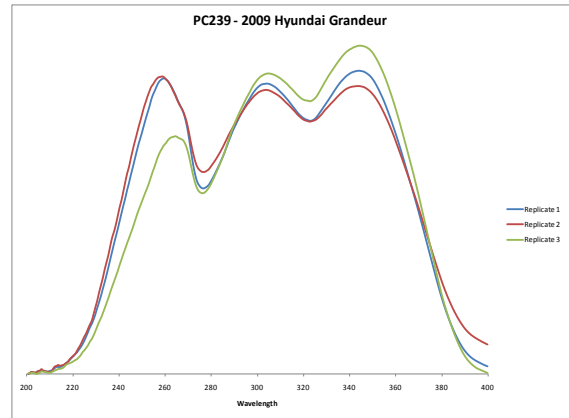
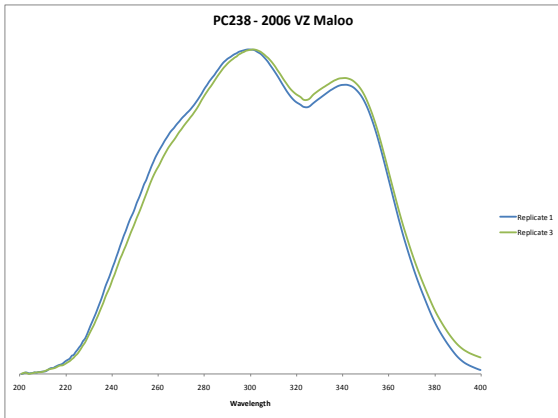
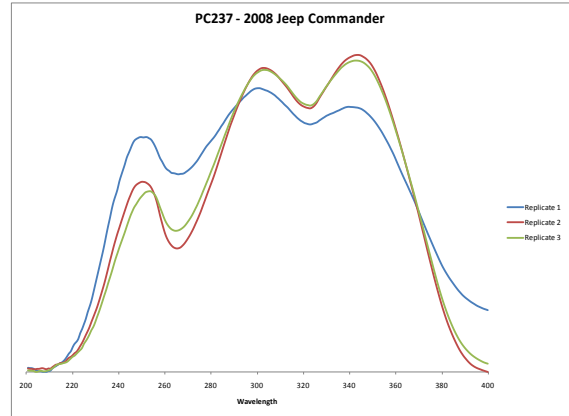
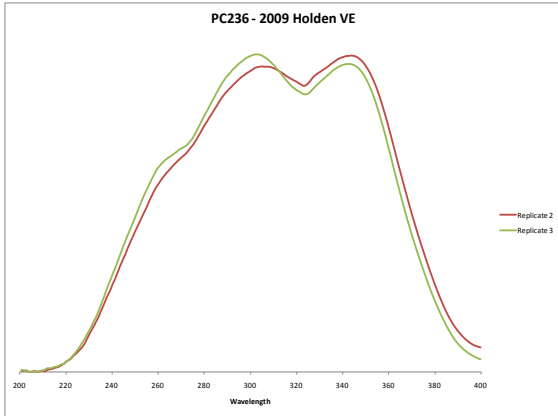


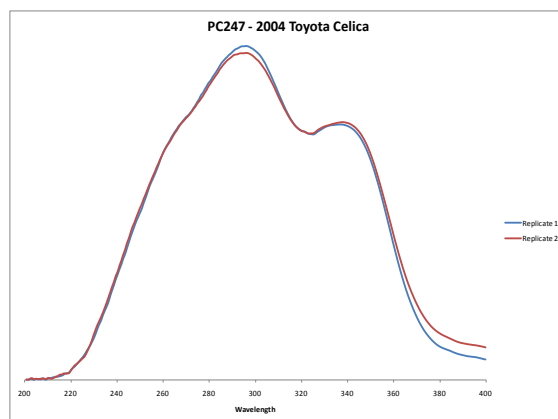
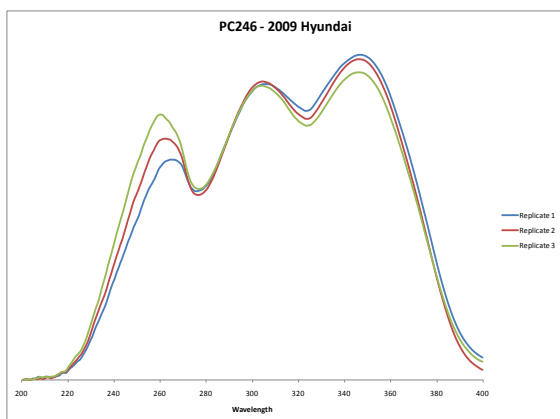
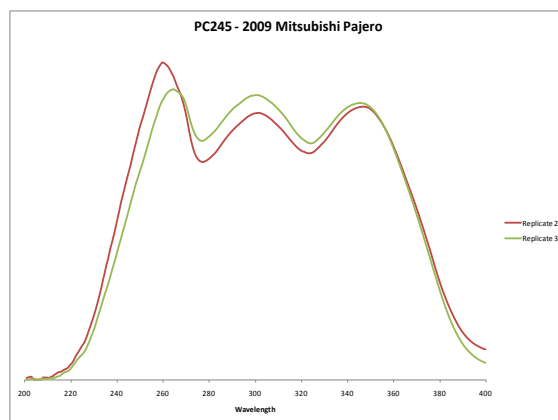
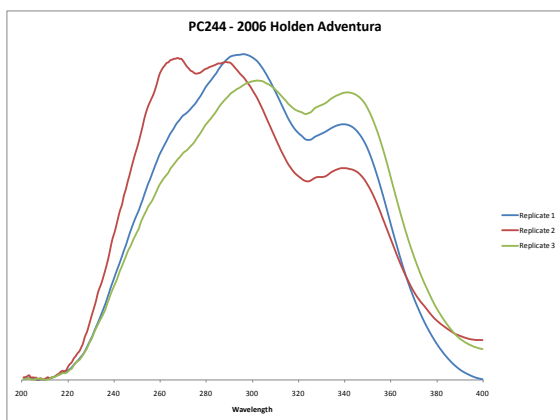
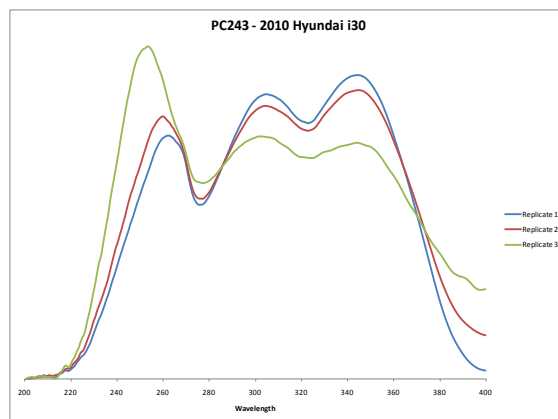
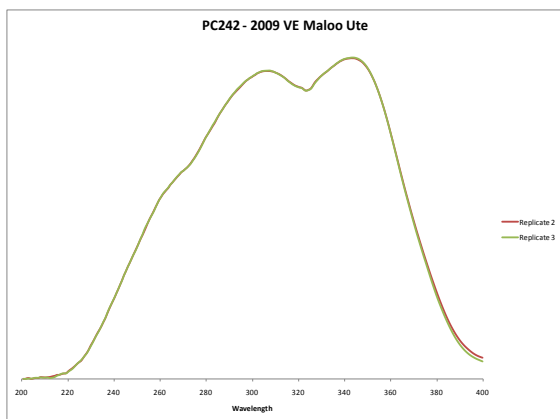


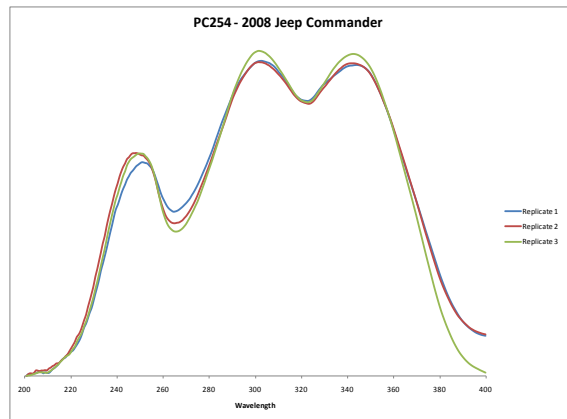
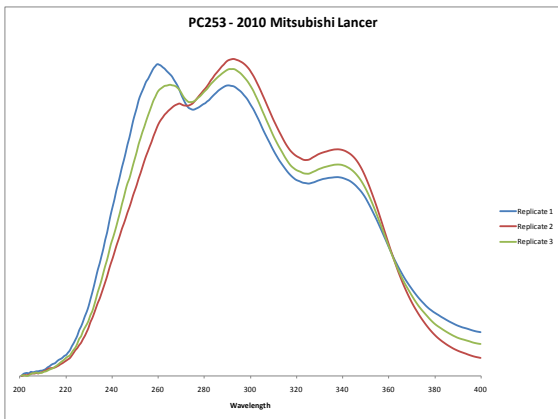
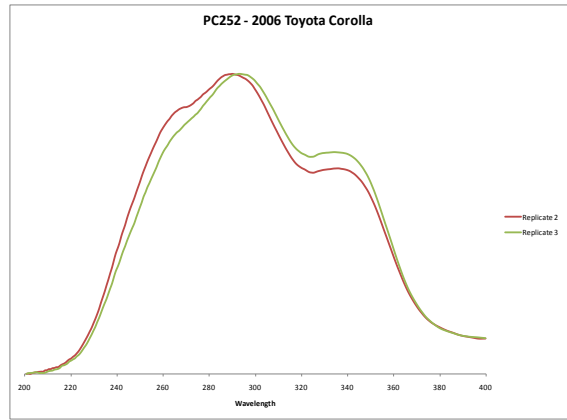
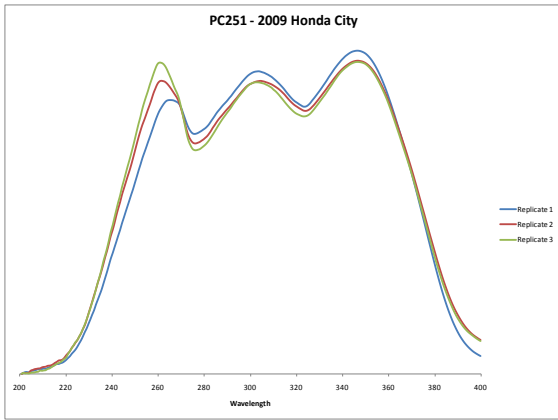
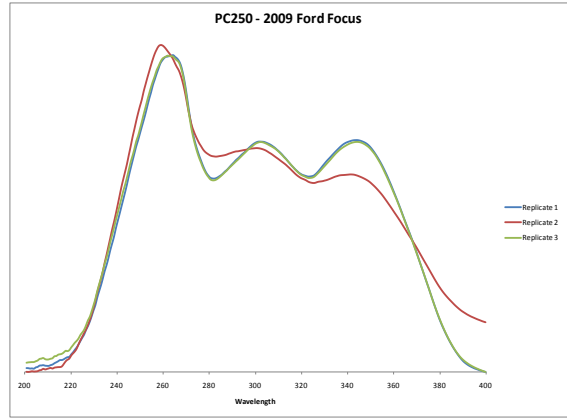
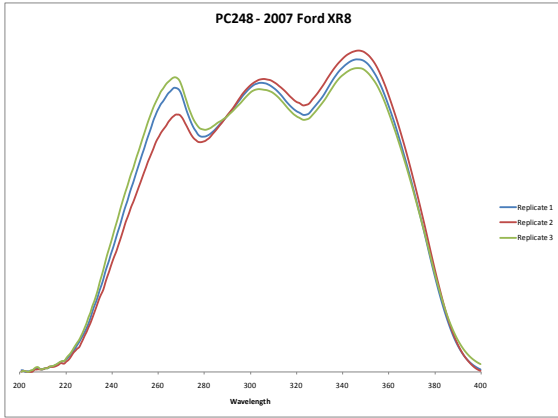


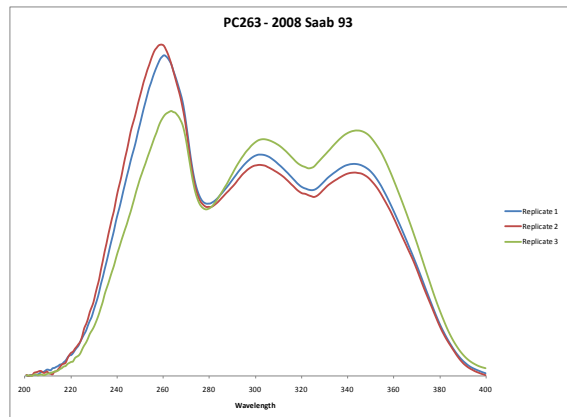
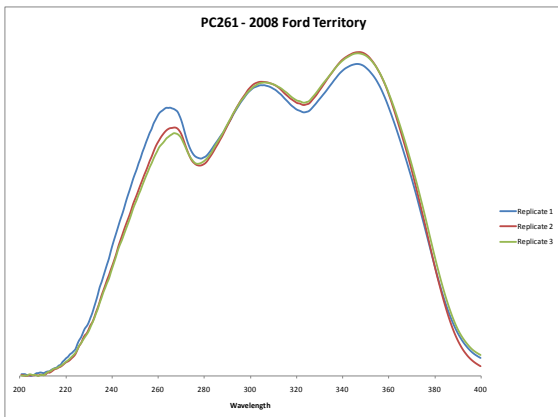
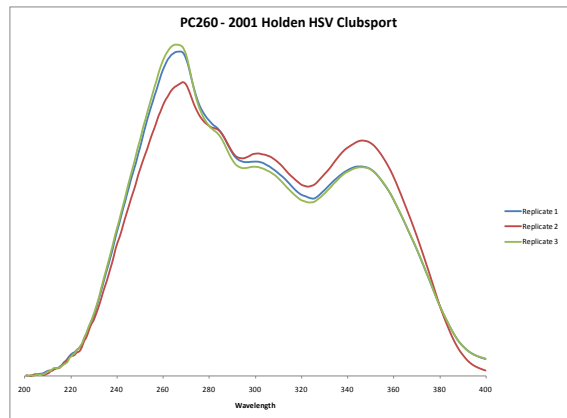
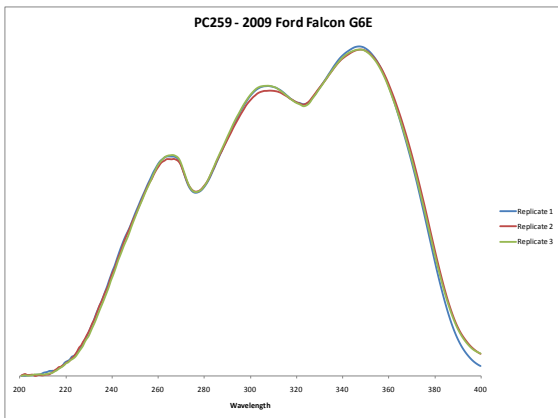
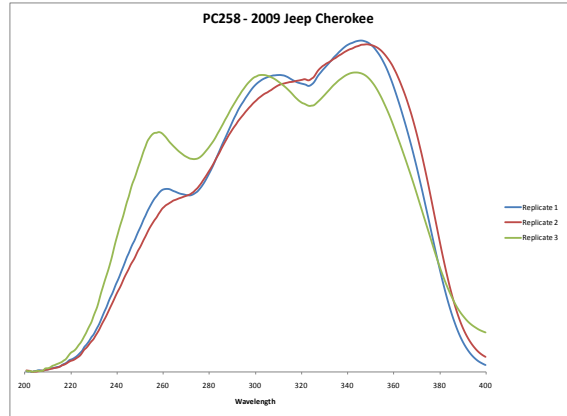
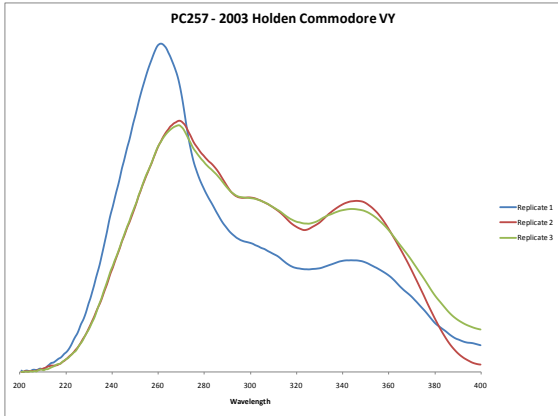




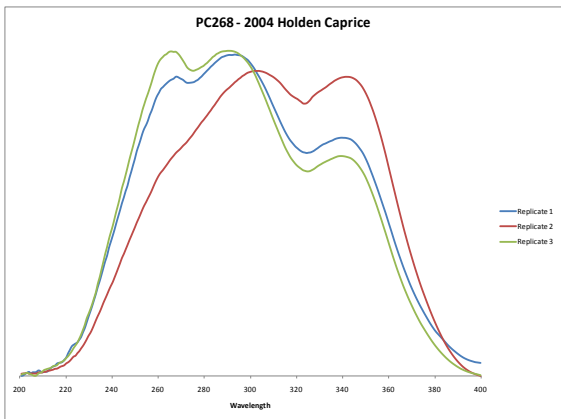
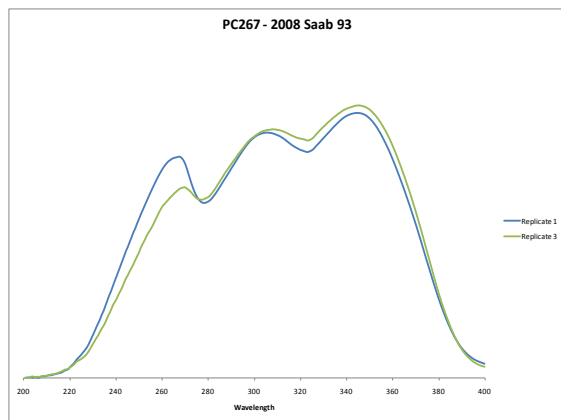
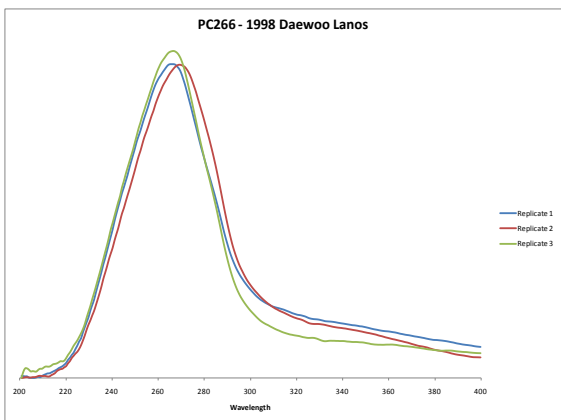
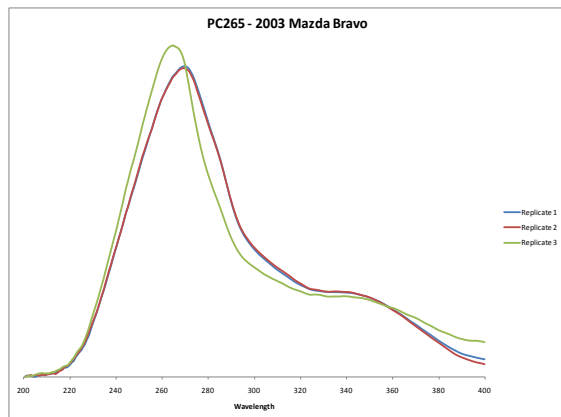
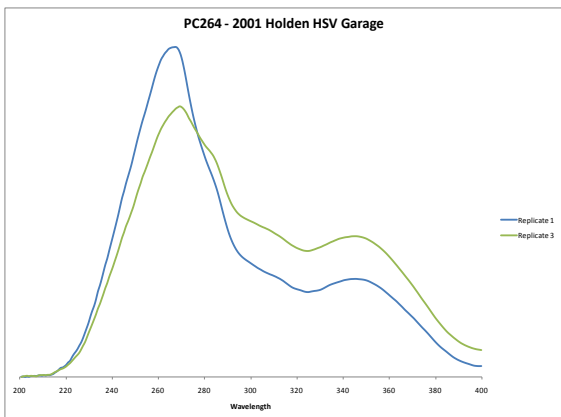






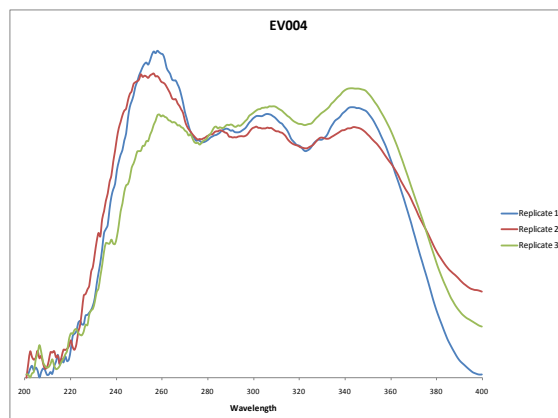
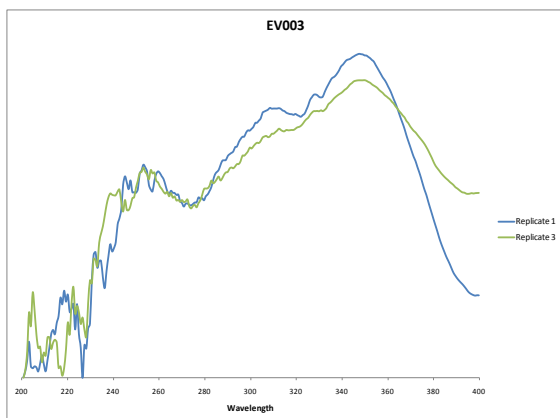
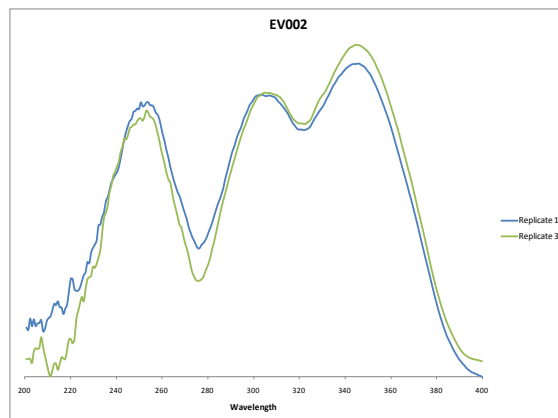
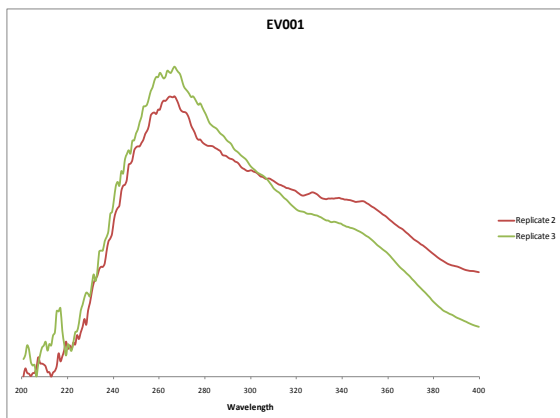


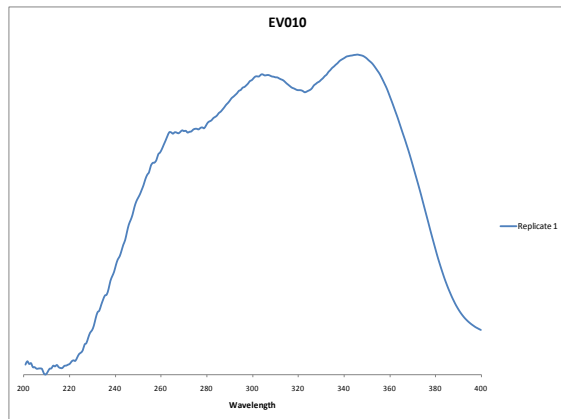
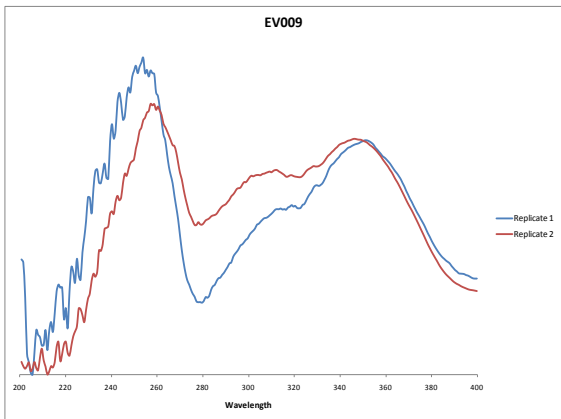
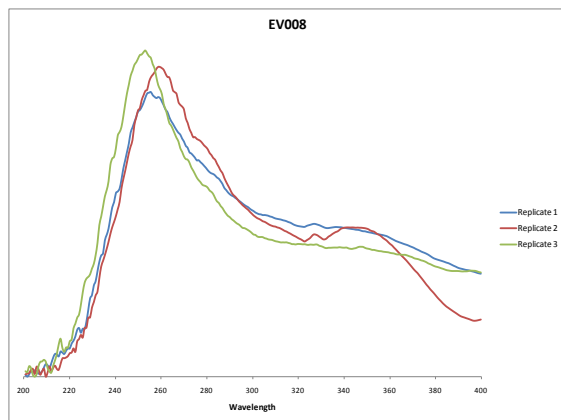
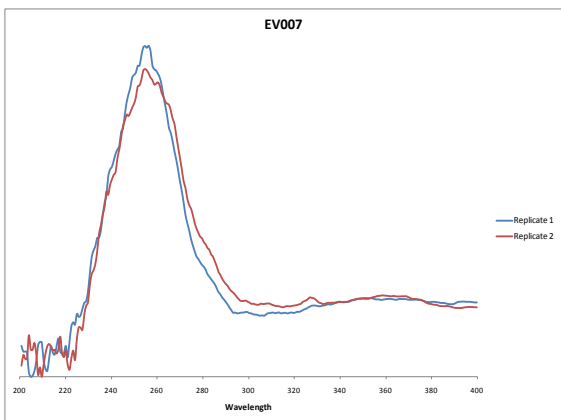
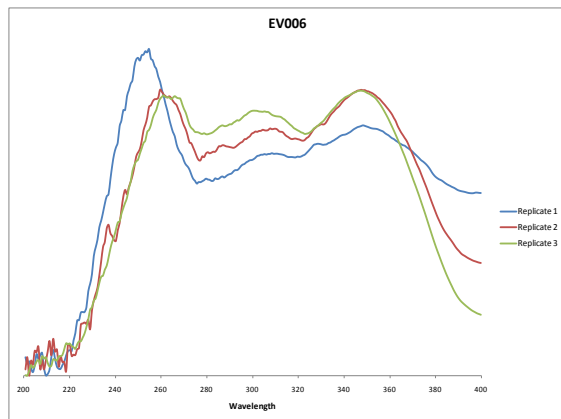
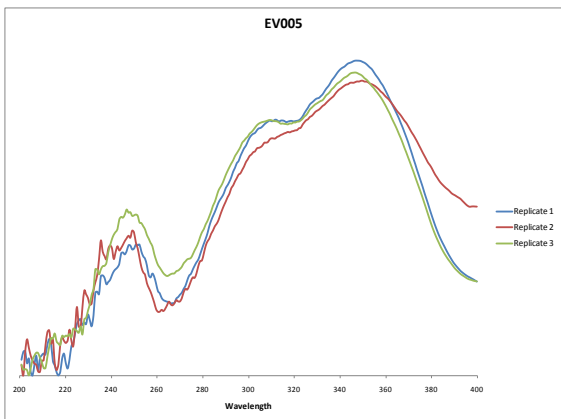


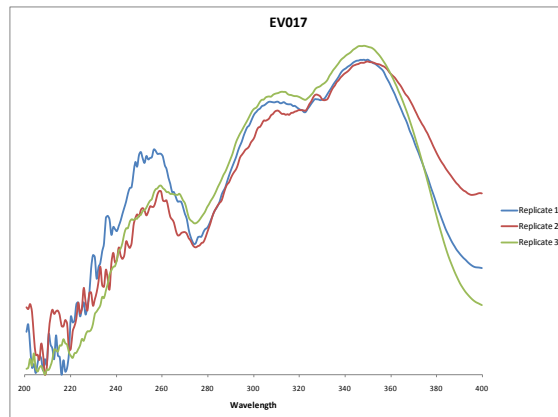
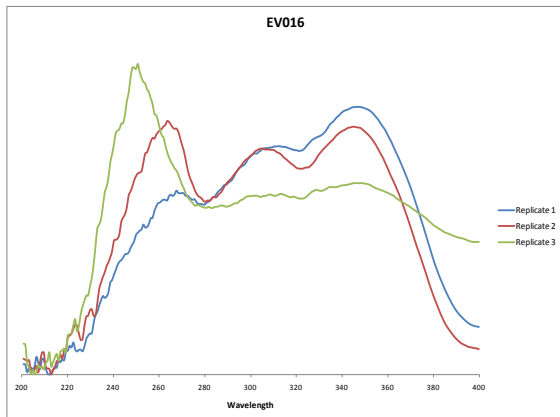
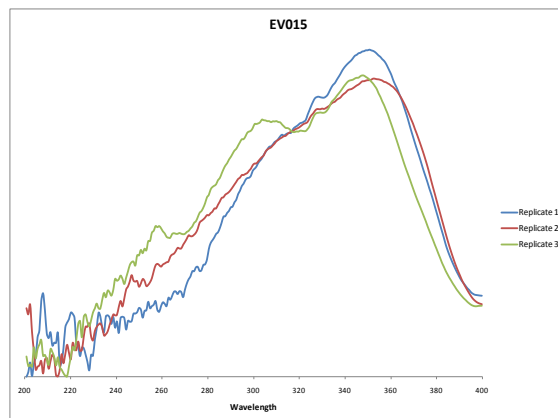
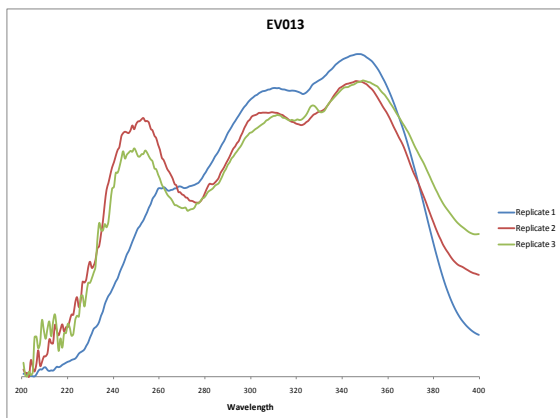
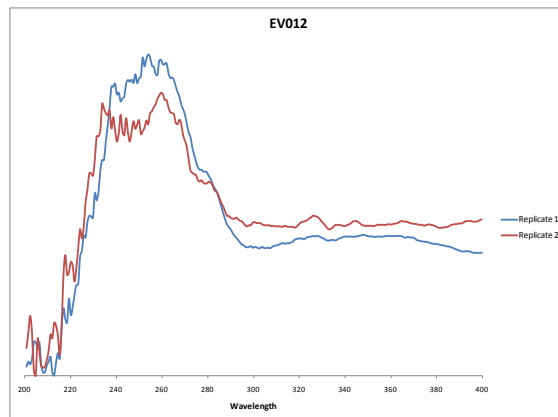
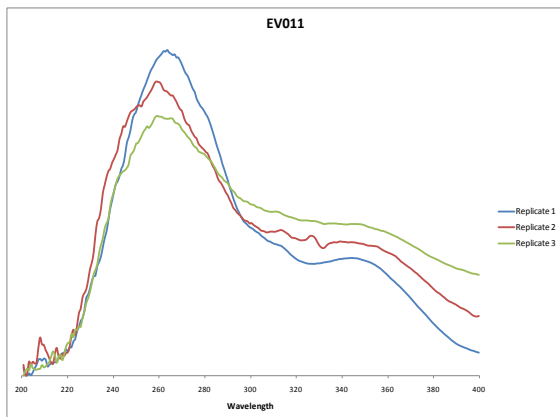


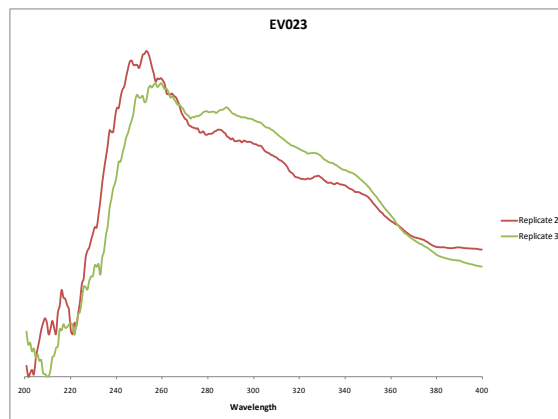
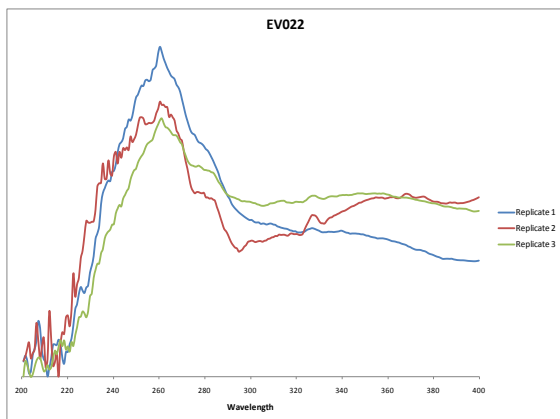
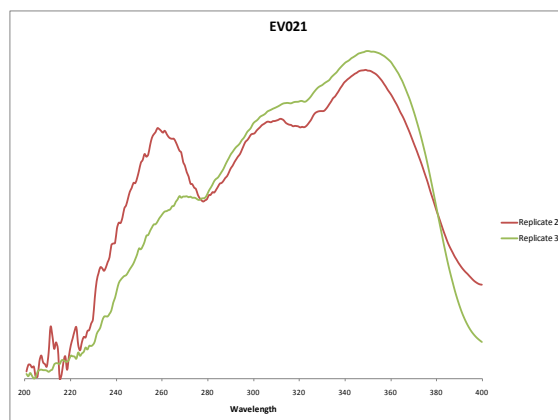
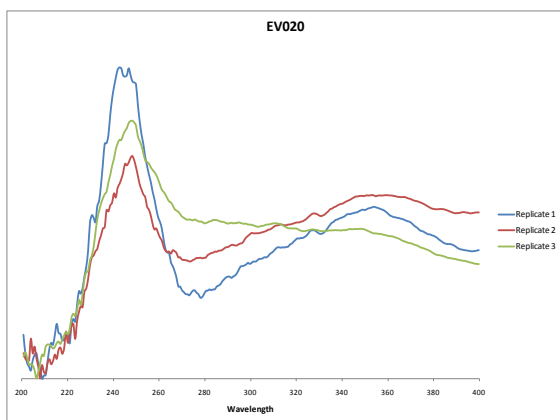
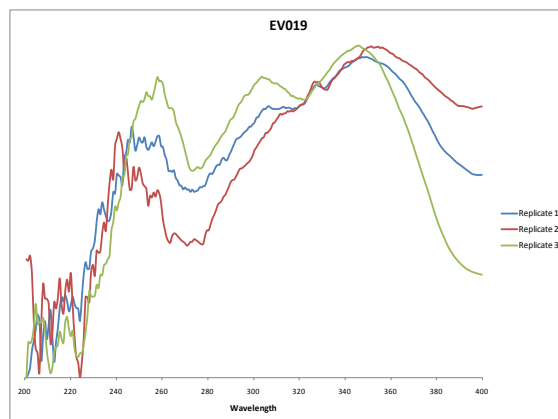
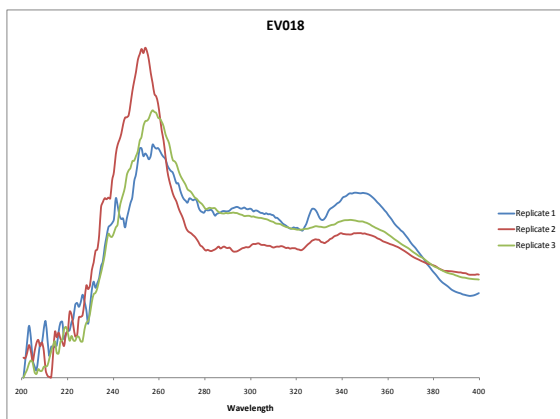
## C.2 External Validation Samples

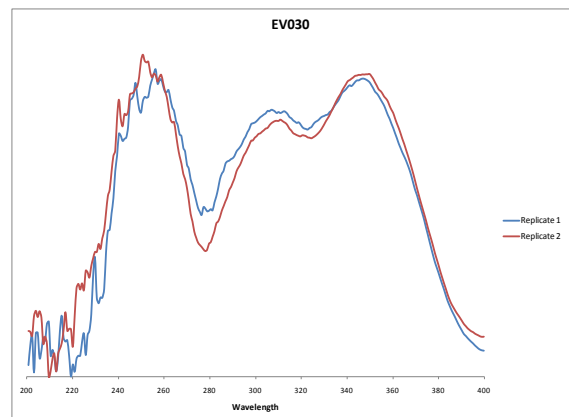
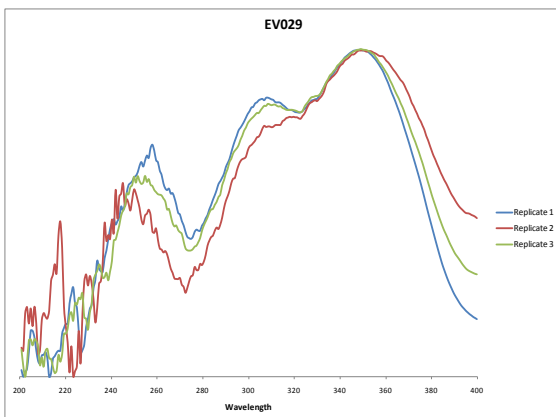
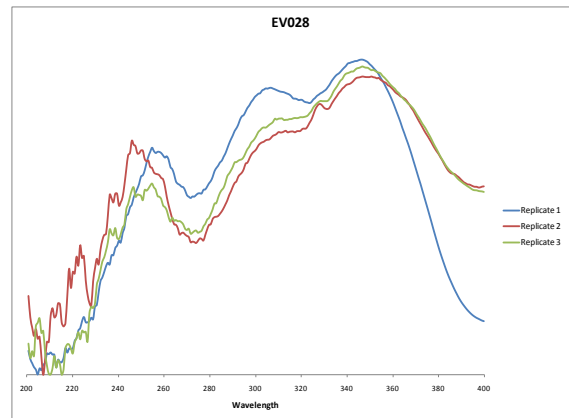
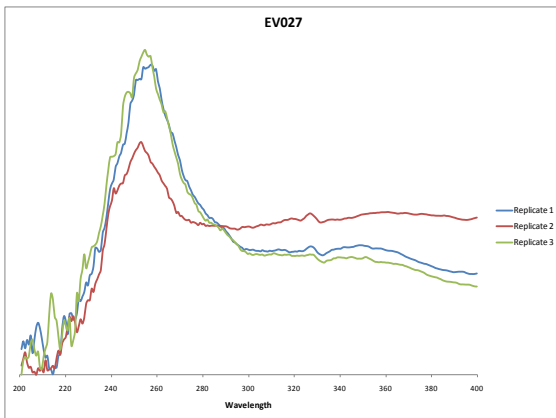
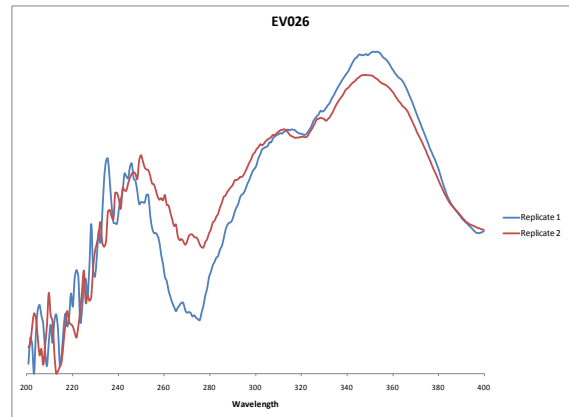
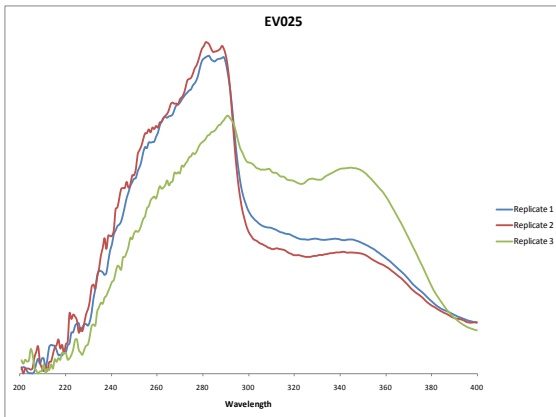
### C.2.1 External Validation Spectra











## C.2.2 Comparison of External Validation and Training Set (averaged spectra)

